Otília da Anunciação Cardoso d'Almeida

NEURAL BASIS OF VISUAL CORTICAL REORGANIZATION MECHANISMS AFTER RETINAL INJURY IN OPTIC NEUROPATHIES

Tese de Doutoramento do Programa de Doutoramento em Ciências da Saúde, ramo de Ciências Biomédicas, orientada pelo Professor Doutor Miguel Castelo-Branco e apresentada à Faculdade de Medicina da Universidade de Coimbra

Setembro 2016

· U C ·

Universidade de Coimbra

DOCTORAL PROGRAM IN HEALTH SCIENCES

FACULTY OF MEDICINE OF UNIVERSITY OF COIMBRA

NEURAL BASIS OF VISUAL CORTICAL REORGANIZATION MECHANISMS AFTER RETINAL INJURY IN OPTIC NEUROPATHIES

Otília da Anunciação Cardoso d'Almeida

September, 2016

The studies referenced in this PhD thesis were carried out at the Visual Neurosciences Laboratory at IBILI - Institute for Biomedical Imaging and Life Sciences, Faculty of Medicine, University of Coimbra, Portugal, and at ICNAS - Institute of Nuclear Sciences Applied to Health, University of Coimbra, Portugal. These were supported in part by an individual fellowship from the Portuguese Foundation for Science and Technology, SFRH/BD/76013/2011.

Cover design: Original artwork by Otília C.d'Almeida.

· U C ·

UNIVERSITY OF COIMBRA

FACULTY OF MEDICINE

NEURAL BASIS OF VISUAL CORTICAL REORGANIZATION MECHANISMS AFTER RETINAL INJURY IN OPTIC NEUROPATHIES

Bases neurais de mecanismos de reorganização do córtex visual em neuropatias óticas

Doctoral Thesis of the Doctoral Programme in Health Sciences, area of Biomedical Sciences, supervised by Professor Miguel Castelo-Branco, MD PhD and presented to the Faculty of Medicine of the University of Coimbra.

Tese de Doutoramento do Programa de Doutoramento em Ciências da Saúde, ramo de Ciências Biomédicas, orientada pelo Professor Doutor Miguel Castelo-Branco e apresentada à Faculdade de Medicina da Universidade de Coimbra.

Otília da Anunciação Cardoso d'Almeida

2016

Scientific Advisor Prof. Miguel Castelo-Branco, M.D., Ph.D.

"As scientists, we step on the shoulders of science,
building on the work that has come before us
aiming to inspire a new generation of young scientists
to continue once we are gone."

Stephen Hawking

TABLE OF CONTENTS

LIST OF ABBREVIATIONS VII

SUMMARY XI

RESUMO XIII

CHAPTER I · INTRODUCTION 15

1 OUTSTANDING RESEARCH CHALLENGES IN VISUAL PLASTICITY MECHANISMS EVOKED BY INPUT DAMAGE: THE ROLE OF STRUCTURAL, NEUROCHEMICAL AND FUNCTIONAL BRAIN IMAGING 17

1.1 The Visual System is especially sensitive to plasticity events 18

2 THE VISUAL CIRCUITRY 20

2.1 The Process of Sight 20

3 WHAT WENT WRONG – DISEASE MODELS OF IMPAIRED RETINOCORTICAL PROCESSING, BASED ON GANGLION CELL DAMAGE AND MITOCHONDRIAL DYSFUNCTION 23

3.1 Mitochondrial diseases and their intriguing neural link 23

3.1.1 *Genetic neuropathies: Leber Hereditary Optic Neuropathy (LHON) and Autosomal Dominant Optic Atrophy (ADOA, Kjer's disease)* 24

3.1.2 *Acquired neuropathy models: type 1 and type 2 Diabetes Mellitus* 25

3.1.3 *Acquired neuropathy model: Multiple Sclerosis and Optic Neuritis* 26

4 FUNDAMENTAL PRINCIPLES OF MAGNETIC RESONANCE IMAGING FOR THE ASSESSMENT OF BRAIN STRUCTURE, FUNCTION, METABOLISM AND NEUROTRANSMISSION 28

4.1 How does MRI work – the underlying physics 28

4.2 Structural neuroimaging (of the brain) 33

4.3 Functional neuroimaging 35

4.3.1 *Localizing early visual areas - The retinotopy* 37

4.4 Neurospectroscopy 39

4.4.1 *Optimization issues - Shimming* 42

4.4.2 *The spectrum: what are we measuring?* 42

5 AIMS 45

6 OUTLINE 47

7 REFERENCES 49

CHAPTER II · LEBER HEREDITARY OPTIC NEUROPATHY 55

CH. II.1 LONG TERM CORTICAL PLASTICITY IN VISUAL RETINOTOPIC AREAS IN HUMANS WITH SILENT RETINAL GANGLION CELL LOSS 57

Ch. II.2 Genetically induced impairment of retinal ganglion cells at the axonal level is linked to extrastriate cortical plasticity 75

Ch. II.3 The neurochemical phenotype of the visual occipital cortex of clinically diagnosed Leber Hereditary Optic Neuropathy patients: a ^{1}H and ^{31}P MR Spectroscopy pilot study 95

CHAPTER III · AUTOSOMAL DOMINANT OPTIC ATROPHY (KJER'S DISEASE) 109

Ch. III.1 A novel cortical neurochemical phenotype in a genetic mitochondrial disorder affecting the retinal ganglion cell 111

CHAPTER IV · TYPE 1 AND TYPE 2 DIABETES MELLITUS 121

Ch. IV.1 Coupling vs. uncoupling of metabolism and neurotransmission in type 2 and type 1 diabetes 123

CHAPTER V · MULTIPLE SCLEROSIS 137

Ch. V.1 Structural assessment of the retinocortical pattern in Multiple Sclerosis 139

CHAPTER VI · CONCLUDING REMARKS 155

LIST OF PUBLICATIONS 165

AGRADECIMENTOS 167

SHORT *CV* 169

List of Abbreviations

^{13}C - Carbon

^{1}H - Hydrogen/Proton

^{31}P - Phosphorus

AcCoA - Acetyl Coenzyme A

AC-PC - Anterior and Posterior Commissure Plane

ADOA - Autosomal Dominant Optic Atrophy

ADP - Adenosine Diphophosphate

Asc - Ascorbate

Asp - Aspartate

ATP - Adenosine Triphosphate

BMI - Body Mass Index

BOLD - Blood Oxygenation Level Dependent

CCT - Cambridge Colour Test

CHESS - Chemical-Shift-Selective

Cho - Choline

CI - Confidence Interval

CNS - Central Nervous System

Cr/PCr - Creatine/Phosphocreatine

CRLB - Crámer-Rao Lower Bounds

CSF - Cerebrospinal Fluid

CSI - Chemical Shift Imaging

CT - Cortical Thickness

DARTEL - Diffeomorphic Anatomical Registration Using the Exponentiated Lie Algebra

DeoxyHb - Deoxygenated Haemoglobin

DIFF - Difference Edited Spectrum

DS - Down Syndrome

DSS - 2,2-Dimethyl-2-Silapentane-5-Sulfonate

DTI - Diffusion Tensor Imaging

EPI - Echo Planar Imaging

ERG - Electroretinography

eTIV - Estimated Total Intracranial Volume

FA - Flip Angle

FAST24 - Fiber Adapted Static Testing 24

FDR - False Discovery Rate

FFT - Fast Fourier Transform

FID - Free Induction Decay

FLAIR - Fluid-Attenuated Inversion Recovery

fMRI - Functional Magnetic Resonance Imaging

FOV - Field-Of-View

Freq - Frequency

FWE - Family Wise Error

GABA - γ-Aminobutyric Acid

GCL - Ganglion Cell Layer

Glc - Glycine

Gln - Glutamine

Glu - Glutamate

GPC - Glycerophosphocholine

GPE - Glycerophosphoetanolamine

GSH - Glutathione

$HbA1_c$ - Glycated Haemoglobin

HC - Healthy Controls

HRF - Haemodynamic Response Function

ICV - Intracranial Volume

ILM - Inner Limiting Membrane

INL - Inner Nuclear Layer

IPL - Inner Plexiform Layer

IRL - Inner Retinal Layer

IS/OS - Inner Segment/Outer Segment Layer

IT - Implicit Time

JT - Jonckheere-Terpstra

Lac - Lactate

LBM - Lesion Belief Maps

LE - Left Eyes

LGN - Lateral Geniculate Nucleus

LH - Left Hemisphere

LHON - Hereditary Optic Neuropathy

LPZ - Lesion Projection Zones

LV - Loss of Variance

MANOVA - Multivariate Analysis of Variance

MD - Mean Defect

MD - Mean Diffusivity

MEGAPRESS - Meshcher–Garwood Point Resolved Spectroscopy

MEIS - Myoid and Ellipsoid Inner Segments

mfERG - Multifocal Electroretinography

MPRAGE - Magnetization-Prepared Rapid Gradient-Echo

MRI - Magnetic Resonance Imaging

MRS - Magnetic Resonance Spectroscopy

MRSI - Magnetic Resonance Spectroscopy Imaging

MS - Mean Sensitivity or Multiple Sclerosis

MSIF - Multiple Sclerosis International Federation

MSnoON - Multiple Sclerosis without Optic Neuritis

MSON - Multiple Sclerosis with Optic Neuritis

mtDNA - Mitochondrial DNA

MVS - Multi-Voxel Spectroscopy

myo-Ins, Mi, Myo - Myo-Inositol

NAA - N-Acetylaspartate

NAAG - N-Acetylaspartylglutamate

NMR - Nuclear Magnetic Resonance

OAD - Oral Antidiabetic Agents

OCT - Optic Coherence Tomography

ON - Optic Neuritis

ONH - Optic Nerve Head

OPL-HFL - Outer Plexiform Layer-Henle Fibre Layer

OPR - Outer Photoreceptor Layer

OR - Optic Radiations

ORL - Outer Retinal Layer Thickness

OVS - Outer Volume Suppression

OxAc - Oxaloacetate

OxyHb - Oxygenated Haemoglobin

PC, PCho - Phosphocholine

PE - Phosphoethanolamine

PERG - Pattern Electroretinography

PET - Positron Emission Tomography

P_i - Inorganic Phosphate

PP - Phosphorylation Potential

ppm - Parts-Per-Million

PRESS - Point Resolved Spectroscopy

Pyr - Pyruvate

RE - Right Eyes

RF - Radiofrequency

RGC - Retinal Ganglion Cells

RH - Right Hemisphere

rmANCOVA - Repeated Measures ANCOVA

RNFL - Retinal Nerve Fibre Layer

ROC - Receiver Operating Characteristic

ROI - Regions-Of-Interest

RPE - Retinal Pigment Epithelium

RRMS - Relapsing-Remitting Multiple Sclerosis

RT - Retinal Thickness

SAP - Standard Automated Perimetry

SC - Superior Colliculus

SD - Standard Deviations

SEM - Standard Error of the Mean

SPECT - Single-Photon Emission Tomography

SPMS - Secondary-Progressive Multiple Sclerosis

STEAM - Stimulated Echo Acquisition Mode

SVS - Single-Voxel Spectroscopy

Syllo-Ins - Scyllo-Inositol

$T1_w$ - T1-Weighted

$T2_w$ - T2-Weighted

TAL - Talairach

Tau - Taurine

TBSS - Tract-Based Spatial Statistics

TCA - Tricarboxylic Acid Cycle

TE - Echo Time

Temp - Temporal

TMS - Tetramethylsilane or Transcranial Magnetic Stimulation

TR - Repetition Time

TSP - 3-(Trimethylsilyl) Propionate

V1 - Primary Visual Cortex

VA - Visual Acuity

VBM - Voxel-Based Morphometry

VOI - Volume-Of-Interest

WHO - World Health Organization

WM-GM - White Matter-Grey Matter

α –KG - α-Ketoglutarate

SUMMARY

The concept of neural reorganization or "brain plasticity" has been one of the most dazzling concepts of contemporary Neuroscience and still inspires intense debates. The belief in a rigid brain structure that remains unchanged throughout life is now obsolete. However the understanding of the limits and extent of neural reorganization and the underlying processes following sensory changes is still controversial and many questions remain unanswered. Existing research reports are often contradictory and the singular pathophysiology underlying each disease and involved neural system prevents the generalization into a common theoretical model.

Comprising all the structures from the retina till the occipital cortex, the visual system is particularly suited to investigate this matter since its organization is well known and seems to be highly sensitive to changes in visual experience. Some studies have identified an association between visual loss and neural atrophy. Others proposed that primary sensory areas of the human visual cortex can still retain a certain degree of plasticity through lifespan, and overt retinal lesions may induce visual cortical reorganization. Likewise, developmental plasticity may cooccur with subtle pathology in preclinical stages of retinal degeneration.

We asked how different visual regions reorganize upon loss of the main output of the retina (ganglion cell axons) and investigated the pathophysiological mechanisms and putative "plasticity" in disease models of retinal ganglion cell death and optic nerve atrophy. Accumulating evidence suggests that mitochondrial impairment contributes to the pathogenesis of several neurodegenerative diseases and is tightly coupled to the functional (including visual) impairment frequently reported in these disorders. This is consistent with the idea that mitochondria are not only the main providers of adenosine triphosphate but also participate in cell death cascades. Due to the elevated metabolic needs of neural tissues such as the retina, optic nerves and brain cells, these are particularly susceptible to limited energy supply as a result of mitochondrial dysfunction.

We evaluated the retinocortical profile of two relevant mitochondriopathies, Leber Hereditary Optic Neuropathy and OPA1-related Autosomal Dominant Optic Atrophy. Moreover, we also studied type 1 and type 2 Diabetes Mellitus and Multiple Sclerosis with and without a previous episode of Optic Neuritis in which visual impairment is a frequent comorbidity. The first two are the most common inherited optic neuropathies, caused by mutations affecting the respiratory chain complexes and oxidative phosphorylation in mitochondria. Despite not being "classical" optic neuropathies, the latter two can be seen respectively as metabolic and demyelinating models of disease that lead to visual impairment due to ganglion cell degeneration and optic nerve atrophy. It has been proven already a strong link between the pathophysiology of these disorders and mitochondrial (dys)function. The mitochondrial defect leads to clinically heterogeneous profiles and different degrees of severity. Therefore the apparently simple concept of "brain plasticity" requires multiple levels of analysis (from genetic to behavioural) combining clinical, structural (shape and size), functional (vascular and synaptic), connectivity and biochemical (metabolism and neurotransmission) data.

We addressed visual reorganization/modification processes using optic coherence tomography to measure thickness of retinal layers, magnetic resonance (MR) imaging to study anatomical changes in anatomical and functionally-defined visual retinotopic maps and ^{1}H and ^{31}P MR Spectroscopy to study the neurochemical environment in vivo of the occipital cortex of these patients. These studies manifested the visual cortex' capacity to alter its structure, function and metabolism in response to (partial) disruption of the sensory input, not necessarily in a negative sense, but possibly also to restore homeostasis.

Several hypotheses can be raised including a massive restructuring of the visual circuitry resultant from cortico-cortical and mainly feedforward connections between the eye and the brain. The reorganization may gather structural and functional phenotypical changes with pathophysiological systems modulation at the level of metabolism and neurotransmission pathways. These models of disease highlight the importance of excitatory/inhibitory balance, neurochemical coupling and also the temporal dependence of these adaptive changes for functionally effective reorganization to occur.

Most of the mitochondrial and neurodegenerative diseases rely on the symptomatic treatments, and often neglect the early impact that mitochondrial and visual (dys)function have on the brain. We believe that the integration of different disease model phenotypic profiles with singular aetiologies and (patho)physiologies, and a multimodal approach may help provide a holistic view on the dichotomy between reorganization and degeneration. This might pave the way for the development of novel therapeutic and rehabilitation techniques that aim to modulate mitochondrial function and promote early plasticity before neurodegeneration dominates in order to prevent or delay functional loss.

Keywords:

Autosomal Dominant Optic Atrophy; cortical plasticity; cortical thickness; Diabetes Mellitus; Leber Hereditary Optic Neuropathy; Magnetic Resonance Imaging; metabolism; Multiple Sclerosis; neural reorganization; neurotransmission; Optic Coherence Tomography; optic neuropathy; retina; retinotopy; spectroscopy.

Resumo

O conceito de reorganização neural ou "plasticidade cerebral" tem sido um dos mais deslumbrantes conceitos da Neurociência contemporânea e ainda fomenta intensos debates. A crença em uma estrutura cerebral que permanece inalterada ao longo da vida é agora obsoleta. Contudo, a compreensão dos limites e magnitude da reorganização neural e dos processos subjacentes após alterações sensoriais é ainda controversa e muitas questões permanecem por responder. Os relatos de investigação são muitas vezes contraditórios e a patofisiologia única na base de cada doença e sistema neural envolvido impede a generalização num modelo teórico comum.

Incluindo todas as estruturas desde a retina até ao córtex occipital, o sistema visual é particularmente adequado para investigar este tópico dado que a sua organização é bem conhecida e parece ser extremamente sensível a alterações na experiência visual. Alguns estudos identificaram uma associação entre perda visual e atrofia neural. Outros propuseram que áreas primárias sensoriais do córtex visual humano podem ainda manter um certo grau de plasticidade ao longo da vida e lesões claras da retina podem induzir reorganização visual cortical. Do mesmo modo, plasticidade no desenvolvimento pode co-ocorrer com patologia subtil em estádios preclínicos de degeneração da retina.

Nós questionámos como diferentes regiões visuais reorganizam após perda do principal output da retina (axónios das células ganglionares) e investigámos os mecanismos pato-fisiológicos e de "plasticidade" putativa em modelos de doença de morte de células ganglionares da retina e atrofia no nervo ótico. Evidência acumulada sugere que o dano mitocondrial contribui para a patogénese de várias doenças neurodegenerativas e que está firmemente acoplado ao défice funcional (incluindo défice visual) frequentemente reportado nestas doenças. Isto é consistente com a ideia de que as mitocôndrias são, não só as maiores fornecedoras de adenosina trifosfato, mas também participam em cascadas de morte celular. Devido às necessidades metabólicas elevadas dos tecidos neurais como a retina, nervos óticos e células cerebrais, estes são particularmente suscetíveis a um fornecimento limitado de energia resultante da disfunção mitocondrial.

Nós avaliámos o perfil retinocortical de duas mitocondriopatias relevantes, Neuropatia Ótica Hereditária de Leber e Atrofia Ótica Autossómica Dominante. Além disso, também estudamos Diabetes Mellitus tipo 1 e tipo 2 e Esclerose Múltipla com e sem episódios prévios de Nevrite Ótica nas quais défice visual é uma co-morbilidade frequente. As duas primeiras são as neuropatias óticas hereditárias mais comuns, causadas por mutações que afetam os complexos da cadeia respiratória mitocondrial e fosforilação oxidativa na mitocôndria. Apesar de não serem neuropatias óticas "clássicas", as duas últimas podem ser vistas respetivamente como modelos de doença metabólico e desmielinizante que levam ao défice visual devido à degeneração das células ganglionares e atrofia do nervo ótico. Já foi provada uma ligação forte entre a patofisiologia destas doenças e a (dis)função mitocondrial. O defeito mitocondrial leva a perfis clínicos heterogéneos e diferentes graus de severidade. Portanto o aparentemente simples conceito de "plasticidade cerebral" requer níveis de análise múltiplos (da genética ao comportamental) combinando informação clínica, estrutural (tamanho e forma), funcional (vascular e sináptica), conectividade e bioquímica.

Nós abordámos os processos de reorganização/modificação visual utilizando tomografia de coerência ótica para medir a espessura das camadas da retina, imagiologia por ressonância magnética (RM) para estudar alterações anatómicas em em mapas visuais retinotópicos definidos funcionalmente e anatomicamente e espetroscopia por MR de ^{1}H e ^{31}P para estudar o ambiente neuroquímico in vivo do córtex occipital destes doentes. Estes estudos manifestam a capacidade do córtex visual para alterar a sua estrutura, função e metabolismo em resposta à interrupção (parcial)

do input sensorial, não necessariamente de um modo negativo, mas possivelmente também para restaurar a homeostase.

Várias hipóteses podem ser formuladas incluindo uma reestruturação massiva dos circuitos visuais resultantes de conexões córtico-corticais e principalmente conexões feedforward entre o olho e o cérebro. A reorganização pode juntar alterações fenotípicas estruturais e funcionais com modulações dos sistemas patofisiológicos fisiológicos ao nível das vias de metabolismo e neurotransmissão. Estes modelos de doença realçam a importância do balanço excitatório/inibitório, o acoplamento neuroquímico e também a dependência temporal destas alterações adaptativas para a ocorrência de uma reorganização funcionalmente eficaz.

A maior parte das doenças mitocondriais e neurodegenerativas dependem de tratamentos sintomáticos e muitas vezes negligenciam o impacto precoce que a (dis)função mitocondrial e visual têm no cérebro. Nós cremos que a integração de perfis de diferentes perfis fenotípicos de modelos de doença com etiologias e (pato)fisiologias singulares e uma abordagem multimodal podem ajudar à obtenção de uma visão holística da dicotomia entre reorganização e degeneração. Isto pode abrir caminho para o desenvolvimento de novas técnicas terapêuticas e de reabilitação, com o objetivo de modular a função mitocondrial e promover plasticidade precoce antes da dominação da neurodegeneração para impedir ou atrasar a perda funcional.

Keywords:

Atrofia Autossómica Ótica Dominante; plasticidade cortical; espessura cortical; Diabetes *Mellitus*; Neuropatia Hereditária Ótica de Leber; Ressonância Magnética; metabolismo; Esclerose Múltipla; reorganização neural; neurotransmissão; Tomografia de Coerência Ótica; neuropatia ótica; retina; retinotopia; espetroscopia.

CHAPTER I

INTRODUCTION

"The brain is a tissue.

It is a complicated, intricately woven tissue, like nothing else we know of in the universe, but it is composed of cells, as any tissue is. They are, to be sure, highly specialized cells, but they function according to the laws that govern any other cells. Their electrical and chemical signals can be detected, recorded and interpreted and their chemicals can be identified; the connections that constitute the brain's woven feltwork can be mapped.

In short, the brain can be studied, just as the kidney can."

David H. Hubel

1 OUTSTANDING RESEARCH CHALLENGES IN VISUAL PLASTICITY MECHANISMS EVOKED BY INPUT DAMAGE: THE ROLE OF STRUCTURAL, NEUROCHEMICAL AND FUNCTIONAL BRAIN IMAGING

"Every man can, if he so desires, become the sculptor of his own brain."

Santiago Ramón y Cajal

Neuroscience has come a long way throughout the 20th century (Chatterjee & Coslett, 2013). There were major discoveries regarding the structure of the cellular units of the nervous system and its anatomy, architecture and function.

In the beginning of the 20th century, the brain was conventionally thought to be a fixed and immutable structure. Its tissue would be fully mature by the end of the critical period, a maturational time-window during which the nervous system of an individual is especially sensitive and adaptable to certain external stimuli. The brain would be already set with its predestined number of connections and neuronal cells along the individual's lifespan. Only during these limited temporal windows, the brain would be receptive to alterations in the external sensory input or experience processes and able to modulate its morphology and physiology (Nahmani & Turrigiano, 2014).

However with new discoveries and the close observation of several events, such as the brain response after injury, started to modify that dogma. Despite some scepticism, some studies of lesion and impairment showed that the brain, even into a small extent, is capable of intrinsically modifying itself in response to environmental changes, even in adult stages. In fact, Santiago Ramón y Cajal, Nobel Laureate of Medicine and Physiology in 1906 for the "recognition of his work on the structure of the nervous system", was one of the first neuroscientists questioning the axiom in which he also firstly believed. He considered that adult brain plasticity, as regeneration after injury was possible, but neurogenesis during the adulthood would be improbable.

Several studies have shown that the brain is capable of re-organization and several authors have already verified it in both animal and humans, through several approaches ranging from artificial (Calford et al., 2000; Darian-Smith & Gilbert, 1994; Kaas et al., 1990; Kaas, Collins, & Chino, 2006; Schmid, Panagiotaropoulos, Augath, Logothetis, & Smirnakis, 2009) to disease related (Baker, Peli, Knouf, & Kanwisher, 2005; Baseler et al., 2002; Baseler, Gouws, & Morland, 2009; Bridge, Thomas, Jbabdi, & Cowey, 2008; Gallo, Bisecco, Bonavita, & Tedeschi, 2015; Jiang et al., 2009; Lam, Kaufman, B'Ann, To, & Matsubara, 2003; Leporé et al., 2010) models of lesion. This capacity is age-dependent as proposed by Margaret Kennard in 1930-40's with her studies with monkeys (Mark, 2013). Accordingly, there is a linear negative relation between the age of the individual at the time of brain lesion, and the functional outcome (Dennis, 2010). However a number of inconsistencies in the supporting data makes the subject very controversial and a matter of intense debate (Baseler et al., 2011; Giannikopoulos & Eysel, 2006; Smirnakis et al., 2005).

Due to the development of new research and diagnostic techniques and also due to the knowledge that these brought, new questions and hypothesis can be raised. We consider here "brain plasticity" as the capability of the brain to change its connections, structure and/or function in response to demand changes with long-lasting alterations (Kolb & Whishaw, 1998; Paillard, 1976; Wandell & Smirnakis, 2009; Will, Dalrymple-Alford, Wolff, & Cassel, 2008). Nowadays there is plenty of evidence that corroborate that plasticity is a veridical phenomenon. Several studies showed that the brain is able to increase the density of cellular networks in areas related to specific high-demanding tasks and due to training, as indirectly shown in the famous study of the London taxi drivers that had higher neuronal density in posterior hippocampus highly important for spatial

representations and navigational skills (Maguire et al., 2000) and the studies of intensive long-term instrumental music training that leads to reproducible behavioural, structural, and functional changes (Herholz & Zatorre, 2012). In addition, studies show that it is possible that certain areas spontaneously get more activation in relation to others due to specific functional needs: several studies showed evidence that striate and extrastriate cortex in early-blind subjects can underlie Braille reading (Amedi, Raz, Pianka, Malach, & Zohary, 2003; R. H. Hamilton & Pascual-Leone, 1998; R. Hamilton, Keenan, Catala, & Pascual-Leone, 2000); in some cases the brain can even reorganize to compensate for injury caused by stroke (Murphy & Corbett, 2009; Teasell, Bayona, & Bitensky, 2005). Clues to identify plasticity findings can be achieved not only by simple clinical evaluation but also by histologic and imaging or neurophysiological techniques such as electrophysiology, anatomic, functional, diffusion and spectroscopy Magnetic Ressonance Imaging (MRI), positron emission tomography (PET), single-photon emission tomography (SPECT), transcranial magnetic stimulation (TMS) and other.

The research of the underlying mechanisms of reorganization or compensation and the time frame of the events that may occur in relation to disease processes may provide clues to develop new tools for therapeutic and neurorehabilitation approaches (Johansson, 2011; Schaechter, 2004).

1.1 The Visual System is especially sensitive to plasticity events

The visual system has very special characteristics. Since early times it has captured the attention of neuroscientists for its complexity. Over time it passed from a simplistic model of eyeballs connecting some obscure area in the brain, to an intermediate complexity system with several specialized cells and subtle particularities (such as the fibre crossing at the optic chiasm) to our actual view (Figure I.1). Today, the visual system comprises the eye and all the connections to the brain. There, an intricate mesh of connections in a hierarchical way, coordinate the way we see the world. Since the cortical visual pathway is composed by so many interconnected structures, why not to believe that, if one would be silenced, some other could underlie compensation for this faulty functioning?

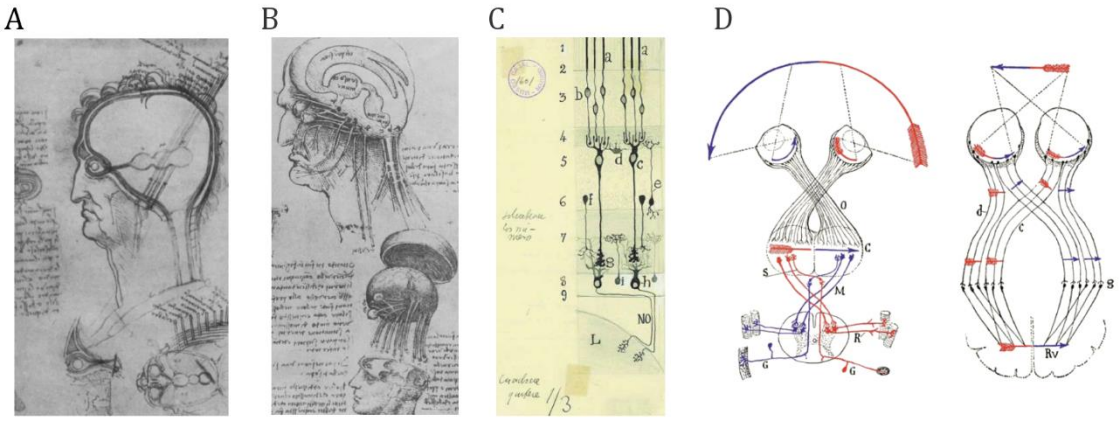

Figure I.1 Representations of sections of the visual system according to the knowledge at (**A, B**) the end of the 15th and (**C, D**) the beginning of the 20th centuries. Leonardo da Vinci drawings of (**A**) the eye and cerebral ventricles of the brain (1490) and of the (**B**) ventricles, optic chiasm, and cranial nerves (1504-1506) (Gross, 1997). Santiago Ramón y Cajal schemes of (**C**) the mammalian retina (layers 1–9), optic nerve (NO in his caption) and the central nervous system (L) and (**D**) the visual system of a (*right*) lower vertebrate and (*left*) a human with emphasis for the inversion of the arrow with the crossing of the optic nerve for the human (Llinás, 2003).

In fact, merit should be attributed to the seminal work of David H. Hubbel and Torsten N. Wiesel, Nobel Laureates of Medicine and Physiology in 1981 for their “discoveries concerning information processing in the visual system" and the pioneers on the modern study of development and plasticity of primary visual cortex (V1) (Constantine-Paton, 2008) with their discoveries on the response properties of cortical neurons their functional arrangement in cats (D. H. Hubel & Wiesel, 1962) and monkeys (D. H. Hubel & Wiesel, 1968).

In the 1960’s, Hubel and Wiesel started to study the physiology of cells in the adult cat visual cortex to understand the evolution of the specific response properties of cortical cells throughout postnatal development. More importantly, they wanted to inspect the role of visual experience in the normal development (D. H. Hubel & Wiesel, 1963; D. H. Hubel, 1982; Wiesel & Hubel, 1963a; Wiesel, 1982). This issue was for long quite intriguing. Behavioural studies showed that animals raised in a dark or stimulusless environment had high impairment of their visual functions. In their experiments, Hubel and Wiesel, induced this conditions by fusing kittens lids by suture, to be able of raising them with light but preventing any form vision (Wiesel & Hubel, 1963b). Their studies suggested that there is an early innate period of development and a later critical period of dramatic experience-dependent plasticity (D. H. Hubel & Wiesel, 1965; Wiesel & Hubel, 1965b). Interestingly, the effects of monocular closure on the visual cortex were more expressive than the ones obtained with binocular occlusion or dark raising (Wiesel & Hubel, 1965a).

Other studies showed that the removal of the primary visual cortex (the area of the cortex that receives first and processes the main visual input from the retina) of a cat did not blind it (Sprague, Levy, DiBerardino, & Berlucchi, 1977). Similar reports showed that a monkey without V1, despite being blind at first regained some visual function (Humphrey, 1974). In humans, the damage to sriate cortex V1 is devastating to all visual functions since it destroys the major source of anatomical input to extrastriate cortical areas and leads to cortical blindness. However, even in humans, some studies showed that, in some cases, when V1 is damaged some alternative pathways may strengthen or be recruited (cortical reorganization) to carry visual information from the eyes to extrastriate visual areas (Baseler, Morland, & Wandell, 1999; Bridge et al., 2010).

This topic is quite interesting in the field of Neuro-ophthalmology. The capacity of the brain to adapt and compensate for injury, especially after the critical period is crucial for the development of new and effective rehabilitation therapies. The plasticity view is gaining more consensus and this is accompanied by the new discoveries in the field. In fact, not only in the visual system, but in other nervous systems, plasticity seems to be a unique feature despite all the controversy around the topic (Huxlin, 2008). The new methodologies that have being developed allowed to reach new paradigms and study in vivo and with more precision both structure (Aguirre et al., 2016; Bence & Levelt, 2005), function (Lemos, Pereira, & Castelo-Branco, 2016) and molecular profile (Nys, Scheyltjens, & Arckens, 2015) of the plasticity potential of neural tissue.

The studies presented in this thesis were based in Magnetic Resonance Imaging methodologies. We used anatomical data to evaluate morphometric measures as cortical thickness and volume/density, functional data to define early visual areas and spectroscopic data to quantify some brain metabolites and neurotransmitters.

2 THE VISUAL CIRCUITRY

"Pictures, propagated by motion along the fibers of the optic nerves in the brain, are the cause of vision"

Isaac Newton

For a long period of time, the sense of vision was especially attributed to the eye, the major sensory organ of the human body. Nowadays, it is known that the vision, or sight, is a complex phenomenon that requires the crosstalk between the eye and the central nervous system – the visual system (Figure I.2).

In fact, humans rely more in the vision over smell or hearing, compared to many other animals, so in an evolutionary way, the humans have developed an extremely complex sight system. Interestingly, the eyes contain around 70% of the sensory receptors of the body and nearly 50% of the cerebral cortex is devoted to visual processes (Light, 2009). The visual system is a sophisticated network comprising the eye, several specialized areas of the brain and its nervous connections that receive transmit and process the visual sensory information from the environment (Kandel, Schwartz, Jessell, Siegelbaum, & Hudspeth, 2012).

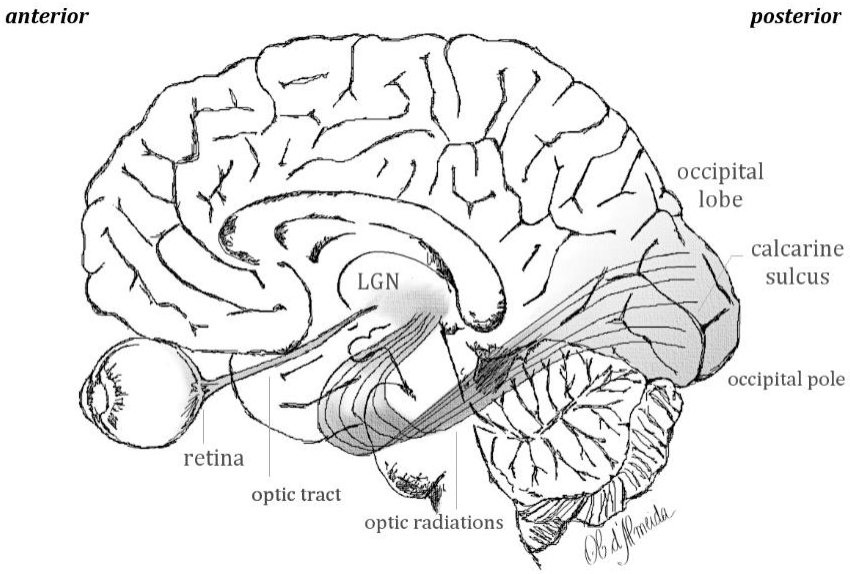

Figure I.2 Hand drawing of the main visual processing pathway from the retina till the early visual areas in the occipital lobe. LGN, Lateral geniculate nucleus.

2.1 The Process of Sight

The visual information travels within the eye in the form of electromagnetic waves (light). It enters the eye through the cornea, and it is focused when passing by the pupil. This system acts like a camera lens controlling for the amount of light entering the eye and the focal length of the image to be projected at the back of the eye – the retina (Figure I.3) (Forrester, Dick, McMenamin, Roberts, & Pearlman, 2015).

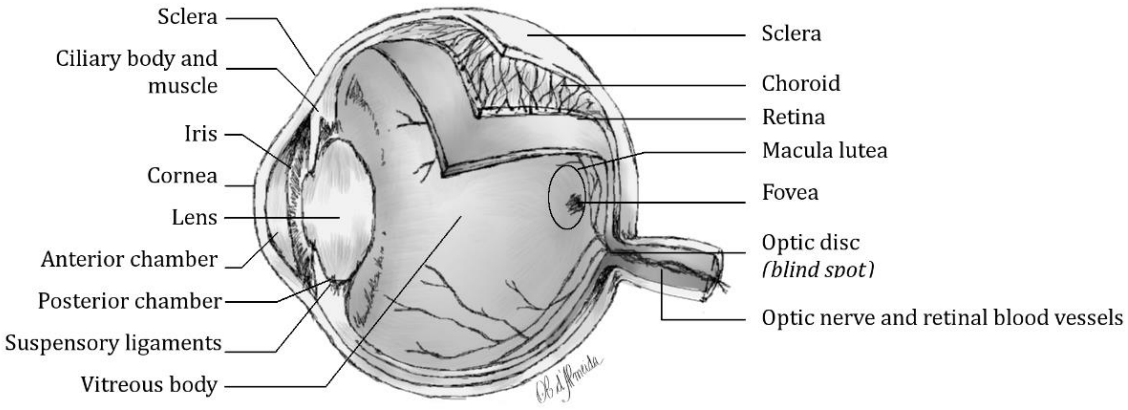

Figure I.3 Hand drawing of a sagittal view of an eye. As a camera has several components, the eye has several layers and specialized cells, and it is the first structure of the visual pathway receiving the visual information in the form of light. Three major layers compose the eye: the sclera including the cornea, maintain, protects and supports the eye; the choroid including the pupil, iris and lens, is rich in blood vessels and provides oxygen and nourishes the tissues; and the retina including cones and rods, converts the light into electric signals to form the image.

Basically, the retina is a neural structure with few hundred micrometres thick arranged in a layered layout. The first layer of the retina receiving the light (the outermost layer) is the photoreceptors layer, composed by specialized cells – rods (*scotopic* vision, or 'night' vision) and cones (*photopic* vision, 'daytime' vision) – that allow the sense of shadow/intensity, and colour, respectively. Here the light pulses are converted into neural electric impulses – *phototransduction*. Thereafter these are transmitted synaptically to bipolar cells, and then to the retinal ganglion cells (RGC) and its axons at the retinal nerve fibre layer (RNFL, the innermost layer). Together with this vertical retinal circuit, lateral retinal connections are established through horizontal and amacrine cells (in the outer and inner synaptic layer respectively). The ganglion cell axons together form the optic nerve that conducts the nervous impulses through the brain (Prasad & Galetta, 2011) (Figure I.4). One particularity of the human visual pathway is optic chiasm a X-shaped space where part of the RGCs axons from each eye converge and segregate into crossed (*decussation*) and uncrossed projections (53%:47%). This pattern is critical for binocular vision since it brings together the information from the halves of each retina that scan the same portion of the visual field (Prasad & Galetta, 2011). Therefore, each optic tract carries RGC axons and information from the ipsilateral temporal retina and the contralateral nasal retina (Figure I.4).

After passing the optic chiasm, the RGC axons of the RNFL terminate in four nuclei (Rodieck, 1979). Three are not considered part of the visual pathway – the superior colliculus (SC), the pretectum of the midbrain and the suprachiasmatic nucleus of the hypothalamus. The lateral geniculate nucleus (LGN) of the thalamus is a laminated structure with different specialized cell types where the majority of the fibres meet. The axons from the LGN cells – optic radiations – transmit a great part of information to different layers and/or sublayers of the primary visual cortex (visual area V1) or striate cortex (*Stria of Gennari*, due to its particular layered Nissl stained appearance). The striate cortex is located at the posterior part of the brain - the occipital lobe (Figure I.2) and it encloses the calcarine cortex around the calcarine fissure from the occipital pole till the lateral aspect of the caudal occipital lobe, corresponding to the anatomically defined Brodmann Area 17. Due to the decussation at the optic chiasm V1 has a full representation of the contralateral visual hemifield. V1 is involved in the initial cortical processing of all visual information necessary for visual perception.

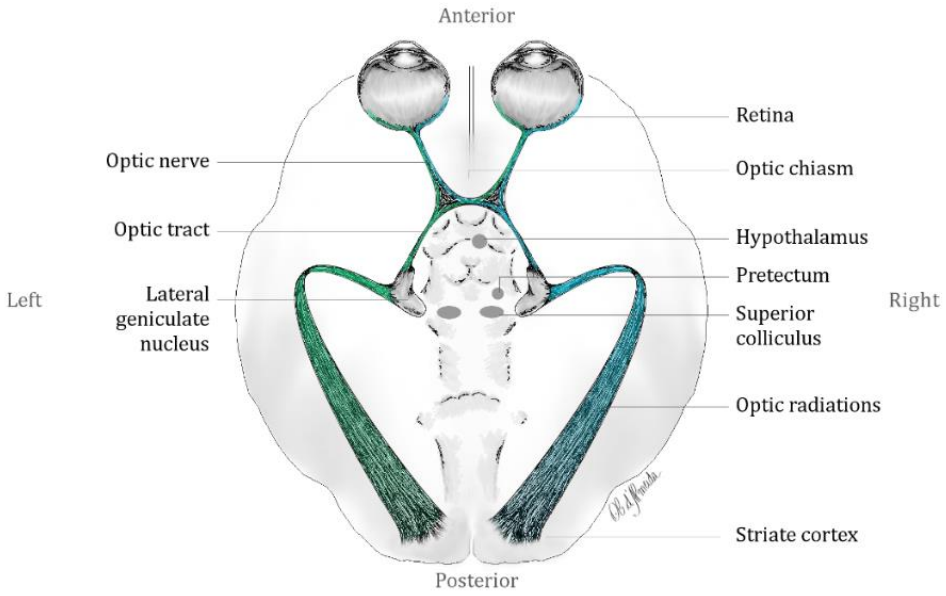

Figure I.4 The visual information flows from the retina till the lateral geniculate nucleus of the thalamus and from there to the striate cortex at the posterior part of the brain. The retinal ganglion cell axons terminate in four nuclei: the suprachiasmatic nucleus of the hypothalamus (for control of diurnal rhythms and hormonal changes); the pretectum of the midbrain (for control of the pupillary light reflex); and the superior colliculus of the midbrain (for control of eye movements) – and one important for visual perception – the lateral geniculate nucleus of the thalamus. The optic nerve crosses in the optic chiasm such as the information of the left visual field is processed by the right hemisphere (blue shade) and the right visual hemifield is processed by the left hemisphere (green shade).

In a review of the visual pathway, in 1979, Hubel and Wiesel wrote *"The lateral geniculate cells in turn send their axons directly to the primary visual cortex. From there, after several synapses, the messages are sent to a number of further destinations: neighboring cortical areas and also several targets deep in the brain. One contingent even projects back to the lateral geniculate bodies; the function of this feedback path is not known. The main point for the moment is that the primary visual cortex is in no sense the end of the visual path. It is just one stage, probably an early one in terms of the degree of abstraction of the information it handles"* (D. Hubel & Wiesel, 1979). In fact, nowadays more than twenty visual cortical areas have been studied and it is known that they follow a very precise hierarchy and are strongly interconnected (Felleman & Van Essen, 1991; Wandell, Dumoulin, & Brewer, 2007). The striate cortex projects to the extrastriate cortex, corresponding roughly to Brodmann areas 18 and 19. Functionally it has been divided into three functional areas, V2, V3, and V4. In the retina low–level visual processing refers to the contrast detection, while intermediate-level visual processing is related to the identification of contours, fields of motion, and the representation of surfaces (Kandel et al., 2012). So the retina detects brightness and colour and transmits the sensory signals to the striate visual cortex V1 that analyse orientation, direction of movement, stereoscopic depth and sends input to extrastriate cortex and to visual association cortex to "perceive" colour, shape/form, location and motion (Wandell, 1995). Thereon, high-level visual areas integrate the information from several sources to obtain "conscious" visual experience (Kandel et al., 2012).

3 WHAT WENT WRONG – DISEASE MODELS OF IMPAIRED RETINOCORTICAL PROCESSING, BASED ON GANGLION CELL DAMAGE AND MITOCHONDRIAL DYSFUNCTION

> *"De todas las reacciones posibles ante una injuria, la más hábil y económica es el silencio."*
> *(Of all the possible reactions to an insult, the most effective and efficient one is silence.)*
>
> ***Santiago Ramón y Cajal***

If developmental plasticity is nowadays commonly accepted, the capacity of the brain to regenerate upon injury or to compensate morphological-, physiological- and/or functionally is still under a highly intense debate. Several studies have attempted to dissect this subject, especially in what concerns to the cortical response upon injury and disease. The results are not always congruent and several limitations subserve the different findings. In addition, different models of disease are constrained by the different pathophysiologic systems that characterize them.

The roman philosopher Marcus Cicero once said *"The face is a picture of the mind as the eyes are its interpreter"*. Since very early, some philosophers considered the eye as a window of the soul and the later identical to the mind. Scientific evidence has proven that the eyes can be indeed considered as windows of the brain. This is not such a farfetched claim since the retina of the eye is nothing more than an extension of the Central Nervous System (CNS) both anatomically and developmentally. In fact, several recognized eye-specific pathologies share the same characteristics of other CNS diseases and vice versa. Many neurodegenerative disorders, commonly known to affect brain and spinal cord have manifestations in the eye, and several times ophthalmologic symptoms precede the CNS conventional diagnosis (London, Benhar, & Schwartz, 2013).

In this thesis four diseases were investigated: Leber Hereditary Optic Neuropathy (LHON) and Autosomal Dominant Optic Atrophy (ADOA), two of the most common genetic optic neuropathies that are typically characterized by the decrease of visual capabilities due to retinal ganglion cell degeneration and optic nerve atrophy; type 1 and type 2 Diabetes Mellitus, not a classical optic neuropathy, but with a high impact in the retina (including the inner layers) and the brain, and; Multiple Sclerosis, that is commonly associated to visual impairment due to optic nerve inflammation – optic neuritis - and consequent ganglion cell degeneration.

3.1 Mitochondrial diseases and their intriguing neural link

Mitochondria is commonly viewed as the cell's powerhouse, responsible for the predominant production of the major cellular energetic currency, adenosine triphosphate (ATP) to meet the energy requirements (R. K. Chaturvedi & Beal, 2013). The higher ATP production occurs through an electron-transport chain/oxidative phosphorylation system - the *"mitochondrial respiratory chain"* (DiMauro & Schon, 2003). In fact mitochondria are multifaceted organelles involved in the biosynthesis of a plethora of pathways ranging from the pyruvate oxidation to the tricarboxylic acid cycle (TCA) and the metabolism of aminoacids, fatty acids and steroids. In addition they help in the maintenance of calcium homeostasis and have a close connection with the cellular stress response, associated with cell death cascades as autophagy and apoptosis processes (Higgins & Coughlan, 2016).

Therefore, not confined to its own walls, the mitochondrion has massive influence in the (proper) functioning of cells and tissues modulating the organism physiology. One of the most unique properties of the mitochondrion is the fact that it possesses its own DNA, the mitochondrial DNA

(mtDNA) for RNA and protein synthesis. Since mtDNA has only 37 genes, the respiratory chain is under control of both mitochondrial and nuclear genomes (Dimauro & Schon, 2003).

However the small size of the mitochondrial genome does not lessen the impact on disease. As a matter of fact, most proteins related to mitochondrial metabolism and mtDNA maintenance are nuclear-encoded and very often mitochondrial disorders are caused by either nuclear and/or mitochondrial genome abnormalities (Taylor & Turnbull, 2005).

Despite being considered rare diseases, these are estimated to affect nearly 10 to 15 persons per 100 000 (Chinnery et al., 2000). Additionally more evidence has shown that in several neurologic disorders that do not have a classical mtDNA mutation may also involve mitochondrial dysfunction, such as in Alzheimer, Huntington and Parkinson Diseases (Rajnish K. Chaturvedi & Beal, 2013).

In this line, mitochondria have shown to play a key role in the pathophysiology of several disorders, not only the ones related to primary mutations in its own DNA, but also in considerable metabolic and neurodegenerative diseases (Nunnari & Suomalainen, 2012).

The main issue when studying mitochondrial disorders is that these present high heterogeneity of clinical features involving multiple organs, tissues and systems leading to physical, developmental, and cognitive disabilities, seizures, vision and/or hearing loss with varying severity. The diagnosis is very frequently hard to acknowledge and nowadays there isn't yet a curative treatment for these patients. The high degree of heterogeneity demands for a multimodal diagnostic approach ranging from clinical to biochemical, functional and structural criteria (Ong, 2014). In addition, it is important to get deeper insight into the pathogenesis of these disorders to develop the most adequate treatment and techniques that would prevent transmission or would allow correcting the genetic defect.

3.1.1 Genetic neuropathies: Leber Hereditary Optic Neuropathy (LHON) and Autosomal Dominant Optic Atrophy (ADOA, Kjer's disease)

Visual damage is a frequent complication appearing in around 50% of mitochondrial diseases and often is the first symptom to appear ranging from injury in the retina to the occipital cortex (Leruez et al., 2014). Within the most prevalent mitochondrial hereditary optic neuropathies are the Leber Hereditary Optic Neuropathy (LHON) and Autosomal Dominant Optic Atrophy (ADOA) that lead to bilateral central vision loss due to mitochondrial dysfunction (Carelli, Ross-Cisneros, & Sadun, 2004).

Leber Hereditary Optic Neuropathy is the most prevalent inherited optic neuropathy caused by a mtDNA mutation, necessary but not sufficient to lead to visual loss (A. A. Sadun, La Morgia, & Carelli, 2011). Interestingly several patients carrying a LHON mutation (*carriers*) may remain asymptomatic even presenting subclinical visual changes such as retinal nerve fibre layer (RNFL) thickening or subtle dyscromatopsia (Alfredo A. Sadun, Morgia, & Carelli, 2011). Some carriers can convert later on and experience severe visual loss with RNFL and optic nerve loss and thinning. Due to the maternal inheritance mode, LHON affects predominantly young adult males (C. Meyerson, Van Stavern, & McClelland, 2015). Despite the lack of reliable primary epidemiologic data it is estimated to affect around 4 per 100 000 people with the three most common point mutations, 11778G>A, 3460G>A and 14484T>C that affect the mitochondrial respiratory complex I (Gorman et al., 2015). The clinical phenotype of LHON patients is widely variable but always present visual dysfunction and sometimes neurologic defects (LHON *'plus'*). Very frequently LHON patients experience monocular painless, acute or subacute, central visual loss. Usually within weeks to months the other eye is also affected. The vision loss may occur subacutely and then stabilize or worsen with the

expansion of the scotoma (region of visual field area of lost or depressed vision) till profound blindness (Alfredo A. Sadun et al., 2011).

Autosomal Dominant Optic Atrophy (ADOA, Kjer's disease) is an autosomal mitochondriopathy since the mutated genes associated to this disorder encode proteins ubiquitously expressed and are imported into the mitochondria for inner mitochondrial inner membrane fusion (Alavi & Fuhrmann, 2013). The most common mutations occur in nuclear-encoded protein OPA1, responsible for more than half of ADOA forms. In addition to the role in mitochondrial fusion, cristae organization and mitochondrial network dynamics processes, OPA1 genes are also important for energy metabolism, control of apoptosis, calcium clearance and maintenance of mitochondrial genome integrity (G. Lenaers et al., 2012).

This neuro-ophthalmic disorder affects particularly the RGCs and leads to blindness due to progressive bilateral atrophy of optic nerve, typically starting the first decade of life (Guy Lenaers et al., 2012). The clinical phenotype of ADOA is quite heterogeneous and not all carriers present visual impairment, even though they may present some extra-ocular subclinical symptoms. However the risk for mutation carriers to develop the symptoms during lifetime is above 80% (Alavi & Fuhrmann, 2013). Characteristically ADOA patients suffer from moderate to high visual loss, associated to very low visual acuity, central or paracentral visual field deficits and dyschromatopsia (Roubertie et al., 2015). Often ADOA include neuro-sensorial symptoms and sometimes can also be syndromic and present neuro-muscular problems (ADOA *'plus'*) that are frequent in mitochondriopathies (Guy Lenaers et al., 2012). The estimated prevalence stands around 1 per 30 000 people worldwide, and 1 per 10 000 in Denmark (founder effect) (Guy Lenaers et al., 2012).

Despite the different aetiologies, LHON and ADOA are both optic neuropathies that share the same characteristic pathologic endpoint. The most intriguing fact is their particular selectivity for the retinal ganglion cell (RGC) and optic nerve degeneration that conducts the visual information from the retina to the brain (Carelli et al., 2007). It is more likely that the high energy requirements for these cells make them strongly susceptible to mitochondrial dysfunction and metabolic insult in the form of reduced ATP synthesis and/or oxidative stress and apoptosis predisposition (Cherise Meyerson, Stavern, & Collin, 2015). Studies show that not only the anterior visual pathway is affected in LHON and ADOA but also the posterior optic pathways. However there are differences in the pattern of structural abnormalities: in LHON posterior optic pathways are affected but other brain regions are spared while in ADOA the WM damage is more diffuse (Messina et al., 2016).

The main concern regarding these two mitochodriopathies is the extreme vulnerability of RGC compared to other tissues and the impact that central visual ganglion cell loss may have in posterior retinocortical pathways and cortical structures. Despite the recent advances in the study of the (patho)physiology underlying these disorders there are not yet any proven effective treatments (Nightingale, Pfeffer, Bargiela, Horvath, & Chinnery, 2016). The understanding of the impact of different patterns of visual deprivation in these conditions will allow better comprehension of the constraints that cortical reorganization patterns impose on visual rehabilitation strategies and hopefully help to optimize and develop new therapeutics.

3.1.2 Acquired neuropathy models: type 1 and type 2 Diabetes Mellitus

Diabetes Mellitus is an escalating, chronic disease estimated to affect nearly 422 million adults worldwide in 2014, compared to the 108 million estimated in 1980 (World Health Organization (WHO), 2016). It is classically characterized by abnormal increase of blood glucose (hyperglycaemia) either due to a deficient insulin (a hormone that regulates the glucose levels in the blood) production by the pancreatic β-cells (type 1 Diabetes) or by predominant insulinoresistance

(type 2 Diabetes) (American Diabetes Association, 2014). Along with severe cardiovascular, kidney and nerve complications, diabetes is one of the leading causes of blindness worldwide. The most common visual co-morbidity of diabetes is diabetic retinopathy, a condition that affects the retinal microvasculature and leads to visual loss. However there are other complications on the optic nerve induced by diabetes such as congenital bilateral optic nerve atrophy and juvenile insulin-dependent diabetes, diabetic papillopathy, anterior ischemic optic neuropathy, posterior ischemic optic neuropathy, and retrobulbar neuritis (Veselinovi & Jovanovi, 2005).

Early in the 60's, Bloodworth reported that *"Diabetic retinopathy is a complex degenerative disease of all elements of the retina, probably due to a fundamental metabolic or enzymatic defect of the cells and is not related to vascular supply (…) the emphasis placed on the undoubtedly important capillary changes is, nonetheless, too great. There is, as yet, no concrete evidence that capillary changes initiate the condition."* (Lieth, Gardner, Barber, & Antonetti, 2000). However very frequently the research on diabetes has hypothesized the vascular abnormalities as the major causative factor for changes in the neuronal function and consequently the vision loss. In fact it is more likely that visual impairment in diabetes is explained by altered neuronal function associated to damage in the neural retina and/or brain. It is clear nowadays that energy metabolism and neuronal activity are tightly coupled. This coupling is the basis for functional MRI and PET imaging that monitors changes in the blood oxygenation and flow and glucose (the main energetic fuel of the neural tissues) oxidation and consumption (Magistretti, Pellerin, Rothman, & Shulman, 1999). Additionally no solid evidence exists to state that microvascular abnormalities precedes neurodegeneration in diabetes and several studies show that neurophysiological changes may occur early after the onset of diabetes both in humans and in experimental animals, even before the occurrence of non-proliferative retinopathy. These studies encompassed several approaches ranging from pattern and multifocal electroretinography (PERG and mfERG) and psychophysical measures such as contrast or colour sensitivity to OCT thickness measures and suggest the early onset of neurodegeneration in the retina of diabetic patients (Lieth et al., 2000). Studies show that in both type 1 and type 2 diabetes, there is a decrease in retinal ganglion cell layer thickness, even with no or minimal retinopathy (Ng et al., 2016; van Dijk et al., 2010).

Regarding the more posterior part of the visual system, the brain has been a little bit neglected compared to other organs in diabetes. In fact not only the retina but also the brain has high energy requirements of the nervous cells. Therefore it is quite straightforward that metabolic disturbances may promote unbalance in the neurotransmission and energetic metabolic signalling pathways in the brain. In addition, the human brain is an especially sensitive structure to insulin, important for memory and reward systems and regulation of eating behaviour and whole body metabolism, increasing the brain susceptibility towards the diabetic status (Heni, Kullmann, Preissl, Fritsche, & Häring, 2015). Therefore, despite not being a classical "optic neuropathy", it is known that neural visual areas are particularly endangered in Diabetes Mellitus. The understanding of the ethology and pathophysiology of diabetes in the brain, the effects of medication and the coupling between neural cells may be helpful to develop more targeted therapies and to identify biomarkers to prevent the early development of the disease, especially type 2 diabetes.

3.1.3 Acquired neuropathy model: Multiple Sclerosis and Optic Neuritis

Multiple Sclerosis is a neurodegenerative disorder and the most prevalent chronic inflammatory demyelinising disorder estimated to affect around 2 million people worldwide by 2013 (Multiple Sclerosis International Federation (MSIF), 2013). The associated symptomatology is quite heterogeneous and usually starts with an acute or subacute episode of a neurologic disturbance

frequently manifested by weakness in one or more limbs, optic neuritis, between others (Inglese, 2006). Sometimes cognitive and psychological problems may also arise. The course of the disease is also very coarse and is usually characterized by defined attacks between cycles of relapses and remissions, followed by full or partial remissions as primary-progressive, relapsing-remitting, secondary progressive MS forms (Lucchinetti & Hohlfeld, 2010; Parisi et al., 2014).

Within the most frequent symptoms in MS are the visual abnormalities due to both afferent (sensory) pathway dysfunction such as visual loss and efferent (motor) visual pathway dysfunction, such as diplopia, or oscillopsia (Costello, 2016). While the efferent problems are caused by lesions in the brainstem or the cerebellum, the visual (sensory) problems are often associated to optic pathway inflammation (Pula & Kattah, 2010). When a MS patient experiments an acute event of blurred vision usually is due to optic neuritis (ON) a common manifestation of MS caused by the demyelination of the optic nerve that is the first clinically demyelinating event in MS in nearly 20% of the patients (Nolan, Narayana, Balcer, & Galetta, 2016). Usually this event only affects one eye and results in visual incapacity with reduced visual acuity and contrast sensitivity in the affected eye by a central scotoma. Usually within the next 6 to 12 months the patient can spontaneously recover its vision and is able to retain good to excellent vision more than 10 years after an attack. However structural and functional impairment of the anterior visual system persist and 35% of ON patients experience recurrences especially more frequent and severe in patients with MS (The Optic Neuritis Study Group, 2004). The visual system may be compromised at any anatomical site from the retinal layers till the occipital visual cortex. Usually, OCT segmentation procedures show ganglion cell layer and retinal nerve fiber layer thinning in all MS subtypes (Saidha et al., 2011). This retinal layer thinning may occur even without any episode of optic neuritis. One very interesting question that remains is the clinical–paraclinical paradox that occurs in MS patients that experience ON. How can these patients recover from visual impairment and even maintain a normal clinical function after such injury? The existence of a critical threshold for fibre loss or compensatory changes at the striate and extrastriate cortical visual areas represent two strong hypotheses (Gallo et al., 2015).

In fact, despite being commonly labelled as a WM disease several studies have already shown that GM structures are also heavily affected as widespread neuronal and axonal loss (Friese, 2016; Pirko, Lucchinetti, Sriram, & Bakshi, 2007) and not only GM dysfunction sometimes precede the WM dysfunction but also can be a major determinant of long-term outcomes and disease burden in MS (Chard & Miller, 2009; Geurts, Calabrese, Fisher, & Rudick, 2012). These neuronal problems affect the clinical, cognitive and motor functions of the patients. Several hypotheses have been formulated to explain the causes of the pathogenesis of MS such as meningeal inflammation, selective neuronal vulnerability, dysregulation of growth factors, glutamate excitotoxicity, mitochondrial deregulation and abnormalities, and the “use-it-and-lose-it” principle (Geurts & Barkhof, 2008). However, the grey matter and vascular pathology have for long been neglected. More recently several studies have focused more and more to aim these aspects of the MS disease (Filippi et al., 2012). In fact with the disease course and aging, the body’s capacity to repair myelin diminishes. Therefore further efforts have to be made to recover neurological damage and stop the progression of the disease before the establishment and appearance of permanent lesions. The study of the pathophysiology of MS lies in the study of preclinical models of disease and patients using advanced molecular, metabolic, anatomical and functional imaging techniques. From bench to clinic, translational and multimodal imaging will allow to test new drugs and stage the disease course to improve disease management (Ciccarelli et al., 2014).

4 FUNDAMENTAL PRINCIPLES OF MAGNETIC RESONANCE IMAGING FOR THE ASSESSMENT OF BRAIN STRUCTURE, FUNCTION, METABOLISM AND NEUROTRANSMISSION

> *"...the single most critical piece of equipment is still the researcher's own brain.*
> *All the equipment in the world will not help us if we do not know how to use it properly, which requires more than just knowing how to operate it.*
> *Aristotle would not necessarily have been more profound had he owned a laptop and known how to program.*
> *What is badly needed now, with all these scanners whirring away, is an understanding of exactly what we are observing, and seeing, and measuring, and wondering about."*
>
> ***Endel Tulving***

In the beginning of the 20th century the development of a new technique revolutionized the Medicine concerning disease detection, diagnosis, and treatment monitoring: Nuclear Magnetic Resonance (NMR). However due to the World War II, and the negative connotation given to the word "nuclear", its name changed to what we commonly call Magnetic Resonance Imaging (MRI). This non-invasive, sophisticated technique allows obtaining detailed, high resolution, 3D images of the body, without the use of ionizing radiation and allows measuring quantitative data, rather than single qualitative, subjective information.

Basically it relies on the physical properties of the nuclei that constitute our body when submitted to changes in the electromagnetic field, namely the hydrogen nuclei. The different acquisition and processing methodologies allow collecting different measures from the signals obtained with MRI (Figure I.5). This is possible due to differences in tissue composition, macro-structural (shape and size) and micro-structural (cellular constituents and its structure) parameters as well as metabolic and physiologic functions (like mitochondrial, metabolic and vascular features) (Chard & Miller, 2009).

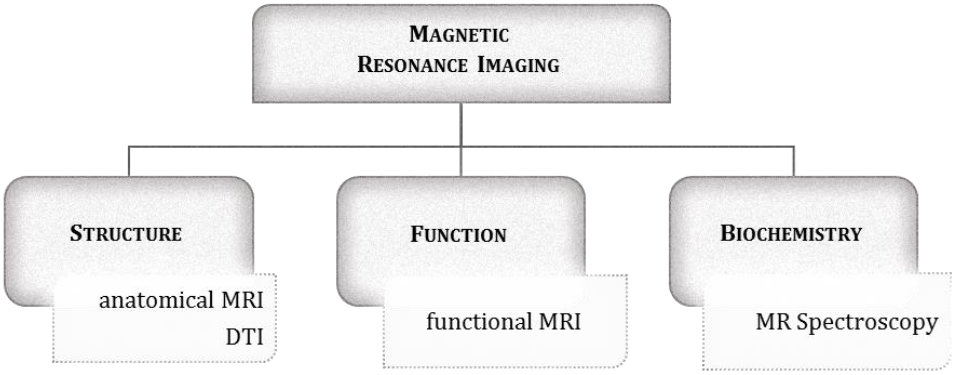

Figure I.5 Diagram of the main MRI techniques used to assess structure (anatomical MRI and diffusion tensor imaging (DTI)), function (functional MRI) and biochemistry (MR spectroscopy).

4.1 How does MRI work – the underlying physics

The fact that basic MRI is based on the behaviour of hydrogen nuclei under electromagnetic field changes makes it particularly well suited to study soft tissues as the brain. In addition, the differences in water content among tissues and organs, and the different water composition in damaged tissues resulting from pathologic processes results in differences in MR images contrast.

Water constitutes about two thirds of the human body weight which means that a large number of the atoms inside the human body are hydrogen atoms.

Several study books (eg. Brown & Semelka, 2003; Horowitz, 1995; Lipton, 2008) and reviews (eg. Jacobs, Ibrahim, & Ouwerkerk, 2007; Pooley, 2005) approach the physics and principles underlying MR imaging technique. To cut the long story short:

An atom is composed of a nucleus surrounded by an electronic shell. The nucleus of each hydrogen atom is built of positively-charged protons that possess random spin movement around its axis (Figure I.6 A). The spinning movement creates its own tiny magnetic field (magnetic moment), giving the proton its own north and south poles, acting as microscopic compass needles. According to the Faraday's Law of Induction (electromagnetic induction), the movement of an electric charge induces an electric current and consequently it creates its own tiny magnetic field.

In a resting state, the protons spin randomly (Figure I.6 B). MRI systems/scanners employ powerful superconductive magnets, which produce a strong magnetic field (B_0, main magnetic field) inside the bore. Inside it the magnetic field B_0 forces protons to align in the same (parallel) or opposite (anti-parallel) direction of that field (Figure I.6 C). These two possible directions are associated to different energy states. Since the lowest energy state is parallel alignment, this is the preferred state and only a minority of protons are aligned anti-parallel to the main magnetic field direction (Pooley, 2005).

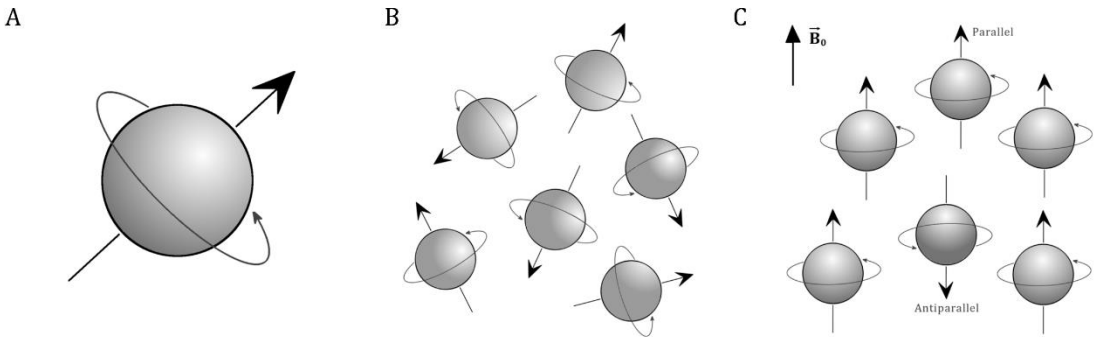

Figure I.6 Representation of the proton spin movement and the effect of a strong magnetic field. (**A**) A proton rotates/spins around its axis creating its own small magnetic field. (**B**) In a basal state, the protons spin in random directions. (**C**) When under a strong magnetic field, the protons align parallel/anti-parallel to this main magnetic field.

In addition, protons not only spin around its axis, but also perform a "wobbling" movement – precession. Therefore there will be forces pointing in opposite directions in the XY plane that will also cancel out. In the z direction (main magnetic field direction) the components will add up (Figure I.7 A). Altogether the aligned spins will constitute a net magnetization (M_z) – *longitudinal magnetization* – that precess circularly around the z-axis with a frequency proportional to the main magnetic field strength. This relation is given by the *Larmor equation* (the proportionality constant is called *gyromagnetic* ratio, γ) (Figure I.7 B, Equation I.1). The stronger the magnetic field B_0 strength, the higher the *precession frequency*, ω_0.

A

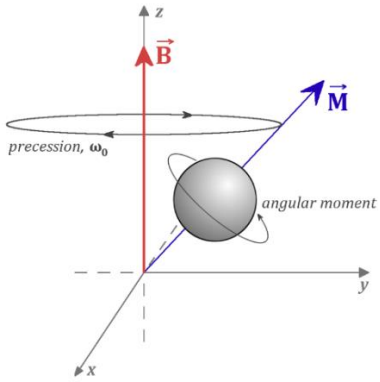

B

$$\omega_0 = \gamma B_0$$

Larmor Equation

(Equation I.1)

Figure I.7 Representation of the net proton magnetization. (**A**) The alignment of the spins will produce a net magnetization precessing around the z-axis (direction of the main magnetic field). (**B**) The angular frequency of precession, ω_0, is proportional to the main magnetic field strength, B_0 and is given by the Larmor equation (**Equation I.1**). The proportion constant, γ, will be dependent on the nucleus (42.58 MHz/T for hydrogen atom).

Representing the protons' moment as vectors in a coordinate system it's clear that vectors "pointing" in opposite directions will cancel out the respective magnetic effects. This is true for both parallel/antiparallel components in the z-direction (Figure I.8 A), and also for the transversal component of the vectors (XY plane, Figure I.8 B). In equilibrium, the net magnetization will be along the z-axis (Figure I.8 C). Since the net magnetization lies in the direction of B_0, no signal can be measured. The magnetization needs to be taken from the equilibrium state.

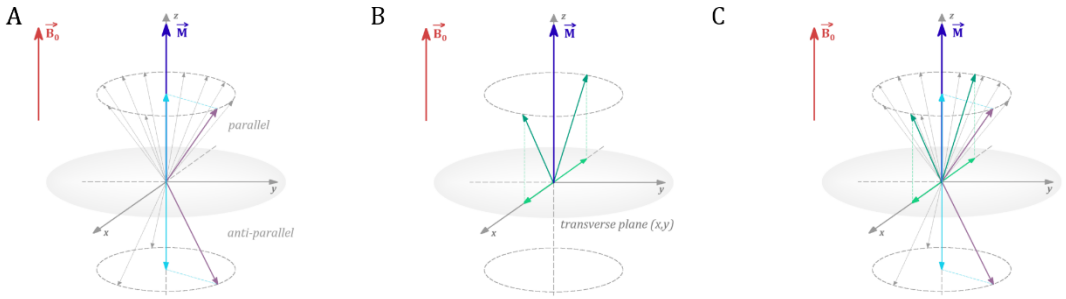

Figure I.8 Vectorial representation of the net proton magnetization. The net magnetic force of the protons (sum of dark green and purple vectors) is represented as a vector. This is formed by two components, one along the z-axis and other along the transverse plane (x,y). (**A**) The parallel and anti-parallel protons along the z-axis will cancel out the magnetic effects of each other (light blue vectors). However only a very small fraction of protons are anti-parallel. The ones that do not cancel out will add up. This magnetization lies longitudinal to the main external magnetic field direction – *longitudinal magnetization*. (**B**) The components on the transverse plane (light green vectors) cancel out with each other. (**C**) Thus, in the reality, the alignment of the spins will produce a net magnetization (dark blue vector) precessing around the z-axis (direction of the main magnetic field).

If a short burst of radiofrequency waves (RF pulse), matching the precession frequency, is sent in a specific alpha angle, the protons will be disturbed and spin out of equilibrium, and change their orientation according to the RF pulse angle – *resonance* – going from a lower to a higher energy state. Beyond re-orienting the net magnetization, the RF pulse aligns the protons in the transversal (XY plane) direction that become "in phase" – *transversal magnetization*. The longitudinal magnetization decreases while the transversal magnetization increases.

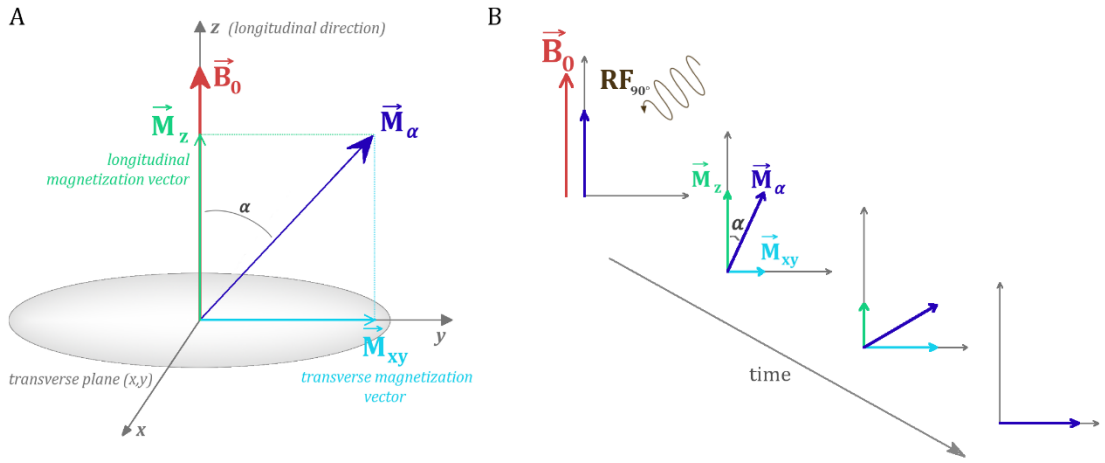

Figure I.9 Vectorial representation of the net proton magnetization when a 90° radiofrequency (RF) pulse is applied. (**A**) The net magnetization has two components: the longitudinal magnetization component lies parallel to the main magnetic field B_0 (M_z) and the transversal magnetization component that is perpendicular to B_0 (M_{xy}). (**B**) When a 90° RF is applied, the net magnetization rotates towards the transverse plane: M_z decreases and M_{xy} increases.

When the RF pulse is switched off, the whole system recovers to the original state – *relaxation*. The transversal magnetizations starts to disappear while the longitudinal magnetization increases back to the original size – *transversal* and *longitudinal magnetization*, respectively (Figure I.9).

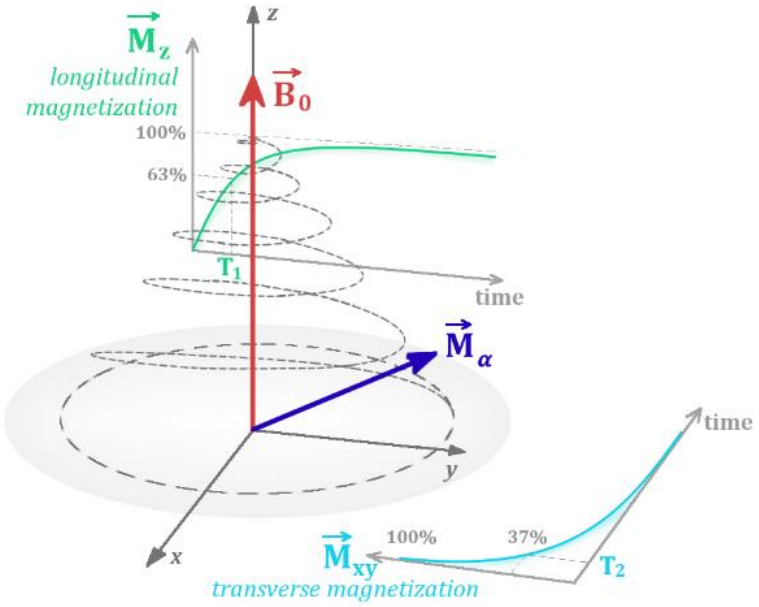

Figure I.10 Vectorial representation of the net proton magnetization after the RF pulse is switched off.

The relaxation process is then composed by two independent events occurring simultaneously (Figure I.10):

- Protons return to their lowest state of energy (aligned to the main magnetic field) releasing energy to the surroundings – T1-relaxation, *recovery*. The time constant T1 is a characteristic parameter of a tissue, depends in B_0 strength and is related to the rate of regrowth of the longitudinal magnetization. It is defined as the time interval for 63% recovery of longitudinal magnetization of M_z assuming a 90° RF pulse. T1 is related to *spin-lattice* interactions.

- Protons also lose phase coherence (in the transverse plane) – T2-relaxation, *dephasing*. During the RF pulse the protons precess "*in phase*". Ideally, the MR scanner field would be homogeneous. However it is not totally uniform. Also each proton that have its own tiny magnetic field influences and is influenced by the surrounding protons small magnetic fields. Consequently, the precession frequencies will be slightly different. So when the RP pulse stops, the protons become out of phase in the transversal plane. The dephasing leads to the cancelling of the transversal magnetic moments, decreasing the transversal magnetization. To account for the inherent inhomogeneity of the magnetic field and the susceptibility effects of the object scanned T2 is commonly called T2* (T2 star) decay or T2* relaxation. The time constant T2 refers to the time interval for 37% loss of original transverse magnetization of M_z after applying a 90° RF pulse. T2 is particularly related to *spin-spin* interactions.

By the Faraday's law of induction, the transverse components of Mz induce an electrical current in the receiver coil/antenna due to the change of the magnetic moment. So the application of the RF pulse generates an immediate electromagnetic signal, a sine wave oscillating at the Larmor frequency – *FID signal* or *Free Induction Decay* – that rapidly decreases due to T2* effects (Figure I.11).

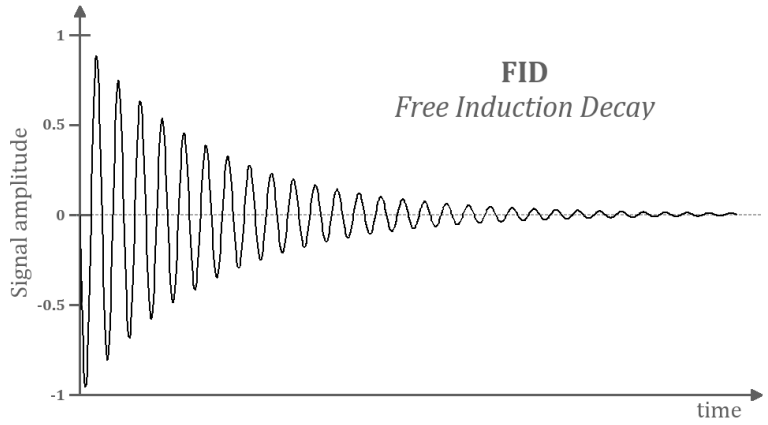

Figure I.11 Representation of the electromagnetic signal received in the coil after the RF pulse. This short-lived sinusoidal signal is called *Free Induction Decay* (FID).

To allow localization, three magnetic field gradients are applied in the 3 main axes, x, y and z. These gradients are basically conducting loops of wire or thin conductive sheets on a cylindrical shell like coils inside the bore (Figure I.12 A). When the current passes through them, a secondary magnetic field is created (Lauterbur, 1973). Therefore they produce calibrated distortions of the main magnetic field in the 3 main directions changing the frequency point-by-point – *spatial encoding*. The raw data is mapped on the so-called *k-space* (Figure I.12 B). The contrast resolution of the image is set by the low spatial frequencies encoded in the centre of the k-space. The details and edges are coded by the high frequency frequencies encoded in the periphery of the k-space. However, the k-space is only understandable after applying the *Fast Fourier Transform* (FFT) translated the time-domain acquired data into reconstructed 3D images. Therefore each pixel of the MRI image is a weighted combination of all the data enclosed in the k-space and each point of k-space encodes for spatial information of the whole MRI image (Zhuo & Gullapalli, 2006).

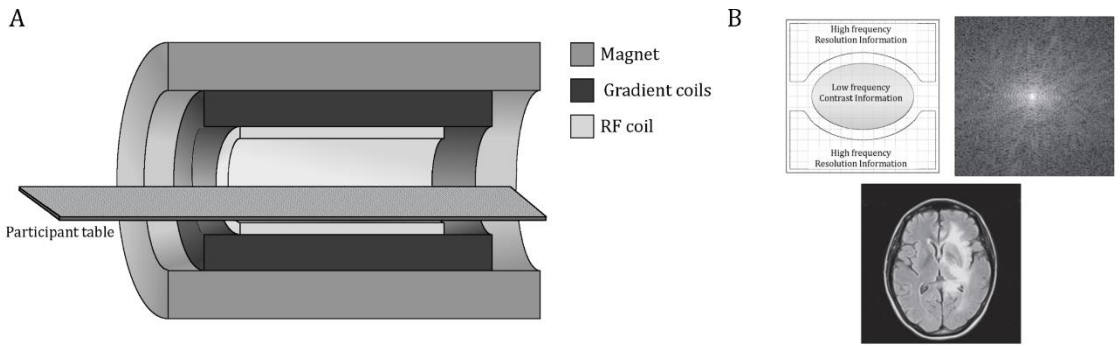

Figure I.12 MRI system. In (**A**) there are represented the three main components of an MR scanner: the magnet that creates a constant magnetic field, B_0; the gradient coils, by providing linear gradations of the magnetic field, allow to perform the spatial encoding of the MR signal and the RF coil that allows the transmission of the RF pulse and the acquisition of the signal after spin relaxation. The raw data is enclosed in the (**B**) k-space that contains the phase (y-dimension) and frequency (x-dimension) direction. By applying the FFT we may achieve the MRI image (**B**, low panel) (**B** is *adapted from* (Zhuo & Gullapalli, 2006)). The image information is predominantly confined in the centre of the k-space, as low spatial frequency information and related to the general shape and image contrast. In contrast, the periphery of the k-space is associated to high spatial frequency information, related to image details, such as edges and spatial resolution.

4.2 Structural neuroimaging (of the brain)

Structural MRI allows to collect qualitative and quantitative information regarding morphometry (size and shape) and integrity of grey and white matter in the brain. The difference between various types of tissues is based on their internal magnetic field variations. The time it takes for the protons to realign with the magnetic field (Figure I.13 A,B), as well as the amount of energy released is a characteristic of a tissue and it depends on the environment and the chemical nature of the molecules.

The time that the net magnetization takes to realign after the RF pulse stops is different from tissue to tissue. The approach used to get different contrasts in a MRI image will rely on the RF pulse and especially in the relaxation times of each tissue (Figure I.13 C,D), namely T1 and T2 constants (Jacobs et al., 2007). Therefore, manipulating the pulse sequence parameters is possible to obtain images with different contrasts for the different tissues (Figure I.13 E,F). Therefore, different tissues have different T1 and T2 constants. In addition, exploring the pulse sequence parameters (the specific number, strength and timing for the application of the RF and gradient pulses) it is possible not only to discriminate between different tissues but also emphasize different aspects of normal and abnormal brain tissue. For example, tissues with high water content (eg. in several pathologic conditions), have long T1 and T2. Applying different pulses with different time intervals – *pulse sequences* – it is possible to discriminate different tissues. This issue is not in the scope of the thesis and therefore will not be developed in here. The most commonly used are T1-weighted images, more suited for anatomic detail (they emphasize the contrast between grey and white matter and fat) and T2-weighted images for detection of pathological alterations (optimally show fluid and abnormalities) (Figure I.13 E,F). These two types of images provide complementary information being both important for abnormalities characterization.

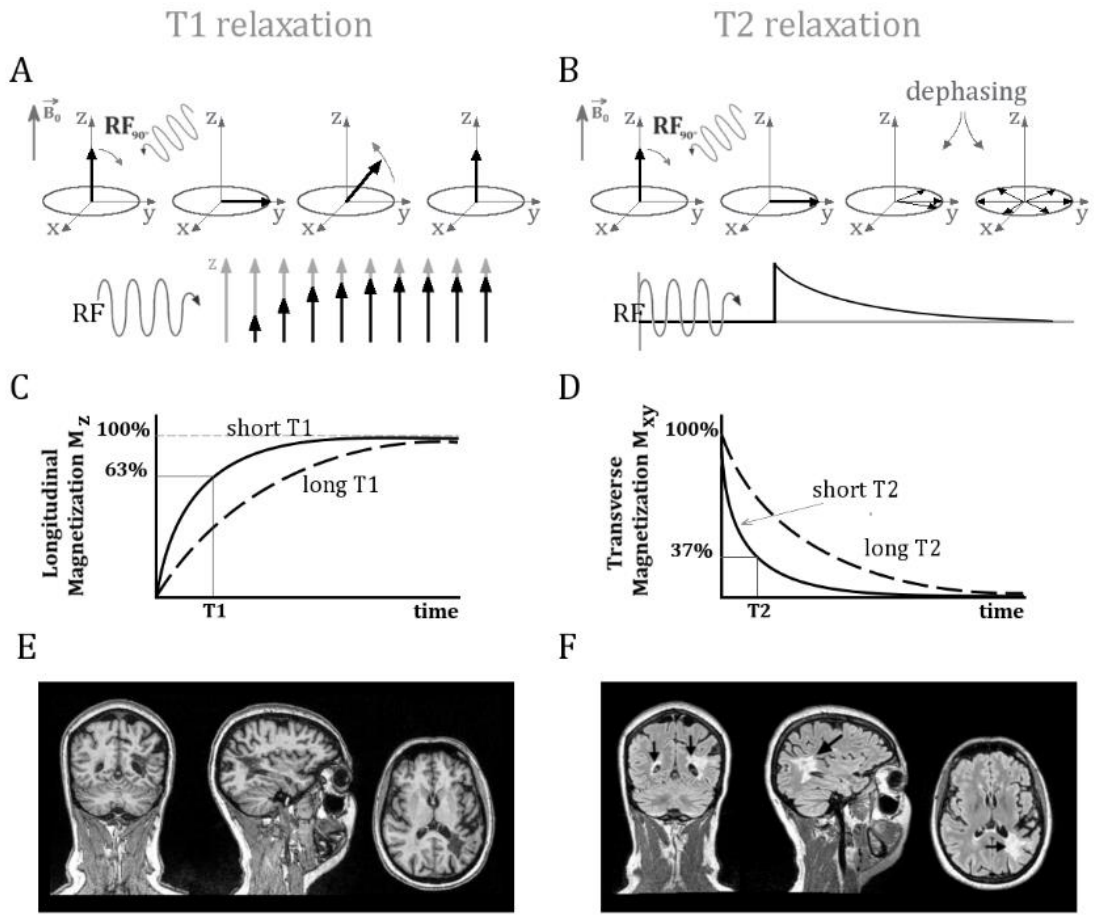

Figure I.13 Schematic representations of the T1 (left panel) and T2 (right panel) relaxation processes occurring during an MRI experiment. When a RF pulse is applied to the system (aligned to the main magnetic field B0) at the Larmor frequency of the precessing spin (in this case the hydrogen) the net magnetization rotates in the angle defined by the RF pulse. When the pulse is switched off it (**A**) tilts towards the main magnetic field direction again, increasing the longitudinal magnetization. By contrast, (**B**) transversal magnetization starts to disappear due to the loss of phase coherence. The time constant (**C**) T1 is the time it takes for the longitudinal component to reach 63% of its final value is characteristic of the tissue. The disappearance of the transverse magnetization component is characterized by the (**D**) transverse relaxation time (spin-spin relaxation time) or T2 which is also characteristic of a tissue and reflects the time it takes for the transverse magnetization to decrease to 37% of its starting value. Playing with these time constants and the pulse sequences it is possible to obtain images more (**E**) "*T1-weighted*" or (**F**) "*T2-weighted*". The different types of images give different contrasts between tissues. The images below are a coronal, sagittal and horizontal planes of the brain of a Multiple Sclerosis patient. In (**E**) the sequence used was a *3D Magnetization-Prepared RApid Gradient-Echo* (MPRAGE), more T1-weighted and in (**F**) a *Fluid-Attenuated Inversion Recovery* (FLAIR) sequence, a special T2-weighted sequence that nulls signal from CSF (in a regular T2-weighted image CSF appears bright, white matter dark grey and grey matter light grey). Notice the good contrast provided by MPRAGE between grey matter (dark grey) and the white matter (light grey) whereas CSF is devoid of signal (black). FLAIR reveals a wide range of lesions, including cortical, periventricular, and meningeal diseases that can be difficult to see on more conventional images (arrows). These two complementary images provide important information about tissue integrity and characterization of abnormalities.

4.3 Functional neuroimaging

> *"During an MRI experiment with an anesthetized mouse, I saw most of the dark lines disappear when the breathing air was switched to pure O2 in order to rescue the mouse as it appeared to start choking. This observation rang a bell."*
>
> ***Seiji Ogawa***

Structural MRI has proven to be a very powerful technique, allowing to study with high spatial resolution the static morphology of tissues, from muscle to brain. At the beginning, the best option to assess some functional parameters was low spatial resolution and invasive method, positron emission tomography (PET), through the injection of radioactive tracers (Chou, 2008).

In 1990's, Ogawa and colleagues developed a new technique based on MRI principles, called functional magnetic resonance imaging (fMRI) (Ogawa, Lee, Kay, & Tank, 1990). Nowadays it is widely used both in clinical and research domains to probe brain function.

The key is that neurons do not have internal reserves of energy in the form of glucose and oxygen, so their firing demands for immediate energy to be brought in quickly. This energy supply comes from blood cells through a process called the haemodynamic response.

The main markers of changes on brain activity are enhanced blood flow, glucose consumption and oxygen consumption (J. C. Siero, Bhogal, & Jansma, 2013; Uludağ, Dubowitz, & Buxton, 2005). Since the 19th century that is known that there is an automatic mechanism by which the blood supply of any part of the cerebral tissue varies according to the activity and chemical changes which underlie the functional action of that part – the neurovascular coupling.

fMRI technique relies essentially on the so-called BOLD – *Blood Oxygenation Level Dependent* – effect (Figure I.14), related to the different magnetic properties of the oxygenated (oxyHb) and deoxygenated (deoxyHb) haemoglobin of the blood cells (Ferris et al., 2006; Ogawa et al., 1990; J. C. W. Siero, Bhogal, & Jansma, 2013). Basically, when a specific population of neurons in a certain region is activated (increases its neural activity), there is an initial drop in oxyHb and an increase of CO2 in the surrounding capillaries due to oxygen consumption. In 2 to 6 seconds, there's an influx of regional blood to increase the levels of oxyHb (decreasing deoxyHb levels). Then the levels of oxyHb drop and deoxyHb increase again. The large rebound in the relative ratios between oxy- and deoxy-haemoglobin during the tissue activation are the fundament of fMRI image formation (Heeger & Ress, 2002). In fact, oxyHb is weakly diamagnetic, while deoxyHb is paramagnetic, inducing an inhomogeneity in the magnetic field translated in changes on the T2 signal, so-called T2*-weighting. The distortion of the magnetic field, promotes the local dephasing of protons and reduces the signal. Consequently, a decrease on the concentration of deoxyHb relative to oxyHb is associated to an increase in image intensity, while an increase on the concentration of deoxyHb is related with a decrease in the intensity of the image (Figure I.14, *below*).

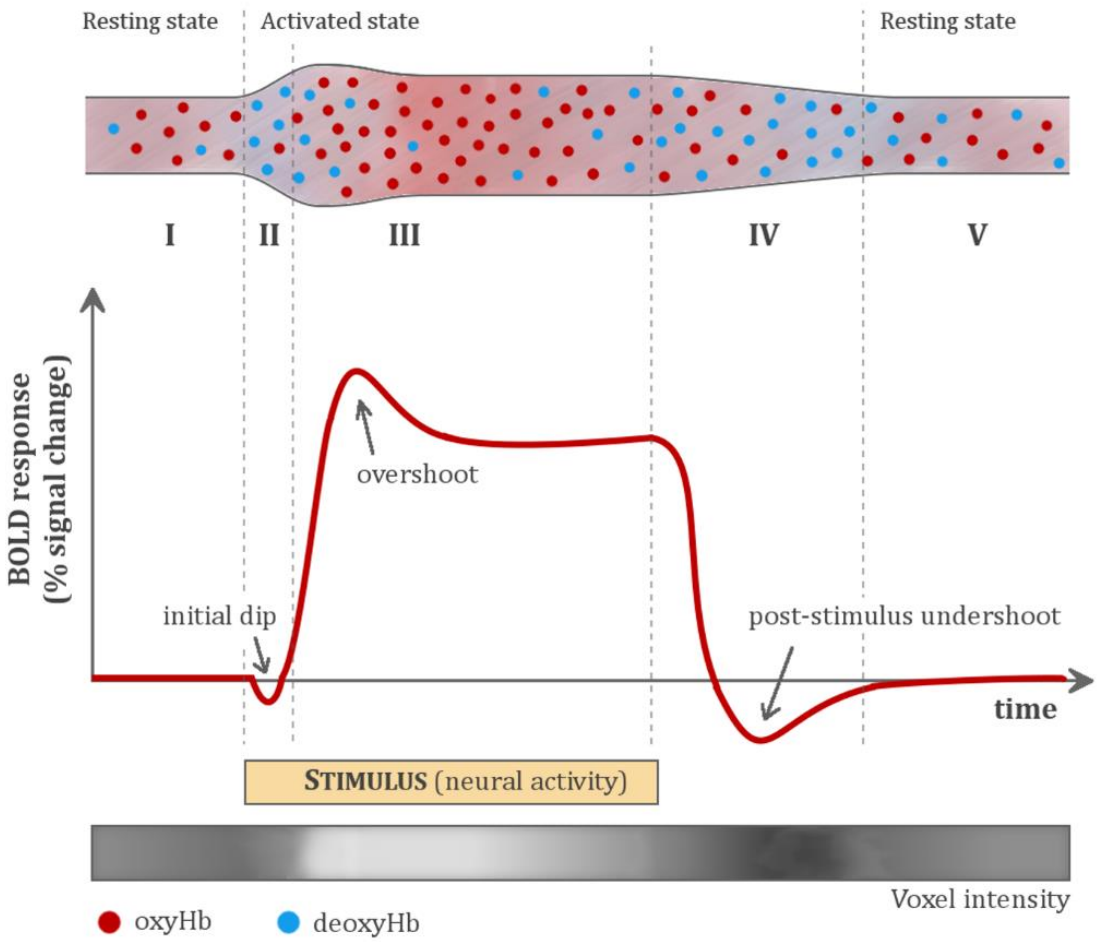

Figure I.14 Diagram of the basic principles underlying the functional MRI technique – the Blood Oxygenated-level dependent, BOLD signal. The fMRI signal reflect the presence of small changes in the homogeneity in the magnetic field due to changes in local blood oxygenation (T2* signal). The image basic units, the voxel, encloses thousands of neurons. (**I**) When a group of neurons that were in a resting state start firing, (**II**) the oxygen demands increase and there is an increase of O_2 consumption. Consequently the levels of deoxyhaemoglobin (deoxyHb) increase and the BOLD signal decreases. Then (**III**) there is a large increase of the signal due to a local increase of the blood flow to supply more O_2 for energetic demands. Therefore the levels of oxyHb relative to deoxyHb increase. Due to the differences in the magnetic properties of oxyHb (weakly diamagnetic, so it has little effect in the local magnetic field) and deoxyHb (paramagnetic - adds an inhomogeneity to local magnetic field), the T2* signal increases – increase of BOLD signal. After the decrease of the blood flow, and the (**IV**) oxyHb (after the oversupply of O_2), (**V**) the signal returns slowly to the baseline. This event is translated into a function – the *haemodynamic response function* (HRF) when stimulus duration is very short (impulse response function). The changes in the magnetization can be translated into variations of voxel intensities throughout time.

4.3.1 Localizing early visual areas - The retinotopy

> *"Only those regional differentiations of the cortical structure had been taken into account, which are apparent in the laminar organization of a cross-sectioned gyrus, in the positioning, size, packing density and distribution of cells, that is, in the cytoarchitectonic differences. Histological differences sensu strictu, that is, details of single cells, appearance of fibrils and tigroid substance as well as details of the structure of cell nuclei, etc., are not used topographically."*
>
> ***Korbinian Brodmann***

Korbinian Brodmann in 1909, published a cytoarchitectonic map of the brain dividing the cerebral cortex into 43 areas (Brodmann, 1909). Brodmann's criteria integrated cell body-stained histological information with structural–functional correlations (K. Zilles & Amunts, 2010). In his work he postulated that each cytoarchitectonic area (Brodmann area, BA) is specifically responsible for a particular function. In fact, at the time, the primary visual area V1 was one of the few cortical areas that could be tested for this claim since it is the first cortical visual area receiving the massive input from the retina creating a neuronal representation of the whole visual field. Brodmann divided the visual (occipital) cortex into three cytoarchitectonic areas, striate BA17, and extrastriate BA18 and BA19.

Recently, new methods allowed to demonstrate that Brodmann's representation of the tri-partition of the occipital cortex into BA17, BA18 and BA19 is a rough representation, with high inter-variability and especially concerning to the extrastriate areas (Amunts, Malikovic, Mohlberg, Schormann, & Zilles, 2000). Moreover these new methodologies showed that instead of three visual areas, there are several dozens of specialized areas in the visual cortex (Karl Zilles & Amunts, 2010). The primary visual area closely overlaps to BA17 and V2 may roughly correspond to BA18. Nevertheless, BA19 and even BA18 should be subdivided into several specific higher visual areas (Amunts et al., 2000).

One of the most singular properties of the visual system is its retinotopic configuration. The 'image' projected from the retina to the LGN, and from the latter to striate and extrastriate cortex have a topographical correspondence. This means that adjacent areas in the retina are projected in adjacent areas in the LGN and thereon in cortical striate V1 and extrastriate V2, V3 and V4 (Figure I. 15 D). Sereno, in 1995 postulated that, using the adequate visual stimuli for fMRI (Engel et al., 1994, Figure I.15 A,B), these cortical visual areas could be defined (Sereno et al., 1995). Not only the mapping from in the retina remains topographic but also within the early visual areas (V1 to V4) retain its topography in a *mirrowed/non-mirrowed* configuration (Figure I.15 C) allowing the computation of *visual field sign maps* (VFS, Sereno, McDonald, & Allman, 1994).

Studies show that there is still an high degree of overlap cytoarchitectonic maps of striate and extrastriate visual areas with functionally-defined visual areas (Wilms et al., 2010; Wohlschläger et al., 2005). However, fMRI-based retinotopic mapping has quickly increased interest over the structural definition as the best noninvasive tool to define the borders of early visual areas (e.g. Wandell & Winawer, 2010). This is due to the fact that a precise delineation allows the establishment of intersubject and interspecies comparisons (Van Essen & Glasser, 2014; Van Essen et al., 2001), better understanding of the functional architecture of visual system in humans (Felleman & Van Essen, 1991; Tootell, Dale, Sereno, & Malach, 1996; Tyler et al., 2005; Van Essen & Dierker, 2007), both in health (Tootell, Hadjikhani, Mendola, Marrett, & Dale, 1998) and disease (Bridge, 2011), quantification of variables as the magnification factor (Duncan & Boynton, 2003)or

the receptive field size and number, and even for source localization in EEG/MEG imaging (Im, Gururajan, Zhang, Chen, & He, 2007). With more sensitivity and specificity, retinotopy allows retrieving more detailed information about visual cortical responses both in health (e.g. Dougherty, Koch, Brewer, Modersitzki, & Wandell, 2003; Rees, Kreiman, & Koch, 2002; Souza & Lee, 2011) and disease (e.g. Baseler et al., 2002, 2009; Duncan, Sample, Weinreb, Bowd, & Zangwill, 2007; Morland, Baseler, Hoffmann, Sharpe, & Wandell, 2001; Olsen et al., 2009).

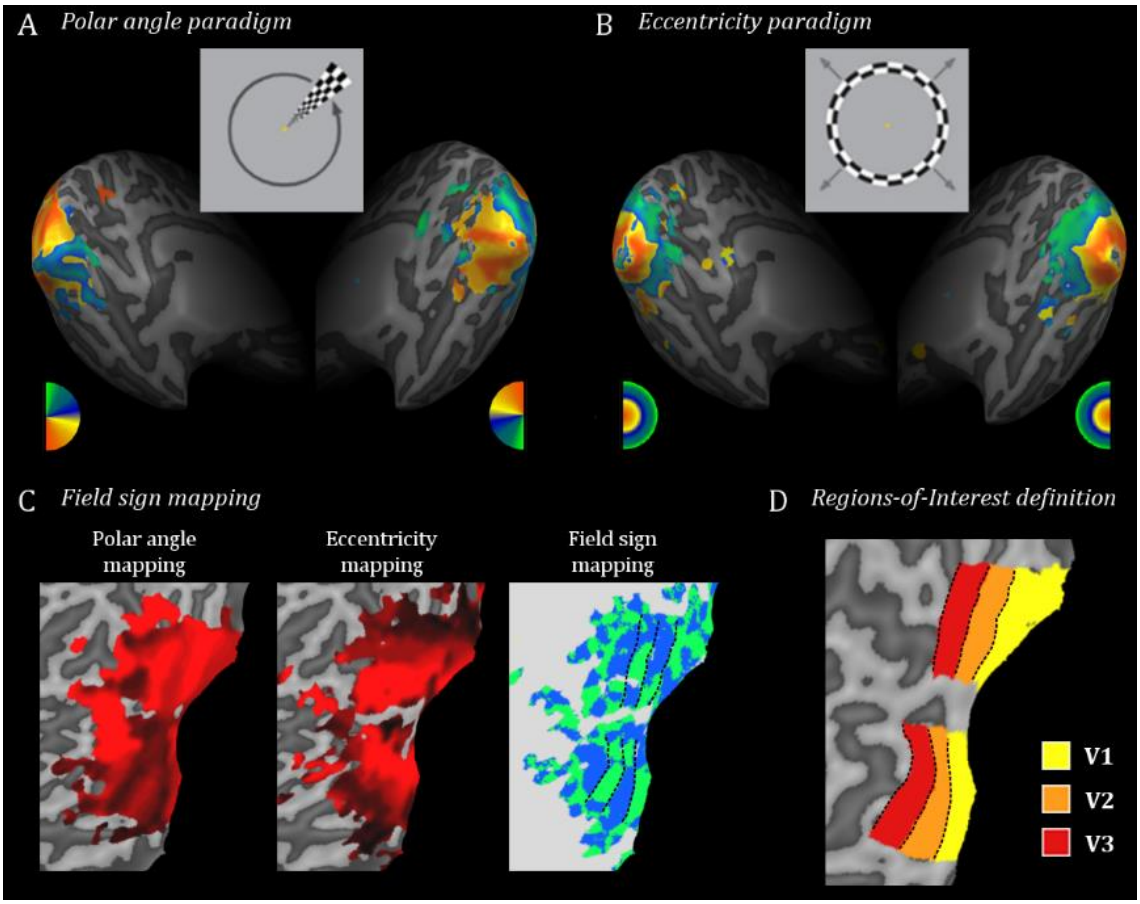

Figure I.15 Cortical Retinotopy as measured by fMRI assesses the correspondence of the topographic projections from the retina to the lateral geniculate nucleus (LGN) layers and from the LGN layers to striate visual area V1 and extrastriate areas V2 and V3 in the cortex. Adjacent areas alternate with a mirror and nonmirror representation of the visual field, corresponding to the horizontal and vertical meridians. So, using adequate visual stimuli fMRI: (**A**) polar angle paradigm – a flickering checkered wedge rotates around the central fixation point (on top of **A**), mapping the angular position regarding the centre of the gaze; and (**B**) eccentricity paradigm – a flickering checkered ring that expands (on top of **B**), mapping the position from posterior to anterior cortex as the stimuli move from centre (fovea) to periphery of the visual field. Using a pseudo-color map overlaid on 3D meshes, early visual areas may be visualized and defined. Both paradigms are "phase encoding" experiments: the result of the continuous repetition of the stimulation and the specific position stimulated corresponds to a relative time point (phase) within one cycle. To further improve the definition of the borders between visual areas (**C**) field sign maps may be computed. These are based on the computation of local gradients - the horizontal and vertical meridians are detectable at locations where the gradients maximally change their direction. Combining the information of the gradients of both polar angle and eccentricity maps it is possible to compute a map that assigns the "*mirror*" (green) or "*non-mirror*" (blue) configuration of an early-visual area. The delineation of the resulting boundaries between early visual areas allows the (**D**) definition of regions-of-interest (ROI) for analysis.

4.4 Neurospectroscopy

> *"Ultimately, biological phenomena involve molecules,*
> *and understanding them involves understanding the underlying chemistry.*
> *In my opinion, this is a particularly exciting area of chemistry. "*
>
> ***Venkatraman Ramakrishnan***

Nuclear Magnetic Resonance Spectroscopy (NMR) was introduced at the end of the 50's as a *"revolutionizing technique in organic chemistry"* (Mountford, Stanwell, Lin, Ramadan, & Ross, 2010). Magnetic Resonance Spectroscopy (MRS) is an application of NMR that acts as an in vivo biopsy of biological tissues. Through the estimation of basal levels of several metabolites it allows to infer about cellular viability, energetics and signalling.

The spectrometer for *in vivo* analysis is the MR scanner that allows not only the acquisition of anatomical images, but also the estimation of metabolites levels or even their distribution within the tissue under investigation (Magnetic Resonance Spectroscopy Imaging, MRSI).

The main difference between MRI and MRS outputs relays on the pulse sequences used for data acquisition. Retrieving the Larmor Equation (Equation I.1), there's a linear relationship between the external magnetic field B_0 influencing the nuclei, and its resonance frequency, ω. The constant, the gyromagnetic ratio γ, is nucleus-specific.

However, a nucleus is frequently part of a chemical compound. Therefore the neighbouring microenvironment promotes an electronic shielding effect on the local magnetic field B_0. This causes a slight difference in the experienced magnetic field, changing the frequency of the nucleus. This frequency difference – *chemical shift* – is the basis for MRS experiment and it gives information about the molecular group carrying the nucleus-of-interest (Drost, Riddle, & Clarke, 2002).

By convention, to make the chemical shift position independent from the field strength, a normalization is performed, expressed in parts per million (ppm), as stated in the Equation I.2:

$$\delta = \frac{\omega - \omega_{ref}}{\omega_{ref}} \times 10^6 \qquad \text{(Equation I.2)}$$

where δ is the chemical shift (in ppm) and ω and ω_{ref} are the frequencies of the compound under investigation and a reference compound, respectively. The reference compounds most widely accepted are tetramethylsilane (TMS) for 1H-NMR and ^{13}C-NMR of compounds in organic solvents and 2,2-dimethyl-2-silapentane-5-sulfonate (DSS) or 3-(trimethylsilyl) propionate (TSP) for aqueous solutions. However, since none of these compounds is found *in vivo* other resonances are commonly used as an internal reference for in vivo MRS. Usually for ^{1}H-MRS of the brain it is used the methyl resonance of N-acetyl aspartate (2.01 ppm) and for ^{31}P-MRS of brain and muscle, the phosphocreatine resonance (0.00 ppm) (R. A. De Graaf, 2007).

The electronic shielding surrounding the nucleus of interest that causes the chemical shift relies not only on the internal chemical bonding but also in chemical binding in the molecule that disturbs the spin system. These electronic interactions are called *J-coupling* and are the cause of the splitting of individual resonances into characteristic multiplets (Stagg & Rothman, 2014).

The resultant signal of a MRS experiment is a function of time with exponentially decreasing high-frequency oscillation – the *free induction decay* (FID, Figure I.11). By applying a *Fast Fourier Transform* (FFT) it is possible to obtain a frequency spectrum plotting of the signal intensity (vertical axis) with the relative frequency shift (horizontal axis) or chemical shift, in ppm, to become independent from the magnetic field strength (Figure I.16). The MRS signal is basically a sum of sine

waves of different unique resonance frequencies (peaks), amplitudes, phases, spin-couplings and relaxation properties (Gallagher, Nemeth, & Hacein-Bey, 2008; Ross & Bluml, 2001). Through signal decomposition, relative levels of each metabolite can be calculated as the area under the curve (peak integral). This is possible since the specific nuclei in a metabolite are associated to a single peak or multiple peaks whose positions in the spectrum are unique and dependent on the chemical shift (Figure I.16).

Usually the signal amplitudes of the spectral peaks are closely proportional to the abundance of the resonating nucleus allowing the estimation of metabolites concentration. However, the analyses are often performed as metabolites ratios between different peaks. Absolute concentrations may be estimated using additional measurements like water quantification (Danielsen & Henriksen, 1994) considering it nearly stable or by using phantoms as reference (Stephan Ulmer, Backens, & Ahlhelm, 2015; M. van der Graaf, 2010).

Very often the molecule has more than one resonating nucleus, and therefore multiple peaks may be observed in the spectra which helps to boost the accuracy of quantification. The MRS spectra is a combination of unique spectral patterns that act as a fingerprint. Thus, to disentangle and identify the individual metabolites the analysis requires to have *a priori* knowledge of the specific chemical/spectral pattern of each potential molecule by experimental MRS acquisition of metabolite solutions or in-silico numerical simulations based on physical and chemical characteristics of the substances (Figure I.16).

A

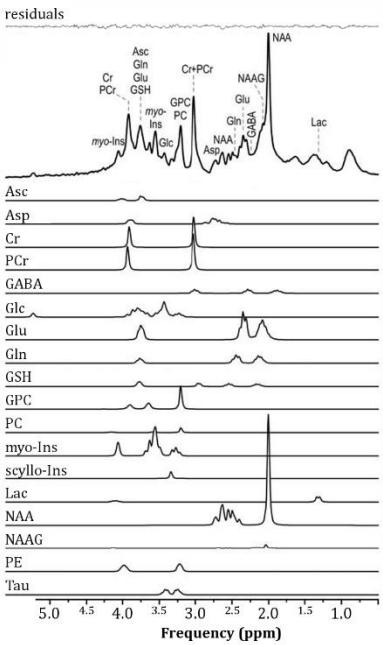

B

Peak #	Name	Freq (ppm)
1	Cr/PCr	3.954
2	Gln/Glu	3.790
3	mI	3.665
4	Tau	3.571
5	GPC/PC/Cho	3.235
6	Cr/PCr	3.045
7	Gln	2.373
8	Glu	2.283
9	NAA	2.026
10	Lac	1.313
11	Lipid	0.872

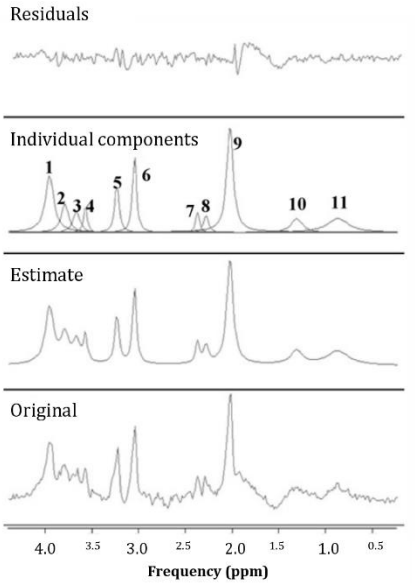

Figure I.16 Schemes of two different post-processing analysis tools of ^{1}H-MRS spectra. In (**A**) LCModel software was used to separate and quantify the components of an ^{1}H-MRS spectrum of a voxel in the occipital lobe of a control participant of the study of Mangia et al., 2013 (*Adapted from* (Mangia et al., 2013)). In (**B**) one represents the quantification procedure of ^{1}H-MRS data using the AMARES quantification algorithm with the jMRI processing package (*Adapted from* (Pravat K Mandal, 2011)). Despite the differences in the methodologic analysis both algorithms show the signal decomposition into the several components (metabolite peaks). Basically, the spectra consist of a scaled sum of spectral patterns from individual metabolites. The spectra are plotted as frequencies (horizontal axis), in ppm, as a function of signal intensity (vertical axis), where the signal intensities are approximately proportional to the metabolites concentrations. The frequencies (ppm) are characteristic of substances due to the different chemical environments surrounding the protons of each molecule. Asc, *ascorbate;* Asp, *aspartate;* Cho, *choline;* Cr, *creatine;* Freq, *frequency;* GABA, *γ-aminobutyric acid;* Glc, *glycine;* Gln, *glutamine;* Glu, *glutamate;* GPC, *glycerophosphocholine;* GSH, *glutathione;* Lac, *lactate;* myo-Ins, mI, *myo-inositol;* NAA, *N-acetylaspartate;* NAAG, *N-acetylaspartylglutamate;* PC, *phosphocholine;* PCr, *phosphocreatine;* PE, *phosphoethanolamine;* ppm, *parts-per-million;* syllo-Ins, *scyllo-inositol;* Tau, *taurine.*

Usually the MRS experiment begins with the acquisition of an anatomic image to define the volume-of-interest within which the MRS data will be collected. Then spectra may be acquired using different techniques. We may divide them into *single-voxel* (SVS) and *multi-voxel* (MVS) spectroscopy (both with short and long echo times).

The major difference is that in SVS the spectroscopy voxel is previously selected, combining slice-selective pulses in 3D space (Bertholdo, Watcharakorn, & Castillo, 2013). The intersection of the three orthogonal planes forms the volume-of-interest (VOI, Figure I.17 A). There are two major sequences for ^{1}H-MRS acquisition: the *Point RESolved Spectroscopy* (PRESS, Figure I.17 B) and the *Stimulated Echo Acquisition Mode* (STEAM, not presented). These two differ on the combination of pulses used (90°-180°-180° and 90°-90°-90°, respectively), applied simultaneously to different field gradients. The signal is restricted to the VOI using *spoiler gradients* that dephase the nuclei outside the VOI reducing this signal. Due to the longer length of the 180° pulses, PRESS takes higher TEs compared to STEAM. In addition, PRESS sequence may present higher chemical-shift displacement artefact and the 90° pulses give more precise localization. However PRESS gives almost two-fold SNR than STEAM (Bertholdo et al., 2013).

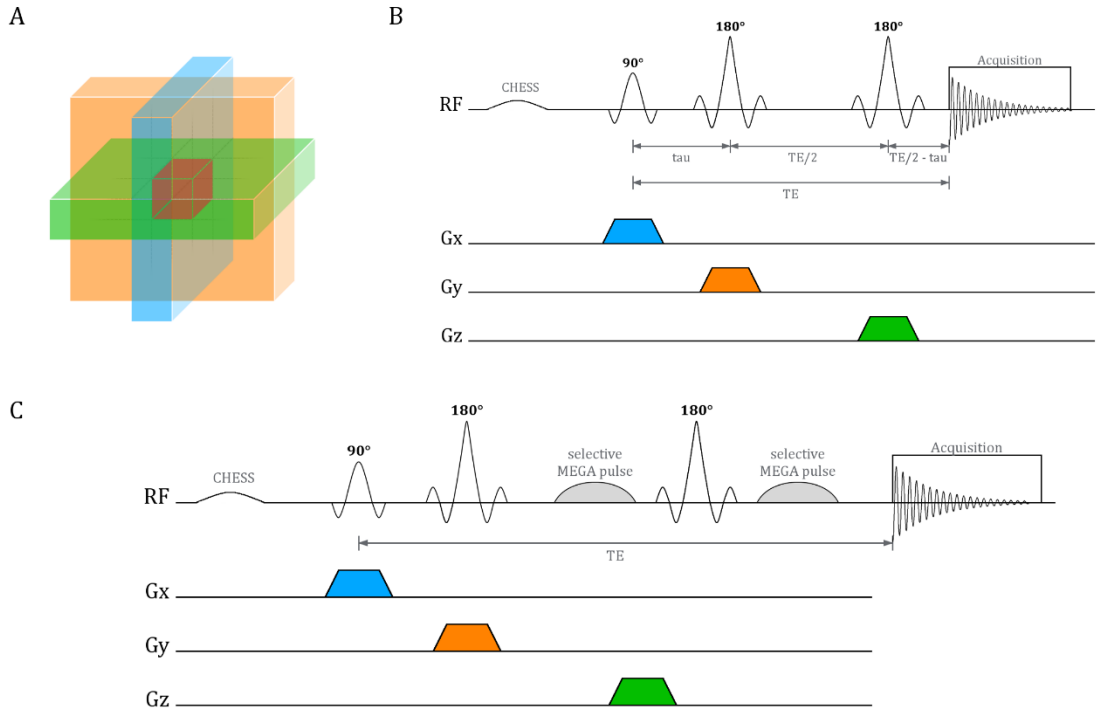

Figure I. 17 Schematic diagrams of (**A**) slice selection method and (**B**) PRESS and (**C**) MEGAPRESS acquisition schemes with CHEmical-Shift-Selective (CHESS) pulse for water suppression. (**A**) Three slice-selective RF pulses in the direction of the three main axis are used to define the ROI in a 90°-180°-180° scheme. (**B**) PRESS sequence.

Magnetic Resonance Spectroscopy Imaging (MRSI) is also called *Chemical Shift Imaging* (CSI) and is a multivoxel acquisition technique. The main goal of CSI is to acquire several voxels in a bigger ROI within a single sequence, allowing to inspect the spatial distribution of the metabolites. Therefore, there are needed phase-encoding gradients (in 2- or 3-dimensions) after the application of RF pulses and the gradient of slice selection to allow the encoding of spatial information (besides the spoiler gradients). The same sequences used for SVS may be applied in multivoxel imaging. The result of MRSI is a matrix of spectra (2D results into a grid corresponding to the field-of-view (FOV) and in 3D results into a volume of grids within one FOV). Usually CSI acquisition takes longer than SVS since

the number of voxels is proportional to the number of phase-encoding steps and to the spatial resolution (Bertholdo et al., 2013). The fact that the FOV is rectangular and gets unwanted signals from outside the brain, especially lipids of the subcutaneous fat, some techniques are used to optimize the FOV, namely the *Outer Volume Suppression* (OVS). Several advantages and disadvantages of both single- and multi-voxel techniques must be taken into account depending the experiment purpose. SVS usually gives high-quality spectrum in a shorter scanning time and have a good field homogeneity resulting in a precise quantification of metabolites. However, due to T2 relaxation, the sequences cannot hold very long TEs. MRSI can give information regarding spatial distribution of metabolites, and the grid allows the repositioning of voxels during the post-processing steps. Nonetheless due to voxel bleeding (voxel contamination from outside signals as a partial volume effect) the quantification may not be as accurate as with SVS (Bertholdo et al., 2013).

4.4.1 Optimization issues - Shimming

One of the major difficulties when performing a MRS acquisition is to have a good SNR. This is important to be able to discriminate the real MRS signal from the background noise and define and quantify each peak-of-interest.

Ideally a MRI magnet would have a perfectly homogeneous magnetic field. However several constraints, electrical and mechanical, as well as variables in the manufacturing process and surrounding structures cause some inhomogeneities in the main magnetic field. Even with perfect design and manufacturing, the placing of an object inside the bore creates local susceptibility effects that changes the main field (Jacobs et al., 2007; Lipton & Kanal, 2008).

During the MRI experiment, to perform the spatial encoding, gradients are used to change the local magnetic field (thus the Larmor frequency of the nuclei). Then the FFT maps the different frequencies (raw data in the k-space) to the spatial location of the spins. If the frequency shift occurs due to a non-homogeneous magnetic field, it results in a distortion on the image. In MRS experiments this is critical for reliable metabolite quantification because the homogeneity of the field determines the spectral resolution.

One technique used to prevent magnetic susceptibility artefacts and overcome this issue is to perform the shimming. The shim coils may be passive or active. The passive shimming is usually configured during magnet installation and consists in affixing pieces of sheet metal or ferromagnetic pellets at specific locations at the outer surface of the scanner. The active shimming consists in producing electric currents that can be adjusted to fine-tune the magnetic field homogeneity using specifically designed coils (Jacobs et al., 2007). By adjusting the homogeneity of the static main magnetic field B0 this method allows the improvement of the quality of the spectra.

4.4.2 The spectrum: what are we measuring?

Magnetic Resonance Spectroscopy (MRS) allows to assess in vivo metabolites levels and distribution in regions-of-interest that are linked to metabolic and physiologic processes of the organism, using suitable equipped MRI scanners and sequence protocols.

Several nuclei can be used in MRS, like hydrogen/proton (^{1}H), phosphorus (^{31}P), carbon (^{13}C), fluorine (^{19}F) and sodium (^{23}Na) (Table I.1). Basically each nuclei that possess spin values of ½ (that makes them little magnets) can be used in MRS experiments. Distinct advantages make the proton the preferential nuclei used for MRS acquisitions in research and particularly in clinical environments (Lin et al., 2012). Most of scanners allow the acquisition of ^{1}H-MRS spectra, due to its technical feasibility and ease of hardware configuration: it uses the standard RF coils and do not

require any extra hardware from the basic coil. Also it is the most sensitive stable nucleus, has a high natural abundance and a high sensitivity (Table I.1). Other nuclei require dedicated coils, tuned to their specific Larmor frequencies and sometimes the infusion of enriched substrates due to its low natural abundance as in ^{13}C-MRS. Also the ^{31}P-MRS does not need the administration of tracers or enriched substrates. Usually, ^{31}P-MRS experiments are performed by utilizing the *Nuclear Overhauser effect* by taking advantage of the higher gyromagnetic ratio of the proton – proton-decoupled ^{31}P-MRS (P. K. Mandal, 2012).

One of the major issues of 1H-MRS is probably the large signal coming from the water molecules that exceeds and overlaps the relatively small metabolites signals. Therefore, several water suppression methods have been developed to overcome this issue (R. A. De Graaf, 2007) such as the *CHEmical Shift Selective* (CHESS) *water suppression* technique (Haase, Frahm, Hänicke, & Matthaei, 1985). Sometimes an additional spectrum without water suppression is acquired to perform line-shape and eddy current corrections and also for quantification purposes (Kreis, 2004).

Table I.1 NMR properties of the most commonly used nuclei for in vivo Magnetic Resonance Spectroscopy Imaging (*Adapted from* de Graaf, 2007; Ulmer, Backens, & Ahlhelm, 2015).

	Spin	**γ (MHz/T)**	**ω_0 at 3T (MHz)**	**Relative Sensitivity (Nucleus)**	**Natural Abundance (%)**	**Concentration *in vivo* (mmol/L)**	**Relative signal *in vivo***
^{1}H (water)	1/2	42.58	127.7	1	99.98	100 000	100
^{1}H (metabolites)	1/2	42.58	127.7	1	99.98	10	0.01
^{31}P	1/2	17.23	51.7	0.066	100	10	0.0007
^{23}Na	3/2	11.26	33.8	0.093	100	50	0.005
^{19}F	1/2	40.05	120.2	0.830	100	<1	<0.001
^{13}C	1/2	10.71	32.1	0.017	1.1	50	0.00001

Three major peaks characterize a ^{1}H-MRS spectrum: the N-acetylaspartate (NAA, ~2.0 ppm), creatine/phosphocreatine (Cr/PCr, ~3.0 ppm) and the choline (Cho, ~3.2 ppm) peaks (Hajek & Dezortova, 2008). However, from 1.5T up, the spectral quality of the ^{1}H-MRS often allows the identification and quantification of lactate, myo-inositol, glutamate, γ-aminobutyric acid (GABA), and lipids. The appearance of these signals are quite influenced by choice of echo time (TE) in particular the lactate signal.

Briefly, NAA is the most prominent signal in ^{1}H-MRS spectra of the human brain (CH3 group resonating at 2 ppm). Despite the debate around its exact role in the nervous system (Moffett, Ross, Arun, Madhavarao, & Namboodiri, 2007), due to its preferential location on the neuronal mitochondria, frequently is used as a neuronal marker proven to be related to neuronal death and/or mitochondrial dysfunction, decreased O_2 consumption and ATP production. Creatine, usually together with PCr, are commonly considered markers of energy metabolism as quick energetic supplies for the biological processes. Their peaks are easily noticeable in both ^{1}H-MRS and ^{31}P-MRS. The signal of Cr/PCr signal dominates in ^{31}P-MRS of the brain and muscle. The signal of Cho of ^{1}H-MRS is used as a marker of membrane status since it incorporates precursors or degradation products of the membrane phospholipids such as phosphocholine (PCho) and glycerophosphocholine (GPC), free cholines, citidine diphosphate choline, acetylcholine, betaine and others. The neurotransmitters glutamate and GABA are usually associated to the excitatory/inhibitory balance of neural cells and allow to assess synaptic activity and plasticity events. Glutamate and glutamine changes have been associated with 'profound metabolic defects' and/or neurotransmission unbalance and GABA is the major inhibitory neurotransmitter of the CNS. Glu and Gln are two relatively abundant amino acids in the human brain that coexist in a highly

dynamic and balanced cycling (Ramadan, Lin, & Stanwell, 2013). The striking structural similarity within the human brain makes their peaks often difficult to resolve. Usually at 3T and above fields, spectra have enough resolution to resolve Glu and Gln. However, to overcome this issue, they are usually referred as a pool named Glx (Glu+Gln). Due to the low concentration of GABA signals from more abundant metabolites often overlap (GABA signals are overlapped by more intense signals arising from NAA at 2.0 ppm, Cr at 3.0 ppm and glutamate (Glu) and glutamine (Gln) at 2.3 ppm. Therefore a recent spectral editing method has been developed (Mullins et al., 2014; Puts & Edden, 2012) - *MEshcher–GArwood Point RESolved Spectroscopy*, MEGAPRESS (Figure 17, 18).

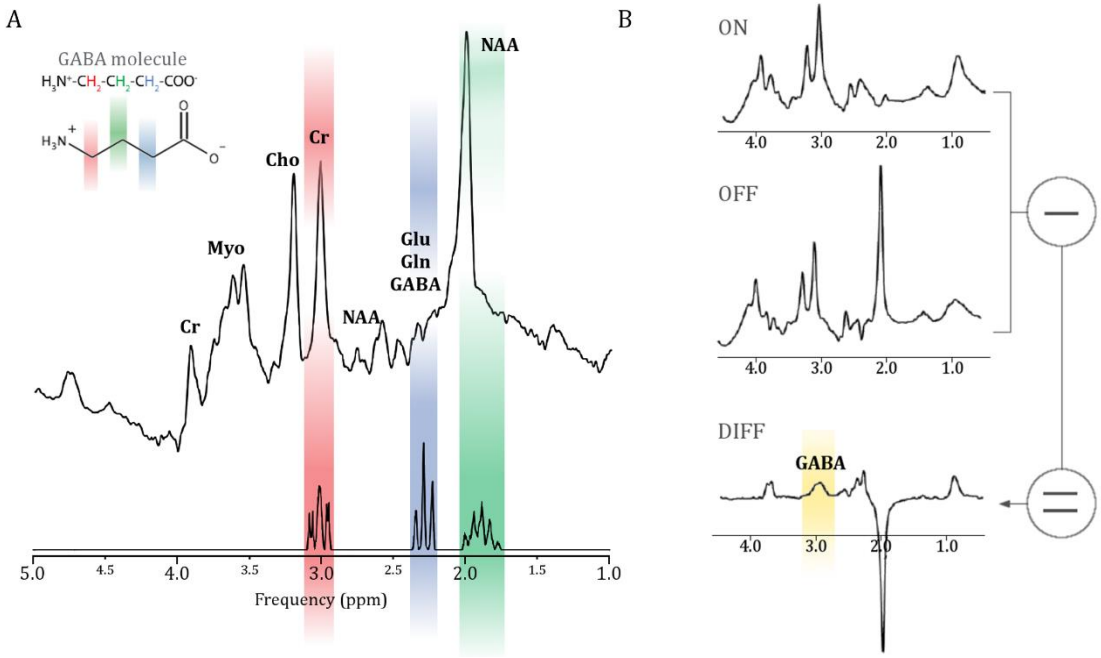

Figure I.18 MRS spectra of γ-aminobutyric acid (GABA). In (**A**) it is represented the spectrum of a 3T 1H-MRS experiment in a human brain. Colour bars show the simulated peak positions of the protons of the GABA molecule (*top left corner*), that are masked in a regular PRESS sequence [*Adapted from* (Puts & Edden, 2012). MEGAPRESS, a GABA-editing sequence was developed to assess GABA levels more accurately. **(B)** By applying editing pulses at 1.9 ppm (ON pulse), GABA signals are modulated, while most of signals are unaffected. Subtracting the ON and OFF (without the editing pulse) scans, the creatine signals overlaying GABA at 3.0 ppm are removed and revealing the GABA signal in the difference edited spectrum (DIFF) [*Adapted from* (Mullins et al., 2014)]. Cho*, choline;* Cr*, creatine;* Gln*, glutamine;* Glu*, glutamate;* myo*, myo-inositol;* NAA*, N-acetylaspartate;* ppm*, parts-per-million.*

The metabolites assessed by ^{31}P-MRS have also a high clinical applicability since these are key-metabolites involved in tissue energy such as high-energy phosphates (ATP and PCr) as final acceptors of energy from mitochondrial oxidative phosphorylation and low-energy metabolites (adenosine diphophosphate (ADP) and inorganic phosphate (P_i)) and membrane metabolism (the "building blocks" for membranes, phosphomonoesters phosphocholine (PC) and phosphoethanolamine (PE) and metabolites involved in the membrane breakdown processes, phosphodiesters glycerophosphocholine (GPC) and glycerophosphoetanolamine (GPE)) and allows inferring relevant parameters as intracellular pH.

The physiologic and metabolic pathways in which these metabolites are involved and their biochemical relevance may be reviewed elsewhere (Agarwal & Renshaw, 2012; Andrade, Otaduy, Park, & Leite, 2014; Bertholdo et al., 2013; R. A. De Graaf, 2007; Hajek & Dezortova, 2008; P. K. Mandal & Akolkar, 2011; Menuel et al., 2010; Mountford et al., 2010; RX, 2001; Stagg & Rothman, 2014; M. van der Graaf, 2010).

5 AIMS

"Science is exploration.
The fundamental nature of exploration is that we don't know what's there.
We can guess and hope and aim to find out certain things,
but we have to expect surprises."

Charles H. Townes

The rationale of this thesis is to understand the "*Neural basis of visual cortical reorganization mechanisms after retinal injury in Optic Neuropathies*".

For long it is known that the brain is a highly flexible structure during developmental stages and very sensitive to manipulations of sensory experience. Yet adult cortical plasticity still remains a very controversial topic. The debate is in general intense and the elucidation of the limits of cortical capability to reorganize in response to afferent damage remains a current challenge in sensory neuroscience. Some authors suggest reorganization in visual cortex of patients with retinal lesions, while others find no evidence of remapping. In this project we focus on human models of visual damage due to impairment in the only cell type in the retina that provides input to brain structures, the ganglion cell and the optic nerve links the eye and the brain for visual processing.

Through a comprehensive array of techniques and defined cohorts we propose to analyse the the neuronal impact (anatomy, function, neurochemistry and metabolism) of impaired retinocortical processing and cortical plasticity in models of ganglion cell degeneration and mitochondrial dysfunction: Leber hereditary optic neuropathy (LHON) and autosomal dominant optic atrophy (Kjer's disease, ADOA), the most common hereditary optic neuropathies, and acquired models of optic neuropathy, type 1 and type 2 Diabetes Mellitus (which affects also the inner retinal structures), a metabolic model of disease and Multiple Sclerosis with and without Optic Neuritis caused by demyelination processes of neural structures.

A critical question in the genetic models is to understand whether mechanisms of damage are due to loss of input and/or to intrinsic cortical dysfunction.

We also aim to understand the interplay between cortical damage and plastic reorganization. We believe that the understanding of the impact of different patterns of visual deprivation will allow better comprehension of the constraints that cortical reorganization patterns impose on visual rehabilitation strategies.

6 OUTLINE

"The eye is the lamp of the body.
If your eyes are healthy, your whole body will be full of light.
But if your eyes are unhealthy, your whole body will be full of darkness."

The Bible, Matt 6:22-23

According to the World Health Organization (World Health Organization (WHO), 2014) more than two hundred million people worldwide are estimated to be visually impaired in which over 30 million are blind. This is a global problem, with major health and socio-economic impact that have been potentiating the international cooperation with several global planning initiatives.

However, it is important to emphasize that the visual system not only involves the eye, but all the relays till the cortex and intracortical processing. Therefore, one should scrutinize comprehensively the system as a whole. For several years science has evolved, not only in what concerns to the know-how, but also methodologically, which allowed to bring new concepts. One revolutionary concept was the one of cortical plasticity, which we may consider as a capability that can be retrieved by which the cortex can structural-, functional- or physiologically change in response to an abnormal sensory experience. In this work we studied several pathologies that have a neuro-ophthalmologic impact with a comprehensive set of techniques.

In **Chapter I** is made an overall "Introduction" to the main concepts that are approached along the thesis. A small historical perspective on the visual plasticity conceptual roots and the main methodologies used are also presented.

Chapter II is subdivided into three sub-chapters. The main model of disease in this chapter is named "*Leber Hereditary Optic Neuropathy*" (LHON), one of the most common hereditary mitochondrial optic neuropathies. **Chapter II.1** focus the occipital cortex of a family of 15 LHON patients, clinically asymptomatic. The plasticity measure of analysis was cortical thickness of functionally-defined early visual cortical areas, assessed by MRI and retinotopy fMRI. **Chapter II.2** aims to establish the bridge between the eye and the cortex in the same cohort of LHON participants from Chapter 2.1. The retinal macular and retinal ganglion cell layer (RNFL) thicknesses were estimated by Optic Coherence Tomography (OCT) and cortical thicknesses by MRI. A new sub-study is being designed to study the neurochemistry of the occipital lobe of a different cohort of LHON participants (**Chapter II.3**) and link neural changes with the thickness of segmented layers of the retina by OCT. A pilot study was already performed to implement a new technique in our lab, 31-phosphorus Magnetic Resonance Spectroscopy Imaging (^{31}P-MRSI). Proton (^{1}H) and ^{31}P-MRS will allow to gather information on neuronal/axonal viability, cellular membrane integrity/turnover and energetics through the quantification of different metabolites involved in energy metabolism, tricarboxylic acid cycle and neurotransmission (^{1}H-MRS) and also high-energy phosphates and membrane phospholipids (^{31}P-MRS).

In **Chapter III** a cortical analysis is performed of "*Autosomic Dominant Optic Atrophy*" (ADOA) patients with the OPA-1 mutation. This is the most frequent hereditary optic neuropathy that shares some phenotype characteristics with LHON but has different pathophysiology. In here, a cohort of 14 ADOA patients were submitted to MRI and Spectroscopy MEGA-PRESS to study anatomically-defined visual cortical structures thickness, GM and WM volumetric changes. GABA, the major inhibitory neurotransmitter of the brain, was estimated through MEGA-PRESS spectroscopy as a surrogate marker of plasticity phenomena and neurotransmission.

Visual problems are one of the major complications of "*type 1 and type 2 Diabetes Mellitus*". **Chapter IV** describes a study on the biochemical changes in the occipital cortex of both Diabetes subtypes in what concerns links to bioenergetics and neurotransmission.

Another model of optic neuropathy is "*Multiple Sclerosis*". The study of this disorder is developed in **Chapter V**. This model is different from the previous one. It is mainly a demyelinating disorder, and the visual complications arise mainly due to the loss/degeneration of the myelin sheet surrounding the axons of the neurons. This is a work-in-progress where in the future we aim to establish the neural correlation between the retinal layer thicknesses and the visual cortical structures thickness.

At last, in **Chapter VI** ("*Concluding remarks*") we provide an overall integrative analysis of the distinct models results and approaches used.

The Chapters II.1, II.2, III and IV are formatted as requested by the journals where the papers were published or submitted for publication, with minor modifications.

7 REFERENCES

Agarwal, N., & Renshaw, P. F. (2012). Proton MR Spectroscopy – Detectable major neurotransmitters of the brain: biology and possible clinical applications. *American Journal of Neuroradiology*, *33*(4), 595–602. doi:10.3174/ajnr.A2587

Aguirre, G. K., Datta, R., Benson, N. C., Prasad, S., Jacobson, S. G., Cideciyan, A. V., … Gennatas, E. D. (2016). Patterns of individual variation in visual pathway structure and function in the sighted and blind. *bioRxiv*, 065441. doi:10.1101/065441

Alavi, M. V., & Fuhrmann, N. (2013). Dominant optic atrophy, OPA1, and mitochondrial quality control: understanding mitochondrial network dynamics. *Molecular Neurodegeneration*, *8*(32), 1–11. doi:10.1186/1750-1326-8-32

Amedi, A., Raz, N., Pianka, P., Malach, R., & Zohary, E. (2003). Early "visual" cortex activation correlates with superior verbal memory performance in the blind. *Nature Neuroscience, 6*(7), 758–766. doi:10.1038/nn1072

American Diabetes Association. (2014). Diagnosis and classification of diabetes mellitus. *Diabetes Care*, *37*(Suppl 1), S81–90. doi:10.2337/dc14-S081

Amunts, K., Malikovic, A., Mohlberg, H., Schormann, T., & Zilles, K. (2000). Brodmann's areas 17 and 18 brought into stereotaxic space-where and how variable? *Neuroimage*, *11*(1), 66–84. doi:10.1006/nimg.1999.0516

Andrade, C. S., Otaduy, M. C. G., Park, E. J., & Leite, C. C. (2014). Phosphorus-31 MR spectroscopy of the human brain: technical aspects and biomedical applications. *International Journal of Current Research and Review*, *6*(9), 41–57.

Baker, C. I., Peli, E., Knouf, N., & Kanwisher, N. G. (2005). Reorganization of visual processing in macular degeneration. *The Journal of Neuroscience*, *25*(3), 614–618. doi:10.1523/JNEUROSCI.3476-04.2005

Baseler, H. A., Brewer, A. A., Sharpe, L. T., Morland, A. B., Jägle, H., & Wandell, B. A. (2002). Reorganization of human cortical maps caused by inherited photoreceptor abnormalities. *Nature Neuroscience*, *5*(4), 364–370. doi:10.1038/nn817

Baseler, H. A., Gouws, A., Haak, K. V., Racey, C., Crossland, M. D., Tufail, A., … Morland, A. B. (2011). Large-scale remapping of visual cortex is absent in adult humans with macular degeneration. *Nature Neuroscience*, *14*(5), 649–655. doi:10.1038/nn.2793

Baseler, H. A., Gouws, A., & Morland, A. B. (2009). The organization of the visual cortex in patients with scotomata resulting from lesions of the central retina. *Neuro-Ophthalmology*, *33*(3), 149–157. doi:10.1080/01658100903050053

Baseler, H. A., Morland, A. B., & Wandell, B. A. (1999). Topographic organization of human visual areas in the absence of input from primary cortex. *The Journal of Neuroscience*, *19*(7), 2619–2627.

Bence, M., & Levelt, C. N. (2005). Structural plasticity in the developing visual system. *Progress in Brain Research*, *147*, 125–139. doi:10.1016/S0079-6123(04)47010-1

Bertholdo, D., Watcharakorn, A., & Castillo, M. (2013). Brain proton magnetic resonance spectroscopy: introduction and overview. *Neuroimaging Clinics of North America*, *23*(3), 359–380. doi:10.1016/j.nic.2012.10.002

Bridge, H. (2011). Mapping the visual brain: how and why. *Eye*, *25*(3), 291–296. doi:10.1038/eye.2010.166

Bridge, H., Hicks, S. L., Xie, J., Okell, T. W., Mannan, S., Alexander, I., … Kennard, C. (2010). Visual activation of extra-striate cortex in the absence of V1 activation. *Neuropsychologia*, *48*(14), 4148–4154.

Bridge, H., Thomas, O., Jbabdi, S., & Cowey, A. (2008). Changes in connectivity after visual cortical brain damage underlie altered visual function. *Brain*, *131*(6), 1433–1444. doi:10.1093/brain/awn063

Brodmann, K. (1909). *Vergleichende lokalisationslehre der großhirnrinde in ihren prinzipien dargestellt auf grund des zellenbaues (English translation available in Garey, L.J. (2006). Brodmann's: Localisation in the cerebral cortex. 3rd Edition. Springer US)*. Barth.

Brown, M. A., & Semelka, R. C. (2003). *MRI: basic principles and applications* (3rd ed.). John Wiley&Sons.

Calford, M. B., Wang, C., Taglianetti, V., Waleszczyk, W. J., Burke, W., & Dreher, B. (2000). Plasticity in adult cat visual cortex (area 17) following circumscribed monocular lesions of all retinal layers. *The Journal of Physiology*, *524*(2), 587–602.

Carelli, V., La Morgia, C., Iommarini, L., Carroccia, R., Mattiazzi, M., Sangiorgi, S., … Valentino, M. L. (2007). Mitochondrial optic neuropathies: how two genomes may kill the same cell type? *Bioscience Reports*, *27*(1-3), 173–184. doi:10.1007/s10540-007-9045-0

Carelli, V., Ross-Cisneros, F. N., & Sadun, A. A. (2004). Mitochondrial dysfunction as a cause of optic neuropathies. *Progress in Retinal and Eye Research*, *23*(1), 53–89. doi:10.1016/j.preteyeres.2003.10.003

Chard, D., & Miller, D. (2009). Grey matter pathology in clinically early multiple sclerosis: evidence from magnetic resonance imaging. *Journal of the Neurological Sciences*, *282*(1), 5–11. doi:10.1016/j.jns.2009.01.012

Chatterjee, A., & Coslett, H. B. (Eds.). (2013). *The roots of cognitive neuroscience: Behavioral neurology and neuropsychology.* Oxford University Press.

Chaturvedi, R. K., & Beal, M. F. (2013). Mitochondrial diseases of the brain. *Free Radical Biology and Medicine*, *63*, 1–29. doi:10.1016/j.freeradbiomed.2013.03.018

Chinnery, P. F., Johnson, M. A., Wardell, T. M., Singh-Kler, R., Hayes, C., Brown, D. T., … Turnbull, D. M. (2000). The epidemiology of pathogenic

mitochondrial DNA mutations. *Annals of Neurology*, *48*(2), 188–193.

Chou, I. (2008). Milestone 19. (1990) Functional MRI. Read my mind. *Nature Milestones Spin*. doi:10.1038/nphys874

Ciccarelli, O., Barkhof, F., Bodini, B., De Stefano, N., Golay, X., Nicolay, K., … Miller, D. H. (2014). Pathogenesis of multiple sclerosis: insights from molecular and metabolic imaging. *The Lancet Neurology*, *13*(8), 807–822. doi:10.1016/S1474-4422(14)70101-2

Constantine-Paton, M. (2008). Pioneers of cortical plasticity: six classic papers by Wiesel and Hubel. *Journal of Neurophysiology*, *99*(6), 2741–2744. doi:10.1152/jn.00061.2008

Costello, F. (2016). Vision disturbances in Multiple Sclerosis. In *Seminars in neurology* (Vol. 36, pp. 185–195). Thieme Medical Publishers.

D'Souza, D. V., Auer, T., Strasburger, H., Frahm, J., & Lee, B. B. (2011). Temporal frequency and chromatic processing in humans: An fMRI study of the cortical visual areas. *Journal of Vision*, *11*(8), 1–17. doi:10.1167/11.8.8

Danielsen, E. R., & Henriksen, O. (1994). Absolute quantitative proton NMR spectroscopy based on the amplitude of the local water suppression pulse. Quantification of brain water and metabolites. *NMR in Biomedicine*, *7*(7), 311–318. doi:10.1002/nbm.1940070704

Darian-Smith, C., & Gilbert, C. D. (1994). Axonal sprouting accompanies functional reorganization in adult cat striate cortex. *Nature*, *368*(6473), 737–740.

De Graaf, R. A. (2007). In vivo NMR spectroscopy: principles and techniques (2nd ed.). John Wiley & Sons.

Dennis, M. (2010). Margaret Kennard (1899-1975): Not a "principle" of brain plasticity but a founding mother of developmental neuropsychology. *Cortex*, *46*(8), 1043–1059. doi:10.1016/j.cortex.2009.10.008

DiMauro, S., & Schon, E. A. (2003). Mitochondrial respiratory-chain diseases. *The New England Journal of Medicine*, *348*(26), 2656–2668.

Dougherty, R. F., Koch, V. M., Brewer, A. A., Fischer, B., Modersitzki, J., & Wandell, B. A. (2003). Visual field representations and locations of visual areas V1/2/3 in human visual cortex. *Journal of Vision*, *3*(10), 586–598. doi:10.1167/3.10.1

Drost, D. J., Riddle, W. R., & Clarke, G. D. (2002). Proton magnetic resonance spectroscopy in the brain: report of AAPM MR Task Group #9. *Medical Physics*, *29*(9), 2177–2197. doi:10.1118/1.1501822

Duncan, R. O., & Boynton, G. M. (2003). Cortical magnification within human primary visual cortex correlates with acuity thresholds. *Neuron*, *38*(4), 659–671.

Duncan, R. O., Sample, P. A., Weinreb, R. N., Bowd, C., & Zangwill, L. M. (2007). Retinotopic organization of primary visual cortex in glaucoma: Comparing fMRI measurements of cortical function with visual field loss. *Progress in Retinal and Eye Research*, *26*(1), 38–56. doi:10.1016/j.preteyeres.2006.10.001

Engel, S. A., Rumelhart, D. E., Wandell, B. A., Lee, A. T., Glover, G. H., Chichilnisky, E. J., & Shadlen, M. N. (1994). fMRI of human visual cortex. *Nature*, *369*, 525.

Felleman, D. J., & Van Essen, D. C. (1991). Distributed hierarchical processing in the primate cerebral cortex. *Cerebral Cortex*, *1*(1), 1–47.

Ferris, C. F., Febo, M., Luo, F., Schmidt, K., Brevard, M., Harder, J. A., … King, J. A. (2006). Functional magnetic resonance imaging in conscious animals: A new tool in behavioural neuroscience research. *Journal of Neuroendocrinology*, *18*(5), 307–318. doi:10.1111/j.1365-2826.2006.01424.x

Forrester, J. V., Dick, A. D., McMenamin, P. G., Roberts, F., & Pearlman, E. (2015). *The eye: basic sciences in practice* (4th ed.). Saunders Ltd.

Friese, M. A. (2016). Widespread synaptic loss in multiple sclerosis. *Brain*, *139*(1), 2–4. doi:10.1093/brain/awv349

Gallagher, T. A., Nemeth, A. J., & Hacein-Bey, L. (2008). An introduction to the Fourier transform: Relationship to MRI. *American Journal of Roentgenology*, *190*(5), 1396–1405. doi:10.2214/AJR.07.2874

Gallo, A., Bisecco, A., Bonavita, S., & Tedeschi, G. (2015). Functional plasticity of the visual system in multiple sclerosis. *Frontiers in Neurology*, *6*(Article 79), 1–3. doi:10.3389/fneur.2015.00079

Geurts, J. J., Calabrese, M., Fisher, E., & Rudick, R. A. (2012). Measurement and clinical effect of grey matter pathology in multiple sclerosis. *The Lancet Neurology*, *11*(12), 1082–1092. doi:10.1016/S1474-4422(12)70230-2

Giannikopoulos, D. V., & Eysel, U. T. (2006). Dynamics and specificity of cortical map reorganization after retinal lesions. *Proceedings of the National Academy of Sciences*, *103*(28), 10805–10810. doi:10.1073/pnas.0604539103

Gorman, G. S., Schaefer, A. M., Ng, Y., Gomez, N., Blakely, E. L., Alston, C. L., … McFarland, R. (2015). Prevalence of nuclear and mitochondrial DNA mutations related to adult mitochondrial disease. *Annals of Neurology*, *77*(5), 753–759. doi:10.1002/ana.24362

Gross, C. G. (1997). Leonardo da Vinci on the brain and eye. *The Neuroscientist*, *3*(5), 347–355.

Haase, A., Frahm, J., Hänicke, W., & Matthaei, D. (1985). 1H NMR chemical shift selective (CHESS) imaging. *Physics in Medicine and Biology*, *30*(4), 341–344. doi:10.1088/0031-9155/30/4/008

Hajek, M., & Dezortova, M. (2008). Introduction to clinical in vivo MR spectroscopy. *European Journal of Radiology*, *67*(2), 185–193. doi:10.1016/j.ejrad.2008.03.002

Hamilton, R. H., & Pascual-Leone, A. (1998). Cortical plasticity associated with Braille learning. *Trends in Cognitive Sciences*, *2*(5), 168–174. doi:10.1016/S1364-6613(98)01172-3

Hamilton, R., Keenan, J. P., Catala, M., & Pascual-Leone, A. (2000). Alexia for Braille following bilateral occipital stroke in an early blind woman. *Neuroreport*, *11*(2), 237–240. doi:10.1097/00001756-200002070-00003

Heeger, D. J., & Ress, D. (2002). What does fMRI tell us about neuronal activity? *Nature Reviews Neuroscience*, *3*(2), 142–151. doi:10.1038/nrn730

Hendrick, R. E. (1994). The AAPM/RSNA physics tutorial for residents: Basic physics of MR imaging: an introduction. *Radiographics*, *14*(4), 829–846. doi:10.1148/radiographics.14.4.7938771

Heni, M., Kullmann, S., Preissl, H., Fritsche, A., & Häring, H.-U. (2015). Impaired insulin action in the human brain: causes and metabolic consequences. *Nature Reviews Endocrinology*, *11*(12), 701–711. doi:10.1038/nrendo.2015.173

Herholz, S. C., & Zatorre, R. J. (2012). Musical training as a framework for brain plasticity: behavior, function, and structure. *Neuron*, *76*(3), 486–502. doi:10.1016/j.neuron.2012.10.011

Higgins, G. C., & Coughlan, M. T. (2016). Mitochondrial fission/fusion and disease. *eLS*, 1–7. doi:10.1002/9780470015902.a0021879

Horowitz, A. L. (1995). *MRI physics for radiologists* (3rd ed.). Springer.

Hubel, D. H. (1982). Evolution of ideas on the primary visual cortex, 1955–1978: A biased historical account. *Bioscience Reports*, *2*(7), 435–469. doi:10.1007/BF01115245

Hubel, D. H., & Wiesel, T. N. (1962). Receptive fields, binocular interaction and functional architecture in the cat's visual cortex. *The Journal of Physiology*, *160*(1), 106–154.

Hubel, D. H., & Wiesel, T. N. (1963). Receptive fields of cells in striate cortex of very young, visually inexperienced kittens. *Journal of Neurophysiology*, *26*, 994–1002.

Hubel, D. H., & Wiesel, T. N. (1965). Binocular interaction reared in striate artificial cortex squint. *Journal of Neurophysiology*, *28*(6), 1041–1059.

Hubel, D. H., & Wiesel, T. N. (1968). Receptive fields and functional architecture of monkey striate cortex. *The Journal of Physiology*, *195*(1), 215–243.

Hubel, D., & Wiesel, W. (1979). Brain mechanisms of vision (A Scientific American book). In *The Brain* (Vol. 241, pp. 84–96). W.H.Freeman & Co Ltd.

Humphrey, N. K. (1974). Vision in a monkey without striate cortex: a case study. *Perception*, *3*(3), 241–255.

Im, C. H., Gururajan, A., Zhang, N., Chen, W., & He, B. (2007). Spatial resolution of EEG cortical source imaging revealed by localization of retinotopic organization in human primary visual cortex. *Journal of Neuroscience Methods*, *161*(1), 142–154. doi:10.1016/j.jneumeth.2006.10.008

Inglese, M. (2006). Multiple sclerosis: new insights and trends. *American Journal of Neuroradiology*, *27*(5), 954–957.

Jacobs, M. A., Ibrahim, T. S., & Ouwerkerk, R. (2007). MR Imaging: Brief Overview and Emerging Applications. *Radiographics*, *27*(4), 1213–1229. doi:10.1148/rg.274065115

Jiang, J., Zhu, W., Shi, F., Liu, Y., Li, J., Qin, W., … Jiang, T. (2009). Thick visual cortex in the early blind. *The Journal of Neuroscience*, *29*(7), 2205–2211. doi:10.1523/JNEUROSCI.5451-08.2009

Johansson, B. B. (2011). Current trends in stroke rehabilitation. A review with focus on brain plasticity. *Acta Neurologica Scandinavica*, *123*, 147–159. doi:10.1111/j.1600-0404.2010.01417.x

Kaas, J. H., Collins, C. E., & Chino, Y. M. (2006). Plasticity of retinotopic maps in visual cortex of cats and monkeys after lesions of the retina or primary visual cortex. In *Plasticity in the Visual System: From genes to circuits* (pp. 205–227). Springer.

Kaas, J. H., Krubitzer, L. A., Chino, Y. M., Langston, A. L., Polley, E. H., & Blair, N. (1990). Reorganization of retinotopic cortical maps in adult mammals after lesions of the retina. *Science*, *248*(4952), 229–231.

Kandel, E. R., Schwartz, J. H., Jessell, T. M., Siegelbaum, S. A., & Hudspeth, A. J. (2012). *Principles of neural science* (5th ed.). McGraw-Hill.

Kolb, B., & Whishaw, I. Q. (1998). Brain plasticity and behavior. *Annual Review of Psychology*, *49*(1), 43–64. doi:10.1146/annurev.psych.49.1.43

Kreis, R. (2004). Issues of spectral quality in clinical 1H-magnetic resonance spectroscopy and a gallery of artifacts. *NMR in Biomedicine*, *17*(6), 361–381. doi:10.1002/nbm.891

Lam, D. Y., Kaufman, P. L., B'Ann, T. G., To, E. C., & Matsubara, J. A. (2003). Neurochemical correlates of cortical plasticity after unilateral elevated intraocular pressure in a primate model of glaucoma. *Investigative Ophthalmology & Visual Science*, *44*(6), 2573–2581. doi:10.1167/iovs.02-0779

Lauterbur, P. C. (1973). Image formation by induced local interactions: examples employing nuclear magnetic resonance. *Nature*, *242*, 190–191.

Lemos, J., Pereira, D., & Castelo-Branco, M. (2016). Visual Cortex Plasticity Following Peripheral Damage To The Visual System: fMRI Evidence. *Current Neurology and Neuroscience Reports*, *16*(10), 1–17. doi:10.1007/s11910-016-0691-0

Lenaers, G., Hamel, C., Delettre, C., Amati-Bonneau, P., Procaccio, V., Bonneau, D., … Milea, D. (2012). Dominant optic atrophy. *Orphanet Journal of Rare Diseases*, *7*(1), 46. doi:10.1186/1750-1172-7-46

Leporé, N., Voss, P., Lepore, F., Chou, Y. Y., Fortin, M., Gougoux, F., … Thompson, P. M. (2010). Brain structure changes visualized in early- and late-onset blind subjects. *Neuroimage*, *49*(1), 134–40. doi:10.1016/j.neuroimage.2009.07.048

Leruez, S., Amati-Bonneau, P., Verny, C., Reynier, P., Procaccio, V., Bonneau, D., & Milea, D. (2014). Mitochondrial dysfunction affecting visual pathways. *Revue Neurologique*, *170*(5), 344–354. doi:10.1016/j.neurol.2014.03.009

Lieth, E., Gardner, T. W., Barber, A. J., & Antonetti, D. A. (2000). Retinal neurodegeneration: early pathology in diabetes. *Clinical & Experimental Ophthalmology*, *28*(1), 3–8. doi:10.1046/j.1442-9071.2000.00222.x

Light, D. B. (2009). The human body: how it works - *The senses* (1st ed.). Chelsea House Publications.

Lin, A., Tran, T., Bluml, S., Merugumala, S., Liao, H. J., & Ross, B. D. (2012). Guidelines for acquiring and reporting clinical neurospectroscopy. In *Seminars in neurology* (Vol. 32, pp. 432–453). Thieme Medical Publishers. doi:10.1055/s-0032-1331814

Lipton, M. L., & Kanal, E. (2008). *Totally accessible MRI: a user's guide to principle, technology, and applications*. Springer.

Llinás, R. R. (2003). The contribution of Santiago Ramón y Cajal to functional neuroscience. *Nature Reviews Neuroscience*, *4*(1), 77–80. doi:10.1038/nrn1011

London, A., Benhar, I., & Schwartz, M. (2013). The retina as a window to the brain-from eye research to CNS disorders. *Nature Reviews Neurology*, *9*(1), 44–53. doi:10.1038/nrneurol.2012.227

Lucchinetti, C. F., & Hohlfeld, R. (2010). *Multiple Sclerosis 3: Blue Books of Neurology Series (Volume 34)* (1st ed.). Saunders.

Magistretti, P. J., Pellerin, L., Rothman, D. L., & Shulman, R. G. (1999). Energy on demand. *Science*, *283*(5401), 496–497. doi:10.1126/science.283.5401.496

Maguire, E. A., Gadian, D. G., Johnsrude, I. S., Good, C. D., Ashburner, J., Frackowiak, R. S., & Frith, C. D. (2000). Navigation-related structural change in the hippocampi of taxi drivers. *Proceedings of the National Academy of Sciences*, *97*(8), 4398–4403. doi:10.1073/pnas.070039597

Mandal, P. K. (2012). In vivo proton magnetic resonance spectroscopic signal processing for the absolute quantitation of brain metabolites. *European Journal of Radiology*, *81*(4), e653–e664. doi:10.1016/j.ejrad.2011.03.076

Mandal, P. K., & Akolkar, H. (2011). A new experimental approach and signal processing scheme for the detection and quantitation of 31P brain neurochemicals from in vivo MRS studies using dual tuned (1H/31P) head coil. *Biochemical and Biophysical Research Communications*, *412*(2), 302–306. doi:10.1016/j.bbrc.2011.07.088

Mangia, S., Kumar, A. F., Moheet, A. A., Roberts, R. J., Eberly, L. E., Seaquist, E. R., & Tkáč, I. (2013). Neurochemical profile of patients with type 1 diabetes measured by 1H-MRS at 4 T. *Journal of Cerebral Blood Flow & Metabolism*, *33*(5), 754–759. doi:10.1038/jcbfm.2013.13

Mark, V. M. (2013). Plasticity. In A. Chatterjee & H. B. Coslett (Eds.), *The roots of cognitive neuroscience: Behavioral neurology and neuropsychology* (pp. 334–348). Oxford University Press.

Menuel, C., Guillevin, R., Costalat, R., Perrin, M., Sahli-Amor, M., Martin-Duverneuil, N., & Chiras, J. (2010). Spectroscopie du phosphore 31 par résonance magnétique: applications en pathologies cérébrales. *Journal of Neuroradiology*, *37*(2), 73–82. doi:10.1016/j.neurad.2009.07.001

Messina, R., Rocca, M., Marzoli, S. B., Petrolini, M., Milesi, I., Darvizeh, F., … Filippi, M. (2016). Regional patterns of brain gray and white matter abnormalities in patients with hereditary optic neuropathies: Dominant Optic Atrophy vs Leber Hereditary Optic Neuropathy (S48. 006). *Neurology*, *86*(16.Supplement), S48–006.

Meyerson, C., Van Stavern, G., & McClelland, C. (2015). Leber hereditary optic neuropathy: current perspectives. *Clinical Ophtalmology*, *9*, 1165–1176.

Moffett, J. R., Ross, B., Arun, P., Madhavarao, C. N., & Namboodiri, A. M. A. (2007). N-Acetylaspartate in the CNS: from neurodiagnostics to neurobiology. *Progress in Neurobiology*, *81*(2), 89–131. doi:10.1016/j.pneurobio.2006.12.003

Morland, A. B., Baseler, H. A., Hoffmann, M. B., Sharpe, L. T., & Wandell, B. A. (2001). Abnormal retinotopic representations in human visual cortex revealed by fMRI. *Acta Psychologica*, *107*(1), 229–247.

Mountford, C. E., Stanwell, P., Lin, A., Ramadan, S., & Ross, B. (2010). Neurospectroscopy: the past, present and future. *Chemical Reviews*, *110*(5), 3060–3086.

Mullins, P. G., McGonigle, D. J., O'Gorman, R. L., Puts, N. A., Vidyasagar, R., Evans, C. J., … Edden. (2014). Current practice in the use of MEGA-PRESS spectroscopy for the detection of GABA. *Neuroimage*, *86*, 43–52. doi:10.1016/j.neuroimage.2012.12.004

Multiple Sclerosis International Federation (MSIF). (2013). Atlas of MS 2013: Mapping Multiple Sclerosis Around the World. *Multiple Sclerosis International Federation*, 1–28.

Murphy, T. H., & Corbett, D. (2009). Plasticity during stroke recovery: from synapse to behaviour. *Nature Reviews Neuroscience*, *10*(12), 861–872. doi:10.1038/nrn2735

Nahmani, M., & Turrigiano, G. G. (2014). Adult cortical plasticity following injury: recapitulation of critical period mechanisms? *Neuroscience*, *283*, 4–16. doi:10.1016/j.neuroscience.2014.04.029

Ng, D. S. K., Chiang, P. P. C., Tan, G., Cheung, C. M. G., Cheng, C.-Y., Cheung, C. Y., … Ikram, M. K. (2016). Retinal ganglion cell neuronal damage in diabetes and diabetic retinopathy. *Clinical & Experimental Ophthalmology*, 1–8. doi:10.1111/ceo.12724

Nightingale, H., Pfeffer, G., Bargiela, D., Horvath, R., & Chinnery, P. F. (2016). Emerging therapies for mitochondrial disorders. *Brain*, *139*, 1633–1648. doi:10.1093/brain/aww081

Nolan, R. C., Narayana, K., Balcer, L. J., & Galetta, S. L. (2016). Optical coherence tomography (OCT) and multiple sclerosis (MS). In A. Grzybowski & P. Barboni (Eds.), *OCT in Central Nervous System Diseases: The eye as a window to the brain* (pp. 87–104). doi:10.1007/978-3-319-24085-5_5

Nunnari, J., & Suomalainen, A. (2012). Mitochondria: in sickness and in health. *Cell*, *148*(6), 1145–1159. doi:10.1016/j.cell.2012.02.035

Nys, J., Scheyltjens, I., & Arckens, L. (2015). Visual system plasticity in mammals: the story of monocular enucleation-induced vision loss. *Frontiers in Systems Neuroscience*, *9*(Article 60), 60. doi:10.3389/fnsys.2015.00060

Ogawa, S., Lee, T. M., Kay, A. R., & Tank, D. W. (1990). Brain magnetic resonance imaging with contrast dependent on blood oxygenation. *Proceedings of the National Academy of Sciences*, *87*(24), 9868–9872.

Olsen, R. K., Kippenhan, J. S., Japee, S., Kohn, P., Mervis, C. B., Saad, Z. S., … Berman, K. F. (2009). Retinotopically defined primary visual cortex in Williams syndrome. *Brain*, *132*, 635–644. doi:10.1093/brain/awn362

Ong, S. B. (2014). Imaging of mitochondrial disorders: A review. In *Advances in Medical Diagnostic Technology* (pp. 99–136). Springer. doi:10.1007/978-981-4585-72-9_5

Paillard, J. (1976). Réflexions sur l'usage du concept de plasticité en neurobiologie. *Journal de Psychologie Normale et Pathologique*, *1*, 33–47.

Parisi, L., Rocca, M. A., Mattioli, F., Riccitelli, G. C., Capra, R., Stampatori, C., … Filippi, M. (2014). Patterns of regional gray matter and white matter atrophy in cortical multiple sclerosis. *Journal of Neurology*, *261*(9), 1715–1725. doi:10.1007/s00415-014-7409-5

Pirko, I., Lucchinetti, C. F., Sriram, S., & Bakshi, R. (2007). Gray matter involvement in multiple sclerosis. *Neurology*, *68*(9), 634–642. doi:10.1212/01.wnl.0000250267.85698.7a

Pooley, R. A. (2005). AAPM/RSNA Physics Tutorial for Residents: Fundamental Physics of MR Imaging. *Radiographics*, *25*(4), 1087–1099. doi:10.1148/rg.254055027

Prasad, S., & Galetta, S. L. (2011). Anatomy and physiology of the afferent visual system. In C. Kennard & R. J. Leigh (Eds.), *Handbook of Clinical Neurology* (Vol. 102, pp. 3–19). Elsevier B.V. doi:10.1016/B978-0-444-52903-9.00007-8

Pula, J. H., & Kattah, J. C. (2010). Diagnosis and treatment of visual disturbances in Multiple Sclerosis. *International Journal of MS Care*, *12*(3), 106–113.

Puts, N. A., & Edden, R. A. (2012). In vivo magnetic resonance spectroscopy of GABA: a methodological review. *Progress in Nuclear Magnetic Resonance Spectroscopy*, *60*, 29–41. doi:10.1016/j.pnmrs.2011.06.001

Ramadan, S., Lin, A., & Stanwell, P. (2013). Glutamate and glutamine: a review of in vivo MRS in the human brain. *NMR in Biomedicine*, *26*(12), 1630–1646. doi:10.1002/nbm.3045

Rees, G., Kreiman, G., & Koch, C. (2002). Neural correlates of consciousness in humans. *Nature Reviews Neuroscience*, *3*(4), 261–270. doi:10.1038/nrn783

Rodieck, R. W. (1979). Visual pathways. *Annual Review of Neuroscience*, *2*, 193–225.

Ross, B., & Bluml, S. (2001). Magnetic resonance spectroscopy of the human brain. *The Anatomical Record*, *265*(2), 54–84. doi:10.1002/ar.1058

Roubertie, A., Leboucq, N., Picot, M. C., Nogue, E., Brunel, H., Le Bars, E., … Hamel, C. P. (2015). Neuroradiological findings expand the phenotype of OPA1-related mitochondrial dysfunction. *Journal of the Neurological Sciences*, *349*(1), 154–160. doi:10.1016/j.jns.2015.01.008

Sadun, A. A., La Morgia, C., & Carelli, V. (2011). Leber's hereditary optic neuropathy. *Current Treatment Options in Neurology*, *13*(1), 109–117. doi:10.1007/s11940-010-0100-y

Saidha, S., Syc, S. B., Durbin, M. K., Eckstein, C., Oakley, J. D., Meyer, S. A., … Calabresi, P. A. (2011). Visual dysfunction in Multiple Sclerosis correlates better with optical coherence tomography derived estimates of macular ganglion cell layer thickness than peripapillary retinal nerve fiber layer thickness. *Multiple Sclerosis Journal*, *17*(12), 1449–1463. doi:10.1177/1352458511418630

Schaechter, J. D. (2004). Motor rehabilitation and brain plasticity after hemiparetic stroke. *Progress in Neurobiology*, *73*(1), 61–72. doi:10.1016/j.pneurobio.2004.04.001

Schmid, M. C., Panagiotaropoulos, T., Augath, M. A., Logothetis, N. K., & Smirnakis, S. M. (2009). Visually driven activation in macaque areas V2 and V3 without input from the primary visual cortex. *PloS One*, *4*(5), e5527. doi:10.1371/journal.pone.0005527

Sereno, M. I., Dale, A. M., Reppas, J. B., Kwong, K. K., Belliveau, J. W., Brady, T. J., … Tootell, R. B. H. (1995). Borders of multiple visual areas in humans revealed by functional magnetic resonance imaging. *Science*, *268*, 889–893.

Sereno, M. I., McDonald, C. T., & Allman, J. M. (1994). Analysis of retinotopic maps in extrastriate cortex. *Cerebral Cortex*, 4, 601–620.

Siero, J. C., Bhogal, A., & Jansma, J. M. (2013). Blood oxygenation level-dependent/functional magnetic resonance imaging: Underpinnings, practice, and perspectives. *PET Clinics*, *8*(3), 329–344. doi:10.1016/j.cpet.2013.04.003

Smirnakis, S. M., Brewer, A. A., Schmid, M. C., Tolias, A. S., Schüz, A., Augath, M., … Logothetis, N. K. (2005). Lack of long-term cortical reorganization after macaque retinal lesions. *Nature*, *435*, 300–307.doi:10.1038/nature03495

Sprague, J. M., Levy, J., DiBerardino, A., & Berlucchi, G. (1977). Visual cortical areas mediating form discrimination in the cat. *Journal of Comparative Neurology*, *172*(3), 441–488. doi:10.1002/cne.901720305

Stagg, C. J., & Rothman, D. L. (Eds.). (2014). *Magnetic resonance spectroscopy: tools for neuroscience research and emerging clinical applications* (1st ed.). Academic Press. doi:10.1016/B978-0-12-401688-0.00025-2

Taylor, R. W., & Turnbull, D. M. (2005). Mitochondrial DNA mutations in human disease. *Nature*

Reviews Genetics, *6*(5), 389–402. doi:10.1038/nrg1606

Teasell, R., Bayona, N. A., & Bitensky, J. (2005). Plasticity and reorganization of the brain post stroke. *Topics in Stroke Rehabilitation*, *12*(3), 11–26. doi:10.1310/6AUM-ETYW-Q8XV-8XAC

The Optic Neuritis Study Group. (2004). Visual function more than 10 years after optic neuritis: experience of the optic neuritis treatment trial. *American Journal of Ophthalmology*, *137*(1), 77–83. doi:10.1016/S0002-9394(03)00862-6

Tootell, R. B. H., Dale, A. M., Sereno, M. I., & Malach, R. (1996). New images from human visual cortex. *Trends in Neurosciences*, *19*(11), 481–489.

Tootell, R. B. H., Hadjikhani, N. K., Mendola, J. D., Marrett, S., & Dale, A. M. (1998). From retinotopy to recognition: fMRI in human visual cortex. *Trends in Cognitive Sciences*, *2*(5), 174–183.

Tyler, C. W., Likova, L. T., Chen, C.-C., Kontsevich, L. K., Schira, M. M., & Wade, A. R. (2005). Extended concepts of occipital retinotopy. *Current Medical Imaging Reviews*, *1*(3), 319–329. doi:10.2174/157340505774574772

Ulmer, S., Backens, M., & Ahlhelm, F. J. (2016). Basic principles and clinical applications of magnetic resonance spectroscopy in neuroradiology. *Journal of Computer Assisted Tomography*, *40*(1), 1–13. doi:10.1097/RCT.0000000000000322

Uludağ, K., Dubowitz, D. J., & Buxton, R. B. (2005). Basic principles of functional MRI. In *Clinical MRI* (pp. 249–287). Elsevier.

van der Graaf, M. (2010). In vivo magnetic resonance spectroscopy: basic methodology and clinical applications. *European Biophysics Journal*, *39*(4), 527–540. doi:10.1007/s00249-009-0517-y

van Dijk, H. W., Verbraak, F. D., Kok, P. H. B., Garvin, M. K., Sonka, M., Lee, K., … Abràmoff, M. D. (2010). Decreased retinal ganglion cell layer thickness in patients with type 1 Diabetes. *Investigative Ophthalmology & Visual Science*, *51*(7), 3660–3665. doi:10.1167/iovs.09-5041

Van Essen, D. C., & Dierker, D. L. (2007). Surface-based and probabilistic atlases of primate cerebral cortex. *Neuron*, *56*(2), 209–225. doi:10.1016/j.neuron.2007.10.015

Van Essen, D. C., & Glasser, M. F. (2014). In vivo architectonics: a cortico-centric perspective. *Neuroimage*, *93*(Pt 2), 157–164. doi:10.1016/j.neuroimage.2013.04.095

Van Essen, D. C., Lewis, J. W., Drury, H. A., Hadjikhani, N., Tootell, R. B. H., Bakircioglu, M., & Miller, M. I. (2001). Mapping visual cortex in monkeys and humans using suface-based atlases. *Vision Research*, *41*(10), 1359–1378.

Veselinovi, D., & Jovanovi, M. (2005). Diabetes Mellitus and optic nerve diseases. *Acta Fac. Med. Naiss*, *22*(3), 145–148.

Wandell, B. A. (1995). *Foundations of vision* (1st ed.). Sinauer Associates Inc.

Wandell, B. A., Dumoulin, S. O., & Brewer, A. A. (2007). Visual field maps in human cortex. *Neuron*, *56*(2), 366–383. doi:10.1016/j.neuron.2007.10.012

Wandell, B. A., & Smirnakis, S. M. (2009). Plasticity and stability of visual field maps in adult primary visual cortex. *Nature Reviews Neuroscience*, *10*(12), 873–884. doi:10.1038/nrn2741

Wandell, B. A., & Winawer, J. (2011). Imaging retinotopic maps in the human brain. *Vision Research*, *51*(7), 718–737. doi:10.1016/j.visres.2010.08.004

Weishaupt, D., Köchli, V. D., & Marincek, B. (2006). *How Does MRI Work? An Introduction to the Physics and Function of Magnetic Resonance Imaging. Journal of Nuclear Medicine* (2nd ed., Vol. 48). Springer.

Wiesel, T. N. (1982). The postnatal development of the visual cortex and the influence of environment. *Bioscience Reports*, *2*(6), 351–377.

Wiesel, T. N., & Hubel, D. H. (1963a). Effects of visual deprivation on morphology and physiology of cells in the cat's lateral geniculate body. *Journal of Neurophysiology*, *26*, 978–993.

Wiesel, T. N., & Hubel, D. H. (1963b). Single-cell responses in striate cortex of kittens deprived of vision in one eye. *Journal of Neurophysiology*, *26*(6), 1003–1017.

Wiesel, T. N., & Hubel, D. H. (1965a). Comparison of the effects of unilateral and bilateral eye closure on cortical unit responses in kittens. *Journal of Neurophysiology*, *28*(6), 1029–1040.

Wiesel, T. N., & Hubel, D. H. (1965b). Extent of recovery from the effects of visual deprivation in kittens. *Journal of Neurophysiology*, *28*(6), 1060–1072.

Will, B., Dalrymple-Alford, J., Wolff, M., & Cassel, J.-C. (2008). The concept of brain plasticity-Paillard's systemic analysis and emphasis on structure and function (followed by the translation of a seminal paper by Paillard on plasticity). *Behavioural Brain Research*, *192*(1), 2–7. doi:10.1016/j.bbr.2007.11.008

Wilms, M., Eickhoff, S. B., Hömke, L., Rottschy, C., Kujovic, M., Amunts, K., & Fink, G. R. (2010). Comparison of functional and cytoarchitectonic maps of human visual areas V1, V2, V3d, V3v, and V4(v). *Neuroimage*, *49*(2), 1171–1179. doi:10.1016/j.neuroimage.2009.09.063

Wohlschläger, A. M., Specht, K., Lie, C., Mohlberg, H., Wohlschläger, A., Bente, K., … Fink, G. R. (2005). Linking retinotopic fMRI mapping and anatomical probability maps of human occipital areas V1 and V2. *Neuroimage*, *26*(1), 73–82. doi:10.1016/j.neuroimage.2005.01.021

World Health Organization (WHO). (2014). Visual impairment and blindness, *Fact Sheet N°282*.

World Health Organization (WHO). (2016). *Global Report on Diabetes*.

Zhuo, J., & Gullapalli, R. P. (2006). AAPM/RSNA physics tutorial for residents: MR artifacts, safety, and quality control. *Radiographics*, *26*(1), 275–297. doi:10.1148/rg.261055134

Zilles, K., & Amunts, K. (2010). Centenary of Brodmann's map - conception and fate. *Nature Reviews Neuroscience*, *11*(2), 139–145. doi:10.1038/nrn2776

CHAPTER II

Leber Hereditary Optic Neuropathy

II.1

- We found unexpected increase in visual cortical thickness in early silent ganglion cell loss (asymptomatic LHON carriers).
- Retinotopically defined area V2 shows evidence for early compensatory plasticity.
- Later in life plasticity migrates further to extrastriate area V3.

II.2

- CT was a very discriminative measure between LHON carriers and controls.
- Increased cortical thickness in V2 and V3 was observed in peripheral regions, as visual field loss, in these mutation carriers.
- Peripheral cortical compensatory plasticity in early visual areas V2/V3 may be triggered by pathology in peripheral RGC axons in combination with potential developmental changes.

Author note: *The ophtalmological analysis was already included in the PhD Thesis of Catarina Mateus, 2015 and are presented here only for contextualization purposes. Now the study is published and new cortical analysis were performed after revision entirely by the author of this Thesis, added to the final version of the (published) manuscript and discussed exclusively in here.*

II.3

- Future work
- ^{1}H and ^{31}P MR Spectroscopy may further elucidate the impact of mitochondrial dysfunction in metabolism and neurotransmission of the occipital cortex of LHON patients.

Ch. II. 1

Long term cortical plasticity in visual Retinotopic areas in humans with silent retinal ganglion cell loss

Otília C. d'Almeida,
Catarina Mateus, Aldina Reis, Manuela M. Grazina, Miguel Castelo-Branco

ABSTRACT

Visual cortical plasticity induced by overt retinal lesions (scotomas) has remained a controversial phenomenon. Here we studied cortical plasticity in a silent model of retinal ganglion cell loss, documented by in vivo optical biopsy using coherence tomography. The cortical impact of non-scotomatous subtle retinal ganglion cell functional and structural loss was investigated in carriers of the mitochondrial DNA 11778G>A mutation causing Leber's hereditary optic neuropathy. We used magnetic resonance imaging (MRI) to measure cortical thickness and fMRI to define retinotopic cortical visual areas V1, V2 and V3 in silent carriers and matched control groups. Repeated Measures analysis of variance revealed a surprising increase in cortical thickness in the younger carrier group (below 21 years of age). This effect dominated in extrastriate cortex, and notably V2. This form of structural plasticity suggests enhanced plastic developmental mechanisms in extrastriate retinotopic regions close to V1 and not receiving direct retinocortical input.

d'Almeida, O. C., Mateus, C., Reis, A., Grazina, M. M., & Castelo-Branco, M. (2013). Long term cortical plasticity in visual retinotopic areas in humans with silent retinal ganglion cell loss. *Neuroimage*, *81*, 222-230. doi:10.1016/j.neuroimage.2013.05.032

1 INTRODUCTION

It is known that the brain is able to optimize neural connectivity, in particular during critical periods (Eysel, 2009). Cortical plasticity is characterized by the modification of wiring of neuronal cortical networks in response to changes in visual experience, leading to structural and functional reorganization. Even though developmental plasticity is a well-established phenomenon, adult plasticity still is a very controversial issue. The ability of the cerebral cortex to adapt to changes in visual experience and mechanisms underlying the compensation of loss of function is still highly debated (Wandell & Smirnakis, 2009). Nevertheless human studies have suggested that during the lifespan the cortex maintains the ability to structurally and functionally reorganize either to increased use or disuse due to lesions (Baseler, Gouws, & Morland, 2009; Bridge et al., 2010; Bridge, Thomas, Jbabdi, & Cowey, 2008).

Animal model studies of artificially induced retinal lesions (for a review see Baseler et al. (2009)) suggest that the cortex preserves a certain degree of plasticity and is capable of rewiring in response to the loss of sensory inputs using the remaining intact portions of the retina. However, the mechanisms of visual plasticity induced by sustained silent loss of afferent retinal inputs in humans have hitherto not been studied.

We have addressed this issue by studying the silent stage of a human model of retinal ganglion cell (RGC) degeneration and death, Leber Hereditary Optic Neuropathy (LHON). LHON is an inherited genetic condition that may lead to the loss of vision that becomes suddenly apparent after years of subtle neural loss. It is one of the most common types of hereditary optic atrophies with an estimated prevalence rate of approximately 1 in 30,000 (Man et al., 2003; Newman & Biousse, 2004). This maternally inherited disorder caused by point mutations in the mitochondrial DNA (Kirkman, Yu-Wai-Man, et al., 2009) is characterized by optic nerve atrophy and reduced retinocortical processing. After clinical onset it leads to bilateral visual impairment with dominant loss of central vision (Kirkman, Korsten, et al., 2009).

Retinocortical information flow is routed from the optic nerve to the lateral geniculate nucleus (LGN) and then dominantly to the primary striate visual cortex (V1). Visual information is then redistributed to extrastriate V2, V3 and higher visual areas (Felleman & Van Essen, 1991). Retinal degeneration does therefore directly deprive V1 from receiving sensory information.

The main aim of this study was to elucidate the structural impact of silent early stage deprivation. An important question was whether indirectly deprived visual extrastriate regions would be affected, or instead reorganize.

It is worth emphasizing that we did not study here overt or late stage clinical cases, where the lack of direct input might lead to manifest cortical atrophy and grey matter thinning. Such overt loss might explain putative cortical atrophy in lesion projection zones (LPZ) of clinically established retinal lesions. Accordingly, a study comparing grey matter density in visual cortex of foveal (age-related macular degeneration) and peripheral (open-angle glaucoma) retinal lesion models using Voxel Based Morphometry revealed reduction in grey matter density in the respective LPZs in the calcarine sulcus (Boucard et al., 2009). This shows that overt lesions as expressed by visual field scotomata may lead to retinotopic-specific structural loss in the visual cortex.

Our study focuses on the impact of widespread but clinically silent early afferent degeneration on primary striate and extrastriate cortex reorganization. We computed cortical thickness (CT) maps in a pedigree of LHON individuals carrying the 11778G>A mitochondrial DNA mutation in functionally defined early visual areas V1, V2 and V3 in comparison with age-matched controls. Importantly, we expected plasticity to occur mainly during cortical development and to be reduced in adulthood due

to decreased plasticity and progression of silent neurodegeneration. It was therefore important to set late developmental cutoffs defined by the onset of early adulthood. We found evidence for differential reorganization in this age-dependent model of silently progressive loss.

2 MATERIAL AND METHODS

2.1 Subjects

We have tested 15 asymptomatic LHON carriers (7 men, 8 women; mean age=29.3±13.50 [*SD*] years; age range, 8–47 years) (Table II.1) that belong to a single homogeneous pedigree of confirmed presence of the mitochondrial DNA 11778G>A mutation (Grazina et al., 2007). Participants from the LHON group were submitted to MRI acquisition and data were compared to subjects from an age-matched control group (n=15 participants; 11 men, 4 women; mean age=26.2±11.45 [*SD*] years; age range, 7–44 years).

Table II.1 Demographics and measures of visual acuity and visual field (MD, mean defect; LV, loss of variance) of both left (LE) and right (RE) eyes of LHON carriers. Normal range: MD±2 dB and a LV<6 dB^2. Visual dysfunction consistent with subclinical loss is evident.

Patient	Gender	Age	Visual Acuity		Visual Field			
					MD (dB)		**LV** (dB^2)	
		(y)	**LE**	**RE**	**LE**	**RE**	**LE**	**RE**
1	M	47	20/16	20/16	0.7	-0.7	3.3	3.8
2	F	47	20/20	20/20	1.7	1.8	4.4	5.2
3	F	43	20/20	20/20	3.8	2.8	10.3	4.9
4	M	41	20/16	20/16	4.0	4.2	8.3	4.0
5	F	40	20/20	20/20	4.4	4.0	6.6	3.1
6	F	39	20/20	20/20	3.8	5.0	7.9	2.1
7	F	37	20/16	20/16	0.9	1.8	5.1	5.2
8	F	30	20/16	20/16	7.8	7.0	9.1	10.8
9	M	21	20/16	20/16	7.8	5.5	20.4	32.3
10	F	22	20/16	20/16	6.6	3.9	26.7	9.2
11	M	17	20/16	20/16	5.0	3.3	24.1	10.9
12	M	19	20/16	20/20	5.2	2.8	15.2	10.5
13	M	10	20/20	20/20	6.9	4.1	15.7	4.3
14	F	18	20/16	20/16	7.6	7.8	6.7	9.2
15	M	8	20/16	20/20	3.1	3.1	7.9	9.9

All participants were submitted to a complete ophthalmological examination, including best-corrected visual acuity obtained with Snellen chart, ocular tension (Goldmann applanation tonometer, slit lamp biomicroscopy and fundus examination (Goldmann lens)). Control subjects were required to have good visual acuity and not to have any visual field defect (as defined by normative data). Our participants from the LHON carrier group had normal ocular examination, with normal visual acuity and no fundus changes. Visual functional evaluation (see Table II.1) showed subclinical impairment in chromatic contrast sensitivity for all colour axes (Cambridge Colour Test – Cambridge Research Systems, Rochester, UK: Protan: p=0.002; Deutan: p=0.006; Tritan: p=0.007). Subtle changes in the visual field sensitivity, in spite of the absence of scotomas (Octopus – Haag-Streit AG, Germany), with impact in the global threshold parameters (mean±*SD*), mean defect (MD): 3.76±2.10 dB; and loss of variance (LV): 8.36±7.31 dB^2, could also be found (Table II.1). The normal range considered for MD and LV is ±2 dB and <6 dB^2, respectively. Structural evaluation of the neural retina was performed using optical coherence tomography, a form of optical biopsy (Stratus OCT3 – Humphrey, Carl Zeiss Meditec, Dublin, CA, USA, axial resolution ~10 μm, for details see below). Exclusion criteria were established pseudophakic and aphakic eyes, significant media opacities, other retinal diseases, high ammetropy (sphere>+4D; cylinder>+2D) and other neuro-

ophthalmologic pathology, besides LHON. The study followed the tenets of the Declaration of Helsinki and was approved by our Institutional Review Board. Informed consent was obtained from each participant, after research procedures had been fully explained.

2.2 Retinal imaging

Optical coherence tomography (Stratus OCT3, Humphrey, Carl Zeiss Inst., CA, USA) provides a cross-sectional tomography of retinal tissue in real time, based on optical interferometry, using infra-red (843 nm), low coherence light. Cross-sectional images of retinal anatomy were thus obtained, with an axial resolution of ≤10 μm. Retinal thickness was computed as a 9 region bidimensional interpolated thickness map, with a central circle of 1 mm diameter and 2 outer circles with diameter of 3 and 6 mm (Figure II.1).

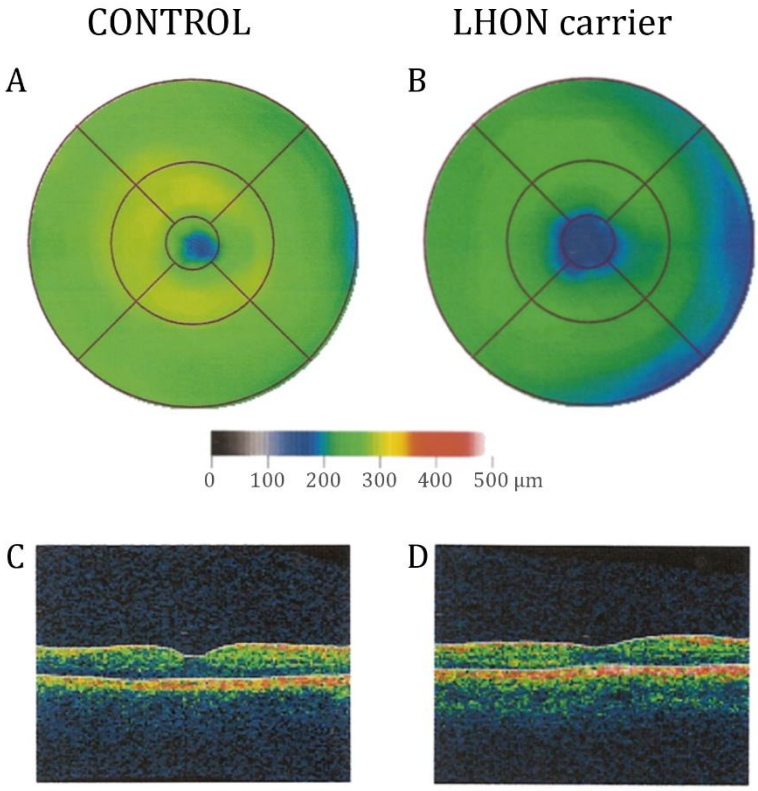

Figure II.1 Ocular imaging data of the left eye of a (*left*: **A**, **C**) CONTROL, 48 years and (*right*: **B**, **D**) a LHON carrier (Table II.1, patient 2), 47 years. (**A**, **B**) Individual OCT neuroretinal thickness maps (colour bar codes this measure in μm) centred on the fovea. Relative macula volume/thickness loss can be documented in the inner rings of LHON carrier (total macular volume 6.24 mm^3) comparing to the CONTROL (total macular volume 7.14 mm^3) (see text for group analysis). Imaging data were obtained across a 6 mm circular area centred in the macula. (**C**, **D**) Sectional retinal scans corresponding to the maps presented on top.

2.3 Stimuli and task design

2.3.1 Retinotopic mapping

Early visual areas are retinotopically arranged in the human visual cortex and *mirror*/*nonmirror* representations of adjacent areas of the visual field correspond to the turning points in horizontal and vertical meridians. Visual field mapping fMRI data were acquired using visual stimuli encoding polar coordinates. We used the standard travelling wave method (phase-encoded retinotopy) (Engel et al., 1994; Sereno et al., 1995). Presented stimuli were: (i) polar angle encoding stimuli (Figure II.2

B) comprising a rotating (anticlockwise) black and white checkered wedge flickering at 8 Hz (48 s full cycle, 4 cycles/scan, three scans per subject) and (ii) an eccentricity mapping paradigm (Figure II.2 C), using an expanding black and white checkered annulus flickering at 8 Hz (48 s each full expansion, 4 expansions/scan, one scan per subject), while the subject was instructed to fix an orange-coloured central point. The stimuli spanned 23°×23° of visual angle (diameter). This method allowed the mapping of the visual field angular position and eccentricity in relation to the centre of the gaze (see below details of fMRI analysis).

2.4 Data acquisition

High resolution MRI data was acquired in a 3T scanner (Siemens Magnetom TrioTim 3T Erlangen, Germany) at the Portuguese Brain Imaging Network, with a 12 channel head coil. The MRI acquisition protocol for each participant was: (i) two 9-minute long T1-weighted ($T1_w$) three-dimensional *Magnetization Prepared Rapid Acquisition Gradient Echo* (MPRAGE) sequences, repetition time (TR) 2.3 s, echo time (TE) 2.98 ms, flip angle (FA) 9°, field of view (FoV) 256×256 mm^2, yielding 160 slices with 1×1×1 mm^3 voxel size; (ii) four functional runs (three polar angle and one eccentricity stimuli) using single shot echo planar imaging (EPI) acquired in the axial plane orthogonal to the anterior commissure covering the occipital, temporal and frontal cortices, TR 2 s, TE 39 ms with a 128×128 imaging matrix, interslice time 76 ms, FA 90°, FOV 256×256 mm^2, yielding 26 slices with 2×2×2 mm^3 voxel size.

2.5 Data analysis

All image processing, cortical thicknesses and retinotopic mapping analyses were performed with BrainVoyager QX 2.2 (Brain Innovation, Maastricht, The Netherlands) (Figure II.2). Thickness values of each visual area were extracted with BVQX toolbox for MATLAB (R2008a, v.7.6.0, The MathWorks, USA). For details on statistical analysis see below.

2.5.1 Anatomical image processing

Structural data processing was as described in Geuze et al. (2008). Anatomical data were converted from DICOM to BrainVoyager's internal data format. To reduce the intensity variations caused by the magnetic field and RF-field inhomogeneities, we applied a bias-field mask (Dale, Fischl, & Sereno, 1999). The two high-resolution T1w anatomical images were averaged, to improve the signal-to-noise ratio. To clean the data we applied a "brain peeling" tool (Goebel, Esposito, & Formisano, 2006) to automatically "skull-strip" and remove the extra-cerebral voxels. The anatomical volumes were re-oriented in relation to the anterior and posterior commissure plane (AC–PC) and transformed to Talairach (TAL) (Talairach & Tournoux, 1988) coordinate system. Thereon, cortex was segmented using automatic segmentation routines (Kriegeskorte & Goebel, 2001) to create mesh representations of each hemisphere. To visualize all cortical activities, from gyri to sulci, we morphed each reconstructed hemisphere, and inflated it. Thereafter, we drew manually a cut along the calcarine fissure and flattened each hemisphere (Fischl, Sereno, & Dale, 1999). Meshes were inflated and flattened for surface map projection (Figure II.2).

2.5.2 Cortical thickness assessment

To allow an accurate segmentation of white matter-grey matter (WM–GM) and GM-cerebrospinal fluid (CSF) boundary and since 0.5 mm resolution is better suited to measure cortical thickness by the Laplace method (Jones, Buchbinder, & Aharon, 2000), TAL anatomical data were converted to high-resolution 0.5×0.5×0.5 mm iso-voxels using sinc interpolation iso-voxels (Geuze et al., 2008).

The subcortical structures and the ventricles were filled as WM. To sort white from grey matter voxels, we used an adaptive region growing step based on locally computed intensity histograms and calculated gradient information. Thereafter, the GM-CSF border was also segmented with a dilation process starting at the WM–GM border. Finally both borders were polished. The final step allowed for the definition of two boundaries translated into two different intensity values, defining the WM–GM and GM–CSF boundaries. The measurement of cortical thickness can lead to miscalculations, in both manual or automatic approaches (Fischl & Dale, 2000), due to the highly convoluted structure of the cortical surface. To reduce the error probability we used an automatic algorithm that applies the second-order partial differential Laplace's equation (Jones et al., 2000). The solution of Laplace's equation is equivalent to smooth transition of intensities between the two boundaries. The program calculates a gradient value for each voxel. Starting at each boundary voxel the algorithm continuously performs small steps along the gradient's direction at each point. The sum of the small step sizes performed between the two borders gives the cortical thickness values (Geuze et al., 2008). After the computation, a cortical thickness map was superimposed in the volumetric (VMR) data file, and then interpolated into the inflated cortical meshes (Figure II.2 A).

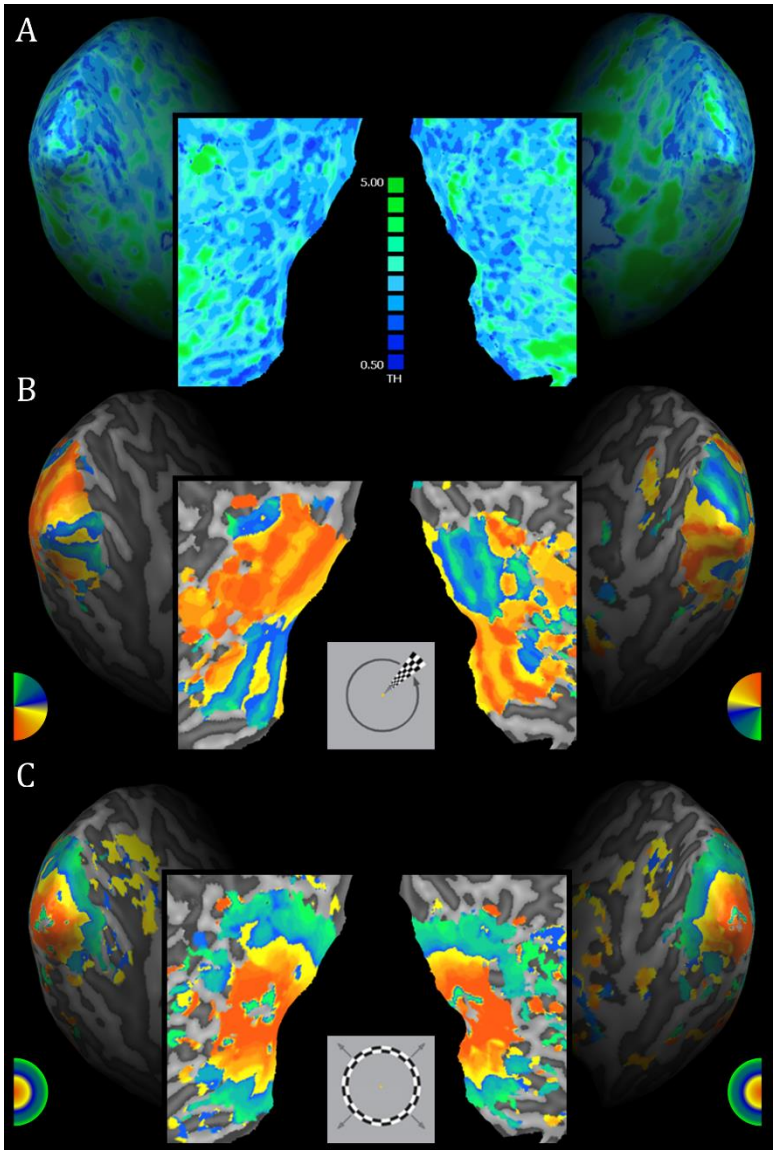

Figure II.2 Occipital inflated (*periphery*) and flattened (*centre*) meshes of a LHON patient (Table *2.1*.1, patient 14). (**A**) Cortical thickness map over the right and left occipital lobes. Due to the high convoluted structure of the cortex we used an automatic algorithm based on the second-order Laplace's equation after the pre-

segmentation of cortical tissues. The output is a pseudo-colour map overlaid on 3D meshes for visualization. Using BVQX tools we can export the thickness map of region-of-interest points. (**B**, **C**) Overlays of retinotopic maps in response to (**B**) polar angle stimuli (maps' angular position regarding the centre of gaze). The position is represented by a colour coded map; and (**C**) eccentricity representations (maps from posterior to anterior cortex as the stimuli move from centre (fovea) to periphery of the visual field).

2.5.3 Functional image processing

The fMRI datasets were pre-processed as follows: slice scan time correction, cubic-spline interpolation, small 3D interscan head motion correction with sinc estimation and interpolation, space domain 3D spatial smoothing (Gaussian filter of 2 mm) and temporal filtering (high pass, 2 cycles per run).

Polar angle maps were obtained from the average of three runs. Both polar angle and eccentricity maps were created based on linear regression analysis (HRF=5 s) and projected onto the TAL anatomical surfaces of each subject. The cross-correlation was calculated for each run, as a function of the time lag (in TR units, 2 s per lag). Lag values at each voxel were encoded in pseudocolours, voxels were included into the statistical map if $r>0.25$ and $p<0.05$.

2.5.4 Retinotopic mapping

Sereno et al. (1994) described an accurate method for delineating early visual areas, using information both from polar angle (Figure II.3 A) and eccentricity (Figure II.3 B) mapping experiments. The eccentricity and polar angle gradients define field sign maps that reflect the mirrored representation of visual areas. Hence, we obtained two-colour code mapping that established the lateral boundaries of the cortical visual areas (Figure II.3 C). Retinotopic areas V1, V2 and V3 were manually defined over flattened meshes for each subject in each hemisphere using BrainVoyager's surface drawing tools (Figure II.3 D). Obtained regions-of-interest (ROIs) were used as "masks" to the analysis of regional cortical thickness.

2.6 Statistical analysis

Each hemisphere was considered individually and a region-of-interest approach was applied. Using a Matlab (MATLAB R2008a, TheMathworks, USA) interface, ROIs were superimposed in the CT maps and the mean values of thickness for each area were calculated. To prevent outlier biases, an outlier removal criterion was considered. This approach consisted in the recalculation of the mean excluding the values deviating more than 3 standard deviations (*SD*) of the mean.

All statistical analyses were performed with IBM SPSS Statistics 20 for Windows (version 20, IBM Corp., Armonk, NY, USA). Parametric tests were performed subsequent to prior verification of normality assumption (non-parametric Kolmogorov–Smirnov test, $p>0.05$). The statistical analysis was based on the General Linear Model multivariate analysis of variance (MANOVA) for homologous ROIs between group comparisons. Further analysis was done in younger and older age cohorts separately (using a developmental cut-off criterion of 21 years, see Introduction). We also calculated Cohen's *d* from *F*-tests to evaluate the effect size of the MANOVA statistical results. In addition, to analyse the spatial specificity of effects we performed between groups independent samples *t*-tests for two anatomically-defined non-visual control regions, precentral and postcentral gyrus.

To analyse ROI thickness differences within each group, we used parametric GLM Repeated Measures ANCOVA (rmANCOVA), setting age as a metric covariate. We also performed a rmANCOVA adding gender as a putative confound. When the data did not meet the assumptions of sphericity, we used the epsilon value to choose the type of correction applied: the Huynh–Feldt (for $\varepsilon>0.75$) or the

Greenhouse–Geisser (for ε<0.75). Repeated Measures ANOVA was performed to assess group differences between visual areas' cortical thickness in each of the two age subgroups.

Multiple comparison *post-hoc* tests were based on the Bonferroni correction. We also checked for correlations between ROIs and between age and visual areas with Pearson's correlation analyses.

Moreover, we performed correlation analysis between retinal thickness measures across eccentricity rings (using OCT Stratus) and thickness of cortical visual areas. All statistical data are presented as the mean ±*SEM* (standard error of the mean). Two-tailed hypothesis testing was performed at a 0.05 significance level.

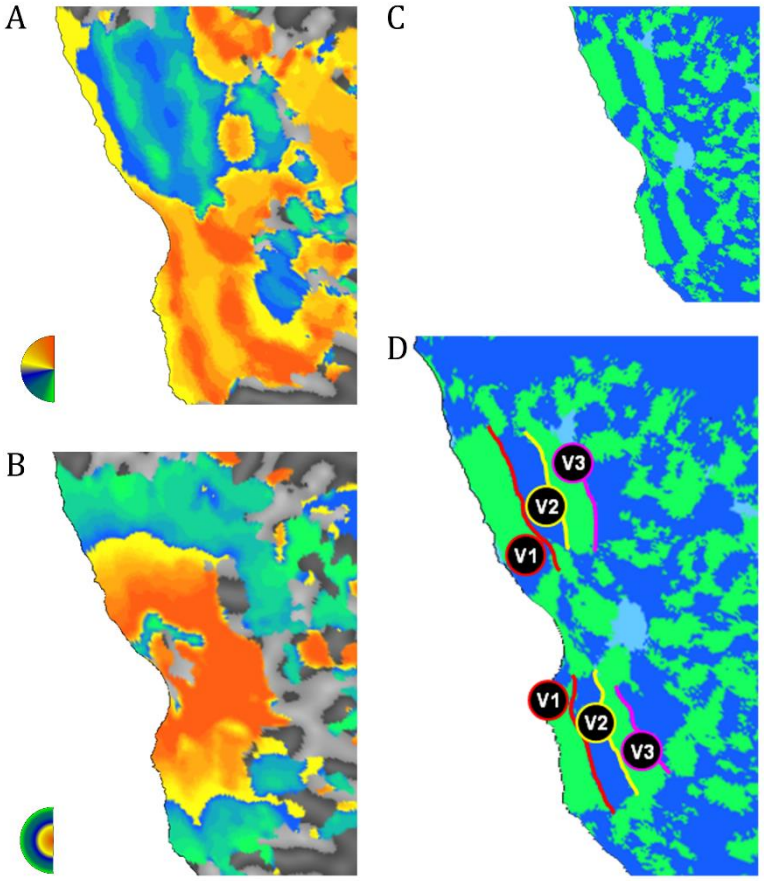

Figure II.3 Functional representation of early visual areas (Table II.1, patient 14). (**A**) Polar angle map. (**B**) Eccentricity map. (**C**) Visual field sign map. This technique provides a better approach to delineate the borders of visual areas. It is based on the local gradient (fastest rate of change direction) of each coordinate, polar angle and eccentricity. (**D**) Since adjacent areas alternate with a *mirror* and *nonmirror* representation of the visual field, corresponding to the horizontal and vertical meridians, with drawing tools, we can define the early visual areas as regions-of-interest for subsequent analysis.

3 RESULTS

Mean cortical thickness was calculated as the average of all vertices inside each functionally defined low-level visual areas V1, V2, and V3 (n=30 hemispheres for each group, see Figures II.2, II.3 and Material and Methods section). As in this genetic condition RGCs are specifically affected, we measured the integrity of the neural retina. We found decreased thickness of the neural retina in the central ring (p<0.05), when compared with controls (Figure II.1), showing the impact of silent RGC loss.

3.1 Cortical thickness in retinotopically defined areas

LHON carriers, bearing silent visual loss, have thicker extrastriate visual cortical areas as compared to controls.

Overall higher values of cortical thickness were observed for the LHON group (Figure II.4). Multivariate analysis MANOVA for visual areas V1, V2 and V3, showed a statistically significant difference between groups for extrastriate areas V2 and V3 (V2: $F(1,58)=7.309$, $p=0.009$, Cohen's $d=0.71$; V3: $F(1,58)=5.539$, $p=0.022$, Cohen's $d=0.62$). Between group comparisons of cortical thickness within the precentral ($t(58)=0.860$) and the postcentral gyrus ($t(58)=1.177$) showed no differences (n.s.), which suggests that we have indeed found a specific pattern of reorganization.

To specifically compare ROIs cortical thickness within each group, we performed rmANCOVA with visual areas' (V1, V2 and V3) cortical thickness as within-subject factor for each group (LHON and control) separately, and adding age as a possible confound.

As expected the control group showed no differences in the mean cortical thickness across visual areas. However, we found that cortical thickness differed significantly across visual areas in LHON carriers (Huynh–Feldt correction, $F(1.746,48.885)=6.059$, $p=0.006$), suggesting differential reorganization processes.

Post hoc tests using the Bonferroni correction, to identify the sources of the main effect, suggested that increased cortical thickness in LHON is due to the difference in thickness between both extrastriate areas V2 and V3 and V1 (V1–V2, $p=0.061$; V1–V3, $p=0.035$) with no evidence for differences between extrastriate regions (n.s.).

Even though the LHON carrier group was balanced in gender, the control group was not. Therefore we performed a Repeated Measures ANOVA, using group as between subject factor, each ROI as within subject factor and both gender and age as covariates. We found that there was neither an interaction between visual areas' cortical thickness with gender nor a gender effect (n.s.).

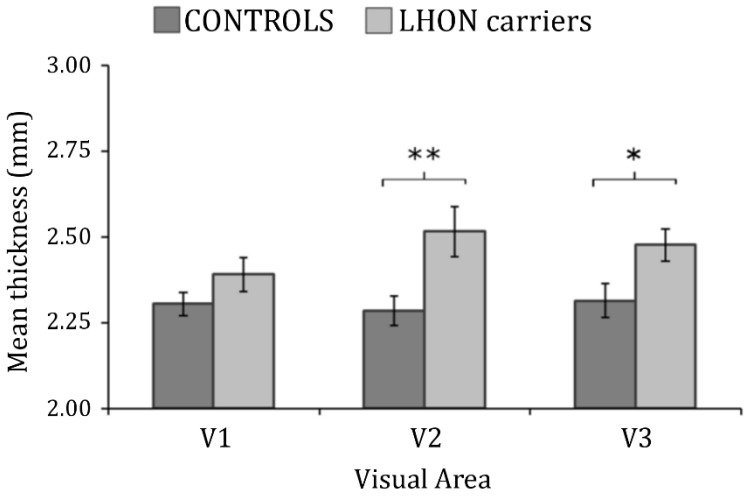

Figure II.4 Mean cortical thickness is significantly higher in LHON carrier group as compared to the CONTROL group, particularly in extrastriate areas V2 and V3. *$p<0.05$; and **$p<0.01$. Error bars correspond to ±1 *SEM*.

3.2 Group differences in cortical thickness across visual areas prior to and after the end developmental maturation

In rmANCOVA, setting age as covariate, both within control and LHON carrier groups a main effect of age was found ($F(1,28)=7.743$, $p=0.010$; $F(1,28)=24.060$, $p<0.001$, respectively). We have

also found in LHON a significant interaction between the effects of visual area mean thickness and age (Huynh–Feldt correction, $F(1.746,48.885)=3.371$, $p=0.049$), suggesting that a neural plasticity profile is consistent with the differential changes in striate vs. extrastriate regions in the group with silent retinal loss.

For this reason, and to probe early vs. post developmental (early adulthood) effects, we have divided each group into two subgroups using the developmental cut-off criterion of 21 years of age ("≤21" and ">21" subgroups).

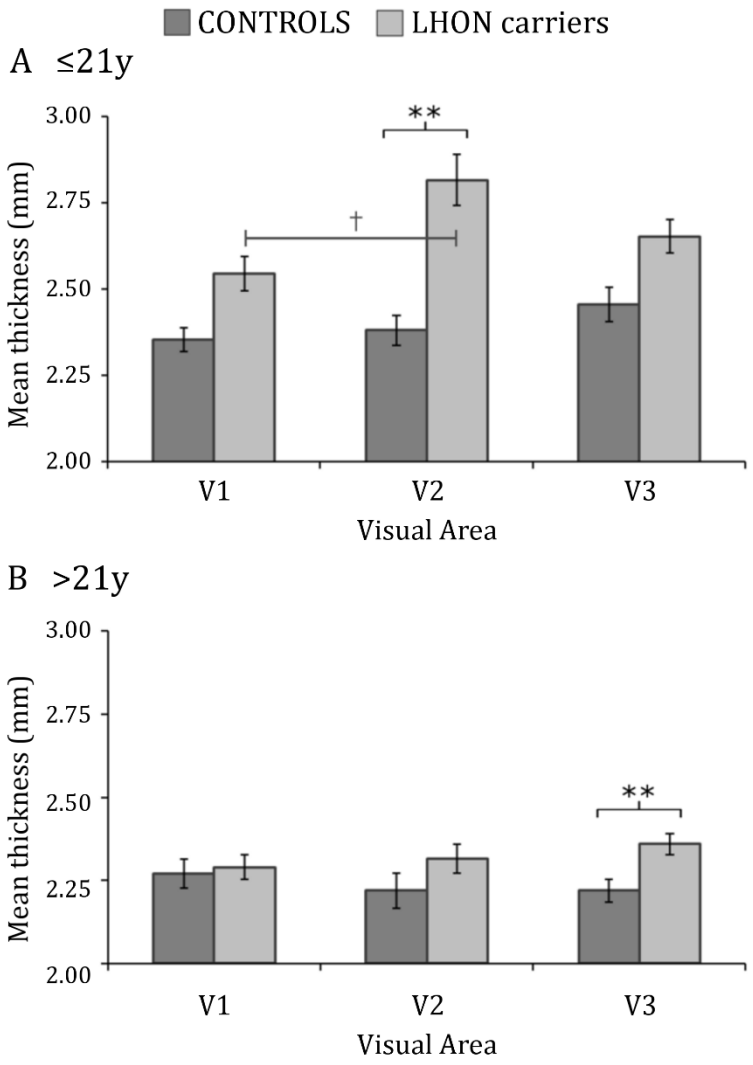

Figure II.5 Mean cortical thickness of each cortical visual area. Results are from a ROI-based analysis of CONTROL and LHON carrier groups with (**A**) age under 21 years; and (**B**) age over 21 years old. $^{**}p<0.01$, $\dagger p<0.053$ *post-hoc* Bonferroni pairwise comparisons. Error bars correspond to ±1 *SEM*.

By splitting each group into "≤21" and ">21" subgroups, we could then perform a group comparison across visual areas using (M)ANOVA. We confirmed that the mean cortical thickness in the LHON carrier group was, on average, higher than that in the control group both under and over 21 years. Figure II.5 shows that this difference is mainly caused by differences in V2 thickness across groups in younger subjects and in V3 in older subjects, suggesting that the differential role of extrastriate areas changes across age. ANOVA analysis showed indeed that there was a generally significant difference in cortical thickness between control and LHON carrier groups, in particular for V2 ($F(1,22)=8.312$, $p=0.009$, Cohen's $d=1.23$) below 21 years old, and in V3 ($F(1,34)=8.934$,

p=0.005, Cohen's d=1.03) in participants over 21 years old. In the two age subgroups we performed a rmANOVA analysis with V1, V2 and V3 (visual area cortical thickness) as the within-subject factors and group (LHON and control) as between-subject factor. We confirmed a significant effect of visual area specific to ≤21 subgroups (F(2,44)=3.288, p=0.047). The visual area effect in the younger age group can, as expected, be attributed mainly to the difference between visual area thickness in the LHON carrier group (F(2,22)=5.606, p=0.011, rmANOVA for ≤21 LHON group), particularly between areas V1 and V2 (Bonferroni post-hoc analysis, p=0.053). These differences were, absent in the >21 subgroup. Figure II.6 shows the examples of cortical thickness in a young LHON carrier and a control.

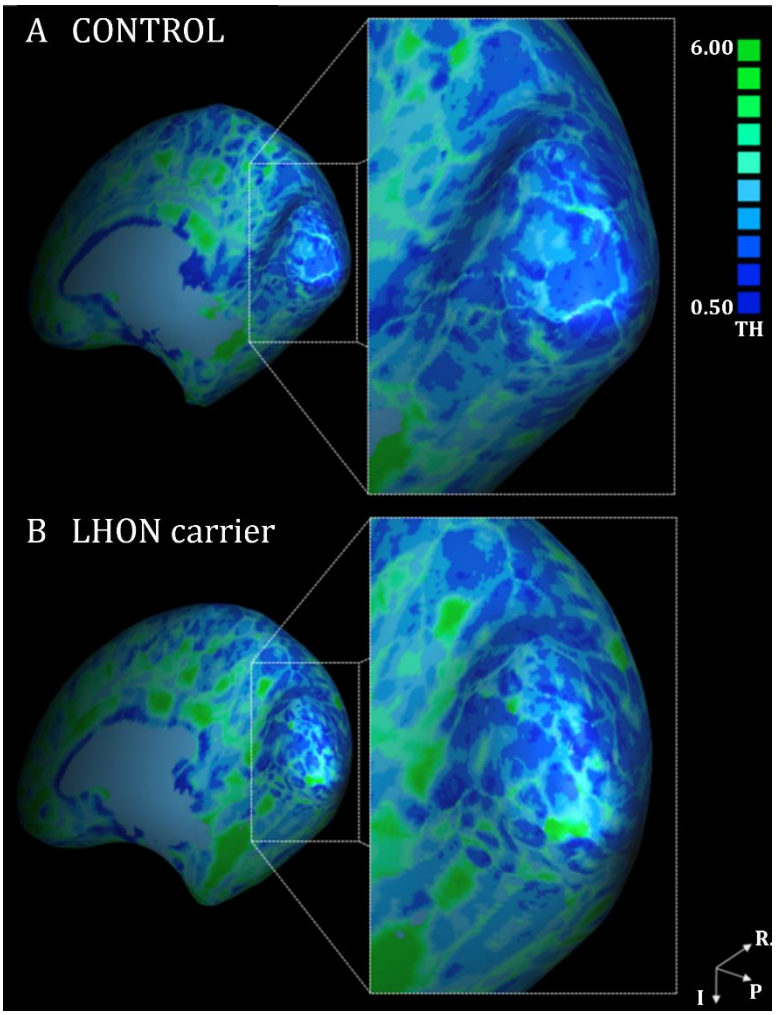

Figure II.6 Cortical thickness maps over inflated meshes. (**A**) CONTROL, 14 years; (**B**) LHON carrier, 17 years (Table *2.1.*1, patient 11). For visual inspection a pseudo-colour cortical thickness map is overlaid on inflated meshes (dark blue, 0.50 mm; light green, 6.00 mm). I, *inferior*; P, *posterior*; R, *right*.

3.3 Regression of cortical thickness with age

Pearson correlation coefficients were computed to identify any potential associations between each individual's visual areas' mean cortical thickness and also age in younger and older groups. We found interesting correlational patterns between visual areal thickness and age for control and LHON groups, both under and over 21 years (see Table II.2). A strong negative correlation was found in the ≤21 years control group between V3 and age, and in the ≤21 years LHON carrier group

between both V2 and V3 and age. Areas within the control group showed no significant early correlation patterns between areas (but only late – in adulthood), in contrast with the LHON group.

Table II.2 Pearson correlation coefficients computed between visual area thickness and age for controls and LHON carrier groups under and over 21 years old.

	CONTROLS				**LHON carriers**			
	mean thickness (mm)				mean thickness (mm)			
	V1	**V2**	**V3**	**Age** (y)	**V1**	**V2**	**V3**	**Age** (y)
Age ≤ 21y								
V1 mean thickness (mm)	1	n.s.	n.s.	n.s.	1	.688 (.013)	.841 (.001)	n.s.
V2 mean thickness (mm)		1	n.s.	n.s.		1	.763 (.004)	-.857 (<.001)
V3 mean thickness (mm)			1	-.772 (.003)			1	-.833 (.001)
Age (y)				1				1
Age > 21y								
V1 mean thickness (mm)	1	.557 (.016)	.529 (.024)	n.s.	1	n.s.	n.s.	n.s.
V2 mean thickness (mm)		1	.633 (.005)	n.s.		1	n.s.	n.s.
V3 mean thickness (mm)			1	n.s.			1	n.s.
Age (y)				1				1

Correlation analysis between global (all lamina) retinal thickness measures across eccentricity rings and cortical thickness measures in LHON carrier group showed only strong significant positive correlations between the most peripheral ring, where the neural retina is still largely preserved, and extrastriate areas V2 (r=0.582, p=0.023) and V3 (r=0.537, p=0.039). Retinal lamina analysis, separating fibre layers from neural cell body layers, using high resolution retinal imaging might be helpful in future studies to further elucidate the correlation patterns found in these patients.

4 DISCUSSION

We found that silent carriers of mitochondrial mutations affecting retinal ganglion cells (Carelli et al., 2007; Inglese, Rovaris, Bianchi, Comi, & Filippi, 2001) have profound changes in brain organization and plasticity, even when structural and functional neural loss is clinically silent and in the absence of scotomas.

Evidence for changed brain organization was expressed by increased cortical thickness that dominated in extrastriate areas throughout early visual development in LHON. This is to our knowledge, the first report describing positive plastic changes in cortical extrastriate regions in an asymptomatic condition leading to subcortical afferent loss.

It is possible that latent mitochondrial dysfunction leads to the here reported developmental plasticity. This interpretation is consistent with the knowledge that mitochondria play important roles in sculpting cytoarchitecture during the development of the nervous system and that the location or properties of mitochondria change in association with developmental processes (for a review see Mattson et al. (2008)). This interpretation is also in line with well documented role of mitochondria in controlling brain plasticity (for a review see Mattson et al. (2008)).

The fact that effect sizes of differences in thickness are larger in V2, which neighbours the region with direct afferent loss (V1) suggests that compensatory developmental plasticity is indeed a major mechanism underlying changes in thickness patterns across visual regions. Taken together, and since V1 suffers from impaired retinocortical input even in preclinical stages, these effects are consistent with a topological mechanism whereby neighbouring area V2 shows increased compensatory thickness. This effect seems to be specific given that non-visual areas (in precentral and postcentral gyrus regions) did not show changes.

Previous studies focused on plasticity related to visual scotomas or other acquired lesions (for a review see Wandell et al. (2009)). Our work addresses a very distinct form of plasticity because here we studied a preclinical carrier stage model of ganglion cell degeneration without visual symptoms in spite of the evidence for subtle psychophysical changes, and absence of scotomas.

Other studies have analysed the structural impact of long-term cortical deprivation and visual loss as assessed by the expected grey matter density changes in the correspondent visual representations (Boucard et al., 2009). These identified losses are to be expected from late stage clinically affected adults in whom neural degeneration and visual symptoms dominate over plasticity which is rather limited at such stages. This was the case of previous work using voxel-based morphometry (VBM) reporting brain degeneration in largely impaired patients with clinically installed LHON, with reduced GM volume in putative (non-retinotopically mapped) visual cortex, with damage in anterior visual pathways and in optic radiations (OR) (Barcella et al., 2010). In our study we addressed prelesional states of silent degeneration spanning developmental windows of available neural plasticity.

The long term period of brain adaptation that we could access largely exceeds the ones often available in experimental situations in which it becomes rather difficult to identify significant remapping or reorganization (Baseler et al., 2011). Accordingly, many studies cover a narrow age span, involve older age groups, and end stage disease. Consequently, neurodegeneration dominates and plastic reorganization mechanisms become barely noticeable (Bridge et al., 2010).

Our combination of retinotopic mapping with cortical thickness measures to identify differences in explicitly localized visual areas V1, V2 and V3 enabled interindividual matching and enhanced the power to detect plastic changes. These visual cortical areas do therefore seem to differently reorganize even in carriers of a mutation leading to abnormal physiology of retinal input cells.

Since maturation of cerebral structures also involves the pruning of neuronal processes, the lack of such pruning is also a potential explanation for the overall early increase in cortical thickness in LHON carriers (Low & Cheng, 2006; Tamnes et al., 2010). In our study, both LHON and control groups showed a pattern of age-dependent cortical thickness decrease which is consistent with previous studies (Salat et al., 2004). Moreover, our correlation results are in agreement with the notion that higher level regions tend to mature later and have a different pattern in LHON and control subjects.

In any case, the most relevant finding in this study was the early increased thickness of extrastriate V2 (and into a smaller extent, V3) representations. Early visual information processing is mainly routed through V1 (receiving direct input from the LGN) and V2 (Felleman & Van Essen, 1991; Kaas, Collins, & Chino, 2006). There is a strong functional relationship between V1 and V2 including feed-forward and feed-back projections (Sincich & Horton, 2005). The possibility that V2 can take over or compensate the loss of function in V1 is also supported by brain damage data from (Bridge et al., 2008).

As stated above our study goes beyond studies in humans or animal models with retinal induced-lesions because in our model there is no overt lesion (scotoma) in the carrier state. The placement of retinal laser lesions in cats and monkeys, monocularly or binocularly produces a lesion projection zone (LPZ) in V1. Neurons inside the LPZ gradually become responsive to stimuli presented to more peripheral, intact retinal locations (Baseler et al., 2009; Giannikopoulos & Eysel, 2006; Kaas et al., 1990). This plastic reorganization has significance but limited spatial extent, being restricted to few neighbouring millimetres in the cortex and may be mediated by local cortico-cortical connections (Calford, Wright, Metha, & Taglianetti, 2003; Darian-Smith & Gilbert, 1994). In spite of the differences between models, balance between growth and regressive factors is likely of equal

importance (Kaas et al., 2006). Accordingly, it is possible that in LHON patients alternative pathways are formed, strengthened and/or recruited, to rescue the functionality that is more rapidly lost in V1. Age dependency of this type of effects (Giedd et al., 1999) suggests that neuroplasticity is dependent on interaction between neurodevelopmental trajectories and neurodegenerative processes.

In sum, we found structural plastic reorganization, in a carrier state disease model of RGC degeneration that is specific to developmental stages, in the absence of visual scotomas. The fact that extrastriate areas show a distinct pattern or reorganization, with specific thickening of V2/V3 in this silent model of afferent loss, may provide clues for the development of effective strategies for rehabilitation.

5 CONCLUSION

These results show that sensory deprivation in early and asymptomatic ganglion cell degeneration leads to differential regional-specific plasticity of regions of human visual cortex. These effects are age dependent, suggesting that early developmental plasticity causes increased thickness in extrastriate cortex. Such unexpected extrastriate structural plasticity overcomes the cortical atrophy expected from neurodegeneration in particular in striate cortex. The evidence of specific structural plasticity of extrastriate area V2 in this model of silent afferent loss reveals the presence of robust compensatory mechanisms with implications for rehabilitation approaches.

6 ACKNOWLEDGMENTS

We do thank the LHON family, as well as all the control subjects that participated in this study. We also thank Carlos Ferreira and João Marques for the help with MRI scanning and Pedro Guimarães for MatLab scripting. We do thank João Pratas for the technical assistance in mtDNA analysis. This work was supported by the Portuguese Foundation for Science and Technology [grant numbers COMPETE, PTDC/SAU-NEU/68483/2006, PIC/IC/82986/2007, PTDC/SAU-ORG/118380, PEst-C/SAU/UI3282/2011 and individual fellowships SFRH/BD/64306/2009 to C.M., SFRH/BD/76013/2011 to O.C.A.].

7 CONFLICTS OF INTEREST

The authors report no conflicts of interest.

8 REFERENCES

Barcella, V., Rocca, M. A., Bianchi-Marzoli, S., Milesi, J., Melzi, L., Falini, A., … Filippi, M. (2010). Evidence for retrochiasmatic tissue loss in Leber's hereditary optic neuropathy. *Human Brain Mapping*, *31*(12), 1900–1906. doi:10.1002/hbm.20985

Baseler, H. A., Gouws, A., Haak, K. V., Racey, C., Crossland, M. D., Tufail, A., … Morland, A. B. (2011). Large-scale remapping of visual cortex is absent in adult humans with macular degeneration. *Nature Neuroscience*, *14*(5), 649–655. doi:10.1038/nn.2793

Baseler, H. A., Gouws, A., & Morland, A. B. (2009). The organization of the visual cortex in patients with scotomata resulting from lesions of the central retina. *Neuro-Ophthalmology*, *33*(3), 149–157. doi:10.1080/01658100903050053

Boucard, C. C., Hernowo, A. T., Maguire, R. P., Jansonius, N. M., Roerdink, J. B. T. M., Hooymans, J. M. M., & Cornelissen, F. W. (2009). Changes in cortical grey matter density associated with long-standing retinal visual field defects. *Brain*, *132*, 1898–1906. doi:10.1093/brain/awp119

Bridge, H., Hicks, S. L., Xie, J., Okell, T. W., Mannan, S., Alexander, I., … Kennard, C. (2010). Visual activation of extra-striate cortex in the absence of V1 activation. *Neuropsychologia*, *48*(14), 4148–4154.

Bridge, H., Thomas, O., Jbabdi, S., & Cowey, A. (2008). Changes in connectivity after visual cortical brain damage underlie altered visual function. *Brain*, *131*(6), 1433–1444. doi:10.1093/brain/awn063

Calford, M. B., Wright, L. L., Metha, A. B., & Taglianetti, V. (2003). Topographic plasticity in primary visual cortex is mediated by local corticocortical connections. *The Journal of Neuroscience*, *23*(16), 6434–6442.

Carelli, V., La Morgia, C., Iommarini, L., Carroccia, R., Mattiazzi, M., Sangiorgi, S., … Valentino, M. L. (2007). Mitochondrial optic neuropathies: how two genomes may kill the same cell type? *Bioscience Reports*, *27*(1-3), 173–184. doi:10.1007/s10540-007-9045-0

Dale, A. M., Fischl, B., & Sereno, M. I. (1999). Cortical surface-based analysis. I:Segmentation and surface reconstruction. *Neuroimage*, *9*(2), 179–194. doi:10.1006/nimg.1998.0395

Darian-Smith, C., & Gilbert, C. D. (1994). Axonal sprouting accompanies functional reorganization in adult cat striate cortex. *Nature*, *368*(6473), 737–740.

Engel, S. A., Rumelhart, D. E., Wandell, B. A., Lee, A. T., Glover, G. H., Chichilnisky, E. J., & Shadlen, M. N. (1994). fMRI of human visual cortex. *Nature*, *369*, 525.

Eysel, U. T. (2009). Adult cortical plasticity. In L. R. Squire (Ed.), *Encyclopedia of Neuroscience* (1st ed., pp. 141–147). Academic Press.

Felleman, D. J., & Van Essen, D. C. (1991). Distributed hierarchical processing in the primate cerebral cortex. *Cerebral Cortex*, *1*(1), 1–47.

Fischl, B., & Dale, A. M. (2000). Measuring the thickness of the human cerebral cortex from magnetic resonance images. *Proceedings of the National Academy of Science*, *97*(20), 11050–11055. doi:10.1073/pnas.200033797

Fischl, B., Sereno, M. I., & Dale, A. M. (1999). Cortical surface-based analysis: II: inflation, flattening, and a surface-based coordinate system. *Neuroimage*, *9*(2), 195–207. doi:10.1006/nimg.1998.0396

Geuze, E., Westenberg, H. G. M., Heinecke, A., de Kloet, C. S., Goebel, R., & Vermetten, E. (2008). Thinner prefrontal cortex in veterans with posttraumatic stress disorder. *Neuroimage*, *41*(3), 675–681. doi:10.1016/j.neuroimage.2008.03.007

Giannikopoulos, D. V., & Eysel, U. T. (2006). Dynamics and specificity of cortical map reorganization after retinal lesions. *Proceedings of the National Academy of Sciences*, *103*(28), 10805–10810. doi:10.1073/pnas.0604539103

Giedd, J. N., Blumenthal, J., Jeffries, N. O., Castellanos, F. X., Liu, H., Zijdenbos, A., … Rapoport, J. L. (1999). Brain development during childhood and adolescence: a longitudinal MRI study. *Nature Neuroscience*, *2*(10), 861–863. doi:10.1038/13158

Goebel, R., Esposito, F., & Formisano, E. (2006). Analysis of functional image analysis contest (FIAC) data with brainvoyager QX: from single-subject to cortically aligned group general linear model analysis and self-organizing group independent component analysis. *Human Brain Mapping*, *27*(5), 392–401. doi:10.1002/hbm.20249

Grazina, M. M., Diogo, L. M., Garcia, P. C., Silva, E. D., Garcia, T. D., Robalo, C. B., & Oliveira, C. R. (2007). Atypical presentation of Leber's hereditary optic neuropathy associated to mtDNA 11778G>A point mutation - A case report. *European Journal of Paediatric Neurology*, *11*(2), 115–118. doi:10.1016/j.ejpn.2006.11.015

Inglese, M., Rovaris, M., Bianchi, S., Comi, G., & Filippi, M. (2001). Magnetization transfer and diffusion tensor MR imaging of the optic radiations and calcarine cortex from patients with Leber' s hereditary optic neuropathy. *Journal of the Neurological Sciences*, *188*(1), 33–36.

Jones, S. E., Buchbinder, B. R., & Aharon, I. (2000). Three-dimensional mapping of cortical thickness using Laplace's Equation. *Human Brain Mapping*, *11*(1), 12–32. doi:10.1002/1097-0193(200009)11:1<12::AID-HBM20>3.0.CO;2-K

Kaas, J. H., Collins, C. E., & Chino, Y. M. (2006). Plasticity of retinotopic maps in visual cortex of cats and monkeys after lesions of the retina or primary visual cortex. In *Plasticity in the Visual System: from genes to circuits* (pp. 205–227). Springer.

Kaas, J. H., Krubitzer, L. A., Chino, Y. M., Langston, A. L., Polley, E. H., & Blair, N. (1990). Reorganization

of retinotopic cortical maps in adult mammals after lesions of the retina. *Science*, *248*(4952), 229–231.

Kirkman, M. A., Korsten, A., Leonhardt, M., Dimitriadis, K., De Coo, I. F., Klopstock, T., … Yu-Wai-Man, P. (2009). Quality of life in patients with leber hereditary optic neuropathy. *Investigative Ophthalmology & Visual Science*, *50*(7), 3112–3115. doi:10.1167/iovs.08-3166

Kirkman, M. A., Yu-Wai-Man, P., Korsten, A., Leonhardt, M., Dimitriadis, K., De Coo, I. F., … Chinnery, P. F. (2009). Gene-environment interactions in Leber hereditary optic neuropathy. *Brain*, *132*(9), 2317–2326. doi:10.1093/brain/awp158

Kriegeskorte, N., & Goebel, R. (2001). An efficient algorithm for topologically correct segmentation of the cortical sheet in anatomical MR volumes. *Neuroimage*, *14*(2), 329–346. doi:10.1006/nimg.2001.0831

Low, L. K., & Cheng, H.-J. (2006). Axon pruning: an essential step underlying the developmental plasticity of neuronal connections. *Philosophical Transactions of the Royal Society of London B: Biological Sciences*, *361*(1473), 1531–1544. doi:10.1098/rstb.2006.1883

Man, P. Y. W., Griffiths, P. G., Brown, D. T., Howell, N., Turnbull, D. M., & Chinnery, P. F. (2003). The epidemiology of Leber hereditary optic neuropathy in the North East of England. *The American Journal of Human Genetic*s, *72*(2), 333–339. doi:10.1086/346066

Mattson, M. P., Gleichmann, M., & Cheng, A. (2008). Mitochondria in neuroplasticity and neurological disorders. *Neuron*, *60*(5), 748–766. doi:10.1016/j.neuron.2008.10.010

Newman, N. J., & Biousse, V. (2004). Hereditary optic neuropathies. *Eye*, *18*(11), 1144–1160. doi:10.1038/sj.eye.6701591

Salat, D. H., Buckner, R. L., Snyder, A. Z., Greve, D. N., Desikan, R. S. R., Busa, E., … Fischl, B. (2004). Thinning of the cerebral cortex in aging. *Cerebral Cortex*, *14*(7), 721–730. doi:10.1093/cercor/bhh032

Sereno, M. I., Dale, A. M., Reppas, J. B., Kwong, K. K., Belliveau, J. W., Brady, T. J., … Tootell, R. B. H. (1995). Borders of multiple visual areas in humans revealed by functional magnetic resonance imaging. *Science*, *268*, 889–893.

Sereno, M. I., McDonald, C. T., & Allman, J. M. (1994). Analysis of retinotopic maps in extrastriate cortex. *Cerebral Cortex*, *4*, 601–620.

Sincich, L. C., & Horton, J. C. (2005). The circuitry of V1 and V2: integration of color, form, and motion. *Annual Review of Neuroscience*, *28*, 303–326. doi:10.1146/annurev.neuro.28.061604.135731

Talairach, J., & Tournoux, P. (1988). *Co-planar stereotaxic atlas of the human brain - 3-dimensional proportional system: an approach to cerebral imaging* (1st ed.). Thieme Medical Publishers.

Tamnes, C. K., Østby, Y., Fjell, A. M., Westlye, L. T., Due-Tønnessen, P., & Walhovd, K. B. (2010). Brain maturation in adolescence and young adulthood: regional age-related changes in cortical thickness and white matter volume and microstructure. *Cerebral Cortex*, *20*(3), 534–548. doi:10.1093/cercor/bhp118

Wandell, B. A., & Smirnakis, S. M. (2009). Plasticity and stability of visual field maps in adult primary visual cortex. *Nature Reviews Neuroscience*, *10*(12), 873–884. doi:10.1038/nrn2741

Ch. II. 2

Genetically induced impairment of retinal ganglion cells at the axonal level is linked to extrastriate cortical plasticity

Catarina Mateus*, **Otília C. d'Almeida***,
Aldina Reis, Eduardo Silva, Miguel Castelo-Branco

**C. Mateus and O. C. d'Almeida contributed equally to this work.*
All cortical MRI data processing and analysis were exclusively performed by O. C. d'Almeida, and are not described elsewhere.

ABSTRACT

Leber hereditary optic neuropathy (LHON) is a maternally inherited mitochondrial disorder, which leads to initially silent visual loss due to retinal ganglion cell (RGC) degeneration. We aimed to establish a link between features of retinal progressive impairment and putative cortical changes in a cohort of 15 asymptomatic patients harbouring the 11778G>A mutation with preserved visual acuity and normal ocular examination. To study plasticity evoked by clinically silent degeneration of RGC we only studied mutation carriers. We phenotyped preclinical silent degeneration from the psychophysical, neurophysiological and structural points of view to understand whether retinal measures could be related to cortical reorganization, using pattern electrophysiology, chromatic contrast sensitivity and high-resolution optical coherence tomography to measure macular, RGC nerve fibre layer as well as inner/outer retinal layer thickness. We then performed correlation analysis of these measures with cortical thickness estimates in functionally mapped retinotopic visual cortex. We found that compensatory cortical plasticity occurring in V2/V3 is predicted by the swelling (indicating deficits of axonal transport and intracellular oedema) of the macular RGC axonal layer. Increased cortical thickness (CT) in V2 and V3 was observed in peripheral regions, like visual field loss, in these mutation carriers. CT was a very discriminative measure between carriers and controls, as revealed by ROC analysis. Importantly, the substantial cortical reorganization that occurs in the carrier state can be used to provide statistical discrimination between carriers and controls to a level that is similar to measures of retinal dysfunction. We conclude that peripheral cortical compensatory plasticity in early visual areas V2/V3 may be triggered by pathology in peripheral RGC axons in combination with potential developmental changes.

Mateus, C.*, **d'Almeida, O. C.***, Reis, A., Silva, E., & Castelo-Branco, M. (2016). Genetically induced impairment of retinal ganglion cells at the axonal level is linked to extrastriate cortical plasticity. *Brain Structure and Function*, *221*(3), 1767-1780. doi:10.1007/s00429-015-1002-2 (*equal contribution)

1 INTRODUCTION

Leber hereditary optic neuropathy (LHON) is a maternally inherited disease associated with mitochondrial DNA (mtDNA) pathogenic point mutations (Carelli et al., 2007). This optic neuropathy is the most frequent mitochondrial disorder (Chinnery et al., 2000). In over 90% of cases it is due to three mtDNA point mutations, respectively, at positions 11778G>A, 14484T>C and 3460G>A, affecting complex I subunit genes of the mitochondrial respiratory chain (Mackey et al., 1996; Man, Turnbull, & Chinnery, 2002; Newman, 2005). LHON leads to degeneration of retinal ganglion cells and their axons in the optic nerve, with a selective loss of the smaller-caliber fibres of the papillomacular bundle in early disease stages (Carelli, Ross-Cisneros, & Sadun, 2004; Sadun, Win, Ross-Cisneros, Walker, & Carelli, 2000).

In a pre-clinical phase, swelling of retinal nerve fibre layer (RNFL) may occur (Carelli et al., 2004; Yu-Wai-Man, Griffiths, Hudson, & Chinnery, 2009) as objectively documented by optical coherence tomography (OCT). In this sense, unaffected carriers (in the pre-clinical phase) may show a thickened RNFL in temporal and inferior quadrants (Savini et al., 2005). Retinal ganglion cell axons display a particular sensitivity to mitochondrial dysfunction. Accordingly, because of loss of mitochondrial complex I function and RNFL (which is rich in mitochondria) oedema occurs due to failure of axonal transport mechanisms and stasis with also swollen mitochondria (E. Nikoskelainen, Sogg, Rosenthal, Friberg, & Dorfman, 1977; Rojas & Gonzalez-Lima, 2010). The fact that oedema is intracellular rather than extracellular renders that it is often labelled as pseudoedema. It is indeed an unusual feature of this disease that axons initially show swelling instead of thinning due to the unique pathophysiology. On psychophysical testing, carriers also show evidence for subtle impairment of optic nerve function, as assessed by chromatic and achromatic contrast sensitivity (CS) (Quiros et al., 2006; Sadun et al., 2006; Ventura et al., 2007).

After clinical onset, the RNFL gradually degenerates and the endpoint is usually optic nerve atrophy with permanent severe loss of central vision and relative sparing of papillary light responses (Carelli et al., 2004). Some studies using magnetic resonance (MR) spectroscopy have found a non selective and isolated involvement of the optic nerve and reported abnormal mitochondrial energy metabolism in the occipital lobe of clinically affected patients (Barbiroli et al., 1995; Cortelli et al., 1991; Lodi et al., 2002). Using voxel-based morphometry (VBM), (Barcella et al., 2010) have described a significant reduced grey matter volume in bilateral visual cortex, and reduced white matter volume in optic chiasm, optic tract and areas located in optic radiations in LHON patients with well-established retinal degeneration and long-term clinical symptoms.

Interestingly, in the pre-symptomatic stage, cortical thickness may actually be increased (d'Almeida, Mateus, Reis, Grazina, & Castelo-Branco, 2013), suggesting early compensatory plasticity that is lost when the disease becomes clinically established. Cortical plasticity is here defined as *"the capacity of the brain to adapt to changing demands by altering its structure"* (Lövdén, Bäckman, Lindenberger, Schaefer, & Schmiedek, 2010; Lövdén, Wenger, Mårtensson, Lindenberger, & Bäckman, 2013). In other words, some studies show that the brain is able to reorganize in response to changed sensory experience (Wandell & Smirnakis, 2009). Recent studies have further established a link between structural brain plasticity and changes in cortical thickness (Engvig et al., 2010; Lövdén et al., 2013). Damage of peripheral input may indeed lead to cortical reorganization (Rosa, Silva, Ferreira, Murta, & Castelo-Branco, 2013). In our previous study (d'Almeida et al., 2013), we used magnetic resonance imaging (MRI) to measure cortical thickness and functional MRI retinotopic mapping to define functionally cortical visual areas V1, V2 and V3 in unaffected LHON mutation carriers (pre-clinical phase). Interestingly, we found that cortical thickness, in particular in extrastriate regions (V2, V3), was significantly higher in LHON carriers as compared to age-matched

controls. This suggests that in the pre-symptomatic stage, cortical thickness may actually be increased due to early compensatory plasticity that is lost when the disease becomes clinically established.

The major aim of this study was to test whether a link can be established between retinal ganglion cell impairment, as measured by high-resolution retinal imaging and visual field testing in Leber hereditary optic neuropathy and such cortical compensatory plasticity in extrastriate cortex, at central and peripheral levels. All patients were mutation carriers (pre-clinical phase). Therefore, RGC degeneration is present, affecting their visual function, such as chromatic contrast sensitivity and peripheral visual function, at a subtle pre-clinical level.

In summary, we analysed the visual and retinocortical phenotype, at central and peripheral levels, of asymptomatic genetically characterized LHON patients (unaffected carriers from the same pedigree) which also allowed the comparison of retinal and cortical markers in statistical classification of the LHON carrier status. We found that the RNFL integrity predicts the cortical status in distinct retinotopically mapped visual areas.

2 METHODS

2.1 Ethics statement

This study and all procedures were reviewed and approved by the Ethics Commission of the Faculty of Medicine of the University of Coimbra (*"Comissão de Ética da Faculdade de Medicina da Universidade de Coimbra"*) and were conducted in accordance with the Declaration of Helsinki. Written informed consent was obtained from participants older than 18 years of age and from parents/guardians in the case of participants younger than 18 years of age after procedures of the study were fully explained.

2.2 Participants

A cohort of 15 asymptomatic LHON carriers from two generations of the same pedigree [mean age±*SD*=29.2±13.4 years; age range (8–47)] was included in the study and was compared with an age-matched control group [n=24; mean age±*SD*=31.3±13.5 years; age range (7–54)]. Asymptomatic LHON patients underwent genetic analysis and the presence of mtDNA 11778G>A mutation was confirmed in all family members (homoplasmic in eleven and heteroplasmic in four participants) (demographic characteristics are summarized in Table II.3). All participants were submitted to a complete ophthalmological examination, including best-corrected visual acuity (VA; decimal scale), slit lamp biomicroscopy, ocular tension measurement (Goldmann applanation tonometer) and fundus examination (Goldman lens). LHON carriers presented a normal ocular examination, good visual acuity (mean±*SD*=1.1±0.1) and no fundus changes. In spite of the absence of a clinical diagnosis, visual field deficits were found. According to Octopus v311 normative database, we found only 6 ''normal'' visual fields (20% of the total sample) in terms of global measures; the remaining 80% showed a mean defect (MD) and/or a loss variance (LV) outside the normal range, with a constant pattern of paracentral defects (see Table II.3 and Figure II.7 for representative visual field defects). Exclusion criteria included retinal and neurological diseases, diabetes even in the absence of retinopathy, significant media opacities, pseudophakic and aphakic eyes and high ammetropies (sphere>±4D; cylinder>±2D).

Table II.3 Demographic characteristics and clinical data of LHON carriers group. M, *male*; F, *female*; RE, *right eye*; LE, *left eye*; MD, *mean defect*; LV, *loss variance*.

Patient	mtDNA 11778G>A Mutation	Heteroplasmic mutational load (%)	Age (years)	Gender	Visual Acuity		Visual Field MD (dB)		Visual Field LV (dB²)		Visual Field Ring 1 (dB)	Visual Field Ring 2 (dB)
					RE	LE	RE	LE	RE	LE	Mean	Mean
1	homoplasmic		47	M	1.2	1.2	-0.7	0.7	3.8	3.3	30.41	26.61
2	heteroplasmic	80.6	46	F	1.0	1.0	1.8	1.7	5.2	4.4	29.16	26.29
3	homoplasmic		43	F	1.0	1.0	2.8	3.8	4.9	10.3	28.31	23.38
4	homoplasmic		41	M	1.2	1.2	4.2	4.0	4.0	8.3	26.35	22.99
5	homoplasmic		40	F	1.0	1.0	4.0	4.4	3.1	6.6	26.63	23.15
6	homoplasmic		39	F	1.0	1.0	5.0	3.8	2.1	7.9	25.06	22.92
7	homoplasmic		37	F	1.2	1.2	1.8	0.9	5.2	5.1	30.06	25.90
8	heteroplasmic	78.8	30	F	1.2	1.2	7.0	7.8	10.8	9.1	21.72	20.98
9	heteroplasmic	78.0	21	M	1.2	1.2	5.5	7.8	32.3	40.4	29.56	20.40
10	homoplasmic		22	F	1.2	1.2	3.9	6.6	9.2	26.7	27.03	22.97
11	homoplasmic		17	M	1.2	1.2	3.3	5.0	10.9	24.1	29.69	23.12
12	homoplasmic		19	M	1.0	1.2	2.8	5.2	10.5	15.2	28.94	23.98
13	homoplasmic		10	M	1.0	1.0	4.1	6.9	6.3	13.7	28.72	22.06
14	heteroplasmic	67.0	18	F	1.2	1.2	7.8	7.6	9.2	6.7	23.72	20.69
15	homoplasmic		8	M	1.0	1.2	3.1	3.1	9.9	7.9	28.47	25.26

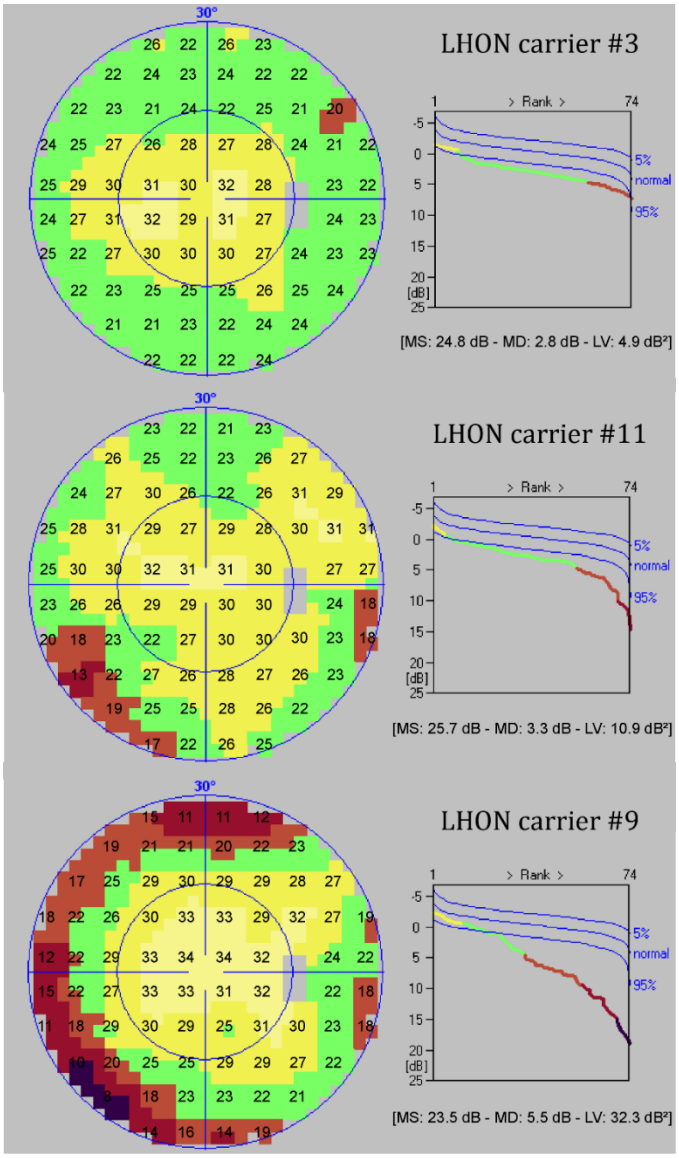

Figure 7 Representative visual field perimetric maps (colour maps depict decibel scale) of LHON carriers. Note a constant pattern of a peripheral defect in visual fields with a relatively preserved sensitivity of central locations as illustrated in the cumulative defect curves.

2.3 Automated static perimetry

In this study, standard automated perimetry (SAP) test was performed, using a commercially available system Octopus version 311 (Haag-Streit AG, Germany) (Reis et al., 2013). Patients were instructed to fixate the central point and report the presence of bright targets, which could appear in 76 different locations within 30° of visual field (program 32, stimulus size: Goldmann III; stimulus duration: 100 ms). Threshold data were obtained with the TOP (tendency oriented perimetry) strategy (Morales, Weitzman, & de la Rosa, 2000), in which every answer at a particular point is taken into account in the adjustments of the neighbouring locations.

The test was performed under monocular conditions, being the first eye tested chosen in a random manner. Performance reliability was assessed by computing false-positive and -negative errors (results with false-positive and -negative errors ≥33% were excluded). Fixation loss was monitored during the testing, with an electronic eye fixation control system that interrupts the examination and notifies if participant is not fixating. Testing restarts thereafter. Global parameters as mean sensitivity (MS), mean defect (MD) and loss variance (LV) were analysed. Mean sensitivity of two concentric rings (ring 1, 15° of radius; ring 2, 30° of radius) was also assessed. According to the normative data from the device, a normal visual field shows a MD between -2 and +2 dB and a LV<6 dB^2.

2.4 Cambridge colour test

We have probed chromatic contrast sensitivities using a computer-controlled psychophysical method, a slightly modified version of Cambridge colour test (CCT; Cambridge Research Systems Lda., CRS, Rochester, UK) (Mateus et al., 2013; Silva et al., 2005). This technique uses three parallel, randomly interleaved staircases, corresponding to simultaneous assessment of the three cone confusion axes (protan, deutan and tritan) modulated in the CIE 1976 u'v' colour space (Trivector version of the test). Each staircase was composed of 11 reversals and the mean of the last 7 reversals was taken as the threshold estimate. The test was performed monocularly (the first eye tested was randomly chosen). Participants had to fixate a screen (21-inch monitor; viewing distance – 180 cm) with a static pattern of circles of various sizes and luminances with superimposed chromatic contrast defining a Landolt-like C-shaped ring (gap size 1.6°; outer diameter 7.6°; inner diameter 3.81°), which forces the participant to use specific colour cues. Six different luminance noise levels were randomly assigned to these patches (8–18 cd/m^2 in steps of two units). Participants were instructed to indicate one out of four possible gap positions (up, down, left or right) of the Landolt C stimulus, by pressing one of four buttons of the response box. Psychophysical thresholds were expressed in CIE 1976 u'v' colour space units. Note that high chromatic thresholds relate to low contrast sensitivity.

2.5 Pattern electroretinogram

We recorded the pattern electroretinogram (PERG; RETIport32, Roland Consult, Germany), which provides information about macular and ganglion cell function, following the ISCEV standards (Bach et al., 2013) and using DTL fibres as recording electrodes. The stimulus consisted in a reversal black and white checkerboard pattern (4.3 reversals per second, rps), with a contrast of 97% and a check size of 0.74°. Stimulus was presented binocularly at a 20-inch monitor (frame rate 60 Hz), at a viewing distance of 1 m. Observers were instructed to fixate at a small red cross in the centre of the screen and fixation was checked by means of online video-monitoring during recording sessions. Refractive errors were corrected for the test distance, when applicable.

The active voltage range of bioelectrical signal was ±100 μV. Signals were amplified with a gain of 100,000 and bandpass filtered (1–100 Hz). We collected 200 artefact-free sweeps to obtain an average waveform (artefact rejection level of 5%). To confirm reproducibility, two PERG measurements were taken. Finally, the amplitudes (μV) and peak time values (ms) of responses for each P-50 and N-95 components and the PERG ratio (N-95 amplitude divided by P-50 amplitude) were analysed.

2.6 Spectral-domain optical coherence tomography (SD-OCT)

OCT (optical coherence tomography) has histology-level resolution, given the optical accessibility of the retina. In this study, we have used Spectralis SD-OCT software version 5.3.2 (Heidelberg Engineering, Heidelberg, Germany) to obtain peripapillary RNFL and retinal thickness (RT) measurements (Laguna et al., 2013). Image acquisition was performed in high-speed mode, providing an axial resolution of 7 μm and a transversal resolution of 14 μm. Participants were instructed to look at an internal fixation light and the stability of the fixation was monitored by an incorporated infrared camera. Concerning RNFL measurements, a circular 3.5 mm scan centred on the optic nerve head was used (768 A-scans) and peripapillary RNFL thickness sectors were evaluated [temporal (315°–45°), superior (45°–135°), nasal (135°–225°) and inferior quadrant (225°–315°)].

We also obtained cross-sectional images centred on the macula, scanning a 20°×20° pattern, with 25 horizontal raster scans (distance between B-scans: 245 μm) and 512 A-scans (ART mode: 20 images averaged). Macular retinal thickness was calculated by computing the distance between the signal from vitreoretinal interface and the signal from basement membrane of the retinal pigment epithelium (RPE), Bruch's membrane complex. We used the RT map analysis protocol, which displays retinal thickness in nine ETDRS subfields. For analysis three concentric rings were considered: ring 1 (1 mm of diameter), ring 2 (3 mm) and ring 3 (6 mm).

Inner retinal layer (IRL) thickness measurements (including nerve fibre layer, ganglion cells layer, inner plexiform layer and inner nuclear layer) were also determined through manual segmentation (Aaker et al., 2010). This was accomplished using Heidelberg software by setting the inner limit of the IRL at the internal limiting membrane and the outer limit at the outer border of the inner nuclear layer (see Figure II.8). We also performed a manual segmentation of macular RNFL thickness (first layer of IRL). Subtracting IRL thickness from the global retinal thickness, we obtained the outer retinal layer thickness (ORL) (including outer plexiform layer, outer nuclear layer, outer limiting membrane, layer of rods and cones and RPE). For IRL, ORL and macular RNFL analysis, we also considered the three rings described above.

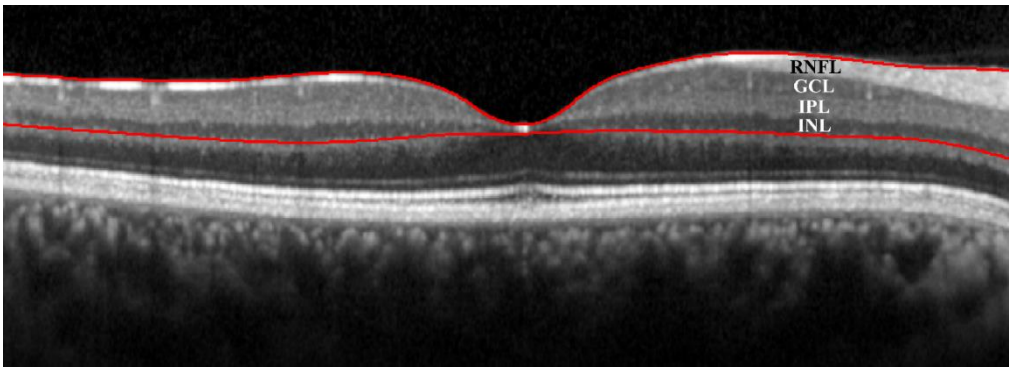

Figure II.8 Spectral domain OCT image of a section through the fovea of the right eye of a control subject showing the segmented inner retinal layer (IRL) (red lines). The following layers of the IRL are shown: retinal nerve fiber layer (RNFL), ganglion cell layer (GCL), inner plexiform layer (IPL) and inner nuclear layer (INL).

In summary, we collected novel high-resolution imaging data (OCT), novel psychophysical and electrophysiological measures for the retinocortical correlations. Given that most of cortical imaging data were reported before (d'Almeida et al., 2013), we only briefly present them here.

2.7 Magnetic resonance imaging (MRI)

The MRI data were acquired in a 3T scanner (Siemens Magnetom TrioTim 3T, Erlangen, Germany) at the Portuguese Brain Imaging Network, with a 12-channel head coil. For each participant we obtained two 9-min long T1-weighted three-dimensional *magnetization-prepared rapid acquisition gradient-echo* (MPRAGE) sequences, repetition time (TR) 2.3 s, echo time (TE) 2.98 ms, flip angle (FA) 9°, field of view (FoV) 256×256 mm^2, yielding 160 slices with 1×1×1 mm^3 voxel size and also four functional runs (three polar angle and one eccentricity stimuli) using single-shot echo-planar imaging (EPI) acquired in the axial plane orthogonal to the anterior commissure covering the occipital, temporal and frontal cortices, TR 2 s, TE 39 ms with a 128x128 imaging matrix, interslice time 76 ms, FA 90°, FoV 256×256 mm^2, yielding 26 slices with 2×2×2 mm^3 voxel size.

The stimuli presented consisted in a polar angle encoding paradigm comprising a rotating (anticlockwise) black and white checkered wedge flickering at 8 Hz (48 s full cycle, 4 cycles/scan, three scans); and an eccentricity mapping paradigm, using an expanding black and white checkered ring flickering at 8 Hz (48 s each full expansion, 4 expansions/scan, one scan), while the participant was instructed to fixate an orange-coloured central point (Figure II.9 A,B). The stimuli spanned 23°×23° of visual angle (diameter). Eye fixation was only monitored online using a video screen which was sufficient to ensure good quality retinotopic maps.

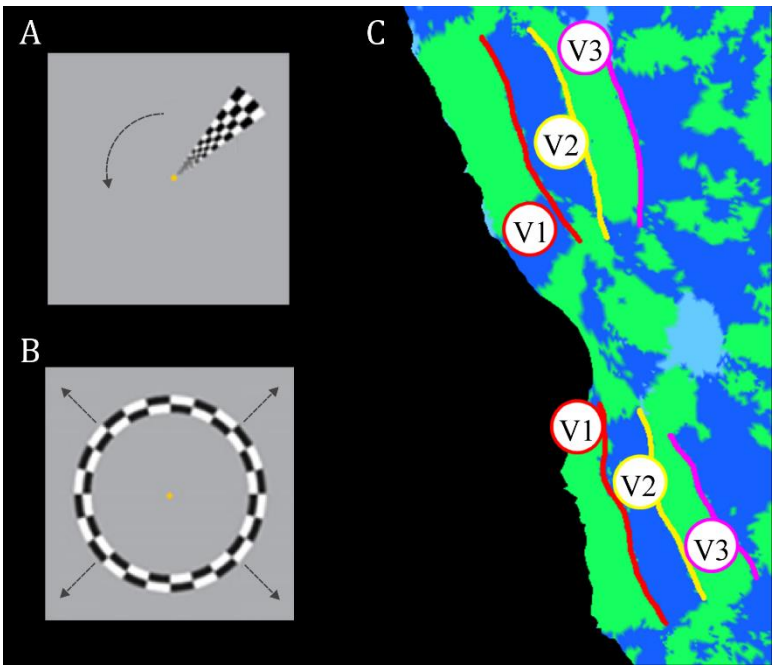

Figure II.9 Functional MRI experiments. Schematic illustration of visual stimuli for functional MRI: (**A**) polar angle paradigm – rotating wedges revolving 360° anticlockwise around the fixation point and (**B**) eccentricity paradigm – expanding ring outward from the fixation point. (**C**) Delineated early visual areas as regions-of-interest based on colour coding of polar angle and eccentricity experiments.

All image processing, cortical thickness and retinotopic mapping were performed with BrainVoyager QX 2.2 (Brain Innovation, Maastricht, The Netherlands). Thickness values of each visual area were extracted with BVQX toolbox for MATLAB (R2008a, v.7.6.0, The MathWorks, USA).

Basically, cortical thickness (CT) was measured through a process that involves four essential steps: (1) high-quality segmentation of the inner and outer cortex boundary of the preprocessed high-quality T1-weighted anatomical 3D data sets. The two anatomical datasets were averaged to get higher signal-to-noise ratio and then were normalized to the Talairach coordinate space; (2) cortical thickness measurement in volume space by the Laplace method (Jones, Buchbinder, & Aharon, 2000); (3) cortical thickness measurement in surface space over inflated meshes; (4) cortical thickness measurement from delineated regions-of-interest (ROIs) based on colour coding of polar angle and eccentricity experiments.

The eccentricity and polar angle gradients define visual field sign maps that reflect the mirrored representation of visual areas (Sereno, McDonald, & Allman, 1994). Hence, we obtained two-colour code map that established the lateral boundaries of the cortical visual areas. Retinotopic areas V1, V2 and V3 were manually defined over flattened meshes for each participant in each hemisphere using Brainvoyager's surface drawing tools (Figure II.9 C). Obtained ROIs were used as ''masks'' to the analysis of regional cortical thickness.

2.8 Statistical analysis

Statistical analysis was performed using statistical software packages (SPSS version 19.0 – SPSS Inc., Chicago, IL; and StatView – SAS, Cary, NC, USA). After verifying statistical assumptions using Shapiro–Wilk normality check and Levène homogeneity tests, comparisons between means were performed with multivariate General Linear Model based on Wilk's Lambda, with Sidak's adjustment for multiple comparisons. To prevent biases caused by violations of independence, we used the mean value of both eyes for all variables, since a significant interocular correlation was found (for control and LHON carrier groups). Pearson coefficient was used for correlation analyses.

The Receiver Operating Characteristic (ROC) curve analyses were also performed using MedCalc version 12.2.1.0 (MedCalc Software, Mariakerke, Belgium) to determine sensitivities at a fixed specificity (approximatey 80 %) for all tested parameters. The relative diagnostic accuracies of functional and structural tests were assessed by comparing areas under the ROC curves (AUC). An AUC equal to 1 represents a perfect discrimination between healthy and mutation carrier groups, whereas an AUC of 0.5 represents chance discrimination. Statistically significant differences between AUC were determined using the method of DeLong et al. (1988). Results with $p<0.05$ were considered statistically significant.

3 RESULTS

3.1 Evidence for impairment of Parvo and Koniocellular contrast sensitivity

We found a significant group effect on chromatic contrast sensitivity [$F(3,21)=3.876$, $p=0.024$, $\eta_p^2=0.356$]. Chromatic thresholds were significantly higher in LHON carriers for protan (red) ($p=0.008$), deutan (green) ($p=0.016$) and tritan (blue) ($p=0.010$) axes, as compared to control participants (Figure II.10).

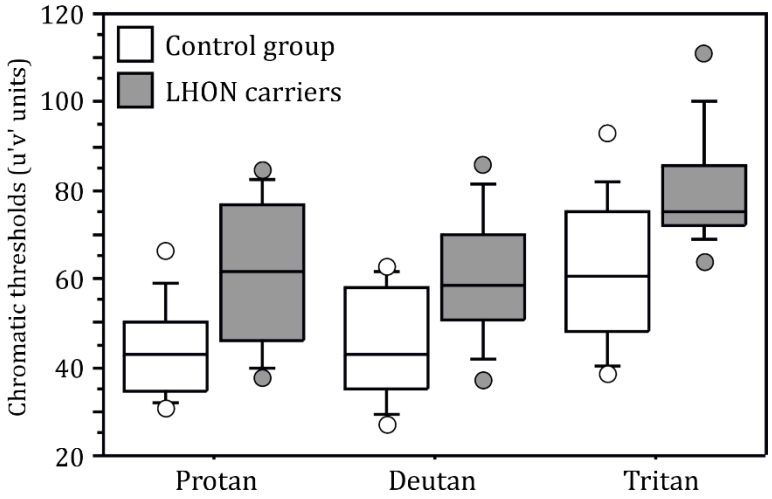

Figure II.10 Chromatic contrast sensitivity thresholds. Significant impairment is observed for the three chromatic axes in patients. Note that higher chromatic thresholds are related to lower contrast sensitivity.

3.2 Assessment of RGC function using the pattern electroretinogram (PERG)

Surprisingly, we found a marginally significant group effect on PERG wave amplitudes [$F(2,23)=3.200$, $p=0.059$, $\eta_p^2=0.218$]. Higher amplitudes of P-50 ($p=0.047$) and N-95 ($p=0.017$) waves were found in LHON carriers, comparing to the control group (Figure II.11; see also a representative example in Figure II.12 A). There were no significant differences in implicit times of both waves, as well as N-95/P-50 ratio between LHON carriers and controls.

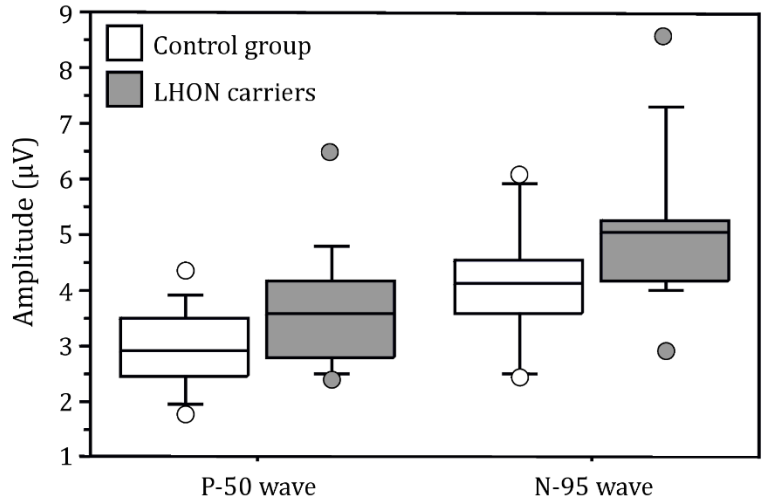

Figure II.11 Ganglion cell function assessed by pattern ERG. LHON carriers show surprisingly higher amplitudes of P-50 and N-95 components of PERG than control group.

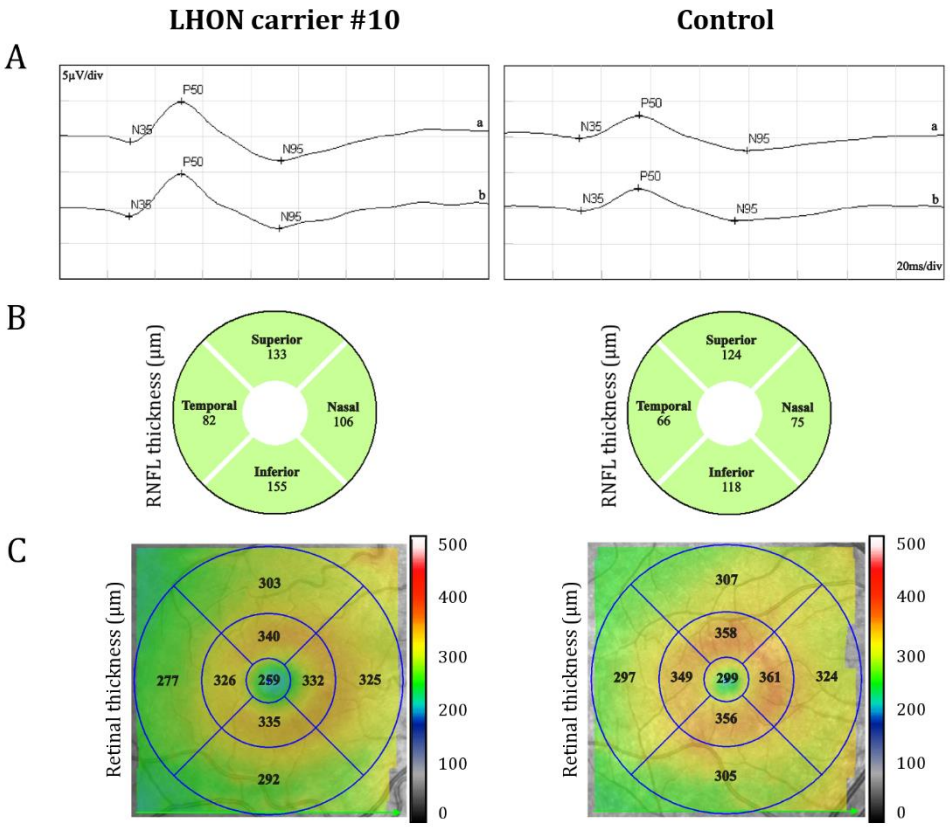

Figure II.12 (**A**) PERG plots, (**B**) OCT—peripapillary RNFL and (**C**) OCT—retinal thickness maps of a representative LHON carrier (#10) and a control subject. Note that carrier #10 presents (**A**) an increase in amplitudes of both P-50 and N-95 waves (a and b, first and second measurements), (**B**) increased peripapillary RNFL thickness and (**C**) decreased retinal thickness (more evident in the most central rings), as compared to the control.

3.3 Evidence for early swelling of papillomacular RNFL bundle

A significant group effect was not found on mean peripapillary RNFL thickness [$F(4,19)=2.364$, $p=0.090$, $\eta_p^2=0.332$]. However, LHON carriers showed an increased RNFL thickness, which was significant for inferior ($p=0.009$) and temporal ($p=0.027$) quadrants (see Figure II.12 B, for a representative example of increased RNFL thickness in Leber carriers group, see Figure II.13). These findings match the observed increases in perimacular RNFL thickness (most peripheric ring) in Leber carriers.

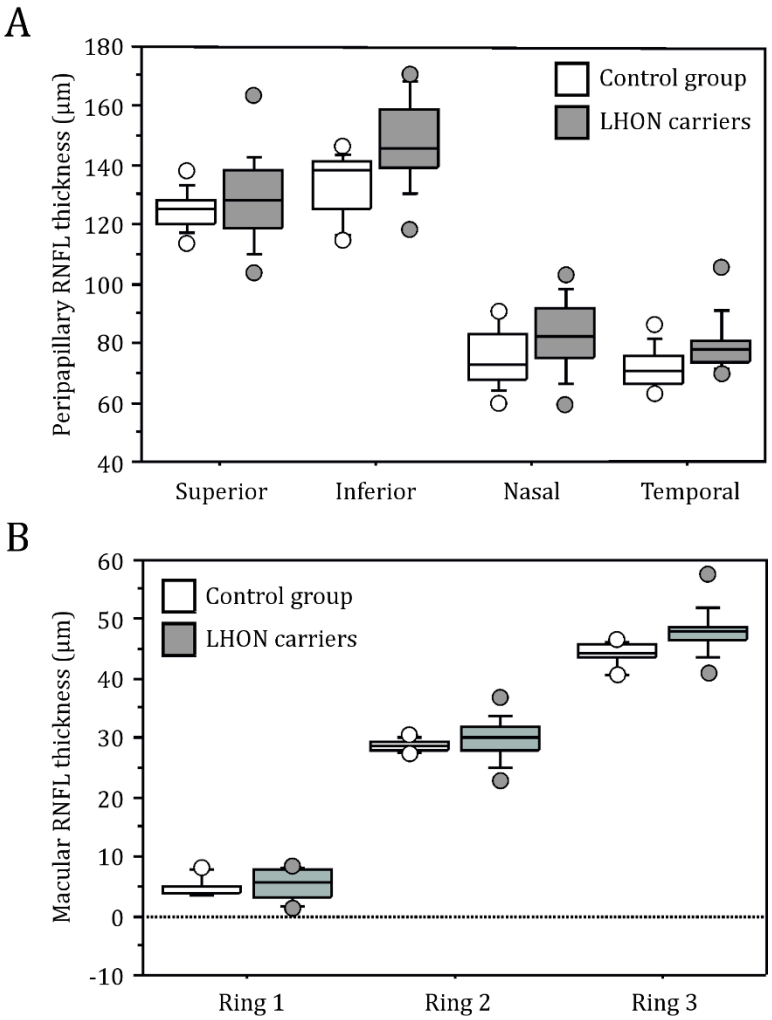

Figure II.13 Pathophysiological RNFL swelling as an early change in LHON carriers. (**A**) Peripapillary RNFL (inferior and temporal quadrants) and (**B**) macular RNFL thickness (ring 3) are significantly increased in the LHON carrier group, comparing with controls.

3.4 Inner retinal layer, macular retinal nerve fibre layer and outer retinal layer thickness measured using spectral domain-OCT

We found a significant group effect on global macular thickness [$F(3,20)=9.066$, $p=0.001$, $\eta_p^2=0.576$] and ORL thickness [$F(3,13)=3.246$, $p=0.057$, $\eta_p^2=0.428$]. By contrast, there was no group effect for IRL and central macular RNFL thickness.

Analysis by rings showed a significant decrease in global macular thickness for the most central rings (ring 1 $p=0.013$; ring 2 $p=0.017$) (Figure II.12 C, representative example of retinal thickness of control groups and LHON carrier, see Figure II.14).

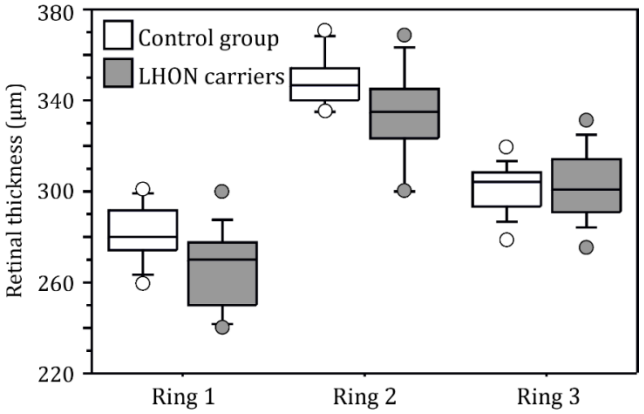

Figure II.14 Retinal thickness assessed by SD-OCT. Macular thickness (most central rings) is significantly decreased in Leber carriers.

We also found a decrease in outer retinal layer thickness for the most central rings (ring 1 p=0.005; ring 2 p=0.017), unlike the inner retinal layer that showed no differences between carriers and controls. On the other hand, we found the expected increase (due to the known pathophysiological swelling) in macular RNFL thickness (most peripheric ring) in Leber carriers (ring 3 p=0.044) (Figure II.13 B).

3.5 Retino-cortical correlation analyses for LHON carriers group

3.5.1 Cortical thickness of retinotopically defined visual areas using functional magnetic resonance imaging

Mean cortical thickness values (average of all vertices inside each functionally defined visual area V1, V2 and V3 from each participant hemispheres) were taken from our previous study (d'Almeida et al. (2013), which showed unexpected early increases in particular in areas V2 and V3; see Figure II.15 for a representative example of cortical thickness of both groups). Figure II.16 shows preserved functional retinotopic data, confirming that we were indeed studying the cortical impact of early retinal ganglion cell functional and structural loss, with associated relative peripheral visual field loss. Significant correlations between retinal and cortical measures were found for asymptomatic LHON group: macular RNFL thickness (ring 3) correlated positively with V2 (r=0.712, p=0.0075) and V3 (r=0.706, p=0.0083). These specific correlation patterns were not found in controls and were not observed for other measures.

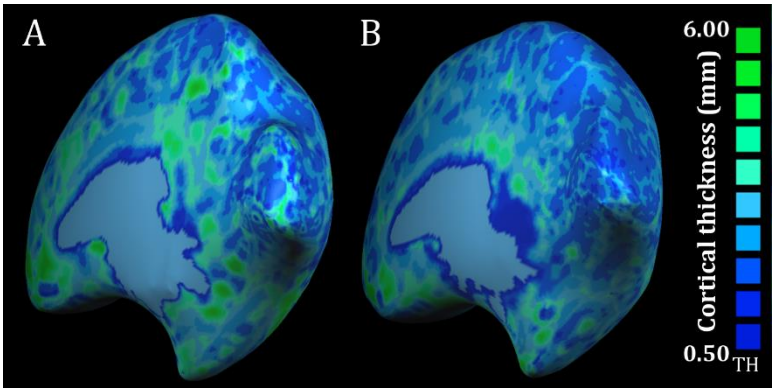

Figure II.15 Representative cortical thickness map (in mm) of (**A**) a LHON carrier #10 and (**B**) a control participant as assessed by magnetic resonance imaging. Note the higher cortical thickness values observed in Leber carrier patients in visual cortex.

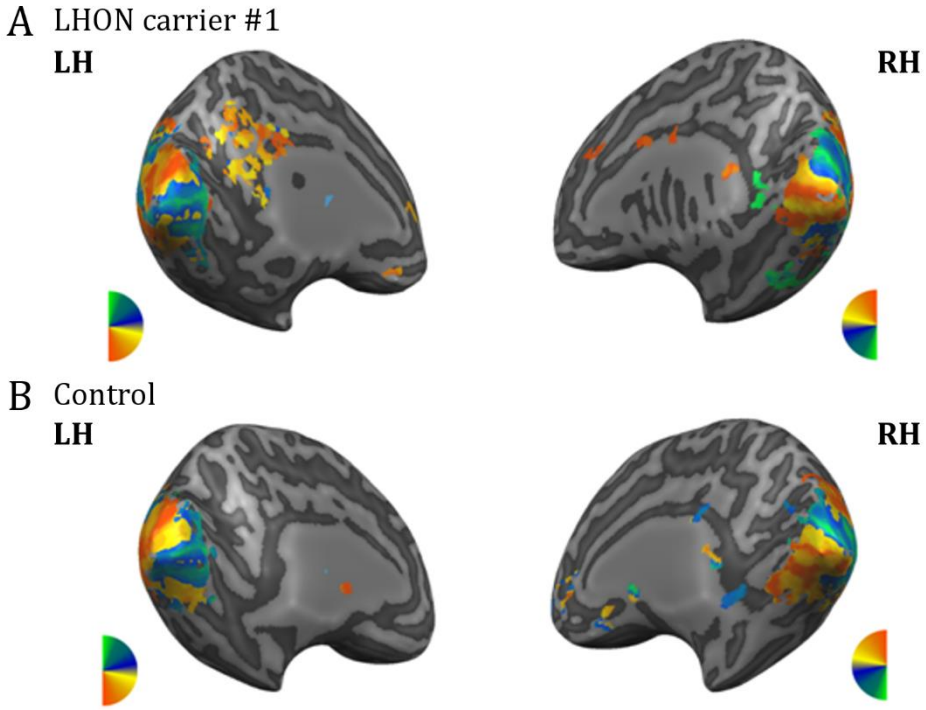

Figure II.16 Representative functional retinotopic data of (**A**) a LHON carrier #1 and (**B**) a control subject. These data show that retinotopic maps are intact despite the relative peripheral visual loss. LH, *left hemisphere*; RH, *right hemisphere*.

Our results suggest a correspondence between the peripheral visual field regions that showed the lowest psychophysical sensitivity, structural evidence for oedematous lesions in the most peripheral rings and highest cortical thickness values of extrastriate visual areas. To further test whether relative peripheral visual field loss was associated with increased extrastriate thickness, we performed a binomial test between concordant and discordant pairs using median separation criteria. The proportion of concordant pairs was significantly larger than discordant pairs (p=0.004, binomial test).

Figure II.17 further corroborates this notion. In the analysis reported in this figure we split cortical retinotopic maps in central, intermediate and peripheral regions and show that increased cortical thickness is significant only in peripheral (R2 and R3) retinotopic V2/V3 regions (p<0.05), in line with the finding of visual field peripheral loss.

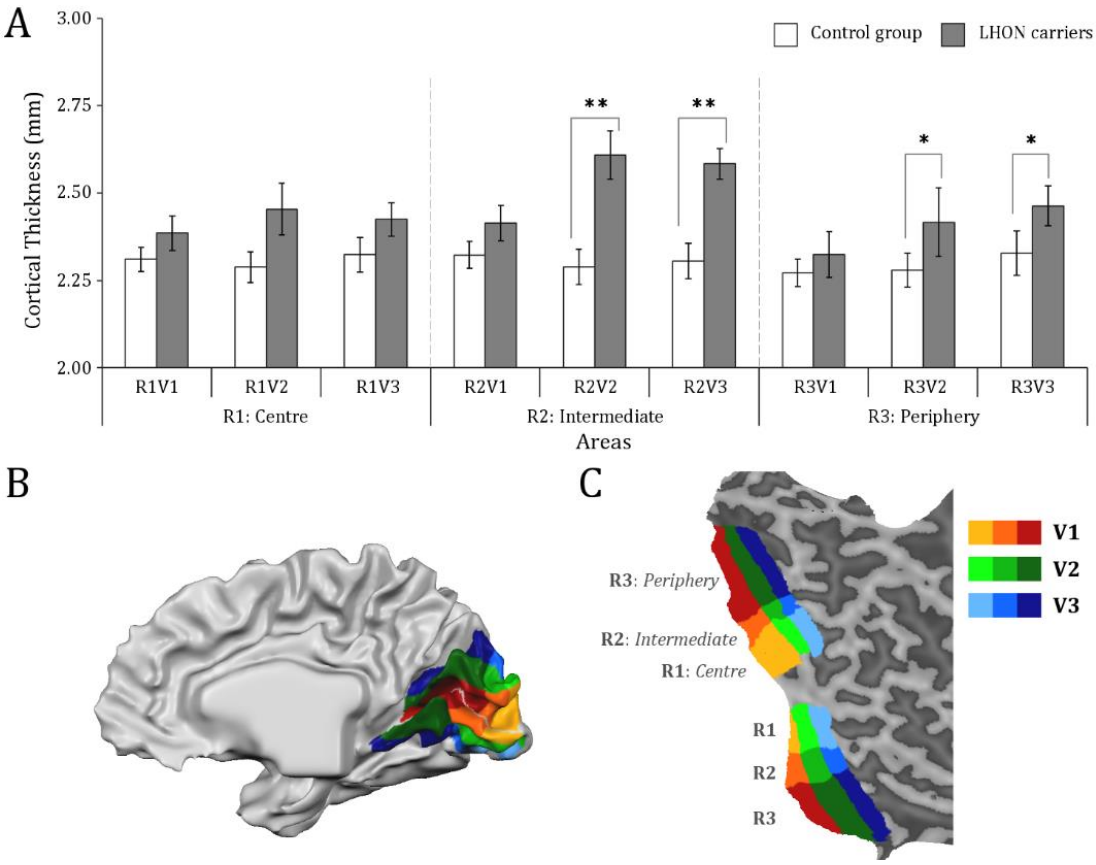

Figure 17 (**A**) Mean cortical thickness differences in central (R1), intermediate (R2) and peripheral (R3) regions as defined in (**B**, **C**). Note that increased cortical thickness in LHON mutation carriers is significant only in the peripheral retinotopic regions (R2 and R3), in line with the finding of visual field peripheral loss. Error bars denote standard error of the mean (±*SEM*). **p<0.01 and *p<0.05.

Finally, regions not suffering from oedema showed the expected positive correlations with central visual field measures (global macular thickness r=0.601, p=0.0160; central ring of ORL thickness r=0.604, p=0.0360).

3.6 ROC curve—sensitivity/specificity analysis

ROC sensitivity curves were generated for all tests. At approximately 80% specificity, the highest sensitivities were found for OCT macular RNFL ring 3 (83%; cut-off 46.25 µm); OCT outer retinal layer (75% for all rings; cutoff ring 1 200.5 µm, ring 2 180.25 µm, ring 3 162 µm); OCT peripapillary RNFL inferior quadrant (73%; cut-off 141.5 µm) and also for CCT Protan (69%; cut-off 50.2 u'v' units) (for more details see Table II.4).

Table II.4 Areas under the receiver operating characteristic (ROC) curve (AUC) and associated 95% confidence interval (CI) are presented for CCT, PERG, OCT and MRI parameters. Sensitivities obtained for each parameter at approximately 80% specificity and criterion values used for that specificity are also presented. CCT, *Cambridge colour test;* PERG, *pattern electroretinogram;* OCT, *optical coherence tomography;* MRI, *magnetic resonance imaging;* RNFL, *retinal nerve fibre layer;* RT, *retinal thickness;* IRL, *inner retinal layer;* ORL, *outer retinal layer;* amp, *amplitude;* IT, *implicit time;* sup, *superior;* inf, *inferior;* temp, *temporal.*

Parameters	AUC	95% CI	*p*-value	Sensitivity/ Specificity (%)	Criteria for 80% Specificity
CCT					
Protan	0.823	0.633, 0.940	<0.0001	69/80	50.2
Deutan	0.774	0.578, 0.909	0.0023	38/80	59.5
Tritan	0.792	0.598, 0.921	0.0012	38/80	76.95
PERG					
P-50 amp	0.710	0.512, 0.862	0.0325	53/82	3.48
N-95 amp	0.743	0.548, 0.886	0.0111	53/82	4.93
N-95/P-50 ratio	0.595	0.398, 0.772	0.3962	40/83	1.56
P-50 IT	0.510	0.318, 0.699	0.9322	13/83	52
N-95 IT	0.564	0.369, 0.746	0.5638	27/79	96
OCT					
Peripapillary RNFL sup	0.597	0.392, 0.780	0.3981	47/83	128.5
Peripapillary RNFL inf	0.800	0.602, 0.928	0.0007	73/83	141.5
Peripapillary RNFL nasal	0.694	0.489, 0.856	0.0653	40/83	85
Peripapillary RNFL temp	0.789	0.590, 0.921	0.0021	67/83	75.5
RT ring 1	0.775	0.574, 0.912	0.0026	67/83	272.5
RT ring 2	0.744	0.541, 0.891	0.0137	67/83	336.5
RT ring 3	0.508	0.310, 0.704	0.9428	27/83	290.13
RT sup	0.589	0.384, 0.773	0.4365	33/83	316.75
RT inf	0.606	0.400, 0.787	0.3535	47/83	312.5
RT nasal	0.656	0.449, 0.826	0.1616	47/83	325.5
RT temp	0.697	0.491, 0.858	0.0629	60/83	302.75
IRL ring 1	0.635	0.394, 0.835	0.3009	42/85	67
IRL ring 2	0.729	0.487, 0.900	0.0577	58/85	155
IRL ring 3	0.573	0.336, 0.788	0.5981	42/85	145.5
ORL ring 1	0.854	0.626, 0.970	0.0001	75/85	200.5
ORL ring 2	0.786	0.548, 0.935	0.0099	75/85	180.25
ORL ring 3	0.781	0.543, 0.932	0.0174	75/85	162
Macular RNFL ring 1	0.507	0.266, 0.746	0.9611	50/83	5
Macular RNFL ring 2	0.583	0.332, 0.806	0.5434	42/83	29.5
Macular RNFL ring 3	0.903	0.671, 0.990	<0.0001	83/83	46.25
MRI					
V1	0.608	0.462, 0.740	0.2719	40/82	2.40
V2	0.673	0.529, 0.796	0.0308	30/82	2.53
V3	0.706	0.563, 0.824	0.0136	33/82	2.49

3.7 Classification accuracy of the mutation carrier state by areas under the ROC curve (AUC)

The AUC is an important measure that summarizes the diagnostic accuracy of each parameter. In our study, we found AUCs up to 0.903 (Table II.4). The parameters that showed higher AUC value were macular RNFL ring 3 (AUC=0.903, $p<0.0001$), outer retinal layer ring 1 (AUC=0.854, $p=0.0001$), CCT Protan (AUC=0.823, $p<0.0001$) and peripapillary RNFL inferior quadrant measures (AUC=0.800, $p=0.0007$).

4 DISCUSSION

In this study, we established a link between early retinal ganglion cell impairment at the axonal level (RNFL), which is known to be reflected in intra-axonal stasis and swelling and increased cortical thickness in extrastriate cortex, in unaffected LHON carriers (mtDNA 11778G>A point mutation). Interestingly, retinal and cortical biological markers could determine the presence of LHON carrier status, as measured by ROC analysis, suggesting that they are tightly coupled. In our previous work (d'Almeida et al., 2013), we found increased cortical thickness in LHON carriers, particularly in extrastriate areas V2/V3. Our work shows that cortical changes are present during clinically silent degeneration of RGC, and importantly, are associated with the presence of relative peripheral visual loss, even when retinotopic maps are still intact.

The association between relative visual field loss in the periphery and cortical thickness suggests that although there is no absolute scotoma, field loss is sufficient to drive cortical changes. Importantly, we could show that increased cortical thickness is significant only in peripheral retinotopic V2/V3 regions, in line with the finding of visual field peripheral loss.

There was no absolute scotoma (defined as a fully blind visual field lesion) and visual field loss was relative but significant. This was not sufficient to disrupt functional retinotopic maps but induced a change in visual experience that could lead to cortical changes (for an earlier review on the effects of visual deprivation on functional and structural organization of the human brain see Noppeney (2007). Since cortical plasticity may also rely in compensatory cortico-cortical connections this might help explain why we find more prominent changes in extrastriate cortex.

LHON carriers showed the expected RNFL swelling that is a pathophysiological marker of early damage in this condition, in particular for temporal and inferior quadrants (Savini et al., 2005). Since these patients show absence of leakage around the disk on fluorescein angiography (Newman, 2005; E. K. Nikoskelainen et al., 1996; Smith, Hoyt, & Susac, 1973), the RNFL swelling does not correspond to an extracellular oedema but rather intracellular oedema (called by some authors, pseudoedema). This RNFL swelling is probably a consequence of impaired axoplasmic transport, due to mitochondrial dysfunction and compensatory increase of mitochondrial biogenesis (Barboni et al. (2010), see also introduction). Only later in the disease process optic atrophy occurs. Vulnerability does nevertheless occur in the pre-clinical stage of this disease (Sadun et al., 2000) and the compromise of the thin RGC-related papillomacular bundle may in particular represent the anatomical substrate for colour vision loss (Carelli et al., 2004; Sadun et al., 2000). This particular psychophysical feature is consistent with the observation that parvo and koniocellular impairment occurs even in asymptomatic carriers before the massive cell death and conversion to the acute stage (Sadun et al., 2006; Ventura et al., 2007). We also found that global macular thickness was decreased, at the cost of the surprising and significant decrease in the outer retinal layer, suggesting that damage at the pre-ganglion level also occurs in the LHON carrier status.

The physiology of preclinical stages may widely differ from after disease onset as also noted above concerning the early pathophysiology of retinal ganglion cell damage. In this context, we found that PERG responses showed a marginally significant early response augmentation that was independent from the changes in RGC-related layers (RNFL and IRL). These results are not inconsistent with a recent study (Guy et al., 2014) that reported a progressive decrease of PERG amplitude in asymptomatic Leber subjects. These findings anticipate a response dampening after conversion to the clinical stage. Moreover, retinal responses may be paradoxically increased in early disease states (Laguna et al., 2013). In that study (Laguna et al., 2013) in Down syndrome (DS) and a trisomic mouse model of DS (Ts65Dn), we found that abnormally high responses may occur in a retina with abnormal cellularity at the RGC level.

Notably, we found that significantly increased visual cortical thickness measures in asymptomatic carriers were correlated with swelling of the macular RGC axons (due to deficits in axonal transport) at the most peripheral ring and significantly associated with relative peripheral visual loss. In other words, compensatory cortical plasticity occurring in particular in peripheral regions of V2 and V3 may be predicted by afferent changes in the thickness of RGC axonal layer (as measured by the segmented macular RNFL) and changed visual peripheral experience, which is an important cause of reorganization (Lövdén et al., 2013; Noppeney, 2007). These findings were specific and other non visual cortical regions showed unchanged thickness. This suggests that early retinal changes are reflected in retinotopically specific plasticity, as assessed by visual cortical thickness, which is a well-established method to study structural plasticity (Engvig et al., 2010; Jiang et al., 2009; Kolb & Whishaw, 1998; Lövdén et al., 2013). The constant pattern of peripheral defects in visual fields, meaning that sensitivity deficits and changed visual experience occurred in the periphery, are significant while not sufficient to disrupt retinotopic maps. The significant association between that relative peripheral visual field loss and increased cortical thickness is indeed suggestive of visual cortical plasticity. Other forms of visual loss (such as colour vision deficits) seem not to induce these forms of reorganization.

However, alternative explanations that might partially contribute to our observations should also be considered, in particular neurodevelopmental changes induced by pervasive mitochondrial dysfunction. Given that neural proliferation and differentiation require high metabolic activity during development, one cannot exclude that changes in metabolic function could also induce changes in cortical thickness. However, it is unlikely that such a pervasive mechanism would explain the regional (V2/V3) and subregional (peripheral) changes identified in this study.

It is relevant to point out that RNFL thickness was among the most sensitive classifiers of the mutation status (and with larger area under the ROC curve) further suggesting an important role in pre-clinical phases. Furthermore, our cortical measures were at least as discriminative as some of the retinal outcomes, suggesting that visual cortical plastic changes and reorganization (d'Almeida et al., 2013) go well in parallel with subtle axonal pathology.

We conclude that retinal ganglion cell impairment at the axonal level in Leber Optic Neuropathy carriers and corresponding relative peripheral visual loss at an early stage is associated with peripheral cortical compensatory plasticity, which dominates in extrastriate cortex and is absent in nonvisual cortex.

5 ACKNOWLEDGMENTS

The authors thank LHON family, as well as all controls for their participation in this study. They also thank Carlos Ferreira and João Marques for helping with MRI scanning and Manuela Grazina and João Pratas for assistance in mtDNA analysis. This research was supported by Portuguese Foundation for Science and Technology Portugal [COMPETE] Strategic project Pest-C/SAU/UI3282/2011 and grants: SFRH/BD/64306/2009 (to CM), SFRH/BD/76013/2011 (to OCA); and also following grants: CENTRO-07-ST24-FEDER-00205, DoIT-Diamarker.

6 REFERENCES

Aaker, G. D., Myung, J. S., Ehrlich, J. R., Mohammed, M., Henchcliffe, C., & Kiss, S. (2010). Detection of retinal changes in Parkinson's disease with spectral-domain optical coherence tomography. Clinical Ophthalmology, 4, 1427–1432. doi:10.2147/OPTH.S15136

Bach, M., Brigell, M. G., Hawlina, M., Holder, G. E., Johnson, M. A., McCulloch, D. L., … Viswanathan, S. (2013). ISCEV standard for clinical pattern electroretinography (PERG): 2012 update. Documenta Ophthalmologica, 126(1), 1–7. doi:10.1007/s10633-012-9353-y

Barbiroli, B., Montagna, P., Cortelli, P., Iotti, S., Lodi, R., Barboni, P., … Zaniol, P. (1995). Defective brain and muscle energy metabolism shown by in vivo 31P magnetic resonance spectroscopy in nonaffected carriers of 11778 mtDNA mutation. Neurology, 45(7), 1364–1369. doi:10.1212/WNL.45.7.1364

Barboni, P., Carbonelli, M., Savini, G., Ramos, C. do V. F., Carta, A., Berezovsky, A., … Sadun, A. A. (2010). Natural history of Leber's hereditary optic neuropathy: longitudinal analysis of the retinal nerve fiber layer by optical coherence tomography. Ophthalmology, 117(3), 623–627. doi:10.1016/j.ophtha.2009.07.026

Barcella, V., Rocca, M. A., Bianchi-Marzoli, S., Milesi, J., Melzi, L., Falini, A., … Filippi, M. (2010). Evidence for retrochiasmatic tissue loss in Leber's hereditary optic neuropathy. Human Brain Mapping, 31(12), 1900–1906. doi:10.1002/hbm.20985

Carelli, V., La Morgia, C., Iommarini, L., Carroccia, R., Mattiazzi, M., Sangiorgi, S., … Valentino, M. L. (2007). Mitochondrial optic neuropathies: how two genomes may kill the same cell type? Bioscience Reports, 27(1-3), 173–184. doi:10.1007/s10540-007-9045-0

Carelli, V., Ross-Cisneros, F. N., & Sadun, A. A. (2004). Mitochondrial dysfunction as a cause of optic neuropathies. Progress in Retinal and Eye Research, 23(1), 53–89. doi:10.1016/j.preteyeres.2003.10.003

Chinnery, P. F., Johnson, M. A., Wardell, T. M., Singh-Kler, R., Hayes, C., Brown, D. T., … Turnbull, D. M. (2000). The epidemiology of pathogenic mitochondrial DNA mutations. Annals of Neurology, 48(2), 188–193.

Cortelli, P., Montagna, P., Avoni, P., Sangiorgi, S., Bresolin, N., Moggio, M., … Lugaresi, E. (1991). Leber's hereditary optic neuropathy: genetic, biochemical, and phosphorus magnetic resonance spectroscopy study in an Italian family. Neurology, 41(8), 1211–1215.

d'Almeida, O. C., Mateus, C., Reis, A., Grazina, M. M., & Castelo-Branco, M. (2013). Long term cortical plasticity in visual retinotopic areas in humans with silent retinal ganglion cell loss. Neuroimage, 81, 222–230. doi:10.1016/j.neuroimage.2013.05.032

DeLong, E. R., DeLong, D. M., & Clarke-Pearson, D. L. (1988). Comparing the areas under two or more correlated receiver operating characteristic curves: a nonparametetric approach. Biometrics, 44(3), 837–845. doi:10.2307/2531595

Engvig, A., Fjell, A. M., Westlye, L. T., Moberget, T., Sundseth, Ø., Larsen, V. A., & Walhovd, K. B. (2010). Effects of memory training on cortical thickness in the elderly. Neuroimage, 52(4), 1667–1676. doi:10.1016/j.neuroimage.2010.05.041

Guy, J., Feuer, W. J., Porciatti, V., Schiffman, J., Abukhalil, F., Vandenbroucke, R., … Lam, B. L. (2014). Retinal ganglion cell dysfunction in asymptomatic G11778A: Leber hereditary optic neuropathy. Investigative Ophthalmology & Visual Science, 55(2), 841–848. doi:10.1167/iovs.13-13365

Jiang, J., Zhu, W., Shi, F., Liu, Y., Li, J., Qin, W., … Jiang, T. (2009). Thick visual cortex in the early blind. The Journal of Neuroscience, 29(7), 2205–2211. doi:10.1523/JNEUROSCI.5451-08.2009

Jones, S. E., Buchbinder, B. R., & Aharon, I. (2000). Three-dimensional mapping of cortical thickness using Laplace's Equation. Human Brain Mapping, 11(1), 12–32. doi:10.1002/1097-0193(200009)11:1<12::AID-HBM20>3.0.CO;2-K

Kolb, B., & Whishaw, I. Q. (1998). Brain plasticity and behavior. Annual Review of Psychology, 49(1), 43–64. doi:10.1146/annurev.psych.49.1.43

Laguna, A., Barallobre, M. J., Marchena, M.-Á., Mateus, C., Ramírez, E., Martínez-Cue, C., … Arbonés, M. L. (2013). Triplication of DYRK1A causes retinal structural and functional alterations in Down syndrome. Human Molecular Genetics, 22(14), 2775–2784. doi:10.1093/hmg/ddt125

Lodi, R., Carelli, V., Cortelli, P., Iotti, S., Valentino, M. L., Barboni, P., … Barbiroli, B. (2002). Phosphorus MR spectroscopy shows a tissue specific in vivo distribution of biochemical expression of the G3460A mutation in Leber's hereditary optic neuropathy. Journal of Neurology, Neurosurgery & Psychiatry, 72(6), 805–807. doi:10.1136/jnnp.72.6.805

Lövdén, M., Bäckman, L., Lindenberger, U., Schaefer, S., & Schmiedek, F. (2010). A theoretical framework for the study of adult cognitive plasticity. Psychological Bulletin, 136(4), 659–676. doi:10.1037/a0020080

Lövdén, M., Wenger, E., Mårtensson, J., Lindenberger, U., & Bäckman, L. (2013). Structural brain plasticity in adult learning and development. Neuroscience and Biobehavioral Reviews, 37(9), 2296–2310. doi:10.1016/j.neubiorev.2013.02.014

Mackey, D. A., Oostra, R.-J., Rosenberg, T., Nikoskelainen, E., Bronte-Stewart, J., Poulton, J., … Howell, N. (1996). Primary pathogenic mtDNA mutations in multigeneration pedigrees with Leber hereditary optic neuropathy. American Journal of Human Genetics, 59(2), 481–485.

Man, P. Y. W., Turnbull, D. M., & Chinnery, P. F. (2002). Leber hereditary optic neuropathy. Journal of Medical Genetics, 39(3), 162–169. doi:10.1136/jmg.39.3.162

Mateus, C., Lemos, R., Silva, M. F., Reis, A., Fonseca, P., Oliveiros, B., & Castelo-Branco, M. (2013). Aging of low and high level vision: from chromatic and achromatic contrast sensitivity to local and 3D object motion perception. PLoS ONE, 8(1), e55348. doi:10.1371/journal.pone.0055348

Morales, J., Weitzman, M. L., & de la Rosa, M. G. (2000). Comparison between tendency-oriented perimetry (TOP) and Octopus threshold perimetry. Ophthalmology, 107(1), 134–142.

Newman, N. J. (2005). Hereditary optic neuropathies: from the mitochondria to the optic nerve. American Journal of Ophthalmology, 140(3), 517–523. doi:10.1016/j.ajo.2005.03.017

Nikoskelainen, E. K., Huoponen, K., Juvonen, V., Lamminen, T., Nummelin, K., & Savontaus, M. L. (1996). Ophthalmologic findings in Leber hereditary optic neuropathy, with special reference to mtDNA mutations. Ophthalmology, 103(3), 504–514.

Nikoskelainen, E., Sogg, R. L., Rosenthal, A. R., Friberg, T. R., & Dorfman, L. J. (1977). The early phase in Leber hereditary optic atrophy. Archives of Ophthalmology, 95(6), 969–978. doi:10.1001/archopht.1977.04450060055002

Noppeney, U. (2007). The effects of visual deprivation on functional and structural organization of the human brain. Neuroscience and Biobehavioral Reviews, 31(8), 1169–1180. doi:10.1016/j.neubiorev.2007.04.012

Quiros, P. A., Torres, R. J., Salomao, S., Berezovsky, A., Carelli, V., Sherman, J., … Sadun, A. A. (2006). Colour vision defects in asymptomatic carriers of the Leber's hereditary optic neuropathy (LHON) mtDNA 11778 mutation from a large Brazilian LHON pedigree: a case-control study. British Journal of Ophthalmology, 90(2), 150–153. doi:10.1136/bjo.2005.074526

Reis, A., Mateus, C., Viegas, T., Florijn, R., Bergen, A., Silva, E., & Castelo-Branco, M. (2013). Physiological evidence for impairment in autosomal dominant optic atrophy at the pre-ganglion level. Archive for Clinical and Experimental Ophthalmology, 251(1), 221–234. doi:10.1007/s00417-012-2112-7

Rojas, J. C., & Gonzalez-Lima, F. (2010). Mitochondrial optic neuropathy: in vivo model of neurodegeneration and neuroprotective strategies. Eye and Brain, 2, 21–37.

Rosa, A. M., Silva, M. F., Ferreira, S., Murta, J., & Castelo-Branco, M. (2013). Plasticity in the human visual cortex: an ophthalmology-based perspective. BioMed Research International, 2013(568354), 1–13. doi:10.1155/2013/568354, 10.1155/2013/568354

Sadun, A. A., Salomao, S. R., Berezovsky, A., Sadun, F., DeNegri, A. M., Quiros, P. A., … Carelli, V. (2006). Subclinical carriers and conversions in Leber hereditary optic neuropathy: a prospective psychophysical study. Transactions of the American Ophthalmological Society, 104, 51–61.

Sadun, A. A., Win, P. H., Ross-Cisneros, F. N., Walker, S. O., & Carelli, V. (2000). Leber's hereditary optic neuropathy differentially affects smaller axons in the optic nerve. Transactions of the American Ophthalmological Society, 98, 223–232.

Savini, G., Barboni, P., Valentino, M. L., Montagna, P., Cortelli, P., De Negri, A. M., … Carelli, V. (2005). Retinal nerve fiber layer evaluation by optical coherence tomography in unaffected carriers with Leber's hereditary optic neuropathy mutations. Ophthalmology, 112(1), 127–131. doi:10.1016/j.ophtha.2004.09.033

Sereno, M. I., McDonald, C. T., & Allman, J. M. (1994). Analysis of retinotopic maps in extrastriate cortex. Cerebral Cortex, 4, 601–620.

Silva, M. F., Faria, P., Regateiro, F. S., Forjaz, V., Januário, C., Freire, A., & Castelo-Branco, M. (2005). Independent patterns of damage within magno-, parvo- and koniocellular pathways in Parkinson's disease. Brain, 128(10), 2260–2271. doi:10.1093/brain/awh581

Smith, J. L., Hoyt, W. F., & Susac, J. O. (1973). Ocular fundus in acute Leber optic neuropathy. Archives of Ophthalmology, 90(5), 349–354. doi:10.1001/archopht.1973.01000050351002.

Ventura, D. F., Gualtieri, M., Oliveira, A. G. F., Costa, M. F., Quiros, P., Sadun, F., … Carelli, V. (2007). Male prevalence of acquired color vision defects in asymptomatic carriers of Leber's hereditary optic neuropathy. Investigative Ophthalmology and Visual Science, 48(5), 2362–2370. doi:10.1167/iovs.06-0331

Wandell, B. A., & Smirnakis, S. M. (2009). Plasticity and stability of visual field maps in adult primary visual cortex. Nature Reviews Neuroscience, 10(12), 873–884. doi:10.1038/nrn2741

Yu-Wai-Man, P., Griffiths, P. G., Hudson, G., & Chinnery, P. F. (2009). Inherited mitochondrial optic neuropathies. Journal of Medical Genetics, 46(3), 145–158. doi:10.1136/jmg.2007.054270

Ch. II. 3

The neurochemical phenotype of the visual occipital cortex of clinically diagnosed Leber Hereditary Optic Neuropathy patients: a ^{1}H and ^{31}P MR Spectroscopy pilot study

ABSTRACT

In this study we aim to assess not only metabolism and neurotransmission but also membrane phospholipid and high-energy phosphate metabolism in the occipital lobe of Leber Hereditary Optic Neuropathy patients. Moreover we want to establish the link between the retinal status evaluated by the thickness of retinal layers and the biochemistry of the occipital visual cortex. Levels of N-acetylaspartate, creatine, choline and glutamate will be measured by PRESS ^{1}H-MRS and GABA will be measured with MEGAPRESS ^{1}H-MRS. Multivoxel ^{31}P chemical shift imaging (CSI) will be also performed to measure high energy phosphates and phospholipids levels and estimate several indexes of readily available free energy in the cell, the efficiency of ATP production and the status of oxidative metabolism in vivo. OCT scans will used to obtain retinal layers thickness.

This is the first study in our lab using in vivo multinuclei magnetic resonance spectroscopy method (^{31}P-MRS). All several technical details had to be acknowledged during the thesis development ranging from MRS data acquisition methodologies involved like proton decoupling and manual shimming to other acquisition and processing protocols associated.

Future work

1 RATIONALE

Cortical reorganization upon direct injury and/or loss of sensory input has been a matter of intense debate in the last years. Despite the controversy, some studies provide strong evidence for potential mechanisms of reorganization in sensory areas in response to afferent damage.

Leber Hereditary Optic Neuropathy (LHON, Leber, 1871) is a maternally inherited disorder, characteristically presenting bilateral acute or subacute loss of vision, mainly in young adult males. The primary aetiology of this disorder is attributed to mitochondrial point mutations that affect genes encoding proteins of the complex I subunits of the mitochondrial respiratory chain (Howell, 1997). The three dominant mitochondrial DNA mutations affecting more than 95% of LHON patients are 11778G>A, 14484T>C, 3460G>A, with an overall prevalence of around 1:45.000 in Europe (Mascialino, Leinonen, & Meier, 2011). The primary mutations together with secondary genetic and/or epigenetic factors (Kirches, 2011) lead essentially to loss of vision upon retinal ganglion cell (RGC) degeneration and optic nerve (ON) atrophy in fibres subserving central vision (Howell, 1997). In fact, RGC axons display a particular sensitivity to mitochondrial dysfunction because of loss of mitochondrial complex I function, retinal nerve fibre layer (RNFL) is rich in mitochondria and oedema occurs due to failure of axonal transport mechanisms and stasis with also swollen mitochondria (Rojas & Gonzalez-Lima, 2010; Zhuo, Luo, & Zhang, 2012).

Several studies have suggested the use of thickness measurements of retinal layers as indicators of the progression of the disease (Hedges et al., 2016; Zhang et al., 2014). In fact subclinical changes in the afferent visual structures seem to occur early in the natural history disease, even in asymptomatic stage. However, not only the retina is affected.

Barcella et al. showed reduced grey matter (GM) volumes bilaterally in primary visual cortex of LHON patients as assessed by Voxel-Based Morphometry (VBM) measures. In addition they also reported the decrease of white matter (WM) volumes in the optic chiasm, optic tract, and bilaterally in the optic radiations (OR) (Barcella et al., 2010). Also a Diffusion Weighted Imaging (DWI) study demonstrated higher mean diffusivity (MD) values in optic radiations (OR) of patients with LHON, especially in those with longer disease duration and no visual acuity recovery. These changes were not detected in unaffected LHON carriers and in extra-visual WM areas (Rizzo et al., 2012).

In our previous study in fifteen Leber Hereditary Optic Neuropathy (LHON) carriers with the 11778G>A mitochondrial mutation (d'Almeida, Mateus, Reis, Grazina, & Castelo-Branco, 2013), we studied the impact of early retinal damage, as assessed by optical coherence tomography (OCT) on the structure of the early cortical visual areas, as evaluated by cortical thickness measurements of retinotopically-defined areas of the visual cortex (d'Almeida et al., 2013). Later on we were able to establish a link between the two (Mateus, d'Almeida, Reis, Silva, & Castelo-Branco, 2016). Our cohort of asymptomatic LHON carriers had normal visual acuity and ocular fundus, minor deficits in visual field sensitivity, lower colour sensitivity, and larger electroretinographic (ERG) responses. OCT measures showed lower retinal thickness and increased peripapillary nerve fibre layer thickness. The most intriguing was the fact that cortical thickness was increased in extrastriate V2 and V3 visual areas that do not receive direct input from the retina (d'Almeida et al., 2013). Despite following the same trend in V1, the differences were not significant and had a much smaller effect size, probably because V1 might be more directly affected by the loss of input. The increase in cortical thickness was correlated with increase of retinal nerve fibre layer thickness (Mateus et al., 2016). These results suggested that, although there is no absolute scotoma, partial field loss is sufficient to drive cortical changes.

Interestingly a study with an animal model of LHON (animals were treated with rotenone, a drug-induced model of mitochondrial dysfunction mimicking Leber neuropathy) showed not only

decreased metabolic capacity in the retina, but also in the superior colliculus (the main recipient region of retinal fibres in rodents), the lateral geniculate nucleus, and primary visual cortex, whereas a compensatory increase in metabolic activity was observed in the secondary visual cortex compared with control values (Rojas, John, Lee, & Gonzalez-Lima, 2009).

In humans, previous studies with in vivo phosphorus MRS (^{31}P-MRS) showed defective mitochondrial function and abnormalities in the levels of high-energy phosphates in the brain of patients carrying mtDNA mutations (Arias-Mendoza, 2004; Barbiroli et al., 1993; Lodi et al., 2002). Decreased energy reserves as evaluated by low phosphorylation potential (PP) and reduced phosphocreatine (PCr) and increased adenosine diphosphate (ADP, related to high levels of inorganic phosphate, P_i) contents in asymptomatic carriers of the 11778 mtDNA mutation were found (Barbiroli et al., 1995). A short report showed also decreased energy supply (low PCr/Pi ratio) in the occipital lobes of three male siblings, with the 11778 mtDNA mutation with clinical history of blindness but with visual recovery (Cortelli et al., 1991). Regarding cortical metabolic and neurotransmitter levels, less is known in this disorder. However, there is some evidence of abnormal WM proton MRS (^{1}H-MRS) profiles of both affected and unaffected LHON mtDNA mutation carriers, even without neurological symptoms and with normal-appearing WM (Jančić et al., 2015; Ostojic et al., 2009).

To further elucidate the impact of mitochondrial dysfunction in metabolism and neurotransmission in carriers of the mitochondrial DNA 11778G>A mutation causing LHON, we aim to study the neurochemical phenotype of the occipital cortex of these patients. We will therefore conduct a comprehensive MRS study combining both ^{1}H- and ^{31}P-MRS. These two techniques will allow to gather information on neuronal/axonal viability, cellular membrane integrity/turnover and energetics through the quantification of different metabolites involved in energy metabolism, tricarboxylic acid cycle and neurotransmission (^{1}H-MRS) and also high-energy phosphates and membrane phospholipids (^{31}P-MRS). Using ^{1}H-MRS, through the PRESS sequence, we will be able to quantify relevant neurotransmitters such as glutamate and glutamine, associated with metabolic defects and/or neurotransmission imbalance, N-acetyl aspartate (NAA) classically related to neuronal death and/or mitochondrial dysfunction and creatine. The major inhibitory neurotransmitter of the central nervous system, γ-aminobutyric acid (GABA) will be measured through a specialized GABA-editing gold-standard technique, MEGA-PRESS sequence.

Through ^{31}P-MRS we will measure PCr, P_i and ATP levels, as well as the content of several membrane phospholipids such as glicerophosphoethanolamine (GPE) and glicerophosphocholine (GPC). We will indirectly estimate several indexes of steady-state mitochondrial functionality, cellular energy reserves and oxidative phosphorylation through the calculus of PP, the maximal rate of ATP biosynthesis ($\%V/V_{max}$), free cytosolic Magnesium (Mg^{2+}) and pH.

To our knowledge this is the first study of the biochemical profile of the occipital lobe of LHON patients, with a comprehensive methodological approach combining both in vivo ^{1}H- and ^{31}P-MRS. Furthermore OCT thickness measures will allow to further correlate retinal and occipital cortex status and neurotransmission. With the study of the biochemistry of the occipital lobe and the retinal structure we will be able to find potentially relevant measures that might be promising in the diagnosis, prognosis, and follow-up of this condition. Moreover this might even allow for the development of new therapeutic strategies in this mitochondrial disorder.

2 MATERIAL AND METHODS

2.1 Participants

Leber Hereditary Optic Neuropathy patients enrolled in this study will be recruited from the Coimbra Hospital and University Centre, after clinical and genetic assessment. The protocol will be also applied to age- and gender- matched control participants recruited from the local community. Exclusion criteria for both groups comprise the presence of glaucoma, diabetes even in the absence of retinopathy or any other eye disease, significant media opacities, pseudophakic and aphakic eyes and high ammetropies (sphere>±4D; cylinder>±2D), surgery or treatment within a period of 6-months. Pregnant or lactating women, participants with severe cardiovascular problems, with cardiac pacemaker or metal implants in the body will be also excluded. All participants included provided they have a negative history of neurological or psychiatric disorders and no neurovascular and structural pathologic alterations that will be checked by an experienced neuroradiologist. The study was already reviewed and approved by our Institutional Review Board (*"Comissão de Ética da Faculdade de Medicina da Universidade de Coimbra"*) and follows the tenets of the Declaration of Helsinki. Written informed consent will be obtained from all participants, after research procedures are fully explained.

We have already acquired data from five participants, clinically evaluated but waiting for genetic diagnosis.

2.2 Visual assessment

A complete ophthalmological examination will be performed on all participants, including best-corrected visual acuity (VA; decimal scale), slit lamp biomicroscopy, ocular tension measurement (Goldmann applanation tonometer) and fundus examination (Goldman lens). Static automated perimetry (SAP) will be performed using a commercially available high resolution Vision Monitor (MonCv3, Metrovision, Pérenchies, France) with the Fiber Adapted Static Testing 24 (FAST24) perimetry procedure. FAST-24 perimetry tests the smallest luminance level that can be detected among 79 fixed dots over the central visual field up to 30 degrees of eccentricity. Here, the testing parameters are identical to those of Goldmann perimeter: the ambient luminance should be kept in a low photopic level and stimulus size is III (26 arc minutes), testing over a white background.

2.2.1 Optic Coherence Tomography

Optic Coherence Tomography (OCT) will be performed on each participant eye to scan the macula (macular cube 512×128×1024 protocol), and the optic disc (optic disc cube 200×200 protocol) using the Cirrus HD-OCT 5000, Software version 6.5 (Carl Zeiss Meditec Inc., Dublin, CA, USA). All patients will be examined with undilated pupils. OCT image segmentation will be performed automatically through the OCT Explorer 4.0 (Iowa Reference Algorithms, Retinal Image Analysis Lab, Iowa Institute for Biomedical Imaging, Iowa City, IA) described in detail elsewhere (Abràmoff, Garvin, & Sonka, 2010; Antony et al., 2011; Garvin et al., 2009). Eleven surfaces will be segmented from each volumetric macula- and optic nerve head- (ONH) centred scan. The algorithm allows the definition of the interfaces of the following layers: inner limiting membrane (ILM), retinal nerve fibre layer (RNFL), ganglion cell layer (GCL), internal plexiform layer (IPL), inner nuclear layer (INL), outer plexiform layer (OPL), OPL-Henle fibre layer (OPL-HFL), photoreceptors inner segment/outer segment layer (IS/OS), IS/OS junction (IS/OSJ), outer photoreceptor layer (OPR), retinal pigment epithelium (RPE) and the choroid (Figure II.18, II.19). All output images will be visually inspected for segmentation errors and manually corrected, if needed. The average thickness

of each layer can be defined as the mean distance between two layers for all A-scan in each central subfield (Figure II.19).

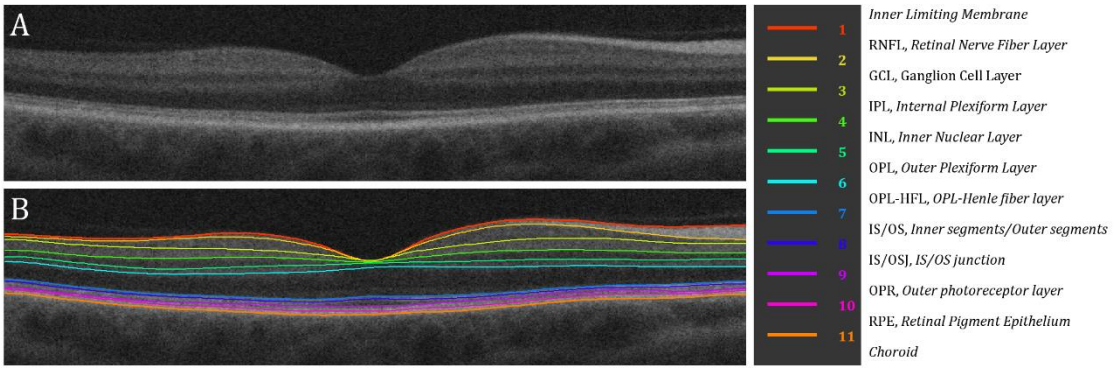

Figure II.18 Representative macular OCT image segmentation. (**A**) Raw data files were automatically segmented using 3-D contextual information and differences in tissue reflectivity into (**B**) 11 surfaces. During the 3D segmentation process the segmentation software identifies the outer boundaries of each retinal layer.

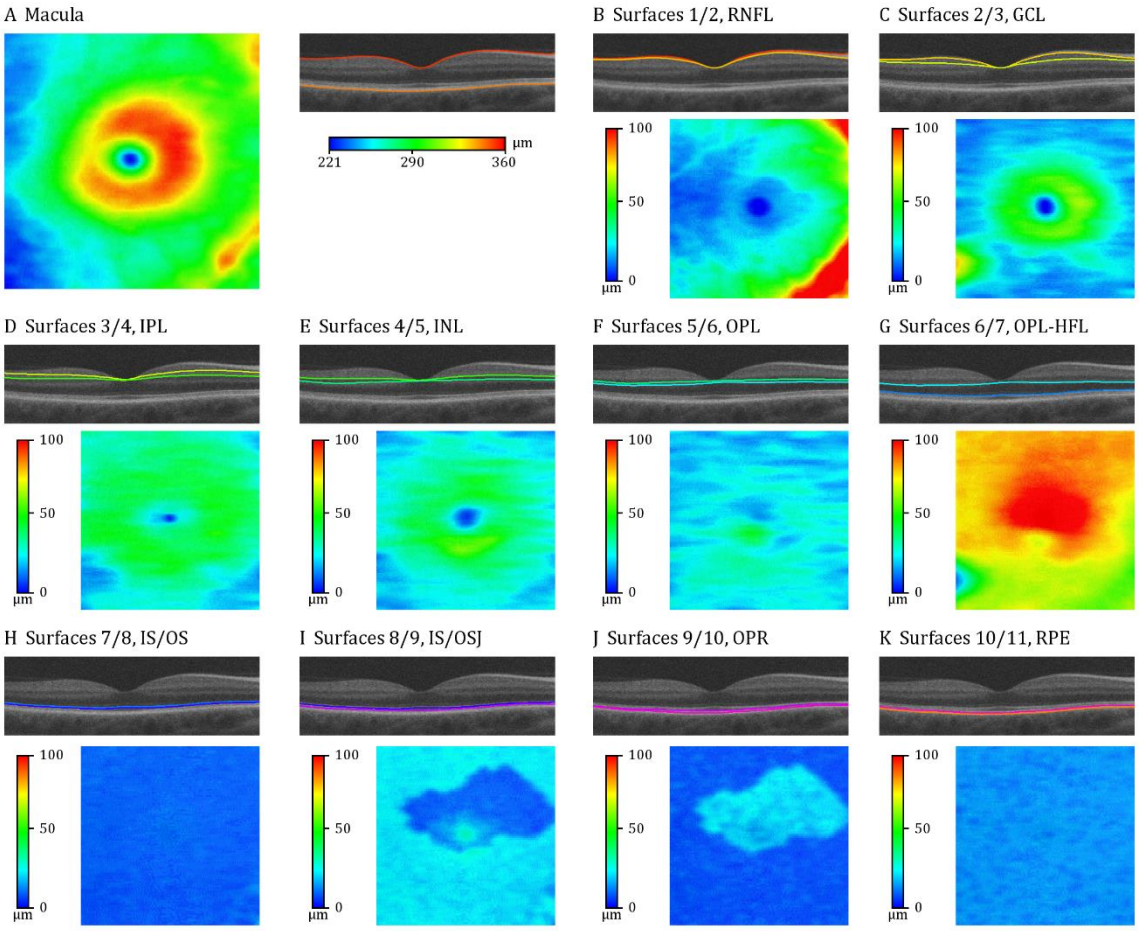

Figure II.19 Representative mean thickness maps for each of the segmented layers of the retina. (**A**) Macula thickness can be defined as the mean distance between the surface (1) inner limiting membrane (ILM) and the interface between the retinal pigment epithelium (RPE) and the choroid. (**B-K**) The algorithm automatically defines 11 surfaces used for computing regional thicknesses. Color-coded thickness maps can also be obtained (blue, thinner; red, thicker). RNFL, *Retinal nerve fibre layer;* GCL, *ganglion cell layer;* IPL, *internal plexiform layer;* INL, *inner nuclear layer;* OPL, *outer plexiform layer;* OPL-HFL, *OPL-Henle fibre layer;* IS/OS, *photoreceptors inner segment/outer segment layer;* IS/OSJ, *IS/OS junction;* OPR, *outer photoreceptor layer*.

2.3 MRI Data acquisition

All participants will be submitted to MRI protocols in a 3T scanner (Siemens Magnetom TrioTim 3T Erlangen, Germany) at the Institute of Nuclear Sciences Applied to Health (ICNAS) using a 12-channel birdcage head coil. One high-resolution T1-weighted ($T1_w$) *three-dimensional Magnetization Prepared Rapid Acquisition Gradient Echo* (MPRAGE; repetition time (TR) 2530 ms, echo time (TE) 3.42 ms, inversion time (TI) 1100 ms, flip angle (FA) 7°, field of view (FoV) 256×256 mm^2, yielding 176 slices with 1×1×1 mm^3 voxel size, GRAPPA acceleration factor=2) will be used to place the ^{1}H-MRS volume of interest (VOI) and to quantify the tissue fraction within the voxel (grey matter (GM), white matter (WM) and cerebrospinal fluid (CSF)).

^{1}H-MR *Point RESolved Spectroscopy* (PRESS, Figure II.20 C) and the MEshcher-GArwood Point RESolved Spectroscopy (MEGAPRESS, Figure II.20 B) sequence will be applied in a 3×3×3 cm^3 voxel positioned medially in the occipital cortex, as described previously in (Violante et al., 2013, Figure II.20 A). The MEGAPRESS sequence (Edden & Barker, 2007; Mescher, Merkle, Kirsch, Garwood, & Gruetter, 1998; Mullins et al., 2014) [TR 1500 ms, TE 68 ms, FA 90°, 196 averages, 1024 data points] will be specifically used to measure GABA levels. In MEGA-PRESS, during odd and even number acquisitions, editing frequency-selective inversion pulses are applied to the GABA-C3 resonance at 1.9 ppm (refocused 'on resonance') and 7.5 ppm (non-refocused 'off resonance') respectively. Since the majority of peaks in the spectrum are undisturbed by the applied editing pulses, subtracting 'on' and 'off' spectra removes these peaks and retains the GABA peak from the spectrum. MEGA-PRESS spectra without the suppression of the water signal (16 averages) will be acquired in the same location to calculate water-scaled GABA concentrations. A PRESS sequence [TR 2000 ms, TE 35 ms, FA 90°, 160 averages, 1024 data points] will be used to evaluate other relevant metabolites such as N-acetylaspartate (NAA), creatine (Cr) and choline (Cho) compounds, glutamate (Glu) and glutamine (Gln) and myo-inositol (Ins). PRESS spectra with unsuppressed water signal (16 averages) will also be acquired to estimate absolute metabolites concentration.

Phosphorus-31 magnetic resonance spectroscopy imaging (^{31}P-MRSI) will be performed on the same session using a dual-tuned ^{31}P/^{1}H volume head coil (RAPID Biomedical GmbH, Rimpar, Germany). First we will acquire one 3D $T1_w$ MPRAGE (repetition time (TR) 2300 ms, echo time (TE) 2.83 ms, inversion time (TI) 900 ms, flip angle (FA) 9°, field of view (FoV) 256×256 mm^2, yielding 128 slices with 1.3×1.3×1.3 mm^3 voxel size) with multi-planar reconstructions to position the ^{31}P-MRS grid for the uniform positioning of the ^{31}P-MRS grid in the mid-sagittal plane with an anterior-posterior commissure (AC-PC) angulation covering all occipital lobe (Figure II.21.A). This MPRAGE will be also used to overlap the MRS grid during the post processing and to account for partial volume effects of the CSF, and measure the fraction of grey and white matter of each analysed voxel. Manual shimming of the B0 magnetic field will be performed. Multivoxel ^{31}P-MRS grid will be placed to cover the whole occipital region with 3D chemical shift imaging (CSI). A weighted phase encoding scheme will be used resulting in an axial slice with a nominal thickness of 26 mm and 16×16 mm^2 in plane resolution (8 averages, TR 2000 ms, TE 2.3 ms, FOV 260×260×80 mm^3, FA 60°, 8 averages, 1024 data points, BW = 2000 Hz, WALTZ4 proton decoupling). The nominal voxel size was 26×26×26 mm^3 (nominal volumes of 17.576 cm^3) and then interpolated to 16×16×16 mm^3, to increase spatial resolution.

2.4 Data analysis

2.4.1 Tissue fraction correction

In order to account for variability of tissue fraction enclosed in the analysed voxel, both ^{1}H- and ^{31}P/^{1}H-MRS anatomical T1-weighted images will be segmented into the three main tissues, grey matter (GM), white matter (WM) and cerebrospinal fluid (CSF) enclosed in spectroscopy voxel (Figure II.20 A, II.21 A). Wherefore an in-house MATLAB (TheMathWorks, USA) scrip relying on the SPM8 (Wellcome Trust Centre for Neuroimaging, Institute of Neurology, UCL, London, UK, http://www.fil.ion.ucl.ac.uk/spm/) and VBM8 toolboxes (http://dbm.neuro.uni-jena.de/vbm8/) will be used.

This script is being adapted to 3D CSI matrices. In this case, the tissue fraction will be calculated for each voxel of interest within the Siemens MRSI acquisition grid for each participant. This work is being done in collaboration with the Nijmegen Imaging Center, The Netherlands.

2.4.2 ^{1}H-MRS MEGA-PRESS and PRESS Data analysis

To measure more accurately GABA levels that are masked by strongly concentrated metabolites (Cr, Glu and NAA) we will use a J-difference editing technique (MEGA-PRESS, Figure II.20 B) (Puts & Edden, 2012). MEGA-PRESS spectroscopy data will be analysed using Gannet GABA-MRS Analysis Tool (Edden, Puts, Harris, Barker, & Evans, 2014) for MATLAB (TheMathWorks, USA). Briefly, a 3 Hz exponential line broadening will be applied to all spectra prior to the Fast Fourier Transform of the time resolved data. After the frequency and phase correction and the outlier rejection, the edited difference spectrum will be generated for each dataset. A nonlinear least-squares fitting will be performed to integrate the ~3.00 ppm GABA (Gaussian model), creatine (Lorentzian model) and the unsuppressed water peak (Lorentzian-Gaussian model).

PRESS data (Figure II.20 C) will be post-processed with LCModel version 6.3 (Provencher, 1993). LCModel analyses the in vivo spectra as a linear combination of prior knowledge in vitro standard basis dataset acquired in a 3T scanner with an identical PRESS sequence with TE 35 ms as in our study. Eddy-current correction and water scaling will be performed. The water scaling will allow the estimation of absolute concentrations presented in institutional units, approximating mmol per Kg wet weight. Spectra will be visually inspected and only metabolites for which Crámer-Rao Lower Bounds (CRLB) are less than 20% will considered for statistical analysis (Provencher, 1993) to exclude poorly fitted data. Only data between chemical shifts of 4.0 and 0.2 ppm (and between 4.0 and 1.8 ppm in case of spectra with major lipid and macromolecules artefacts) will be analysed. Total NAA (tNAA) in the form of N-acetylaspartate and N-acetylaspartylglutamate (NAA+NAAG), and Glx in the form of glutamate plus glutamine (Glu+Gln) and total creatine (Cr+PCr) will be analysed as a sum. Glu and Gln were also analysed separately. We will also look for myoinositol (Ins), taurine (tau) and choline compounds in the form of glycerophosphocholine and phosphocholine (GPC+PCh) levels (Figure II.20). Partial volume correction for CSF fraction will be performed automatically during the model fitting (http://s-provencher.com/pub/LCModel/manual/manual.pdf) using the equation described by Ernst et al. (Ernst, Kreis, & Ross, 1993).

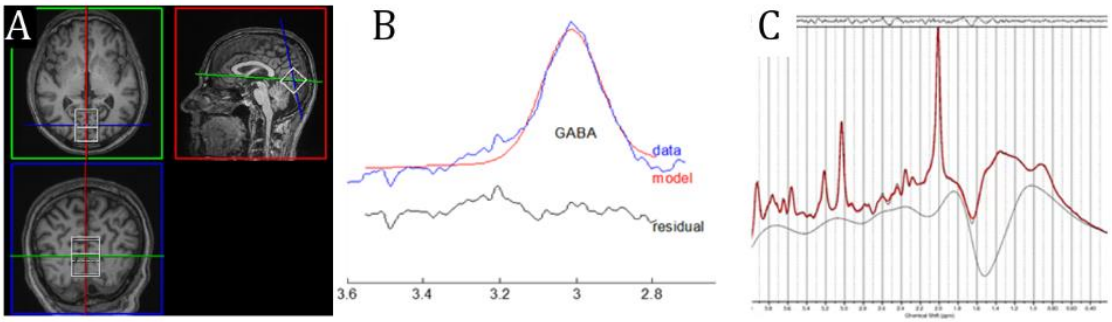

Figure II.20 Spectroscopic acquisition and data processing. ^{1}H-MRS will be acquired in a (**A**) single voxel placed medially in the occipital cortex. Two complementary ^{1}H-MRS acquisition sequences will be used to acquire (**B**) MEGA-PRESS edited GABA signal (analyzed through Gannet) and (**C**) PRESS spectrum (analyzed through LCModel) to estimate NAA, tCr, tCho, Ins, Glu and Gln levels. In (**C**), are represented the processed data (black solid line), the LCModel fitted spectrum (red solid line), the residuals (grey solid line, on top) and the baseline (light grey solid line). GABA, *γ-aminobutyric acid*; Gln, *glutamine*; Glu, *glutamate*; myo, *myoinositol*; NAA, *N-acetylaspartate*; tCho, *total choline*; tCr, *total creatine*.

2.4.3 ^{31}P-MRSI: CSI – chemical shift imaging

^{31}P-MRS spectra will be analysed through jMRUI (version 5.2). jMRUI (Naressi et al., 2001; Stefan et al., 2009) allows to analyse and quantify advanced time-domain MRS data. Signals of residual water will be filtered using a Hankel Lanczos Singular Values Decomposition (HLSVD, Van den Boogaart et al., 1994) and metabolite quantification will be performed through the AMARES algorithm (Vanhamme, van den Boogaart, & Van Huffel, 1997) with soft constraints. Starting values, chemical shifts and J-coupling will be provided as prior knowledge information (Hamilton, Patel, Forton, Hajnal, & Taylor-Robinson, 2003). Exploratory analyses are being performed using the fitting routine from syngo software (syngo MR B19, Siemens Healthcare, Germany) software. Post-processing steps include 200 ms Hanning filter, zero filling to 2048 points, Fourier transformation, phase, baseline and frequency shi-ft correction and curve fitting (Figure II.21).

We will also indirectly estimate several indexes of steady-state mitochondrial functionality, cellular energy reserves and oxidative phosphorylation through the calculus of PP (Veech, Lawson, Cornell, & Krebs, 1979), the maximal rate of ATP biosynthesis (%V/V_{max}) (Nioka et al., 1987), free cytosolic Mg^{2+} concentration (Iotti et al., 1996) and pH (Barker, Butterworth, Boska, Nelson, & Welch, 1999; Petroff et al., 1985). Analysis will be focused on voxels located on the occipital lobe.

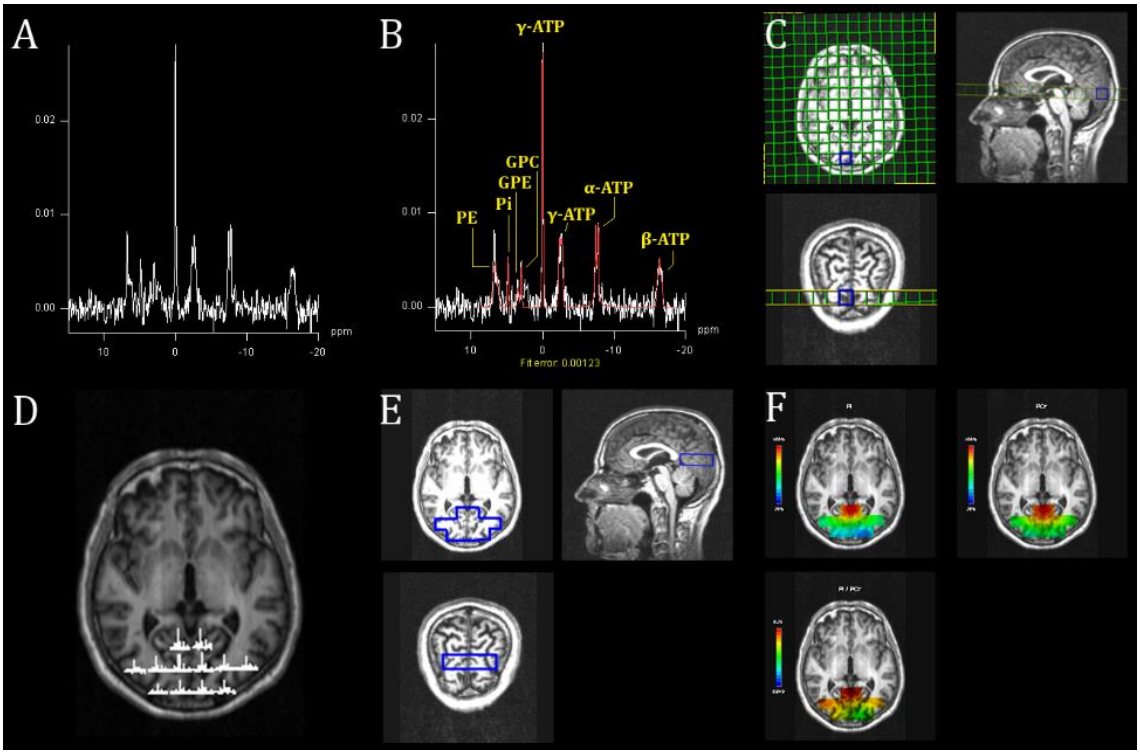

Figure II.21 ^{31}P-MRS acquisition and data processing. Representative (**A**) spectra of a voxel (raw spectrum (white) and with the (**B**) modelled fit (red) overlaid selected from (**C**) one 16×16×16 mm^3 voxel in the right ventral occipital lobe. Some peaks are represented by these fitting: inorganic phosphate, P_i; gamma-, alpha-, and beta-adenosine triphosphate, γ-, α-, β-ATP; phosphocreatine, PCr; phosphomonoesters, PE. (**D**) Spectral maps may be obtained for (**E**) each voxel-of-interest from the acquisition. In the selected voxels syngo may calculate coloured (**F**) metabolite maps that allow a quick visual inspection of the regional distribution of a particular metabolites (P_i, *up left*; PCr, *right*) or ratio between two metabolites (P_i/PCr ratio, *below*).

2.5 Statistical analysis

All statistical analyses will be performed using the IBM SPSS Statistics (IBM Corp., Armonk, NY, USA) package. Kolmogorov-Smirnov (K-S) test with Lilliefors correction will be performed for each evaluated variable to check for data normality (p>0.05). Analyses will be performed between LHON and control group using parametric multivariate analysis of variance (MANOVA) for homologous OCT regions and MRS metabolites concentrations and ratios, whenever possible. We also will calculate Cohen's d from F-tests to evaluate the effect size of the MANOVA statistical results. When data do not met normality assumptions, Mann-Whitney U tests will be used instead.

To analyse OCT thickness differences within each group, we will use parametric GLM Repeated Measures ANCOVA (rmANCOVA), setting age as a metric covariate and analyze gender as a putative confound. When data do not meet the assumptions of sphericity, we will use the epsilon value to choose the type of correction to apply: the Huynh–Feldt (for $\varepsilon > 0.75$) or the Greenhouse–Geisser (for $\varepsilon \leq 0.75$). Multiple comparison post-hoc tests between OCT layers thickness will be based on the Bonferroni correction.

Spearman correlation analyses (r_s) will be performed within each group between some metabolites (namely NAA, glutamate, GABA) and retinal layers thickness measures (namely RNFL and GCL). A false discovery rate (*FDR*) set to 0.15 will be used to control for multiple comparisons in bivariate correlation p-values using the Benjamini–Hochberg procedure (Benjamini & Hochberg, 1995).

All statistical data will be presented as the mean ± *SEM* (standard error of the mean). Two-tailed hypothesis testing will be performed at a 0.05 significance level, with 0.06 trend level.

3 AKNOWLEDGEMENTS

I would like to acknowledge the kind welcome in the Biomedical MR research group of Professor Arend Heerschap (Department of Radiology, the Radboud University in the Nijmegen Medical Centre, Nijmegen, The Netherlands) for a short internship from 15th to 19th of September of 2014. There I acquired hands-on experience on how to perform ^{31}P-MRS experiments of humans and also learned how to process the data, discussed and learned about human and animal MRS data acquisition in general and about the methodologies and processing protocols involved. I would also like to thank Anne Rijpma (Biomedical MR research group, Radboud University, Nijmegen Medical Centre, Nijmegen, The Netherlands) for her help with several steps of ^{31}P-MRS acquisition and analysis details.

This work has been supported by the grant PTDC/DTP-EPI/0929/2012 - "Translational bigenomics investigation in Leber´s Hereditary Optic Neuropathy: genotype-phenotype Correlation". O.C.A. was supported by the Portuguese Foundation for Science and Technology with the individual scholarship SFRH/BD/76013/2011.

4 REFERENCES

Abràmoff, M. D., Garvin, M. K., & Sonka, M. (2010). Retinal imaging and image analysis. *IEEE Reviews in Biomedical Engineering*, *3*, 169–208. doi:10.1109/RBME.2010.2084567

Antony, B., Abràmoff, M. D., Tang, L., Ramdas, W. D., Vingerling, J. R., Jansonius, N. M., … Garvin, M. K. (2011). Automated 3-D method for the correction of axial artifacts in spectral-domain optical coherence tomography images. *Biomedical Optics Express*, *2*(8), 2403–2416. doi:10.1364/BOE.2.002403

Arias-Mendoza, F. (2004). In vivo magnetic resonance spectroscopy in the evaluation of mitochondrial disorders. *Mitochondrion*, *4*(5), 491–501. doi:10.1016/j.mito.2004.07.034

Barbiroli, B., Montagna, P., Cortelli, P., Iotti, S., Lodi, R., Barboni, P., … Zaniol, P. (1995). Defective brain and muscle energy metabolism shown by in vivo 31P magnetic resonance spectroscopy in nonaffected carriers of 11778 mtDNA mutation. *Neurology*, *45*(7), 1364–1369. doi:10.1212/WNL.45.7.1364

Barbiroli, B., Montagna, P., Martinelli, P., Lodi, R., Iotti, S., Cortelli, P., … Zaniol, P. (1993). Defective brain energy metabolism shown by in vivo 31P MR spectroscopy in 28 patients with mitochondrial cytopathies. *Journal of Cerebral Blood Flow & Metabolism*, *13*(3), 469–474. doi:10.1038/jcbfm.1993.61

Barcella, V., Rocca, M. A., Bianchi-Marzoli, S., Milesi, J., Melzi, L., Falini, A., … Filippi, M. (2010). Evidence for retrochiasmatic tissue loss in Leber's hereditary optic neuropathy. *Human Brain Mapping*, *31*(12), 1900–1906. doi:10.1002/hbm.20985

Barker, P. B., Butterworth, E. J., Boska, M. D., Nelson, J., & Welch, K. M. A. (1999). Magnesium and pH imaging of the human brain at 3.0 Tesla. *Magnetic Resonance in Medicine*, *41*(2), 400–406.

Benjamini, Y., & Hochberg, Y. (1995). Controlling the false discovery rate: a practical and powerful approach to multiple testing. *Journal of the Royal Statistical Society. Series B (Methodological)*, *57*(1), 289–300.

Cortelli, P., Montagna, P., Avoni, P., Sangiorgi, S., Bresolin, N., Moggio, M., … Lugaresi, E. (1991). Leber's hereditary optic neuropathy: genetic, biochemical, and phosphorus magnetic resonance spectroscopy study in an Italian family. Neurology, 41(8), 1211–1215.

d'Almeida, O. C., Mateus, C., Reis, A., Grazina, M. M., & Castelo-Branco, M. (2013). Long term cortical plasticity in visual retinotopic areas in humans with silent retinal ganglion cell loss. *Neuroimage*, *81*, 222–230. doi:10.1016/j.neuroimage.2013.05.032

Edden, R. A. E., & Barker, P. B. (2007). Spatial effects in the detection of γ-aminobutyric acid: improved sensitivity at high fields using inner volume saturation. *Magnetic Resonance in Medicine*, *58*(6), 1276–1282. doi:10.1002/mrm.21383

Edden, R. A. E., Puts, N. A. J., Harris, A. D., Barker, P. B., & Evans, C. J. (2014). Gannet: a batch-processing tool for the quantitative analysis of gamma-aminobutyric acid–edited MR spectroscopy spectra. *Journal of Magnetic Resonance Imaging*, *40*(6), 1445–1452. doi:10.1002/jmri.24478

Ernst, T., Kreis, R., & Ross, B. D. (1993). Absolute quantitation of water and metabolites in the human brain. I. Compartments and water. *Journal of Magnetic Resonance, Series B*, *102*(1), 1–8. doi:10.1006/jmrb.1993.1055

Garvin, M. K., Abràmoff, M. D., Wu, X., Russell, S. R., Burns, T. L., & Sonka, M. (2009). Automated 3-D Intraretinal Layer Segmentation of Macular Spectral-Domain Optical Coherence Tomography Images. *IEEE Transactions on Medical Imaging*, *28*(9), 1436–1447. doi:10.1109/TMI.2009.2016958

Hamilton, G., Patel, N., Forton, D. M., Hajnal, J. V., & Taylor-Robinson, S. D. (2003). Prior knowledge for time domain quantification of in vivo brain or liver 31P MR spectra. *NMR in Biomedicine*, *16*(3), 168–176. doi:10.1002/nbm.821

Hedges, T. R., Gobuty, M., Manfready, R. A., Erlich-Malona, N., Monaco, C., & Mendoza-Santiesteban, C. E. (2016). The Optical Coherence Tomographic profile of Leber Hereditary Optic Neuropathy. *Neuro-Ophthalmology*, *40*(3), 107–112. doi:10.3109/01658107.2016.1173709

Howell, N. (1997). Leber hereditary optic neuropathy: how do mitochondrial DNA mutations cause degeneration of the optic nerve? *Journal of Bioenergetics and Biomembranes*, *29*(2), 165–173.

Iotti, S., Frassineti, C., Alderighi, L., Sabatini, A., Vacca, A., & Barbiroli, B. (1996). In vivo assessment of free magnesium concentration in human brain by 31P MRS. A new calibration curve based on a mathematical algorithm. *NMR in Biomedicine*, *9*(1), 24–32. doi:10.1002/(SICI)1099-1492(199602)9:1<24::AID-NBM392>3.0.CO;2-B

Jančić, J., Dejanović, I., Radovanović, S., Ostojić, J., Kozić, D., Đurić-Jovičić, M., … Kostić, V. (2015). White matter changes in two Leber's Hereditary Optic Neuropathy pedigrees: 12-year follow-up. *Ophthalmologica*, *235*(1), 49–56. doi:10.1159/000441089

Kirches, E. (2011). LHON: mitochondrial mutations and more. *Current Genomics*, *12*(1), 44–54.

Leber, T. (1871). Ueber hereditäre und congenital-angelegte sehnervenleiden. *Graefe's Archive for Clinical and Experimental Ophthalmology*, *17*(2), 249–291.

Lodi, R., Carelli, V., Cortelli, P., Iotti, S., Valentino, M. L., Barboni, P., … Barbiroli, B. (2002). Phosphorus MR spectroscopy shows a tissue specific in vivo distribution of biochemical expression of the G3460A mutation in Leber's hereditary optic neuropathy. *Journal of Neurology, Neurosurgery & Psychiatry*, *72*(6), 805–807. doi:10.1136/jnnp.72.6.805

Mascialino, B., Leinonen, M., & Meier, T. (2011). Meta-analysis of the prevalence of Leber hereditary optic neuropathy mtDNA mutations in Europe. *European Journal of Ophtalmology*, *22*(3), 461–465.

Mateus, C., d'Almeida, O. C., Reis, A., Silva, E., & Castelo-Branco, M. (2016). Genetically induced impairment of retinal ganglion cells at the axonal level is linked to extrastriate cortical plasticity. *Brain Structure and Function*, *221*(3), 1767–1780. doi:10.1007/s00429-015-1002-2

Mescher, M., Merkle, H., Kirsch, J., Garwood, M., & Gruetter, R. (1998). Simultaneous in vivo spectral editing and water suppression. *NMR in Biomedicine*, *11*(6), 266–272. doi:10.1002/(SICI)1099-1492(199810)11:6<266::AID-NBM530>3.0.CO;2-J

Mullins, P. G., McGonigle, D. J., O'Gorman, R. L., Puts, N. A., Vidyasagar, R., Evans, C. J., … Edden. (2014). Current practice in the use of MEGA-PRESS spectroscopy for the detection of GABA. *Neuroimage*, *86*, 43–52. doi:10.1016/j.neuroimage.2012.12.004

Naressi, A., Couturier, C., Devos, J. M., Janssen, M., Magneat, C., de Beer, R., & Graveron-Demilly, D. (2001). Java-based graphical user interface for the MRUI quantitation package. *Magnetic Resonance Materials in Physics, Biology and Medicine*, *12*(2-3), 141–152. doi:10.1007/bf02668096

Nioka, S., Chance, B., Hilberman, M., Subramanian, H. V., Leigh, J. S., Veech, R. L., & Forster, R. E. (1987). Relationship between intracellular pH and energy metabolism in dog brain as measured by 31P-NMR. *Journal of Applied Physiology*, *62*(5), 2094–2102.

Ostojic, J., Jancic, J., Kozic, D., Semnic, R., Koprivsek, K., Prvulovic, M., & Kostic, V. (2009). Brain white matter 1 H MRS in Leber optic neuropathy mutation carriers. *Acta Neurologica Belgica*, *109*(4), 305–309.

Petroff, O. A., Prichard, J. W., Behar, K. L., Alger, J. R., den Hollander, J. A., & Shulman, R. G. (1985). Cerebral intracellular pH by 31P nuclear magnetic resonance spectroscopy. *Neurology*, *35*(6), 781–788.

Provencher, S. W. (1993). Estimation of metabolite concentrations from localized in vivo proton NMR spectra. *Magnetic Resonance in Medicine*, *30*(6), 672–679. doi:10.1002/mrm.1910300604

Puts, N. A., & Edden, R. A. (2012). In vivo magnetic resonance spectroscopy of GABA: a methodological review. *Progress in Nuclear Magnetic Resonance Spectroscopy*, *60*, 29–41. doi:10.1016/j.pnmrs.2011.06.001

Rizzo, G., Tozer, K. R., Tonon, C., Manners, D., Testa, C., Malucelli, E., … Lodi, R. (2012). Secondary post-geniculate involvement in Leber's Hereditary Optic Neuropathy. *PLoS ONE*, *7*(11), 1–7. doi:10.1371/journal.pone.0050230

Rojas, J. C., & Gonzalez-Lima, F. (2010). Mitochondrial optic neuropathy: in vivo model of neurodegeneration and neuroprotective strategies. *Eye and Brain*, *2*, 21–37.

Rojas, J. C., John, J. M., Lee, J., & Gonzalez-Lima, F. (2009). Methylene blue provides behavioral and metabolic neuroprotection against optic neuropathy. *Neurotoxicity Research*, *15*(3), 260–273. doi:10.1007/s12640-009-9027-z

Stefan, D., Di Cesare, F., Andrasescu, A., Popa, E., Lazariev, A., Vescovo, E., … Graveron-Demilly, D. (2009). Quantitation of magnetic resonance spectroscopy signals: the jMRUI software package. *Measurement Science and Technology*, *20*(10), 104035. doi:10.1088/0957-0233/20/10/104035

Van den Boogaart, A., Van Ormondt, D., Pijnappel, W. W. F., De Beer, R., & Ala-Korpela, M. (1994). Removal of the water resonance from 1H magnetic resonance spectra. *Mathematics in Signal Processing*, *3*, 175–195.

Vanhamme, L., van den Boogaart, A., & Van Huffel, S. (1997). Improved method for accurate and efficient quantification of MRS data with use of prior knowledge. *Journal of Magnetic Resonance*, *129*(1), 35–43.

Veech, R. L., Lawson, J. W., Cornell, N. W., & Krebs, H. A. (1979). Cytosolic phosphorylation potential. *Journal of Biological Chemistry*, *254*(14), 6538–6547.

Violante, I. R., Ribeiro, M. J., Edden, R. A. E., Guimarães, P., Bernardino, I., Rebola, J., … Castelo-Branco, M. (2013). GABA deficit in the visual cortex of patients with neurofibromatosis type 1: genotype-phenotype correlations and functional impact. *Brain*, *136*(Pt 3), 918–925. doi:10.1093/brain/aws368

Zhang, Y., Huang, H., Wei, S., Gong, Y., Li, H., Dai, Y., … Yan, H. (2014). Characterization of macular thickness changes in Leber's hereditary optic neuropathy by optical coherence tomography. *Experimental and Therapeutic Medicine*, *14*(1), 105.

Zhuo, Y., Luo, H., & Zhang, K. (2012). Leber hereditary optic neuropathy and oxidative stress. *Proceedings of the National Academy of Sciences*, *109*(49), 19882–19883. doi:10.1073/pnas.1218953109

CHAPTER III

Autosomal Dominant Optic Atrophy (Kjer's Disease)

III. 1

- Impaired cortical physiology with structural sparing was found in ADOA patients given the identified GABAergic changes in the occipital cortex, without volumetric changes.
- This cortical physiological alteration may be relevant for the exploration of hitherto unexpected brain dysfunction.

CH. III. 1

A NOVEL CORTICAL NEUROCHEMICAL PHENOTYPE IN A GENETIC MITOCHONDRIAL DISORDER AFFECTING THE RETINAL GANGLION CELL

Otília C. d'Almeida,

Inês R. Violante, Bruno Quendera, Miguel Castelo-Branco

ABSTRACT

Purpose: It has remained a mystery why some genetic mitochondrial disorders only affect some cell types such as the retinal ganglion cell. Concerning the brain, this is particularly intriguing given that retinal and cortical function are often tightly linked in health and disease. Moreover, neurotransmission and metabolism are strongly associated, which motivated our investigation of a putative neurochemical and/or structural phenotype in autosomal dominant optic neuropathy (ADOA), a disease model where the ganglion cell is known to be the main target.

Methods: We acquired in vivo structural and biochemical proton magnetic resonance imaging data using (^{1}H-MRS) of 14 ADOA and 11 age-matched control participants focusing the occipital lobe.

Results: We found evidence for reduced occipital γ-aminobutyric acid (GABA) in the absence of cortical or subcortical atrophy as assessed by cortical thickness and volumetric measures. No changes in other metabolites were found, namely N-acetylaspartate (NAA) or glutamate.

Conclusions: These results suggest that mitochondrial disorders that were previously believed to only affect retinal function also affect cortical physiology, especially the GABAergic system and support the notion of a tight link between metabolism and neurotransmission. Future studies should address the impact of this novel phenotype on visual and cognitive function as identified in other disorders.

d'Almeida, O. C., Violante, I. R., Quendera, B., & Castelo-Branco, M. A novel cortical neurochemical phenotype in a genetic 1 mitochondrial disorder affecting the retinal ganglion cell. (*Submitted* - 2016)

1 INTRODUCTION

Several neurodegenerative and mitochondrial inherited diseases are strongly associated to both mitochondrial dysfunction and optic nerve atrophy (for review see Maresca et al. (2013)). In fact, due to the high-energy demands, the visual pathway is especially susceptible to mitochondrial dysfunction.

Autosomic dominant optic atrophy (ADOA, Kjer's disease, MIM #165500) is the most common hereditary mitochondrial disease (Carelli, Ross-Cisneros, & Sadun, 2004) with an estimated prevalence of 1 in 25 000 in Northern England (Yu-Wai-Man & Chinnery, 2013). ADOA is a genetic disorder with progressive degeneration that *"commences as a degeneration of retinal ganglion cells, with secondary ascending optic atrophy and changes of the corresponding tract and areas in the lateral geniculate body"* (Kjer, Jensen, & Klinken, 1983). Genetic studies have associated the disorder to mutations mainly in the nuclear gene OPA1 on chromosome 3q28-q29 (Delettre et al., 2000) that encodes for mitochondrial proteins.

These mutations have an impact on the subunit I of the mitochondrial transport chain leading to the disruption of mitochondrial dynamics and influencing the normal mitochondrial fusion and fission balance (Williams et al., 2012; Yu-Wai-Man, Trenell, Hollingsworth, Griffiths, & Chinnery, 2011). Phenotypically this disorder is characterized by moderate to severe central vision deterioration and/or blindness due to optic nerve atrophy and retinal nerve fibre layer (RNFL) degeneration (Votruba et al., 1998). Despite the well documented expression of ADOA as optic nerve pathology (Williams et al., 2012; Williams, Morgan, & Votruba, 2010), less is known regarding the impact on the brain. A previous study showed that OPA1 gene is ubiquitously expressed in both retina, optic tract and brain (Bette, Schlaszus, Wissinger, Meyermann, & Mittelbronn, 2005) rendering quite intriguing the classical assumption of the predominant selectivity for retinal ganglion cells (RGC) in genetic mitochondrial disorders.

In here we aimed to investigate the cortical phenotype of ADOA that leads to the loss of central vision with optic nerve atrophy and retinal ganglion cell degeneration. We performed cortical thickness and volumetric analysis, and also biochemical analysis in vivo using proton MR Spectroscopy (^{1}H-MRS) in the occipital cortex of OPA1-ADOA patients to assess metabolism and neurotransmission.

2 METHODS

2.1 Participants

We have tested 14 ADOA patients (5 males, mean age±*SD*=35.8±17.50 years) belonging to different pedigrees (Table III.1). These participants are a subgroup from the ones described elsewhere from the visual function point of view (Reis et al., 2013). The diagnosis was mainly based on classical clinical evaluation and also on genetic assessment (OPA1 mutation analysis). Participants from the ADOA group were submitted to MRI acquisition and data were compared to an age-matched control group (11 participants; 5 males, mean age±*SD*=33.3±10.84 years). All participants were checked for the presence of other neuro-ophthalmologic pathology, besides ADOA). The study followed the tenets of the Declaration of Helsinki and was approved by our Institutional Review Board. Informed consent was obtained from each patient and after procedures of the research had been fully explained.

Table III.1 Demographic characteristics of the ADOA participants. LE, *left eye*; RE, *right eye*.

ID	Gender	Age (y)	Visual Acuity		Family	Mutation	
			LE	RE		at coding DNA level	at protein level
1	F	56	0.1	0.1	D	c.2708_2711del	p.Val903Glyfs*3
2	F	16	0.5	0.5	A	c.869 G>A	p.Arg290Gln het
3	M	19	0.3	0.3	A	c.869 G>A	p.Arg290Gln het
4	F	40	0.3	0.3	A	c.869 G>A	p.Arg290Gln het
5	F	33	0.16	0.16	I	No mutation identified	
6	F	48	0.6	0.6	B	c.2708_2711del	p.Val903Glyfs*3
7	F	76	0.2	0.2	B	c.2708_2711del	p.Val903Glyfs*3
8	M	19	0.4	0.4	C	c.2131 C>T	p.Arg711*het
9	M	39	0.1	0.1	F	No mutation identified	
10	F	41	0.5	0.5	F	No mutation identified	
11	M	31	0.2	0.3	L	No mutation identified	
12	M	47	0.1	0.1	D	c.2708_2711del	p.Val903Glyfs*3
13	F	16	0.2	0.3	H	No mutation identified	
14	F	20	0.2	0.3	K	No mutation identified	

2.2 MRI Data acquisition

In this study we acquired high resolution MRI data was in a 3T scanner (Siemens Magnetom TrioTim 3T Erlangen, Germany), with a 12 channel head coil. For each participant, two three-dimensional *Magnetization Prepared Rapid Acquisition Gradient Echo* (MPRAGE) sequences were acquired (repetition time (TR) 2.3 s, echo time (TE) 2.98 ms, flip angle (FA) 9°, field of view (FoV) 256×256 mm^2, yielding 160 slices with 1×1×1 mm3 voxel size). ^{1}H-Magnetic Resonance Spectroscopy was also performed in a 3×3×3 cm^3 voxel positioned medially in the occipital cortex (Figure III.1 A). *Point RESolved Spectroscopy* (PRESS, TE=30 ms, 160 averages) and *MEshcher-GArwood Point RESolved Spectroscopy* (MEGA-PRESS, TE=68 ms, TR=1.5 s, 196 averages) sequences were used to estimate Glutamate and GABA, respectively.

2.3 MRI Data Analysis

All image processing and morphometric procedures to estimate cortical thickness were performed with BrainVoyager QX 2.8 (Brain Innovation, Maastricht, The Netherlands). Structural data pre-processing was similar to the described in d'Almeida et al. (2013). To improve statistical group-level analysis and be able to use anatomically-defined regions of interest (ROI), a cortical-based alignment procedure was used (Geuze et al., 2008). This procedure enhances the quality of the alignment between brains over the Talairach registration, using the curvature information of the cortex. Cortical thickness was estimated using an automatic algorithm that applies the second-order partial differential Laplace's equation (Jones, Buchbinder, & Aharon, 2000). After the computation, a cortical thickness map was superimposed in the VMR data file, and then interpolated into the spherical cortical meshes. Using BVQX tools, ROIs were superimposed in the CT maps and the mean values of thickness for each area were calculated. To prevent outlier biases, an outlier removal criterion was considered. This approach consisted in the recalculation of the mean excluding the values deviating more than 3 standard deviations (*SD*) of the mean.

Volumetric analysis were conducted using SPM8 (Wellcome Trust Centre for Neuroimaging, Institute of Neurology, UCL, London, UK, http://www.fil.ion.ucl.ac.uk/spm/) and VBM8 toolboxes (http://dbm.neuro.uni-jena.de/vbm8/) running in Matlab (MATLAB R2013a, TheMathworks, USA) environment. Briefly, the following steps were followed: (1) two MPRAGE images were aligned and averaged to increase the SNR; (2) the image was manually centred to the anterior commissure and re-aligned onto the AC-posterior commissure (PC) axis; (3) through VBM8, the image was automatically corrected for field inhomogeneity, normalized to MNI space and segmented into three main tissues based on probabilistic maps, grey matter (GM), white matter (WM) and cerebrospinal fluid (CSF) using the Diffeomorphic Anatomical Registration using the Exponentiated Lie algebra

(DARTEL) algorithm (Ashburner, 2007); (4) the GM and WM modulated images were smoothed with a Gaussian kernel of 8mm (FWHM).

We used a standard, independent t-test with an absolute threshold masking of 0.1 to investigate structural changes (including both GM and WM volumes) between ADOA and control groups in SPM8 software. Statistical inferences were made at $p<0.05$ (corrected for multiple comparisons using Family Wise Error (*FWE*)).

2.4 ^{1}H-MRS Data analysis

To measure GABA levels more accurately we used a J-difference editing technique (MEGA-PRESS) (Puts & Edden, 2012). MEGA-PRESS data were analysed using Gannet GABA-MRS Analysis Tool (Edden, Puts, Harris, Barker, & Evans, 2014) version 2.0 for MATLAB (R2013a, v.8.1.0, TheMathWorks, USA). A 3 Hz exponential line broadening was applied to all spectra prior to the Fast Fourier Transform of the time resolved data. After the frequency and phase correction and the outlier rejection, the edited difference spectrum was generated for each dataset. Gannet uses nonlinear least-squares fitting to integrate the ~3.00 ppm GABA (Gaussian 126 model) and creatine (Lorentzian model). GABA signal will be referred as GABA$^+$ to account for the contamination by homocarnosine and macromolecule signals.

PRESS spectra were analysed using the LCModel version 6.3 (Provencher, 1993) using a linear combination of prior knowledge in vitro standard basis set. All spectra were visually inspected. Only metabolites for which Crámer-Rao Lower Bounds (CRLB) were less than 22% were considered for statistical analysis. The analysis window covered chemical shifts between 4.0 and 0.2 ppm (and between 4.0 and 1.8 ppm in case of spectra with major lipid and macromolecules artefacts). The analysed metabolites covered aspartate (Asp), glutamate (Glu), glutathione (GSH), myo-inositol (Ins), glycerophosphocholine+phosphocholine (GPC+PCh), N-acetylaspartate+N-acetylaspartylglutamate (tNAA) and the pool glutamate+glutamine (Glx). All ^{1}H-MRS metabolites levels were normalized to the total creatine+phosphocreatine (tCr) signal to reduce inter-subject variability.

2.5 Statistical analysis

All statistical analyses were performed with IBM SPSS Statistics 22 for Windows (version 22, IBM Corp., Armonk, NY, USA). Parametric independent *t*-tests were performed to compare ROI thicknesses and metabolite ratios between groups. Whenever normality assumption was not met (Shapiro-Wilk test, $p<0.05$), Mann-Whitney tests were used instead. Two-tailed hypothesis testing were performed at a 0.05 significance level.

3 RESULTS

3.1 ^{1}H-Magnetic Resonance Spectroscopy Analysis

The fractions of GM, WM and CSF enclosed in the acquired voxel were estimated using an in-house MATLAB script relying on the SPM8-VBM8 toolboxes. No differences in tissue content were found between ADOA and control groups (Figure III.1 B).

We acquired MEGA-PRESS data to measure free GABA levels and PRESS data to measure some relevant metabolites in the occipital cortex of both ADOA patients and healthy controls. We found a markedly decrease for GABA$^+$/tCr ratio [Mann-Whitney $U=115.0$, $p=0.011$] in ADOA patients, compared to healthy controls while no differences were found in Glu/tCr ratio (Figure III.1 C,D).

There were no differences on the other metabolites ratios (Asp, GSH, Ins, GPC+PCh and tNAA) between groups.

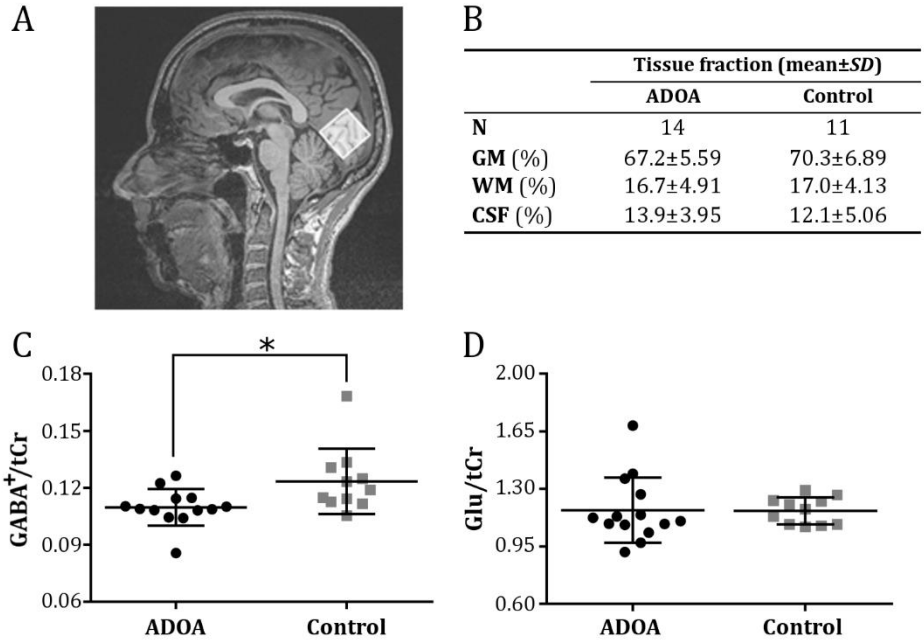

	Tissue fraction (mean±*SD*)	
	ADOA	Control
N	14	11
GM (%)	67.2±5.59	70.3±6.89
WM (%)	16.7±4.91	17.0±4.13
CSF (%)	13.9±3.95	12.1±5.06

Figure III.1 MRS acquisition and analysis. (**A**) Representative positioning of the occipital voxel for MRS PRESS and MEGA-PRESS acquisitions and the respective (**B**) mean tissue fraction for both ADOA and control groups. Cortical (**C**) $GABA^+$/total creatine (tCr) and (**D**) Glu/tCr levels for both groups (ADOA, black circles; Controls, grey squares). **p*=0.011. Graphs depict individual values, mean and standard deviation.

3.2 MRI Structural analysis

3.2.1 Cortical thickness analysis

We estimated mean cortical thickness in several anatomically-defined occipital areas and both pre- and postcentral gyri of both hemispheres and compared the averages between groups. Occipital areas comprised Brodmann areas 17, 18 and 19, as a proxy for primary visual area V1, extrastriate areas V2/V3 and higher level areas, respectively, and also several relevant gyri (cuneus, precuneus and inferior, middle and superior occipital gyri). No significant differences were found for any of the analysed regions.

3.2.2 SPM/VBM analysis

We performed whole-brain voxel-based morphometry to examine white matter volumetric differences between the ADOA patients and controls in the visual tract. Two clusters showed reduced volume in WM images of ADOA patients compared to controls in post-chiasma structures [cluster 1: peak T= 6.60; Z= 4.89; x,y,z=11, -3, -17; $p_{FWEcorr}$= 0.014; cluster 2: peak T= 7.11; Z= 5.12; x,y,z=-9, -3, -17; $p_{FWEcorr}$= 0.005] (Figure III.2).

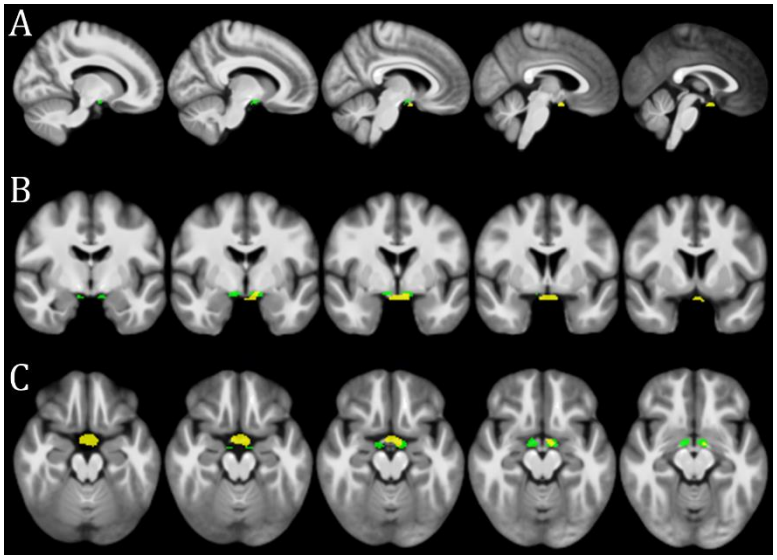

Fiure III.2 Results of VBM analysis presented at a voxel-level *p-value*<0.001, *uncorrected* (only for visualization purposes), with smoothing *FWHM*=8cm^3 on (**A**) sagittal, (**B**) coronal and (**C**) axial MRI slices. Voxels showing significant GM (yellow) and WM (green) relative volume differences are overlaid on an average image of all participants. Note that neither cortical nor subcortical regions seem to be affected and alterations are present only in chiasmatic regions (after correction for multiple comparisons).

4 DISCUSSION

In this work we report a significant decrease of GABA$^+$/tCr levels in the occipital lobe of ADOA patients reflecting GABAergic dysfunction. Interestingly structural changes assessed by volumetric VBM and cortical thickness measures were not observed in the occipital cortex of these patients.

OPA1-ADOA and Leber Hereditary Optic Neuropathy (LHON) are the two major inherited optic neuropathies. Despite having different genetic basis, ADOA and LHON share several clinical pathological endpoints, with retinal ganglion cells (RGC) degeneration, optic atrophy, and frequently central visual loss related to mitochondrial dysfunction (Yu-Wai-Man, Griffiths, Hudson, & Chinnery, 2009). Given the tight relation between retina and cortex in both health and disease (Haak et al., 2014) the most puzzling fact is the apparent special selectivity for RGCs in these disorders.

In our recent work, with asymptomatic LHON individuals we found evidence for enhanced developmental mechanisms of cortical plasticity in extrastriate cortex, not receiving direct retinocortical input from lateral geniculate nucleus (d'Almeida et al., 2013). We also found that this regionally-specific cortical reorganization might be triggered by changes in macular retinal ganglion cell axonal layer thickness (Mateus, d'Almeida, Reis, Silva, & Castelo-Branco, 2016). Here we did not find structural cortical changes in the occipital lobe of ADOA patients, evaluated with both cortical thickness and volumetric measures, as based on the anatomical definition of our ROIs. However our results go in line with the findings of Rocca et al. (2015) that used VBM and Tract-Based Spatial Statistics (TBSS) to assess regional GM and WM changes in ADOA patients. They found significant WM atrophy of the chiasm and optic tract. However, no areas of GM atrophy were found.

Given the interconnection between mitochondrial functioning, metabolism and neurotransmission, we also measured several metabolite and neurotransmitters levels in the occipital lobe of the ADOA patients. Since the basis of the pathophysiology relies on impaired mitochondrial functioning we would expect alterations in some markers of metabolism and neurotransmission, but they were not found. A previous study with OPA1 patients revealed several brain imaging abnormalities but with normal creatine, N-acetylaspartate and choline levels (Roubertie et al., 2015). In our study we only found changes on the major inhibitor neurotransmitter

GABA (normalized for creatine level). In fact, GABA is a surrogate marker of inhibitory neurotransmission, and commonly associated to brain function (Edden, Muthukumaraswamy, Freeman, & Singh, 2009; Violante et al., 2013).

We speculate that such changes in the inhibitory tonus may have an impact on the structural plasticity as suggested before, even in adulthood (Spolidoro, Sale, Berardi, & Maffei, 2009). This may indeed be associated to the observed lower levels of GABA in the visual cortex, without volumetric changes. In this line, lowering of GABA levels, possibly linked with modulation of other substances such as IGF1 (Maya-Vetencourt et al., 2012), could potentially serve as a homeostatic mechanism to prevent early degeneration in the occipital cortex due to retinal ganglion cell impairment. Future studies might be helpful in elucidating the nature of these mechanisms, for example by measuring GABA-A receptor binding potential which could be addressed by PET imaging.

In sum, we provide evidence for impaired cortical physiology with structural sparing in ADOA, given the identified GABAergic changes in the occipital cortex, without volumetric changes. These results suggest a novel cortical physiological alteration that may be relevant for the exploration of hitherto unexpected brain dysfunction, of this retinal ganglion cell disorder. Future studies should address the impact of this novel phenotype on visual and cognitive function, such as identified in other disorders.

5 ACKNOWLEDGMENTS

We would also like to thank Aldina Reis and Catarina Mateus for technical assistance with the ophthalmology assessment. This work was supported by the following grants: FCT-UID/4539/2013 – COMPETE, POCI-01- 0145-FEDER-007440. O.C.A. was supported by the Portuguese Foundation for Science and Technology with the individual scholarship SFRH/BD/76013/2011. I.R.V. is funded by the Wellcome Trust (103045/Z/13/Z).

6 REFERENCES

Ashburner, J. (2007). A fast diffeomorphic image registration algorithm. *Neuroimage*, *38*(1), 95–113. doi:10.1016/j.neuroimage.2007.07.007

Bette, S., Schlaszus, H., Wissinger, B., Meyermann, R., & Mittelbronn, M. (2005). OPA1, associated with autosomal dominant optic atrophy, is widely expressed in the human brain. Acta *Neuropathologica*, *109*, 393–399. doi:10.1007/s00401-004-0970-8

Carelli, V., Ross-Cisneros, F. N., & Sadun, A. A. (2004). Mitochondrial dysfunction as a cause of optic neuropathies. *Progress in Retinal and Eye Research*, *23*(1), 53–89. doi:10.1016/j.preteyeres.2003.10.003

d'Almeida, O. C., Mateus, C., Reis, A., Grazina, M. M., & Castelo-Branco, M. (2013). Long term cortical plasticity in visual retinotopic areas in humans with silent retinal ganglion cell loss. *Neuroimage*, *81*, 222–230. doi:10.1016/j.neuroimage.2013.05.032

Delettre, C., Lenaers, G., Griffoin, J., Gigarel, N., Lorenzo, C., Belenguer, P., … Hamel, C. P. (2000). Nuclear gene OPA1, encoding a mitochondrial dynamin-related protein, is mutated in dominant optic atrophy. *Nature Genetics*, *26*(2), 207–210. doi:10.1038/79936

Edden, R. A. E., Muthukumaraswamy, S. D., Freeman, T. C. A., & Singh, K. D. (2009). Orientation discrimination performance is predicted by GABA concentration and gamma oscillation frequency in human primary visual cortex. *The Journal of Neuroscience*, *29*(50), 15721–15726. doi:10.1523/JNEUROSCI.4426-09.2009

Edden, R. A. E., Puts, N. A. J., Harris, A. D., Barker, P. B., & Evans, C. J. (2014). Gannet: a batch-processing tool for the quantitative analysis of gamma-aminobutyric acid–edited MR spectroscopy spectra. *Journal of Magnetic Resonance Imaging*, *40*(6), 1445–1452. doi:10.1002/jmri.24478

Geuze, E., Westenberg, H. G. M., Heinecke, A., de Kloet, C. S., Goebel, R., & Vermetten, E. (2008). Thinner prefrontal cortex in veterans with posttraumatic stress disorder. *Neuroimage*, *41*(3), 675–681. doi:10.1016/j.neuroimage.2008.03.007

Haak, K. V., Langers, D. R., Renken, R., van Dijk, P., Borgstein, J., & Cornelissen, F. W. (2014). Abnormal visual field maps in human cortex: a mini-review and a case report. *Cortex*, *56*, 14–25. doi:10.1016/j.cortex.2012.12.005

Jones, S. E., Buchbinder, B. R., & Aharon, I. (2000). Three-dimensional mapping of cortical thickness using Laplace's Equation. *Human Brain Mapping*, *11*(1), 12–32. doi:10.1002/1097-0193(200009)11:1<12::AID-HBM20>3.0.CO;2-K

Kjer, P., Jensen, O. A., & Klinken, L. (1983). Histopathology of eye, optic nerve and brain in a case of dominant optic atrophy. *Acta Ophthalmologica*, *61*(2), 300–312.

Maresca, A., la Morgia, C., Caporali, L., Valentino, M. L., & Carelli, V. (2013). The optic nerve: a "mito-window" on mitochondrial neurodegeneration. *Molecular and Cellular Neurosciences*, *55*, 62–76. doi:10.1016/j.mcn.2012.08.004

Mateus, C., d'Almeida, O. C., Reis, A., Silva, E., & Castelo-Branco, M. (2016). Genetically induced impairment of retinal ganglion cells at the axonal level is linked to extrastriate cortical plasticity. *Brain Structure and Function*, *221*(3), 1767–1780. doi:10.1007/s00429-015-1002-2

Maya-Vetencourt, J. F., Baroncelli, L., Viegi, A., Tiraboschi, E., Castren, E., Cattaneo, A., & Maffei, L. (2012). IGF-1 restores visual cortex plasticity in adult life by reducing local GABA levels. *Neural Plasticity*, *2012*, ArticleID: 250421. doi:10.1155/2012/250421

Provencher, S. W. (1993). Estimation of metabolite concentrations from localized in vivo proton NMR spectra. *Magnetic Resonance in Medicine*, *30*(6), 672–679. doi:10.1002/mrm.1910300604

Puts, N. A., & Edden, R. A. (2012). In vivo magnetic resonance spectroscopy of GABA: a methodological review. *Progress in Nuclear Magnetic Resonance Spectroscopy*, *60*, 29–41. doi:10.1016/j.pnmrs.2011.06.001

Reis, A., Mateus, C., Viegas, T., Florijn, R., Bergen, A., Silva, E., & Castelo-Branco, M. (2013). Physiological evidence for impairment in autosomal dominant optic atrophy at the pre-ganglion level. *Archive for Clinical and Experimental Ophthalmology*, *251*(1), 221–234. doi:10.1007/s00417-012-2112-7

Rocca, M. A., Bianchi-Marzoli, S., Messina, R., Cascavilla, M. L., Zeviani, M., Lamperti, C., … Filippi, M. (2015). Distributed abnormalities of brain white matter architecture in patients with dominant optic atrophy and OPA1 mutations. *Journal of Neurology*, *262*(5), 1216–1227. doi:10.1007/s00415-015-7696-5

Roubertie, A., Leboucq, N., Picot, M. C., Nogue, E., Brunel, H., Le Bars, E., … Hamel, C. P. (2015). Neuroradiological findings expand the phenotype of OPA1-related mitochondrial dysfunction. *Journal of the Neurological Sciences*, *349*(1), 154–160. doi:10.1016/j.jns.2015.01.008

Spolidoro, M., Sale, A., Berardi, N., & Maffei, L. (2009). Plasticity in the adult brain: lessons from the visual system. *Experimental Brain Research*, *192*, 335–341. doi:10.1007/s00221-008-1509-3

Violante, I. R., Ribeiro, M. J., Edden, R. A. E., Guimarães, P., Bernardino, I., Rebola, J., … Castelo-Branco, M. (2013). GABA deficit in the visual cortex of patients with neurofibromatosis type 1: genotype-phenotype correlations and functional impact. *Brain*, *136*(Pt 3), 918–925. doi:10.1093/brain/aws368

Votruba, M., Fitzke, F. W., Holder, G. E., Carter, A., Bhattacharya, S. S., & Moore, A. T. (1998). Clinical features in affected individuals from 21 pedigrees with dominant optic atrophy. *Archives of Ophthalmology*, *116*(3), 351–358.

Williams, P. A., Morgan, J. E., & Votruba, M. (2010). Opa1 deficiency in a mouse model of dominant optic atrophy leads to retinal ganglion cell

dendropathy. *Brain*, *133*, 2942–2951. doi:10.1093/brain/awq218

Williams, P. A., Piechota, M., von Ruhland, C., Taylor, E., Morgan, J. E., & Votruba, M. (2012). Opa1 is essential for retinal ganglion cell synaptic architecture and connectivity. *Brain*, *135*(2), 493–505. doi:10.1093/brain/awr330

Yu-Wai-Man, P., & Chinnery, P. F. (2013). Dominant optic atrophy: novel OPA1 mutations and revised prevalence estimates. *Ophthalmology*, *120*(8), 1712. doi:10.1016/j.ophtha.2013.04.022

Yu-Wai-Man, P., Griffiths, P. G., Hudson, G., & Chinnery, P. F. (2009). Inherited mitochondrial optic neuropathies. *Journal of Medical Genetics*, *46*(3), 145–158. doi:10.1136/jmg.2007.054270

Yu-Wai-Man, P., Trenell, M. I., Hollingsworth, K. G., Griffiths, P. G., & Chinnery, P. F. (2011). OPA1 mutations impair mitochondrial function in both pure and complicated dominant optic atrophy. *Brain*, *134*(4), e164(1–5). doi:10.1093/brain/awq288

CHAPTER IV

Type 1 and Type 2 Diabetes Mellitus

IV. 1

- Metabolic marker changes dominate in type 1 and type 2 diabetes and a neurometabolic profile is prevalent in the latter.
- Changes in neurotransmission are linked with metabolic control.
- An association between GABA and $HbA1_c$ suggests a tight coupling between neurometabolism and systemic metabolic control.

Ch. IV. 1

Coupling vs. uncoupling of metabolism and neurotransmission in type 2 and type 1 diabetes

Otília C. d'Almeida,

Ines R. Violante, Bruno Quendera, Carlos Ferreira, Carolina Moreno, Leonor Gomes, Luísa Ribeiro, Miguel Castelo-Branco

ABSTRACT

Aims/Hypothesis. The potential neural impact of metabolic deficits in diabetes remains an outstanding question, given the critical dependence of the brain on glucose availability. This raises the hypothesis whether metabolic changes are directly linked with neurotransmission levels, and whether these serve as pathophysiological markers.

Methods. We addressed this issue in two separate cross-sectional in vivo proton magnetic resonance spectroscopy (^{1}H-MRS) studies of 10 type 1 and 26 type 2 diabetic patients, and the respective age-matched control groups. Absolute concentrations of γ-aminobutyric acid (GABA), total N-acetylaspartate (tNAA), total creatine (tCr), glutamate, and glutamine levels were estimated in the grey matter of occipital cortex. All diabetic patients were medicated with insulin and/or oral anti-diabetics.

Results. We found a primary reduction of tCr in type 1 diabetes which levels were not correlated (unlike in controls) with the unchanged levels of other neurotransmitters/metabolites. In type 2 diabetes we identified a joint reduction in the concentrations of metabolites and neurotransmitters of interest. In this group and respective controls we found positive correlations between tNAA, tCr and Glx (glutamate+glutamine pool) suggesting substantial coupling between glutamatergic neurotransmission and metabolism via the Tricarboxylic Acid cycle. Importantly, a positive correlation was found in type 2 diabetes between GABA and glycated haemoglobin ($HbA1_c$) levels supporting a relation between neurotransmission and metabolic control. Furthermore we showed that the significant GABA differences between the type 2 diabetes group and controls were present in the absence of insulin therapy.

Conclusions/interpretation. Our findings support a strong relationship between abnormal neurotransmission, metabolic control and neurometabolism markers in type 2 diabetes. We suggest that metabolic imbalance precedes and underlies dysfunctional neurotransmission. In controlled type 1 diabetes neurometabolic processes are relatively spared and uncoupled. Future studies will be needed to further unravel neural-metabolic coupling in diabetic individuals as a function of medication and glycaemic states.

d'Almeida, O. C., Violante, I. R., Quendera, B., Ferreira, C., Moreno, C., Gomes, L., Ribeiro, L. & Castelo-Branco, M. Coupling vs. uncoupling of metabolism and neurotransmission in type 2 and type 1 diabetes. (*Submitted* - 2016)

1 INTRODUCTION

Type 1 and type 2 Diabetes Mellitus comprise a wide range of complications during their natural history including microvascular and macrovascular pathologies, neuropathies, and organ specific complications including the eye, the kidney and the heart (American Diabetes Association, 2014). Despite the focus on the non-neural effects of diabetes, the neural tissue is highly energy-dependent relying heavily on glucose content for ATP generation. Therefore the brain is a potential target of damage from impaired glucose metabolism (Biessels, Kappelle, Bravenboer, Erkelens, & W.H., 1994; McCall, 2004).

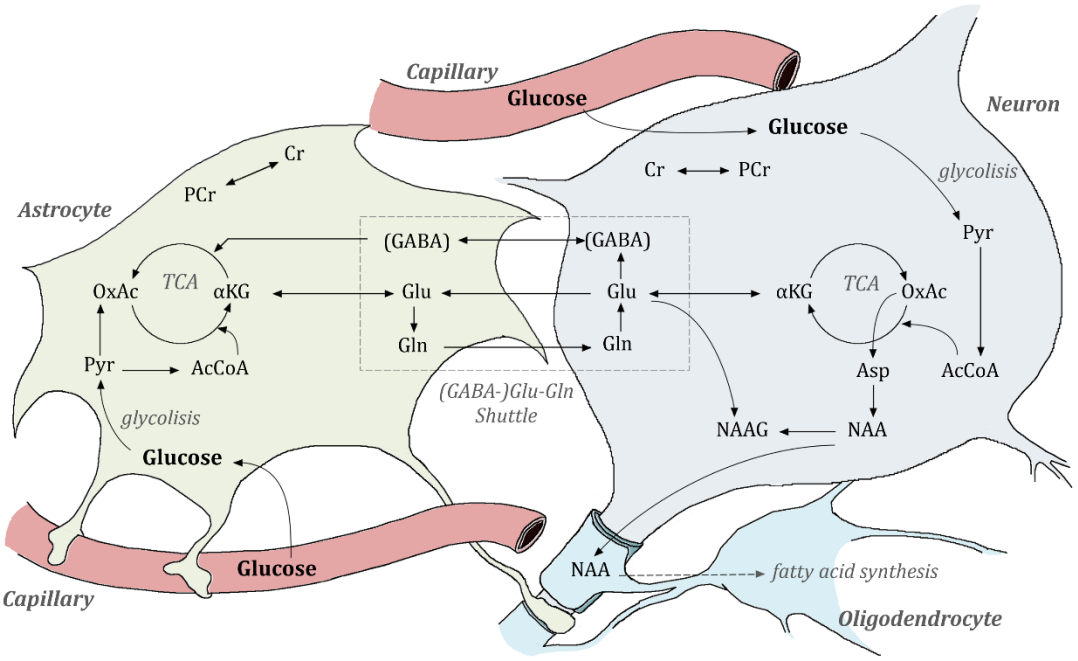

Figure IV.1 Simplified scheme of the astrocyte-neuron interplay and the main glucose metabolic pathways in the brain. Glucose enters both astrocytes and neurons and is oxidized through glycolysis into pyruvate (Pyr) to obtain ATP. Pyruvate is metabolized into acetyl coenzyme A (AcCoA) which reacts with oxaloacetate (OxAc) of the tricarboxylic acid (TCA) cycle to produce large amounts of energy (ATP). In astrocytes, pyruvate carboxylation also produces oxaloacetate for replacement of TCA cycle intermediates. α-ketoglutarate (*α*KG), a TCA intermediate, can form glutamate (Glu). In astrocytes, glutamate is catalysed into glutamine (Gln) acting as a reservoir for glutamate in neurons ((GABA-)glutamate-glutamine shuttle) where it is released as transmitter or converted into γ-aminobutyric acid (GABA) in GABAergic neurons. GABA and glutamate can be re-accumulated in the astrocytes and re-enter either the (GABA-)glutamate-glutamine cycle or the TCA cycle. In neurons, N-acetylaspartate (NAA) is synthesized from aspartate (Asp), via transamination of oxaloacetate and acetyl coenzyme A, crucial for myelin lipid turnover and bioenergetics. Together with glutamate, it is the precursor of N-acetylaspartylglutamate (NAAG). NAA is the most abundant acetylated metabolite in the human brain and can be an important pool of acetate supply for acetyl-CoA synthesis in glial cells.

The extent into which alterations in energy-producing metabolic pathways have repercussions at the neurotransmission level is an important question concerning the diabetic brain. This issue is relevant as there is a tight relationship between brain, the metabolism of glucose and the production of several key neurotransmitters (Figure IV.1), such as γ-aminobutyric acid (GABA) and glutamate. Glutamatergic and GABAergic signalling are strongly dependent on the interactions between astrocytes and neurons that are pivotal to the production, reuse and metabolism of both glutamate and GABA. GABA, glutamate and glutamine are not only neurotransmitters, responsible for the excitatory/inhibitory balance, but are also viewed as energetic metabolites closely coupled to the tricarboxylic acid (TCA) cycle, contributing to the recycling and/or production of its intermediates. Astrocytic and neuronal interactions are relevant through the (GABA-)glutamate-glutamine shuttle

(Figure IV.1) as well as in the context of energy production (for a review see (Hertz & Rodrigues, 2014; Hertz, 2013; Mergenthaler, Lindauer, Dienel, & Meisel, 2013)).

Proton Magnetic Resonance Spectroscopy (^{1}H-MRS) is a technique that allows for the in vivo evaluation of biochemical and metabolic changes, as well as, if tuned for particular neurotransmitters, the global indirect assessment of synaptic neurotransmission in the brain in a rapid and non-invasive way. Using ^{1}H-MRS a previous study suggested the existence of alterations in inhibitory (GABAergic) and possibly also excitatory (indirectly assessed by the levels of the glutamate+glutamine pool (Glx)) neurotransmission in several brain regions in a small cohort of 7 patients (not explicitly mentioning the type of diabetes) with the specific complication of Diabetic Neuropathy (Petrou et al., 2012).

The purpose of this work was to investigate, in two parallel studies, the alterations in the basal levels of several metabolites of interest in the occipital cortex of patients with type 1 and type 2 diabetes by ^{1}H-MRS comparing each to distinct age-matched control groups. Importantly, we focused on the same region of the brain, the occipital lobe, rich in grey matter and with relatively high energy requirements (J. J. Harris & Attwell, 2012). GABA levels were quantified using the MEGA-PRESS sequence. Other relevant metabolites levels, namely N-acetylaspartate (putative neuronal marker and related to energy metabolism), creatine compounds (associated with bioenergetics and membrane turnover), and both glutamate and glutamine were measured using the PRESS sequence.

Given the importance of the interaction between neurotransmission, metabolic activity and astrocytic-neuronal interactions (Figure IV.1) we investigated whether substrates of bioenergetics and neurotransmitters are directly linked in diabetes. We expect that the findings of this work potentially contribute to disclose the relation of such pathophysiologic mechanisms in diabetes and to identify biomarkers and targets for prevention and/or therapy of neural damage.

To our knowledge this is the first study to examine neurometabolism and neurotransmission of both type 1 and type 2 diabetic patients, in comprehensive cohorts and age-matched control groups.

2 RESEARCH DESIGN AND METHODS

2.1 Participants

We have separately studied two cohorts of 10 type 1 and 26 type 2 diabetic patients recruited from the Coimbra Hospital and University Centre. In both studies, spectroscopy data were acquired from two age-matched control groups. Participant characteristics are given in Table IV.1.

Table IV.1 General characterization of the sample groups.

	Type 1 diabetes	**Control group 1**	***p*-value**
N	10	16	-
Mean Age [±*SD*] (y)	35.2 [4.87]	33.1 [7.58]	0.428
M:F	7 : 3	9 : 7	0.483
BMI [±*SD*] (kg/m2)	26.1 [3.67] (N=8)	24.7 [3.86]	0.401
Disease duration [±*SD*] (y)	24.3 [3.28] (N=9)	-	-
HbA1$_c$ level (%)	8.3 [1.79] (N=7)	-	-
HbA1$_c$ level (mmol/mol)	66.9 [19.79] (N=7)	-	-
MRI alterations	no	no	-

	Type 2 diabetes	Control group 2	*p*-value
N	26	16	-
Mean Age [±*SD*] (y)	62.0 [8.45]	63.3 [9.16]	0.648
M:F	15 : 11	8 : 8	0.627
BMI [±*SD*] (kg/m2)	29.9 [4.72]	25.0 [3.59]	0.001
Disease duration [±*SD*] (y)	15.8 [5.21] (N=25)	-	-
$HbA1_c$ level (%)	7.9 [1.26]	-	-
$HbA1_c$ level (mmol/mol)	62.4 [13.80]	-	-
MRI alterations	no	no	-

Sample sizes were based on previous human studies assessing absolute GABA (neurotransmission) (Petrou et al., 2012) and creatine (metabolism) (Sorensen, Siddall, Trenell, & Yue, 2008) levels in the brain using ^{1}H-MRS (Li, Wang, & Gonen, 2003). Also, as type 2 diabetes accounts for 90% to 95% of all diagnosed cases of diabetes in adults (Centers for Disease Control and Prevention, 2011) we were not able to recruit the same number of patients with type 1 diabetes as in other groups.

Diabetic patients that enrolled this study were over 18 years-old and were diagnosed according to the WHO criteria. Exclusion criteria for all groups comprehended the presence of cataract, glaucoma, any other eye disease, surgery or treatment within a period of 6-months and severe nonproliferative (ETDRS level > 35) or proliferative retinopathy. Pregnant or lactating women, participants with chronic or severe kidney disease or acute kidney injury, severe cardiovascular problems, with cardiac pacemaker or metal implants in the body were also excluded. All participants reported no history of neurological or psychiatric disorders and had no neurovascular and structural pathologic alterations as assessed by an experienced neuroradiologist. Control participants had no history of diabetes.

In order to evaluate the patients' metabolic control level, blood samples were collected for analysis of glycated haemoglobin ($HbA1_c$). This was assessed by high-performance liquid chromatography (Variant II, Bio-Rad). All type 1 diabetes patients were taking insulin and in the type 2 diabetes group, 19 were taking oral antidiabetic agents (OAD) and 6 were taking insulin alone or in conjunction with OAD. One type 2 diabetic participant had no reference of medication.

The study was reviewed and approved by our Institutional Review Board (*"Comissão de Ética da Faculdade de Medicina da Universidade de Coimbra"*) and followed the tenets of the Declaration of Helsinki. Written informed consent was obtained from all participants, after research procedures had been fully explained.

2.2 MRI data acquisition

MRI acquisitions were conducted on a 3T MRI scanner (Siemens Magnetom 3T TimTrio, Erlangen, Germany) at the Institute of Nuclear Sciences Applied to Health (ICNAS, University of Coimbra) using a 12-channel birdcage head coil. Each participant underwent conventional high-resolution T1-weighted three-dimensional *Magnetization Prepared Rapid Acquisition Gradient Echo* (MPRAGE) sequence [repetition time (TR) 2530 ms, echo time (TE) 3.42 ms, inversion time (TI) 1100 ms, flip angle (FA) 7°, field of view (FoV) 256×256 mm^2, yielding 176 slices with 1×1×1 mm^3 voxel size].

MRS spectra were acquired in a 3×3×3 cm^3 voxel positioned medially in the occipital cortex (Figure IV.2 A), as described previously in (Violante et al., 2013), to make a compromise between voxel localization and signal-to-noise ratio (Mullins et al., 2014). The volume-of-interest was

specifically chosen to cover a high content of grey matter (Table IV.2). GABA levels were measured in all participants using the *MEshcher-GArwood Point RESolved Spectroscopy* (MEGA-PRESS) sequence (Edden & Barker, 2007; Mescher, Merkle, Kirsch, Garwood, & Gruetter, 1998) [TR 1500 ms, TE 68 ms, FA 90°, 392 averages, 1024 data points]. Editing frequency-selective inversion pulses were applied to the GABA-C3 resonance at 1.9 ppm (refocused 'on resonance') and 7.5 ppm (non-refocused 'off resonance') during odd and even number acquisitions, respectively. Since the majority of peaks in the spectrum are undisturbed by the applied editing pulses, subtracting 'on' and 'off' spectra removes these peaks and retains the GABA peak from the spectrum. To calculate water-scaled GABA concentrations, MEGA-PRESS spectra without the suppression of the water signal (32 averages) were acquired in the same location.

In addition, participants were submitted to a *Point RESolved Spectroscopy* (PRESS) sequence acquisition [TR 2000 ms, TE 35 ms, FA 90°, 160 averages, 1024 data points] to evaluate other relevant metabolites such as N-acetylaspartate (NAA) and creatine (Cr) compounds, glutamate (Glu) and glutamine (Gln). PRESS spectra with unsuppressed water signal (16 averages) were also acquired to estimate absolute metabolite concentration.

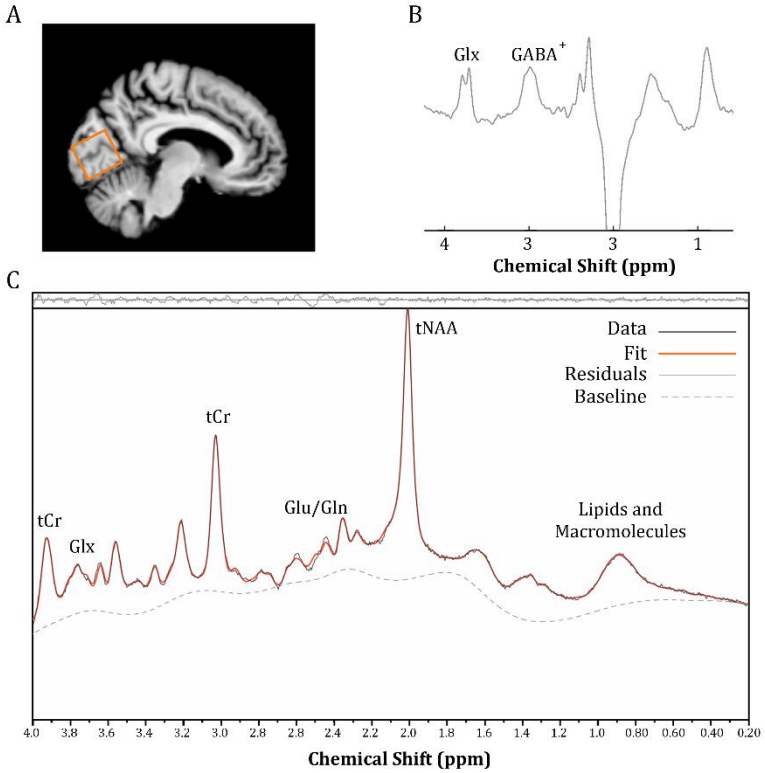

Figure IV.2 Spectroscopic acquisition and data processing. Sagittal view of a (**A**) representative magnetic resonance spectroscopy voxel acquired in the grey matter rich occipital lobe. Two ^{1}H-MRS acquisition sequences were used to acquire (**B**) MEGA-PRESS edited γ-aminobutyric acid (GABA^{+}) signal (analysed through Gannet) and (**C**) PRESS spectrum (analysed through LCModel) to estimate total N-acetylaspartate (tNAA), total creatine (tCr), glutamate (Glu), glutamine (Gln) and glutamine+glutamate pool (Glx) levels. In (**C**), it is shown the processed data (black solid line), the LCModel fitted spectrum (red solid line), the residuals (grey solid line, on top) and the baseline (light grey solid line).

2.3 Data analysis

To determine the fraction of grey matter (GM), white matter (WM) and cerebrospinal fluid (CSF) enclosed in the acquired voxel, anatomical T1-weighted images were segmented (Table IV.2). The procedure was done using an in-house MATLAB (R2013a, v.8.1.0, TheMathWorks, USA) script

relying on the SPM8 (Wellcome Trust Centre for Neuroimaging, Institute of Neurology, UCL, London, UK, http://www.fil.ion.ucl.ac.uk/spm/) and VBM8 toolboxes (http://dbm.neuro.uni-jena.de/vbm8/).

Table IV.2 Mean Grey Matter (GM), White Matter (WM), and Cerebrospinal Fluid (CSF) fractions (and standard deviations, *SD*) of spectroscopy voxel in the occipital cortex of type 1 and type 2 diabetes and the respective control groups.

		Tissue fraction (mean±*SD*)		
	N	**GM** (%)	**WM** (%)	**CSF** (%)
Type 1 diabetic	10	70.7 ± 8.45	15.7 ± 4.30	10.9 ± 3.96
Control group 1	16	70.0 ± 4.86	17.3 ± 5.45	11.9 ± 3.70
Type 2 diabetic	26	65.1 ± 7.30	20.1 ± 6.10	13.1 ± 4.64
Control group 2	16	62.0 ± 8.56	17.8 ± 7.55	16.8 ± 6.18

GABA signals appear at 3.0, 2.3 and 1.9 ppm. Since these are masked by strongly concentrated metabolites (Cr, Glu and NAA) a J-difference editing technique (MEGA-PRESS) was used to measure GABA signals more accurately (Puts & Edden, 2012). MEGA-PRESS data were analysed using Gannet GABA-MRS Analysis Tool (Edden, Puts, Harris, Barker, & Evans, 2014) version 2.0 for MATLAB (R2013a, v.8.1.0, TheMathWorks, USA). A 3 Hz exponential line broadening was applied to all spectra prior to the Fast Fourier Transform of the time resolved data. After the frequency and phase correction and the outlier rejection, the edited difference spectrum was generated for each dataset (Figure IV.2 B). Gannet uses nonlinear least-squares fitting to integrate the ~3.00 ppm GABA (Gaussian model), creatine (Lorentzian model) and the unsuppressed water peak (Lorentzian-Gaussian model). The GABA signal was analysed relative to water content and herein will be referred as GABA+ to consider the contribution due to homocarnosine and macromolecule signals (Edden et al., 2014). Since GABA concentration is highly dependent on the tissue composition (Durst et al., 2015; Ganji et al., 2014; Jensen, Frederick, & Renshaw, 2005) and GABAergic activity occurs mostly in the GM, lesser in the WM and is almost negligible in the CSF, we corrected GABA concentration using the method proposed by Harris et al (A. D. Harris, Puts, & Edden, 2015). Hence the tissue corrected GABA concentration ($GABA^{+}_{corr}$) was measured as:

$$GABA^{+}_{corr} = \frac{GABA^{+}}{f_{GM} + 0.5 f_{WM}}$$

, where fGM and fWM are the fractions of GM and WM, respectively.

Post-processing and quantification of PRESS data was performed with LCModel version 6.3 (Provencher, 1993). The in vivo spectra were analysed as a linear combination of prior knowledge in vitro standard basis dataset acquired with a PRESS sequence with TE 35 ms in a 3T scanner as in our study. Eddy-current correction and water scaling was performed. This enabled estimation of absolute concentrations presented in institutional units, approximating mmol per Kg wet weight. Only metabolites for which Crámer-Rao Lower Bounds (CRLB) were less than 20% were considered for statistical analysis (Provencher, 1993) to exclude poorly fitted data. Spectra were analysed between chemical shifts of 4.0 and 0.2 ppm (and between 4.0 and 1.8 ppm in case of spectra with major lipid and macromolecules artefacts). Total NAA (tNAA) as the pool of N-acetylaspartate and N-acetylaspartylglutamate (NAA+NAAG), total creatine (tCr) as the pool of creatine and phosphocreatine (Cr+PCr) and Glx as the pool glutamate plus glutamine (Glu+Gln) (Figure IV.2 C) were analysed as a sum. Glu and Gln were also analysed separately. Partial volume correction for CSF fraction was performed automatically during the model fitting (http://s-

provencher.com/pub/LCModel/manual/manual.pdf) using the equation described by Ernst et al. (Ernst, Kreis, & Ross, 1993).

2.4 Statistical analysis

All statistical analyses were performed using IBM SPSS Statistics (version 22.0, IBM Corp., Armonk, NY, USA). Due to spectra quality constraints, one PRESS spectrum of both control groups and type 2 diabetes group were excluded from analysis and also two MEGA-PRESS spectra in the control group for type 1 diabetes group. Variables from these spectra were excluded from the analysis with a pairwise approach. Data normality (p>0.05) assumption was verified for each evaluated variable (age, disease duration, $HbA1_c$ levels, BMI, $GABA^+_{corr}$, Gln, Glu, Glx, tCr, tNAA) with the Kolmogorov-Smirnov test with Lilliefors correction. Analyses were performed between diabetic groups and each specific age-matched control group, using parametric independent samples t-tests, whenever possible. When the data did not meet normality assumptions, Mann-Whitney U tests were used instead. Two-tailed hypothesis testing was performed at a 0.05 significance level, with 0.06 trend level. Spearman correlation analyses (r_s) were performed within each group between age, body mass index (BMI), tCr, tNAA, Glx and $GABA^+_{corr}$ levels, and for diabetic groups, also for both disease duration and $HbA1_c$ levels. A false discovery rate (*FDR*) set to 0.15 was used to control for multiple comparisons in bivariate correlation p-values using the Benjamini–Hochberg procedure (Benjamini & Hochberg, 1995).

3 RESULTS

3.1 Creatine levels are primarily affected in type 1 diabetes patients

tCr concentrations measured from PRESS spectra were compared between type 1 diabetes group and its matched control group (Figure IV.3 A). We found a significant difference in tCr levels between groups (t(23)=-2.329, p=0.029), with lower creatine levels in diabetic patients (Figure IV.3 A). There were no significant differences in the absolute levels of the other metabolites (tNAA, Gln, Glu, Glx and $GABA^+_{corr}$) (Figure IV.3).

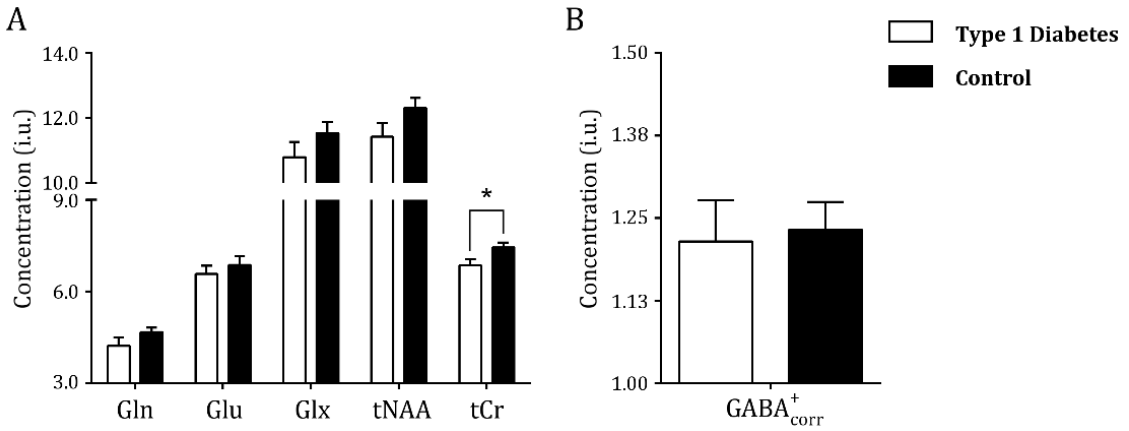

Figure IV.3 Mean metabolite levels in type 1 diabetes and age-matched control group, in institutional units (i.u.). (**A**) Gln, Glu, Glx, tNAA, and tCr levels were estimated from PRESS data and (**B**) $GABA^+_{corr}$ levels were estimated from MEGA-PRESS data. Total creatine levels were lower in diabetic group. $GABA^+_{corr}$, tissue corrected γ-aminobutyric acid; Gln, glutamine; Glu, glutamate; Glx, glutamine+glutamate; tCr, total creatine; tNAA, total N-acetylaspartate. *p<0.05. Error bars correspond to ± 1 *SEM*.

After *FDR* correction, no correlations were found in the type 1 diabetes group between any of the variables tNAA, tCr, Glx, $GABA^{+}_{corr}$, age, disease duration, BMI and $HbA1_c$ levels. However in the age-matched control group there were positive correlations between tCr and both tNAA (r_s=0.70, p=0.004) and Glx (r_s=0.77, p=0.001), tNAA and Glx (r_s=0.60, p=0.017) and a mild correlation between $GABA^{+}_{corr}$ levels and tNAA (r_s=0.57, p=0.034).

3.2 Both metabolic and neurotransmission markers are altered in type 2 diabetes patients

First, we evaluated the putative changes of tCr levels between type 2 diabetes patients and the age-matched control group. The concentration of tCr was significantly different (t(20.873)=-2.120, p=0.046), being lower in the group of diabetic patients compared to controls. Therefore we did not use ratios relative to creatine and used the water peak area instead.

To evaluate neuronal integrity and metabolic status, we compared tNAA levels between both groups. Mean tNAA levels in type 2 diabetes were significantly lower than in the control group (t(38)=-2.480, p=0.018) (Figure IV.4 A).

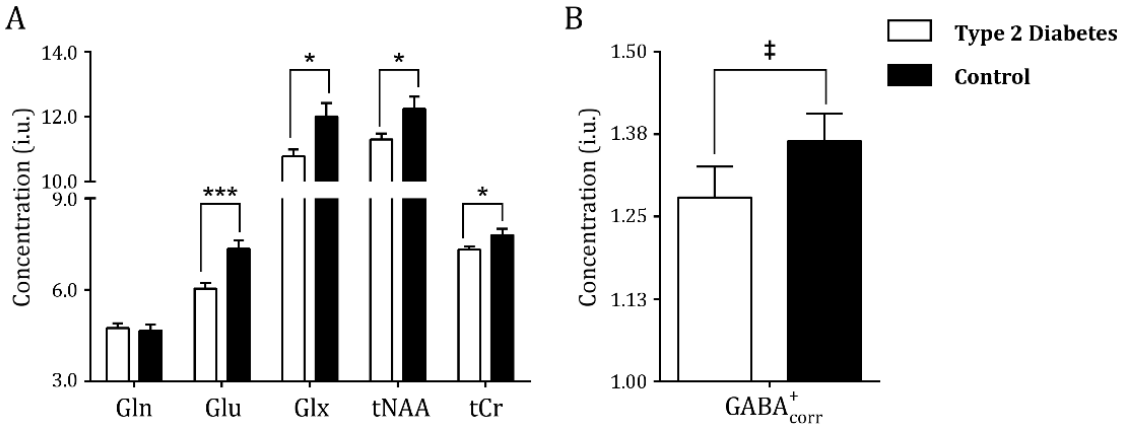

Figure IV.4 Mean metabolite levels in type 2 diabetes and age-matched control group, in institutional units (i.u.). (**A**) Gln, Glu, Glx, tNAA, and tCr levels were estimated from PRESS data and (**B**) $GABA^{+}_{corr}$ levels were estimated from MEGA-PRESS data. There was a global decrease on metabolites levels in the type 2 diabetes group, except for glutamine (Gln). $GABA^{+}_{corr}$, tissue corrected γ-aminobutyric acid; tCr, total creatine; tNAA, total N-acetylaspartate. ***p<0.001, **p<0.01, *p<0.05, ‡p=0.052. Error bars correspond to ± 1 *SEM*.

Neurochemical profiles related to neurotransmission were evaluated by measuring PRESS Gln, Glu, Glx, (Figure IV.4 A) and MEGA-PRESS GABA levels corrected for CSF fraction ($GABA^{+}_{corr}$) (Figure IV.4 B) using independent samples t-tests and the Mann-Whitney U test. We found statistical differences for Glu and Glx (Glu: U=61, p<0.001; Glx: t(20.924)=-2.609, p=0.016), with lower levels in diabetic patients. $GABA^{+}_{corr}$ concentration was also lower in type 2 diabetes compared to the age-matched non-diabetic group (U=133, p=0.052).

As expected, after *FDR* correction, correlation analysis in type 2 diabetes group showed positive associations between age and disease duration (r_s=0.66, p<0.001), $HbA1_c$ levels and BMI (r_s=0.44, p=0.026) and a negative association between disease duration and tNAA (rs=-0.46, p=0.024). Interestingly, $GABA^{+}_{corr}$ and $HbA1_c$ levels were positively correlated (r_s=0.45, p=0.021) supporting an intriguing relation between neurotransmission and metabolic control. For both type 2 diabetes group and the age-matched control group, there was a negative correlation between age and Glx (type 2 diabetes: r_s=-0.43, p=0.034; control: r_s=-0.61, p=0.016), positive correlations between tCr and both tNAA (type 2 diabetes: r_s=0.49, p=0.012; control: r_s=0.91, p<0.001) and Glx (type 2 diabetes:

r_s=0.48, p=0.014; control: r_s=0.75, p=0.001) and between tNAA and Glx (type 2 diabetes: r_s=0.51, p=0.010; control: r_s=0.72, p=0.002).

3.3 Evaluation of effects in the absence of insulin therapy

To exclude the potential impact of the insulin medication, we re-evaluated the type 2 diabetes group by removing the patients that were taking insulin alone or in conjunction with OAD (OAD-type-2) and compared it with the control group, age-matched for type 2 diabetes.

Overall the results remained similar: OAD-type-2 diabetes group had significantly higher BMI (t(32)=3.682, p=0.001) and lower tCr (t(31)=-2.405, p=0.022) and tNAA (t(20.591)=-2.281, p=0.033) levels when compared with the control group. Glu (U=-41, p=0.001), Glx (t(22.696)=-2.689, p=0.013) and $GABA^{+}_{corr}$ (U=77, p=0.013) were also significantly diminished in the OAD-type-2 diabetic group.

4 DISCUSSION

This is the first report to assess, with a comprehensive set of spectroscopy methods, changes in neurotransmitter and neurometabolic intermediate levels in the brain in both type 1 and type 2 diabetes. We ran two independent studies with separate age-matched control groups using PRESS and MEGA-PRESS ^{1}H-MRS, which allowed to dissect both GABA/glutamate levels (not possible with more conventional methods, and not achieved in previous studies) and their relation with bioenergetics, linked to NAA and Cr metabolism.

Our results suggest that type 1 diabetes patients have relatively preserved bioenergetics, except for the Cr/PCr system. In contrast, type 2 diabetes patients showed more global neurometabolic disturbances in the occipital cortex. Importantly, we found evidence for reduction of glutamate and GABA levels in type 2 diabetes patients that could be associated with changes in bioenergetics. This relation is intriguing, and may relate to fluctuation patterns in glucose levels (McCall, 2004). In any case, these findings suggest the brain as a special target in diabetes type 2, in line with central insulinoresistance (Blázquez, Velázquez, Hurtado-Carneiro, & Ruiz-Albusac, 2014).

MRS is one of the most promising techniques to assess in vivo, brain biochemistry and neurotransmission. A major issue in previous studies is that results are often reported as metabolite concentration ratios relative to total creatine (tCr) and/or N-acetylaspartate (tNAA). This choice is based in the assumption that the tCr and tNAA concentrations are nearly constant, which might not be case for a chronic metabolic disease. Accordingly, we found both in type 1 and type 2 diabetes lower levels of tCr and tNAA. It is important to emphasize that we used an unsuppressed water reference as it can give more reliable quantitative estimates (Li et al., 2003). The high-energy demands of the brain can be fulfilled efficiently in strategic sites by the Cr/PCr system (Andres, Ducray, Schlattner, Wallimann, & Widmer, 2008) and its decreases found in both types of diabetes may be a signal for energetic imbalance.

NAA is stored exclusively in neurons and is often interpreted as evaluating the status of neuronal integrity. However, evidence shows that this standard association maybe more complex, given its relation with the Tricarboxylic Acid (TCA) cycle (Figure IV.1), myelin lipid turnover and bioenergetics and astrocyte-neuron signalling (J. R. Moffett, Ross, Arun, Madhavarao, & Namboodiri, 2007) (Patel et al., 2004). This explains that concomitant metabolic disturbances can be associated to the tNAA reductions in Diabetes Mellitus. NAA is the most abundant acetylated metabolite in the human brain and is an important pool of acetate to supply for acetyl-CoA synthesis in glial cells (John R Moffett, Arun, Ariyannur, & Namboodiri, 2013). The decrease in NAA levels in type 2 diabetes could be due to different NAA anabolism and catabolism flux rates. When glucose metabolism in

neurons is impaired, NAA metabolism in astrocytes can act as a non-glucose energy source to maintain acetyl-coA and acetate levels to support for TCA functioning.

Glutamate and GABA have dual roles in the CNS. Their pools are commonly compartmentalized into a neurotransmitter and a metabolic pool (Erecińska & Silver, 1990; Waagepetersen, Sonnewald, & Schousboe, 1999). Glutamate is the major excitatory neurotransmitter in the CNS and despite being rapidly synthesized de novo in astrocytes, it is mainly recycled and replenished for neurons through the glutamate-glutamine shuttle (Figure IV.1). Under normal conditions, glutamate has a high flux rate and is closely coupled with the high-energy demands for brain functioning. Glutamate is preferentially synthesized by aspartate aminotransferase. It relates to alpha-ketoglutarate, and contributes to replenish the substrates of the TCA cycle for energy production. This reaction also contributes to an additional aspartate supply from oxaloacetate and formation of NAA by acetylation. If the aspartate aminotransferase activity is reduced in diabetic brain, synthesis of both NAA and alpha-ketoglutarate from glutamate becomes compromised, reducing energy production. In addition to the impact in the NAA metabolism, there is also tight coupling between glucose metabolism and the synaptic activity involving the (GABA-)glutamate-glutamine cycle (Hyder et al., 2006). In fact, as represented in Figure IV.1, glucose oxidation may strongly influence the recycling of neurotransmitters, being the proportion between the first and the glutamate-glutamine cycle close to 1:1 (Hertz & Rodrigues, 2014; Rothman, Behar, Hyder, & Shulman, 2003; Sibson et al., 1998).

Future studies should investigate the pathogenic role of glutamate and GABA transporter dysfunctions as well as the relation to the role of the glucose-transporter activity through the blood-brain-barrier (BBB) in diabetes which is known to be impaired in chronic hyperglycaemia (Gjedde & Crone, 1981; Matthaei, Horuk, & Olefsky, 1986; Pardridge, Triguero, & Farrell, 1990).

A ^{1}H-MRS study of occipital cortex of type 1 diabetes patients (with disease duration >5 years) showed reduced glutamate and tNAA levels (Mangia et al., 2013). The authors suggested that reduced levels of glutamate and NAA may reflect partial neuronal loss/dysfunction. Importantly, the patients had clamped glycaemia at 300±15 mg/dL (16.7±0.8 mmol/L), and ours were medicated with insulin. We also found a only trend for lower levels of these metabolites which can reflect the effects of insulin medication and the glycaemic status. However our type 2 diabetes group had lower Glutamate, Glx and tNAA levels. We suggest that these changes can reflect early dysfunction in the TCA cycle.

Alterations in NAA and glutamate regulation have also been verified in other diseases such as schizophrenia (Ohrmann et al., 2005). Moreover, even when differences in concentration levels are not found, a decoupling between the two metabolites may occur in schizophrenia (Kraguljac, Reid, White, den Hollander, & Lahti, 2012). An important distinction is that that diabetes is a metabolic disorder in the first place and neurotransmission alterations probably occur downstream.

A previous study (omitting the type of diabetes) found reduced GABA levels in the insula of 7 Diabetic Neuropathy patients (Petrou et al., 2012), which we found only in type 2 diabetic patients.

Importantly, we found an intriguing positive correlation between GABA and $HbA1_c$ levels in type 2 diabetes patients, establishing an association between the inhibitory neurotransmission mediated by GABA and metabolic control. The correlation with poorer metabolic control suggests that GABA reduction may actually be adaptive or at least not pathogenic. In fact, steady-state GABA levels have a double-edged biological impact, depending on the physiological system (Ribeiro, Violante, Bernardino, Edden, & Castelo-Branco, 2015).

In our study, we found neurometabolic uncoupling for type 1 diabetes patients (unlike controls) whilst for type 2 diabetes patients we observed positive correlations between NAA, tCr and Glx as in controls, suggesting differential coupling/uncoupling between metabolism and neurotransmission.

As a limitation of this study, ^{1}H-MRS alone does not allow to infer the rates/fluxes of the reactions. Compartmental models and invasive dynamic studies with ^{13}C might be helpful to get deeper insights into neuroglial mechanisms that are affected in diabetes (Mason, Petersen, Lebon, Rothman, & Shulman, 2006).

We conclude that neurotransmission vs. metabolic coupling is profoundly changed in diabetes with a distinct pattern in type 1 and type 2 diabetes, as demonstrated by using a comprehensive neurospectroscopy approach. Metabolic marker changes dominate in both and a neurometabolic profile is prevalent in diabetes type 2. We found that changes in neurotransmission are linked with metabolic control. These changes may be adaptive or maladaptive depending on the physiologic system. In addition, these changes are different from neurological diseases in which neurotransmitter changes are the primary event. The association between GABA and $HbA1_c$ suggests a tight coupling between neurometabolism and systemic metabolic control that should be addressed in the future by studies. Finally, it will be important to establish in the future whether the neurometabolic coupling identified here can be related to the central insulinoresistance that has been claimed to occur in diabetes type 2.

5 ACKNOWLEDGEMENTS

We do thank all the diabetic participants, as well as all the control subjects that participated in this study.

6 FUNDING

This work was supported by the following grants: “DoIT-Diamarker”, a consortium for the discovery of novel biomarkers in Diabetes type 2, FCT-UID/NEU/04539/2013 - COMPETE, POCI-01-0145-FEDER-007440 and QREN-COMPETE "Genetic susceptibility of multisystemic complications of Diabetes type 2: novel biomarkers for diagnosis and monitoring of therapy"; CENTRO-07-0224-FEDER-002005/SCT_2011_02_005_4816, From Molecules to Man. O.C.A. was supported by the Portuguese Foundation for Science and Technology with the individual scholarship SFRH/BD/76013/2011. I.R.V. is funded by the Wellcome Trust (103045/Z/13/Z).

7 DISCLOSURE STATEMENT

The authors declare no potential conflicts of interest.

8 AUTHOR CONTRIBUTIONS

O.C.A. contributed to study design and execution, researched and interpreted the data and wrote and edited the manuscript. I.R.V. contributed to study execution and reviewed the manuscript. B.Q., C.F., C.M., L.G. and L.R. contributed to study execution and data acquisition. M.C.-B. contributed to the study concept and design and the interpretation of the data and reviewed and edited the manuscript. O.C.A. and M.C.-B. are the guarantors of the study and, as such, had full access to all the data in the study and take responsibility for the integrity of the data and the accuracy of the data analysis.

9 REFERENCES

American Diabetes Association. (2014). Diagnosis and classification of diabetes mellitus. *Diabetes Care*, *37*(Suppl 1), S81–90. doi:10.2337/dc14-S081

Andres, R. H., Ducray, A. D., Schlattner, U., Wallimann, T., & Widmer, H. R. (2008). Functions and effects of creatine in the central nervous system. *Brain Research Bulletin*, *76*(4), 329–343. doi:10.1016/j.brainresbull.2008.02.035

Benjamini, Y., & Hochberg, Y. (1995). Controlling the false discovery rate: a practical and powerful approach to multiple testing. *Journal of the Royal Statistical Society. Series B (Methodological)*, *57*(1), 289–300.

Biessels, G. J., Kappelle, a. C., Bravenboer, B., Erkelens, D. W., & W.H., G. (1994). Cerebral function in diabetes mellitus. *Diabetologia*, *37*, 643–650.

Blázquez, E., Velázquez, E., Hurtado-Carneiro, V., & Ruiz-Albusac, J. M. (2014). Insulin in the brain: its pathophysiological implications for states related with central insulin resistance , type 2 diabetes and alzheimer ' s disease. *Frontiers in Endocrinology*, *5*, 1–21. doi:10.3389/fendo.2014.00161

Centers for Disease Control and Prevention. (2011). *National diabetes fact sheet: national estimates and general information on diabetes and prediabetes in the United States, 2011*. Atlanta, GA: US Department of Health and Human Services, Centers for Disease Control and Prevention. Atlanta, GA: US Department of Health and Human Services, Centers for Disease Control and Prevention (Vol. 201).

Durst, C. R., Michael, N., Tustison, N. J., Patrie, J. T., Raghavan, P., Wintermark, M., & Velan, S. S. (2015). Noninvasive evaluation of the regional variations of GABA using magnetic resonance spectroscopy at 3 Tesla. *Magnetic Resonance Imaging*, *33*(5), 611–617. doi:10.1016/j.mri.2015.02.015

Edden, R. A. E., & Barker, P. B. (2007). Spatial effects in the detection of γ-aminobutyric acid: improved sensitivity at high fields using inner volume saturation. *Magnetic Resonance in Medicine*, *58*(6), 1276–1282. doi:10.1002/mrm.21383

Edden, R. A. E., Puts, N. A. J., Harris, A. D., Barker, P. B., & Evans, C. J. (2014). Gannet: a batch-processing tool for the quantitative analysis of gamma-aminobutyric acid–edited MR spectroscopy spectra. *Journal of Magnetic Resonance Imaging*, *40*(6), 1445–1452. doi:10.1002/jmri.24478

Erecińska, M., & Silver, I. A. (1990). Metabolism and role of glutamate in mammalian brain. *Progress in Neurobiology*, *35*(4), 245–296. doi:10.1016/0301-0082(90)90013-7

Ernst, T., Kreis, R., & Ross, B. D. (1993). Absolute quantitation of water and metabolites in the human brain. I. Compartments and water. *Journal of Magnetic Resonance, Series B*, *102*(1), 1–8. doi:10.1006/jmrb.1993.1055

Ganji, S. K., An, Z., Banerjee, A., Madan, A., Hulsey, K. M., & Choi, C. (2014). Measurement of regional variation of GABA in the human brain by optimized point-resolved spectroscopy at 7 T in vivo. *NMR in Biomedicine*, *27*(10), 1167–1175. doi:10.1002/nbm.3170

Gjedde, A., & Crone, C. (1981). Blood-brain glucose transfer: repression in chronic hyperglycemia. *Science*, *214*(4519), 456–457.

Harris, A. D., Puts, N. A. J., & Edden, R. A. E. (2015). Tissue correction for GABA-edited MRS: Considerations of voxel composition, tissue segmentation, and tissue relaxations. *Journal of Magnetic Resonance Imaging*, *42*(5), 1431–1440. doi:10.1002/jmri.24903

Harris, J. J., & Attwell, D. (2012). The energetics of central nervous system white matter. *The Journal of Neuroscience*, *32*(1), 356–371. doi:10.1523/JNEUROSCI.3430-11.2012.The

Hertz, L. (2013). The Glutamate-Glutamine (GABA) Cycle: Importance of Late Postnatal Development and Potential Reciprocal Interactions between Biosynthesis and Degradation. *Frontiers in Endocrinology*, *4*, 59. doi:10.3389/fendo.2013.00059

Hertz, L., & Rodrigues, T. B. (2014). Astrocytic-neuronal-astrocytic pathway selection for formation and degradation of glutamate/GABA. *Frontiers in Endocrinology*, *5*, 42. doi:10.3389/fendo.2014.00042

Hyder, F., Patel, A. B., Gjedde, A., Rothman, D. L., Behar, K. L., & Shulman, R. G. (2006). Neuronal-glial glucose oxidation and glutamatergic-GABAergic function. *Journal of Cerebral Blood Flow & Metabolism*, *26*(7), 865–877. doi:10.1038/sj.jcbfm.9600263

Jensen, J. E., Frederick, B. D., & Renshaw, P. F. (2005). Grey and white matter GABA level differences in the human brain using two-dimensional, J-resolved spectroscopic imaging. *NMR in Biomedicine*, *18*(8), 570–576. doi:10.1002/nbm.994

Kraguljac, N. V, Reid, M. A., White, D. M., den Hollander, J., & Lahti, A. C. (2012). Regional decoupling of N-acetyl-aspartate and glutamate in schizophrenia. *Neuropsychopharmacology*, *37*(12), 2635–2642. doi:10.1038/npp.2012.126

Li, B. S. Y., Wang, H., & Gonen, O. (2003). Metabolite ratios to assumed stable creatine level may confound the quantification of proton brain MR spectroscopy. *Magnetic Resonance Imaging*, *21*(8), 923–928. doi:10.1016/S0730-725X(03)00181-4

Mangia, S., Kumar, A. F., Moheet, A. A., Roberts, R. J., Eberly, L. E., Seaquist, E. R., & Tkáč, I. (2013). Neurochemical profile of patients with type 1 diabetes measured by 1H-MRS at 4 T. *Journal of Cerebral Blood Flow & Metabolism*, *33*(5), 754–759. doi:10.1038/jcbfm.2013.13

Mason, G. F., Petersen, K. F., Lebon, V., Rothman, D. L., & Shulman, G. I. (2006). Increased brain monocarboxylic acid transport and utilization in type 1 diabetes. *Diabetes*, *55*(4), 929–934. doi:10.2337/diabetes.55.04.06.db05-1325

Matthaei, S., Horuk, R., & Olefsky, J. M. (1986). Blood-brain glucose transfer in diabetes mellitus: decreased number of glucose transporters at blood-brain barrier. *Diabetes*, *35*(10), 1181–1184.

McCall, A. L. (2004). Cerebral glucose metabolism in diabetes mellitus. *European Journal of Pharmacology*, *490*(1), 147–158. doi:10.1016/j.ejphar.2004.02.052

Mergenthaler, P., Lindauer, U., Dienel, G. A., & Meisel, A. (2013). Sugar for the brain: The role of glucose in physiological and pathological brain function. *Trends in Neurosciences*, *36*(10), 587–597. doi:10.1016/j.tins.2013.07.001

Mescher, M., Merkle, H., Kirsch, J., Garwood, M., & Gruetter, R. (1998). Simultaneous in vivo spectral editing and water suppression. *NMR in Biomedicine*, *11*(6), 266–272. doi:10.1002/(SICI)1099-1492(199810)11:6<266::AID-NBM530>3.0.CO;2-J

Moffett, J. R., Arun, P., Ariyannur, P. S., & Namboodiri, A. M. A. (2013). N-Acetylaspartate reductions in brain injury: impact on post-injury neuroenergetics, lipid synthesis, and protein acetylation. *Frontiers in Neuroenergetics*, *5*, 11. doi:10.3389/fnene.2013.00011

Moffett, J. R., Ross, B., Arun, P., Madhavarao, C. N., & Namboodiri, A. M. A. (2007). N-Acetylaspartate in the CNS: from neurodiagnostics to neurobiology. *Progress in Neurobiology*, *81*(2), 89–131. doi:10.1016/j.pneurobio.2006.12.003

Mullins, P. G., McGonigle, D. J., O'Gorman, R. L., Puts, N. A., Vidyasagar, R., Evans, C. J., … Edden. (2014). Current practice in the use of MEGA-PRESS spectroscopy for the detection of GABA. *Neuroimage*, *86*, 43–52. doi:10.1016/j.neuroimage.2012.12.004

Ohrmann, P., Siegmund, A., Suslow, T., Spitzberg, K., Kersting, A., Arolt, V., … Pfleiderer, B. (2005). Evidence for glutamatergic neuronal dysfunction in the prefrontal cortex in chronic but not in first-episode patients with schizophrenia: a proton magnetic resonance spectroscopy study. *Schizophrenia Research*, *73*(2), 153–157. doi:10.1016/j.schres.2004.08.021

Pardridge, W. M., Triguero, D., & Farrell, C. R. (1990). Downregulation of blood-brain barrier glucose transporter in experimental diabetes. *Diabetes*, *39*(9), 1040–1044.

Patel, A. B., de Graaf, R. A., Mason, G. F., Kanamatsu, T., Rothman, D. L., Shulman, R. G., & Behar, K. L. (2004). Glutamatergic neurotransmission and neuronal glucose oxidation are coupled during intense neuronal activation. *Journal of Cerebral Blood Flow & Metabolism*, *24*(9), 972–985. doi:10.1097/01.WCB.0000126234.16188.71

Petrou, M., Pop-Busui, R., Foerster, B. R., Edden, R. A., Callaghan, B. C., Harte, S. E., … Feldman, E. L. (2012). Altered excitation-inhibition balance in the brain of patients with diabetic neuropathy. *Academic Radiology*, *19*(5), 607–612. doi:10.1016/j.acra.2012.02.004

Provencher, S. W. (1993). Estimation of metabolite concentrations from localized in vivo proton NMR spectra. *Magnetic Resonance in Medicine*, *30*(6), 672–679. doi:10.1002/mrm.1910300604

Puts, N. A., & Edden, R. A. (2012). In vivo magnetic resonance spectroscopy of GABA: a methodological review. *Progress in Nuclear Magnetic Resonance Spectroscopy*, *60*, 29–41. doi:10.1016/j.pnmrs.2011.06.001

Ribeiro, M. J., Violante, I. R., Bernardino, I., Edden, R. A. E., & Castelo-Branco, M. (2015). Abnormal relationship between GABA, neurophysiology and impulsive behavior in neurofibromatosis type 1. *Cortex*, *64*, 194–208. doi:10.1016/j.cortex.2014.10.019

Rothman, D. L., Behar, K. L., Hyder, F., & Shulman, R. G. (2003). In vivo NMR studies of the glutamate neurotransmitter flux and neuroenergetics: implications for brain function. *Annual Review of Physiology*, *65*(1), 401–427. doi:10.1146/annurev.physiol.65.092101.142131

Sibson, N. R., Dhankhar, A., Mason, G. F., Rothman, D. L., Behar, K. L., & Shulman, R. G. (1998). Stoichiometric coupling of brain glucose metabolism and glutamatergic neuronal activity. *Proceedings of the National Academy of Sciences*, *95*(1), 316–321.

Sorensen, L., Siddall, P. J., Trenell, M. I., & Yue, D. K. (2008). Differences in metabolites in pain-processing brain regions in patients with diabetes and painful neuropathy. *Diabetes Care*, *31*(5), 980–981.

Violante, I. R., Ribeiro, M. J., Edden, R. A. E., Guimarães, P., Bernardino, I., Rebola, J., … Castelo-Branco, M. (2013). GABA deficit in the visual cortex of patients with neurofibromatosis type 1: genotype-phenotype correlations and functional impact. *Brain*, *136*(Pt 3), 918–925. doi:10.1093/brain/aws368

Waagepetersen, H. S., Sonnewald, U., & Schousboe, A. (1999). The GABA paradox: Multiple roles as metabolite, neurotransmitter, and neurodifferentiative agent. *Journal of Neurochemistry*, *73*(4), 1335–1342. doi:10.1046/j.1471-4159.1999.0731335.x

CHAPTER V

Multiple Sclerosis

v. 1

- Work-in-progress/Future work
- *"The final goal is to correlate retinal thickness layers with brain GM areas and infer regression models that may help to identify and characterize pathophysiological aspects of MS that may be sometimes overlooked in the monitoring of the evolution of the disease."*
- We will also study the effects of acute ON in the retino-cortical phenotypic profile of MS patients and the underlying anterograde and/or retrograde trans-synaptic damage in MS.

Ch. V. 1

Retinocortical structural phenotyping in multiple sclerosis

ABSTRACT

Visual impairment is a frequent complication of multiple sclerosis, even when no overt optic nerve pathology is present. Visual dysfunction may arise from damage either from several parts of the visual circuitry, from the retina to the cortex. One of the most common manifestations is optic neuritis (ON), an inflammatory condition of the optic nerve leading to demyelination that is usually associated to optic nerve atrophy. Despite the association with the white matter dysfunction due to fibre demyelination, increasing evidence points to a critical role of the grey matter that is also affected in MS and sometimes may even precede WM dysfunction. In our study we aim to establish the structural correlates of the retinocortical phenotype of MS patients with and without ON.

Fifty-nine patients with established diagnosis of multiple sclerosis (MS) and 64 age- and gender-matched healthy volunteers (HC) underwent optic coherence tomography (OCT) and 3T brain MRI. The MS group was further subdivided into two separate subgroups regarding the history of optic neuritis (ON): the ones without previous episode of ON (MSnoON) and the ones that had at least one previous episode of Optic Neuritis (MSON) mono- or binocularly. Cortical volumes of several occipital visual areas, BA17 and BA18, the precuneus, the cuneus, the lateraloccipital cortex, the pericalcarine, the lingual, the fusiform gyri and the thalamus were estimated with FreeSurfer software. Total lesion volumes were also estimated and the level of disability was measured by the Expanded Disability Status Scale and the Multiple Sclerosis Severity Score.

We found a statistical significant linear trend for lower volumes (normalized to total intracranial volume) in all ROIs from controls to MSnoON and then to MSON. The stronger linear trend was found for the thalamus, with evidenced lower volumes in the MSON group. The OCT images were segmented into 11 layers and we are still working in segmentation corrections and analysis issues.

The final goal is to correlate retinal thickness layers with brain GM areas and infer regression models that may help to identify and characterize pathophysiological aspects of MS that may be sometimes overlooked in the monitoring of the evolution of the disease.

Work-in-progress/Future Work

1 INTRODUCTION

The retina is recognized as an extension of the central nervous system (CNS) commonly tagged as a "window" of the brain. In fact, in many putative CNS diseases ophthalmological changes often precede the pattern of central neuronal damage that leads to the manifestation of the typical clinical symptoms (London et al., 2013).

Multiple sclerosis is one of the most prevalent debilitating chronic neurological diseases affecting young adults. According to World Health Organization it affects around 2.5 million people worldwide, especially in Europe and North America (WHO, 2006). Despite being the consensus that it has a neuroinflammatory aetiology classically related to white matter dysfunction due to axonal demyelization, many studies showed that the cortical grey matter tissue may also be affected (Friese, 2016; Riccitelli et al., 2012; Zivadinov and Minagar, 2009). In fact, there are evidences that diffuse GM atrophy can occur early-on and be even predictive of long-term outcomes (Chard and Miller, 2009). However it is still controversial the relation between cortical impairment occurs and white matter dysfunction (Geurts and Barkhof, 2008).

Despite the prevailing association to the motor and cognitive complications, the afferent visual pathway is commonly compromised in MS and is often underlies the first signs of the disease (Balcer et al., 2015; Zimmermann et al., 2014). Previous studies showed that visual field abnormalities are closely associated to neuroaxonal damage and may be a valuable marker to monitor MS disability burden (Ortiz-Perez et al., 2016). The optic nerve is a relevant target but the fact that the retina is devoid of myelin does not rule out its contribution to functional changes that tend to persist during the course of the disease (Green et al., 2010).

The most often reported visual co-morbidities of MS patients are optic neuritis (ON) and eye movement dysfunction, such as nystagmus and diplopia (Balcer et al., 2015). These problems are very common, but rarely lead to full blindness. In fact, acute optic neuritis, an inflammation of the optic nerve, leads to moderate to severe visual impairment but the affected ON patients usually have complete or near-complete clinical recovery (Optic Neuritis Study Group, 1991). However, the visual pathway may become compromised from the structural- and/or functional point of view (Gallo et al., 2015; Kolappan et al., 2009). This clinical-radiological paradox has been of interest for both clinicians and researchers (Hackmack et al., 2012). ON is characterized by the demyelination of the optic nerve fibres that conduct visual information from retina to the cortex. However, visual impairment does often occur even in the absence of optic neuritis episodes (Balcer et al., 2015).

The pathway for visual processing comprises the retina, the optic nerves, lateral geniculate nucleus (LGN) of the thalamus (anterior visual pathway) and thereon to occipital visual areas through optic radiations for image processing in multiple cortical visual areas (posterior visual pathway). The study of these structures is nowadays possible in vivo through the development of specialized imaging techniques and data processing tools. Optic coherence tomography (OCT) is a tool that features a truly in vivo biopsy of the neural tissue of the eye, the retina. Several studies already proven the clinical and research value of OCT in Multiple Sclerosis (Hanson et al., 2016). Through new segmentation algorithms it is possible to distinguish and segment several sub-millimetric layers of this tissue and estimate the mean thickness of each area.

In addition, new and improved MRI sequences have provided the opportunity to get morphometric measures of the neocortex and subcortical structures in the brain, as well as to obtain parameters that allow the assessment of the status of the white matter tracts.

In our study, we use OCT to measure whole retinal and multiple retinal layer thicknesses and we will correlate these measures with high-resolution extracted volumes of the thalamus, BA17 and

BA18 (a proxy for striate and extrastriate visual areas, respectively) and other occipital visual areas, using FreeSurfer implemented algorithms. We will also expand our analysis by studying the effects of acute ON in the retino-cortical phenotypic profile of MS patients.

With this approach we intend to establish the structural correlates of the retino-cortical visual phenotype in MS evaluated by morphometric measures. The analysis of ON patients will allow us to study the effects of anterograde and/or retrograde trans-synaptic damage in MS.

2 MATERIAL AND METHODS

2.1 Participants

In our study 59 consecutive MS patients (mean age [±*SD*]: 36.8 [7.28]; age range: 22-54y; M/F: 20/39) regularly followed in the Department of Neurology of the Coimbra University and Hospital Centre (Coimbra, Portugal) were enrolled. Inclusion criteria were as follows: age between 18 to 60 years old with definite diagnosis of MS according to the 2010 McDonald criteria (Polman et al., 2011), relapsing-remitting (RRMS) or secondary-progressive (SPMS) subtypes (RRMS/SPMS: 51/8), and Portuguese language skills adequate for cognitive testing. A group of 64 healthy volunteers (mean age [±*SD*]: 36.8 [9.87]; age range: 21-58y; M/F: 22/42), matched for age, gender and education with MS patients, was recruited from the local community and served as healthy controls (HC) (Table V.1).

Exclusion criteria for all participants were as follows: history of neurological (other than MS in patient group) or systemic disease; a severe visual, auditory or language impairment preventing cognitive assessment; history of psychiatric illness, with the exception of stable mild to moderate depressive symptoms; starting or stopping antidepressants in the previous 2 months; alcohol, drug or substance abuse; head injury resulting in loss of consciousness; recent cognitive evaluation (within 1 year); conditions that would preclude MRI and, for MS patients, steroid treatment within the last 30 days before data acquisition.

The Multiple Sclerosis group was later subdivided into two separate subgroups regarding the optic neuritis history. Thirty-six participants did not have previous episode of Optic Neuritis and/or any active optic inflammation at least till 1 month before the examination (MSnoON) and 21 patients had at least one previous episode of Optic Neuritis (MSON) mono- or binocularly.

This study was approved by the local Ethics Committees (CHUC and UC) and followed the tenets of Helsinki. After a full explanation of the study, all participants gave written informed consent.

Table V.1 Demographic and clinical data. (EDSS*, Kurtzke expanded disability status scale;* eTIV*, estimated total intracranial volume;* MSSS*, Multiple sclerosis severity score;* MSON*, Multiple sclerosis with optic neuritis;* MSnoON*, Multiple sclerosis without optic neuritis;* $T1_w$*, T1-weighted;* $T2_w$*, T2-weighted*)

	Controls	**Multiple Sclerosis**		
		MS (All)	**MSnoON**	**MSON**
N	64	57	36	21
Mean age [±*SE*] (y)	36.8 ± 9.86	37.0 ± 7.41	36.3 ± 8.46	38.3 ± 5.10
Gender [m:f]	22 : 42	19 : 38	12 : 24	7 : 14
Disease duration [±*SE*] (y)	-	11 ± 6.8	10 ± 6.5	12 ± 7.2
EDSS [±*SE*]	-	2.5 ± 1.53	2.4 ± 1.48	2.7 ± 1.62
MSSS [±*SE*]	-	3.3 ± 2.09	3.1 ± 2.03	3.6 ± 2.21
$T1_w$ WM lesion volume (mL)	-	5.3 ± 4.43	4.4 ± 2.98	6.9 ± 5.95
$T2_w$ WM lesion volume (mL)	-	16.5 ± 15.70	14.7 ± 12.98	19.4 ± 19.51
eTIV (mL)	1510.50 ± 177.175	1521.57 ± 149.697	1501.27 ± 146.847	1556.36 ± 151.647

2.2 Clinical assessment

A full medical history and detailed neuroophthalmological examination were obtained for all patients. The following clinical and demographic data was collected: age, gender, handedness, years of education, age of disease onset, age of diagnosis, disease duration and current disease-modifying treatment (Table V.1). Physical disability was evaluated using the detailed Kurtzke Expanded Disability Status Scale (EDSS) (Kurtzke, 1983) and the Multiple Sclerosis Severity Score (MSSS) (Baghizadeh et al., 2013). For HC, medical history was obtained by an interview preceding assessment.

2.3 Optic Coherence Tomography

Optic Coherence Tomography (OCT) is and advanced technique in ophthalmology that provides a noninvasive, high-resolution biopsy of the posterior segment of the eye. In here, OCT was performed on each participant eye to scan the macula (macular cube 512×128×1024 protocol, Figure V.1), and the optic disc (optic disc cube 200×200 protocol, Figure V.2) using the Cirrus HD-OCT 5000, Software version 6.5 (Carl Zeiss Meditec Inc., Dublin, CA, USA). All patients were examined with undilated pupils. OCT image segmentation was performed automatically through the OCT Explorer 4.0 (Iowa Reference Algorithms, Retinal Image Analysis Lab, Iowa Institute for Biomedical Imaging, Iowa City, IA) described in detail elsewhere (Abràmoff et al., 2010; Antony et al., 2011; Garvin et al., 2009). Basically, twelve surfaces were segmented using 3D contextual information and differences in tissue reflectivity (Figure V.3). These surfaces were segmented from each volumetric macula- and optic nerve head- (ONH) centred scan. The algorithm allows the definition of the interfaces of the following layers: the retinal nerve fibre layer (RNFL) limited by the inner limiting membrane (ILM), the ganglion cell layer (GCL), the internal plexiform layer (IPL), the inner nuclear layer (INL), the outer plexiform layer (OPL), the Henle fibre layer (HFL), the myoid and ellipsoid inner segments (MEIS), the photoreceptors inner segment/outer segment layer (IS/OS), the outer photoreceptor layer (OPR) and the inner and outer retinal pigment epithelium layer (RPE) limited by the choroid. All output images will be visually inspected for segmentation errors and manually corrected, if needed. The average thickness of each layer can be defined as the mean distance between two layers for all A-scans in each central subfield.

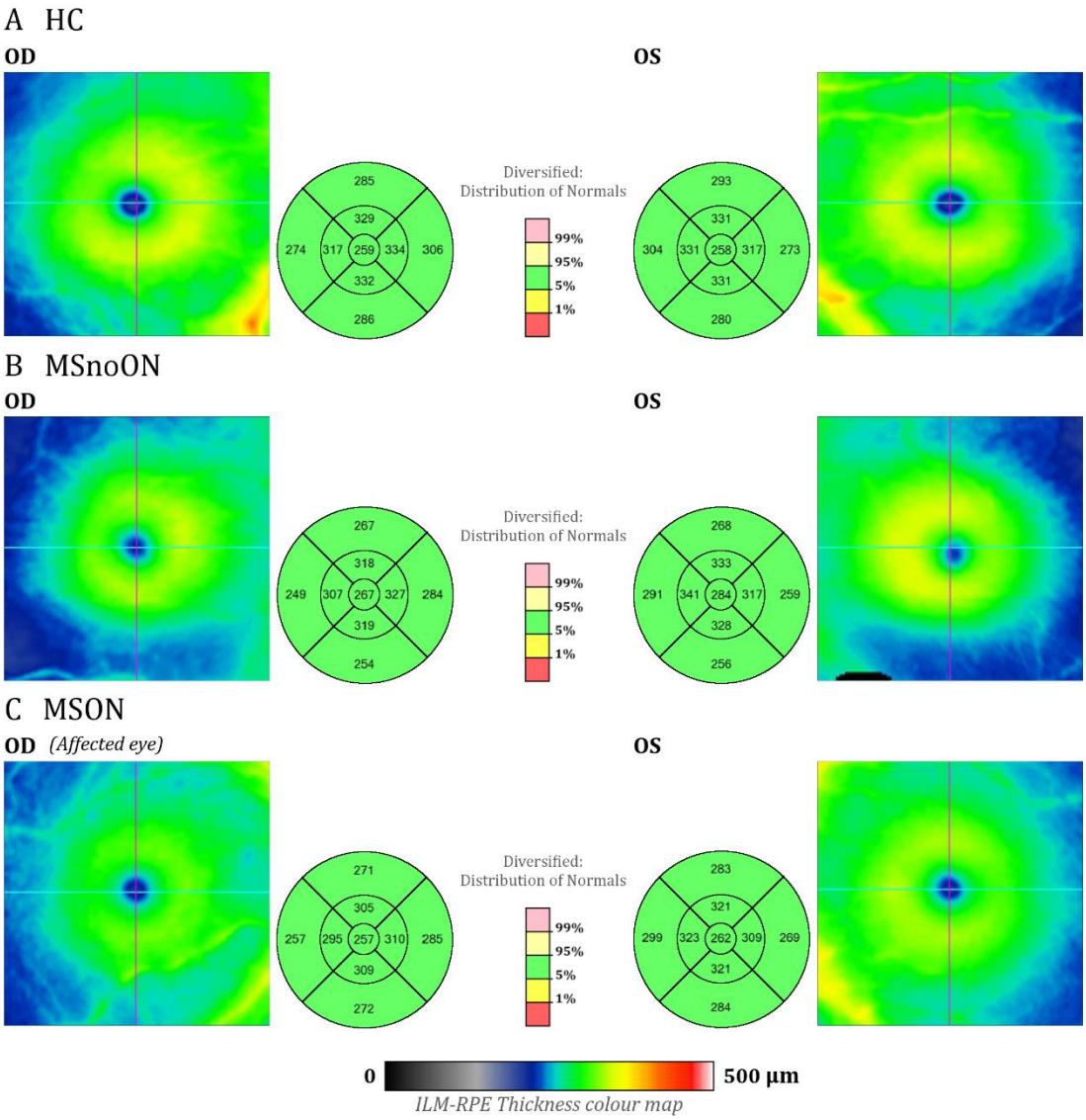

Figure V.1 Representative examples of macular thickness maps measured by Cirrus OCT in (**A**) an healthy control (HC, female, 32y), (**B**) a multiple sclerosis patient without optic neuritis (MSnoON, female, 30y) and (**C**) a multiple sclerosis patient with at least one episode of acute optic neuritis (MSON, female, 30y). The MSON patient had a previous episode of acute optic neuritis (ON) 5 years before image acquisition, in the right eye. Deviation maps show the deviation of macular measurements from healthy controls from the Cirrus internal database, as probability distributions. OD, *Right eye;* OS, *Left eye;* ILM, *Internal limiting membrane;* RPE, *Retinal pigment layer*.

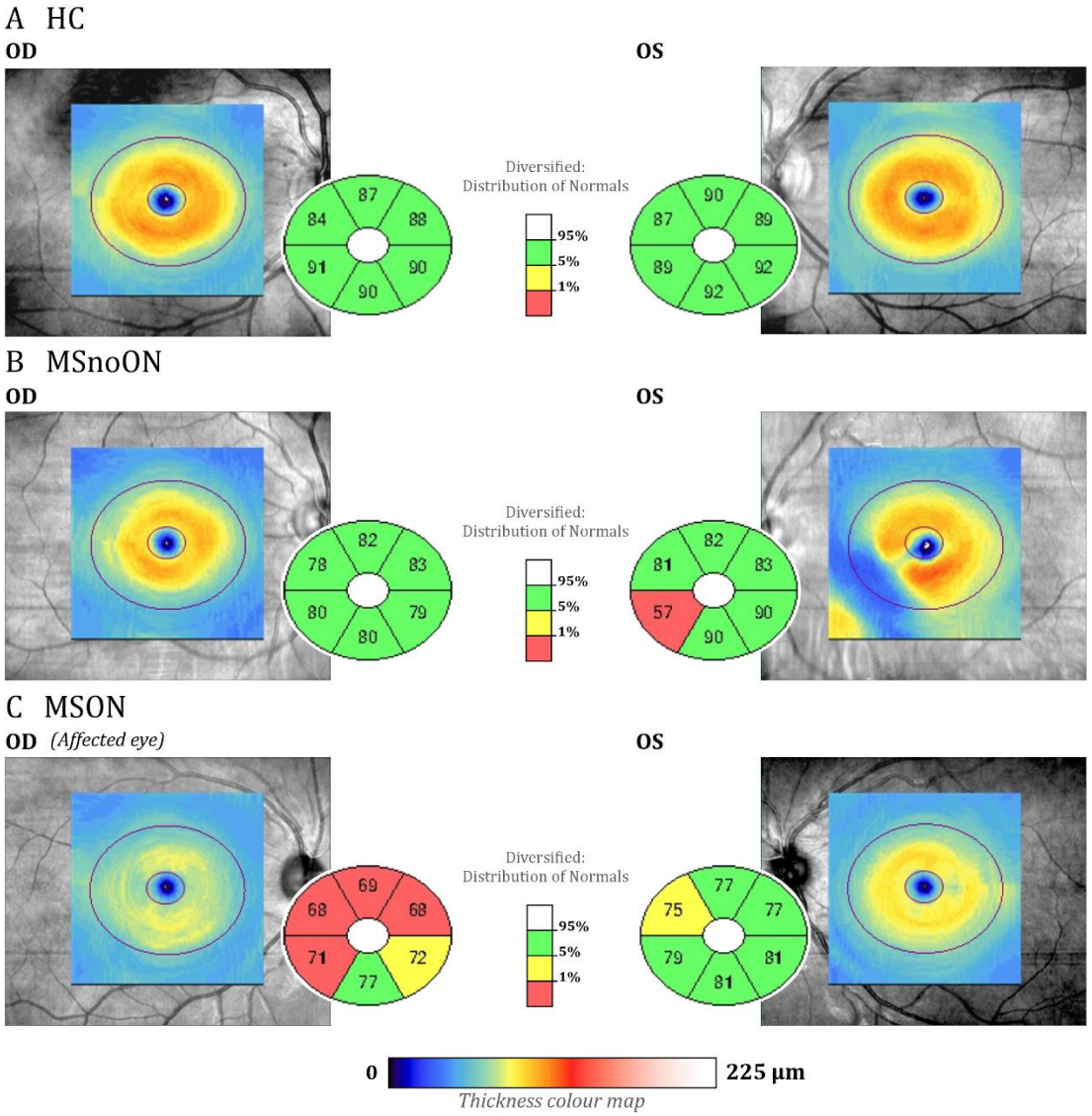

Figure V.2 Representative examples of ganglion cell layer (GCL) thickness maps measured automatically by Cirrus OCT in the same participants from Figure 1: (**A**) an healthy control (HC, female, 32y), (**B**) a Multiple Sclerosis patient without Optic Neuritis (MSnoON, female, 30y) and (**C**) a multiple sclerosis patient with at least one episode of acute optic neuritis (MSON, female, 30y). The MSON patient had a previous episode of acute optic neuritis (ON) 5 years before image acquisition, in the right eye. Deviation maps show the deviation of GLC thickness measurements from healthy controls of the Cirrus internal database, as probability distributions. Sectoral maps show mean GCL thicknesses at superotemporal, superior, superonasal, inferonasal, inferior, and inferotemporal sectors of each participant's eye. OD, *Right eye;* OS, *Left eye;* ILM, *Internal limiting membrane;* RPE, *Retinal pigment layer.*

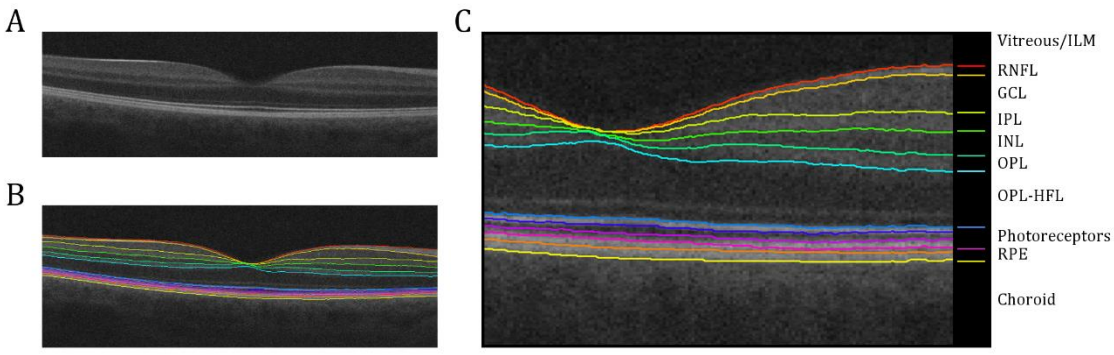

Figure V.3 Representative example of macular OCT image. (**A**) Cross-sectional scans at the level of fovea were automatically segmented into (**B**) 12 surfaces. (**C**) The 3D segmentation process the segmentation software

identifies the outer boundaries of each retinal layer. All output images are being visually inspected for segmentation errors and manually corrected, if needed. The average thickness of each layer can be defined as the mean distance between two layers for all A-scan in each central subfield. ILM*, Inner limiting membrane;* RNFL*, Retinal nerve fibre layer;* GCL*, Ganglion cell layer;* IPL*, Internal plexform layer;* INL*, Inner nuclear layer;* OPL*, Outer plexiform layer;* HFL*, Henle fibre layer;* Photoreceptors*, including the myoid and ellipsoid of inner segments, the inner segment/outer segment and the outer boundary of OPR;* RPE*, retinal pigment epithelium, including the inner and outer boundaries of RPE.*

2.4 MRI data acquisition and preprocessing

All the participants were submitted to 3T MRI scanning (Siemens Magnetom TrioTim 3T Erlangen, Germany) at the *Institute of Nuclear Sciences Applied to Health* (ICNAS) using a 12-channel birdcage head coil. Two high-resolution T1-weighted ($T1_w$) three-dimensional *Magnetization Prepared Rapid Acquisition Gradient Echo* (MPRAGE sequence: repetition time (TR) 2530 ms, echo time (TE) 3.42 ms, inversion time (IT) 1.1 s, flip angle (FA) 7°, field of view (FoV) 256×256 $mm^{2,}$ yielding 176 slices with 1×1×1 mm^3 voxel size) were acquired for each participant as well as a sagittal *3D Fluid Attenuated Inversion Recovery* (FLAIR sequence: TR 5 s, TE 388 ms, IT 1.8 s, FoV 250×250 mm^2, yielding 160 slices with 1×1×1 mm^3 voxel size) to improve the detection of brain lesions in patients with MS (Gramsch et al., 2015).

2.4.1 Data preprocessing using FreeSurfer

Cortical surface reconstruction and volumetric segmentation were performed using a semi-automatic pipeline through FreeSurfer (version 5.3.0, http://surfer.nmr.mgh.harvard.edu/) in a Linux (CentOS 6) platform. The main procedure was followed as described elsewhere (Dale, Fischl, & Sereno, 1999; B. Fischl, Sereno, & Dale, 1999). Briefly, two anatomic high-resolution $T1_w$ images were corrected for motion, averaged and registered to the Talairach space. The average image was intensity normalized (Sled, Zijdenbos, & Evans, 1998) and skull-striped using hybrid watershed algorithms and surface deformation procedures (Ségonne et al., 2004). Subcortical voxels were segmented and labeled into 40 structures (B. Fischl et al., 2002, 2004). Cortical gray/white matter border and pial surface were tessellated and the topological defects were automatically corrected (B. Fischl, Liu, & Dale, 2001; Ségonne, Pacheco, & Fischl, 2007). The folded surface was inflated and registered to an averaged spherical surface atlas based on the individual cortical folding pattern (Bruce Fischl, Sereno, Tootell, & Dale, 1999). Intensity gradients were estimated to deform the surface and optimally define the transition between tissue classes (Dale et al., 1999). Cortical thickness measures were estimated as the average of the distance between the pial surface and the closest point on the opposite surface (GM-WM) and the distance between GM-WM and the corresponding point on the opposite surface (pial) (B. Fischl & Dale, 2000). The cortical labeling of the brain was based on the Desikan-Killiany and Brodmann areas atlas focusing the occipital lobe. Our regions-of-interest (ROI) were: BA17 and 18 (corresponding roughly to striate and extrastriate visual areas respectively), the precuneus, the cuneus, the lateraloccipital cortex, the pericalcarine, the lingual, the fusiform gyri and the thalamus (Figure V.4). We also analysed pre- and post-central gyri as control areas not implicated in visual processes.

Several checkpoints were made to visually inspect for processing inaccuracies regarding the skull-stripping quality, WM, GM and pial surfaces segmentation and subcortical labelling. Whenever possible, manual edits were made and the subsequent steps re-executed. Of the 59 MS participants included in the study, two datasets were excluded due to bad quality data and poor subcortical segmentation and cortical reconstructions.

Volumes were corrected for the *estimated* total intracranial volume (eTIV) as a measure of the relationship between the intracranial volume (ICV) and the spatial linear transformation to the MNI305 space (Buckner et al., 2004).

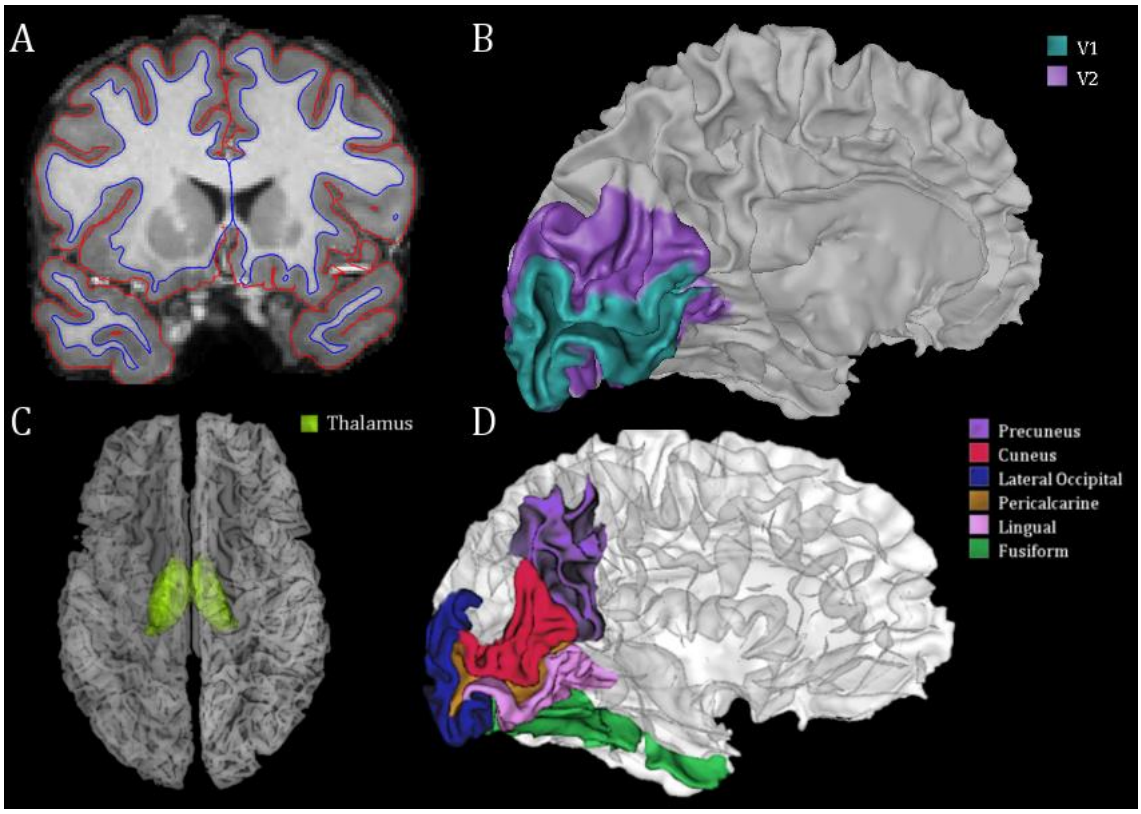

Figure V.4 Structural MRI reconstructions. (**A**) Coronal view of one of the participants. Segmentation procedures were based on FreeSurfer algorithms that automatically defined pial/grey matter (red lines) and grey/white matter (blue lines) interfaces. Our main regions-of-interest were: (**B**) BA17 and 18 (corresponding roughly to striate and extrastriate visual areas respectively), (**C**) the thalamus, (**D**) the precuneus, the cuneus, the lateraloccipital cortex, the pericalcarine, the lingual and the fusiform gyri. Pre- and post-central gyri were also considered for analysis as non-visual control areas (*data not shown*).

2.4.2 $T1_w$ and $T2_w$ lesion segmentation

A fully automated method, based on a lesion growth algorithm (Schmidt et al., 2012), was used to assess the total T2-hyperintense white matter lesion load from FLAIR images ($T2_w$ lesion volume, Table V.1). This algorithm is implemented in the Lesion Segmentation Toolbox (http://www.applied-statistics.de/lst, version 1.2.3) for SPM. The algorithm combines information from both $T1_w$ and FLAIR images. $T1_w$ images were segmented on the three main tissue classes (GM, WM and CSF). Adding this information to the FLAIR intensities, lesion belief maps (LBM) were estimated. A kappa value of 0.3 was used to threshold the maps to binary lesion maps that were expanded through hyperintense voxels of the FLAIR image to obtain lesion probability maps. The kappa value choice was based on previous studies and visual inspection of some datasets. Once lesion probability maps have been calculated binary lesion masks were visually inspected and, if necessary, manually corrected using MRIcron software (www.mricro.com/mricron). Total lesion burden (T2) was calculated from these maps.

$T1_w$ lesion volumes ($T1_w$ lesion volume, Table V.1) were automatically estimated for each participant's using Freesurfer as non-white matter hypointensities (see Methods described above).

2.5 Statistical analysis

All statistical analyses were performed using the IBM SPSS Statistics 22 (IBM Corp., Armonk, NY, USA) package. Descriptive statistics were employed for population characterization. Gender differences were performed between groups using Pearson Chi-Square test.

Conventionally, innate variations in head size should be taken into account for regional volumetric analysis (Buckner et al., 2004) for which several approaches are used based on the estimated total intracranial volume (eTIV). In this work we analysed the regions-of-interest (ROI) volumes as a fraction of the eTIV (permillage, ‰).

Prior to the group comparisons, normality tests were performed using the Kolmogorov-Smirnov test, to choose the appropriate statistical approaches. One-way ANOVA was used to compare each ROI thickness between MS and CNT groups whenever possible. Otherwise, Mann-Whitney *U* was used instead.

The MS group was further dichotomized for the occurrence of previous event of acute optic neuritis. Therefore a severity grading scale was employed considering [0=HC (best), 1=MSnoON, 2=MSON (worst)]. To test for a trend across the three groups, we used the Jonckheere-Terpstra (JT) test for ordered alternatives (Ali et al., 2015). Effect sizes of JT test were calculated by z/sqrt(N).

We will also perform correlation analysis between retinal layers thicknesses and cortical/subcortical volumes adjusted for multiple comparisons.

Graph values are reported as mean±*SEM* (standard error of the mean). For all analyses, two-tailed hypothesis testing was performed at a 0.05 significance level values.

3 RESULTS

3.1 Demographical and clinical characteristics

We studied 57 patients with multiple sclerosis, 36 without previous episode of optic neuritis (MSnoON) and 21 with previous acute episode of optic neuritis (MSON), and compared them to 64 participants of an age- and gender-matched healthy control group [age: $\chi^2(2)=0.825$, $p=0.662$, gender: $\chi^2(2)=0.015$, $p=0.993$].

There were no differences between MSnoON and MSON patients, regarding the other clinical variables analysed such as disease duration, EDSS and MSSS scores and $T1_w$ and $T2_w$ lesion loads. There were no differences in age and gender for both MS subgroups and the controls.

3.2 MRI volume in anatomically-defined visual areas

3.2.1 Multiple sclerosis patients have lower occipital volumes than healthy participants

Average volumes of each anatomically-defined region-of-interest was estimated as the total voxel count within the labelled area for each hemisphere. For each participant, the mean volume of the homologue regions between hemispheres was considered for statistical analysis. All ROI volumes were normalized for the head size variability and are reported as volume fractions of eTIV (permillage, ‰).

One-way ANOVA analysis showed a generalized significant decrease ($p<0.05$) in volumes of MS comparing to HC (Table V.2), not only in cortical visual areas, but also in thalamus and visually-neutral areas such as post- and precentral gyri.

Table V.2 Mean volumes of the ROIs for both healthy controls and multiple sclerosis groups and the respective between-groups statistics results.

	HC (mean ± *sd* ‰)	MS (mean ± *sd* ‰)	*F*-test	*p*-value
V1	2.85 ± 0.33	2.62 ± 0.38	F (1,120)=13.239	<0.001
V2	7.26 ± 0.72	6.73 ± 0.84	F (1,120)=14.268	<0.001
cuneus	4.75 ± 0.50	4.46 ± 0.63	F (1,120)=7.744	0.006
fusiform	10.72 ± 1.08	10.10 ± 1.12	F (1,120)=9.473	0.003
lateraloccipital	14.37 ± 1.52	13.6352 ± 0.97	F (1,120)=7.004	0.009
lingual	8.36 ± 1.51	7.5366 ± 1.14	F (1,120)=18.494	<0.001
pericalcarine	2.78 ± 0.37	2.5213 ± 0.47	F (1,120)=11.148	0.001
precuneus	12.43 ± 1.25	11.8549 ± 1.39	F (1,120)=5.691	0.019
thalamus	9.59 ± 0.73	8.2223 ± 1.29	F (1,120)=53.601	<0.001
postcentral gyrus	6.51 ± 0.63	6.1440 ± 0.78	F (1,120)=8.447	0.004
precentral gyrus	8.24 ± 0.70	7.9029 ± 0.85	F (1,120)=5.686	0.019

3.2.2 Multiple Sclerosis patients have lower volumes in occipital visual areas that receive direct retinocortical input from the retina regardless having had previous optic neuritis episode or not

The multiple sclerosis group was further subdivided into two subgroups regarding the clinical history of optic neuritis: the MSnoON subgroup, without any previous episode of Optic Neuritis and/or any active optic inflammation at least till 1 month before the examination and the MSON subgroup, that had at least one previous episode of Optic Neuritis (MSON) mono- or binocularly. Thus, we considered three grades of disease severity [0=no disease, 1=MSnoON, 2=MSON] and conducted a Jonckheere-Terpstra test for ordered alternatives. We found that there was a statistical significant linear trend for lower volumes in all ROIs with disease severity (Figure V.5, Table V.3). The ROI with a stronger linear trend was the thalamus, with evidenced lower volumes with the increased severity.

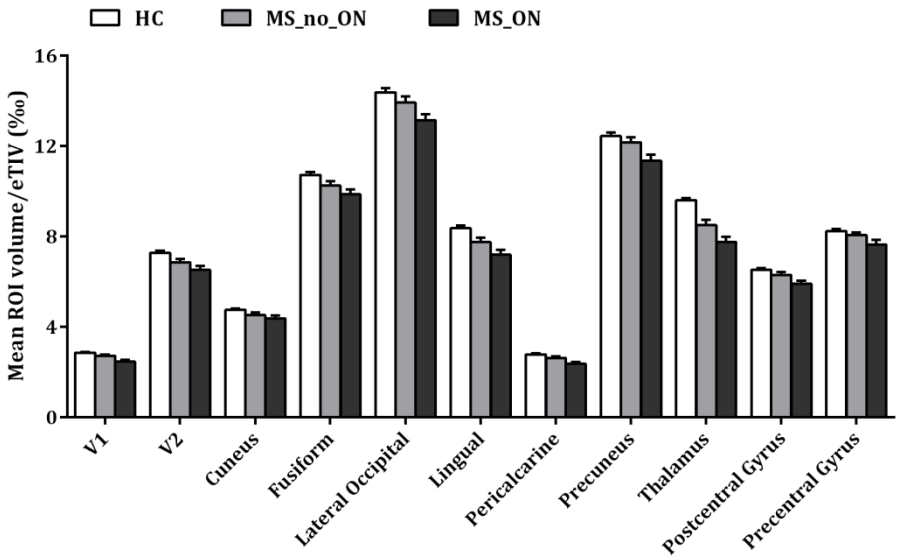

Figure V.5 Mean volumes normalized to eTIV (permillage, ‰) of anatomically-defined occipital regions of healthy controls (HC) and multiple sclerosis patients without previous acute event of optic neuritis (MSnoON) and with previous acute event of optic neuritis (MSnoON). Considering a progressive severity scale, where 0=HC, 1=MSnoON and 2= MSON, it is noticeable the progressive decrease in volume ratio. See Text and Table V.3 for statistics. Error bars denote *SEM*.

Table V.3 Statistical results for the Jonckheere-Terpstra (JT) test for ordered alternatives [0=HC, 1=MSnoON, 2=MSON]. T_{JT}, *JT test statistic*; z, *Standardized test statistic*; r_{JT}, *Effect size.*

	T_{JT}	z	p-value	r_{JT}
V1	1336	-4.290	<0.001	-0.39
V2	1432	-3.815	<0.001	-0.35
cuneus	1640	-2.784	0.005	-0.25
fusiform	1592	-3.022	0.003	-0.27
lateraloccipital	1596	-3.002	0.003	-0.27
lingual	1341	-4.266	<0.001	-0.39
pericalcarine	1403	-3.958	<0.001	-0.36
precuneus	1608	-2.943	0.003	-0.27
thalamus	**879**	**-6.554**	**<0.001**	**-0.60**
postcentral gyrus	1553	-3.215	0.001	-0.29
precentral gyrus	1754	-2.220	0.026	-0.20

4 DISCUSSION

In this work we aim to establish the structural correlates between the retina and occipital visual cortex of multiple sclerosis (MS) patients and age- and gender-matched control (HC) groups. Furthermore the multiple sclerosis group was subdivided concerning the clinical history of optic neuritis (ON). MSON subgroup includes MS patients that had at least one episode of acute ON before data acquisition and MSnoON patients never had any episode of acute ON. Additionally, we investigated changes at the level of the thalamus, a central deep-grey matter structure within the visual pathway.

This work has three sections. In the first part, we analyzed the cortical profile of several ROIs in the occipital visual cortex in patients with Multiple Sclerosis and an age- and gender-matched control group. The second part aims to analyze the effects of optic neuritis in mean thickness of eight retinal layers (Figure V.3). The goal for the third part of this work is to establish the neural correlates between the retina and the cortex structural measures. In this line we will correlate the volumes of the visual cortical areas and the thalamus with the thicknesses of retinal layers.

MR imaging is an established technique in the diagnostic criteria of MS and disease monitoring (Tallantyre and Robertson, 2016). This is not only because it allows to visualize the surrogate markers of demyelination, the $T2_w$ and $T1_w$ lesions, but also due to the introduction of new MRI biomarkers that allow to detect and quantify the degree of pathologic tissue in MS. Immunohistochemistry, pathologic and MRI studies have shown that, despite the typical classification of MS as a WM disease, due to the inflammatory demyelination, there is an extensive and progressive atrophy of GM. Moreover, GM pathology has been associated to neurological and neuropsychological measures of MS disability in higher degree than other MRI measures (Geurts et al., 2012). The GM loss have been suggested to be related to cell (glial and neuronal) and/or synaptic damage (Wegner et al., 2006). Although it is still under debate, some studies indicate some regional dominance for early GM atrophy, especially in the thalamus and other subcortical structures (Chard and Miller, 2009; Cifelli et al., 2002). The atrophy in the thalami driven by silent microstructural thalamic alterations even in normal appearing brain tissue seems to be a solid finding (Deppe et al., 2016). One limitation of this study is the assessment of LGN volume. However, due to the intrinsic difficulty of this endeavour due to its small size, the thalamus was analyzed as a whole. In our work the higher difference relied on the thalamus, that appears here as an especially sensitive structure to MS pathology. Additionally we found that all MS patients had lower cortical volumes in all the other ROIs analyzed, especially in the patients with prior acute ON as assessed by a trend analysis. However, the effects appear to be global since differences were also seen in our ROIs not related to visual processing, the pre- and postcentral gyri. This is quite interesting due to the clinical-

radiological paradox (Hackmack et al., 2012). The fact is that most of the demyelinating lesions that cause ON in MS occur essentially at the optic nerve. The ON leads to moderate to severe visual impairment. Frequently the patients have a (near) complete clinical recovery. However a permanent structural and functional damage persists.

The investigation of retinocortical patterns of damage is still a *work-in-progress* of this study. Regression/correlation analyses between the cortical and retinal variables defining the respective phenotypes are needed such patterns.

Several studies showed that there is a progressive thinning of RNFL layer in patients with MS, even in the absence of ON, usually accompanied by clinically relevant visual deficits (Talman et al., 2010; Walter et al., 2012). However, the decrease is particularly accentuated in MS patients with a history of ON (Sakai et al., 2011). In fact longitudinal studies hypothesized that the RNFL thinning is greater than the expected in normal aging due to retrograde trans-synaptic degeneration along with the progressive loss of retinal ganglion cells, especially if ON occurs (Balk et al., 2014; Petzold et al., 2010). In addition the study of Balk and colleagues (Balk et al., 2014) showed that the atrophy pattern occurred only in the inner retinal layers. They also found a significant decrease in cortical thickness of primary and secondary visual cortex, but only in MS following ON (Balk et al., 2014). It is important to emphasize that the morphometric variable was not the same and does not reflect the same parameters/ROIs. In another longitudinal study within one year the authors found that the RNFL thinning in MS was specifically associated with visual cortex atrophy and it was significantly influenced by N-acetyl-aspartate levels (putative neuronal marker) and the lesion volume within optic radiations, independently from having ON (Gabilondo et al., 2014). However, other studies reported lower thickness in GCL-inner plexiform layer in all MS subtypes that correlate better with vision and disability than RNFL thickness measures (Saidha et al., 2011). Despite some differences across studies, trans-synaptic degeneration is a consistent hypothesis in MS.

The cortical volumes estimated from different software (FreeSurfer, FSL and SPM) are different and therefore caution should be taken on correlations with clinical and/or cognitive variables (Popescu et al., 2016). Nonetheless, there is a general agreement that GM is reduced in MS. The regional specificity may be related to differences in susceptibility to injury by inflammation and/or differences in neuroprotective or neuroplasticitiy responses and pathologic processes.

Visual impairment is frequent in MS, usually in the form of acute optic neuritis episodes that may compromise the integrity of the neural retina, both structural- and functionally (Balcer et al., 2015). Since our participants were not suffering from acute episodes, vision was relatively preserved. In a longitudinal study of Balk and colleagues, a plateau effect on the retinal atrophy was suggested, supporting the advantage of early therapeutic interventions (Balk et al., 2016). In addition, new advanced methods for statistical analysis are being developed for application in this field. Multivariate methods, as support vector machines, using SPM information of GM differences have already proven to be very informative and able to classify with high sensitivity and specificity MS patients at the single case level (Bendfeldt et al., 2012). The analysis of the multivariate patterns of degeneration in both retina and brain may be critical to define several clinical endpoints, monitor disease progression and even help promote the best therapeutic in the relevant time window.

5 ACKNOWLEDGEMENTS

This research was supported by a grant from Biogen. This work was supported by the following grants: FCT-UID/NEU/04539/2013 and COMPETE-POCI-01-0145-FEDER-007440. Otília C. d'Almeida was funded by the Portuguese Foundation for Science and Technology (grant SFRH/BD/76013/2011).

6 REFERENCES

Abràmoff, M. D., Garvin, M. K., & Sonka, M. (2010). Retinal imaging and image analysis. IEEE *Reviews in Biomedical Engineering*, *3*, 169–208. doi:10.1109/RBME.2010.2084567

Ali, A., Rasheed, A., Siddiqui, A. A., Naseer, M., Wasim, S., & Akhtar, W. (2015). Non-parametric test for ordered medians: the Jonckheere Terpstra test. *International Journal of Statistics in Medical Research*, *4*(2), 203–207. doi:10.6000/1929-6029.2015.04.02.6 Accepted

Antony, B., Abràmoff, M. D., Tang, L., Ramdas, W. D., Vingerling, J. R., Jansonius, N. M., … Garvin, M. K. (2011). Automated 3-D method for the correction of axial artifacts in spectral-domain optical coherence tomography images. *Biomedical Optics Express*, *2*(8), 2403–2416. doi:10.1364/BOE.2.002403

Baghizadeh, S., Sahraian, M. A., & Beladimoghadam, N. (2013). Clinical and demographic factors affecting disease severity in patients with multiple sclerosis. *Iranian Journal of Neurology*, *12*(1), 1–8.

Balcer, L. J., Miller, D. H., Reingold, S. C., & Cohen, J. A. (2015). Vision and vision-related outcome measures in multiple sclerosis. *Brain*, *138*, 11–27. doi:10.1093/brain/awu335

Balk, L. J., Cruz-Herranz, A., Albrecht, P., Arnow, S., Gelfand, J. M., Tewarie, P., … Green, A. J. (2016). Timing of retinal neuronal and axonal loss in MS: a longitudinal OCT study. *Journal of Neurology*, *63*(7), 1323–1331. doi:10.1007/s00415-016-8127-y

Balk, L. J., Twisk, J. W. R., Steenwijk, M. D., Daams, M., Tewarie, P., Killestein, J., … Petzold, A. (2014). A dam for retrograde axonal degeneration in multiple sclerosis? Journal of Neurology, Neurosurgery, and Psychiatry, 1–8. doi:10.1136/jnnp- 2013-306902

Bendfeldt, K., Klöppel, S., Nichols, T. E., Smieskova, R., Kuster, P., Traud, S., … Borgwardt, S. J. (2012). Multivariate pattern classification of gray matter pathology in multiple sclerosis. *Neuroimage*, *60*(1), 400–408. doi:10.1016/j.neuroimage.2011.12.070

Buckner, R. L., Head, D., Parker, J., Fotenos, A. F., Marcus, D., Morris, J. C., & Snyder, A. Z. (2004). A unified approach for morphometric and functional data analysis in young, old, and demented adults using automated atlas-based head size normalization: reliability and validation against manual measurement of total intracranial volume. *Neuroimage*, *23*(2), 724–738. doi:10.1016/j.neuroimage.2004.06.018

Chard, D., & Miller, D. (2009). Grey matter pathology in clinically early multiple sclerosis: evidence from magnetic resonance imaging. *Journal of the Neurological Sciences*, *282*(1), 5–11. doi:10.1016/j.jns.2009.01.012

Cifelli, A., Arridge, M., Jezzard, P., Esiri, M. M., Palace, J., & Matthews, P. M. (2002). Thalamic neurodegeneration in multiple sclerosis. *Annals of Neurology*, *52*(5), 650–653. doi:10.1002/ana.10326

Dale, A. M., Fischl, B., & Sereno, M. I. (1999). Cortical surface-based analysis: I. Segmentation and surface reconstruction. *Neuroimage*, *9*(2), 179–194. doi:10.1006/nimg.1998.0395

Deppe, M., Krämer, J., Tenberge, J.-G., Marinell, J., Schwindt, W., Deppe, K., … Meuth, S. G. (2016). Early silent microstructural degeneration and atrophy of the thalamocortical network in multiple sclerosis. *Human Brain Mapping*, *37*(5), 1866–1879. doi:10.1002/hbm.23144

Fischl, B., & Dale, A. M. (2000). Measuring the thickness of the human cerebral cortex from magnetic resonance images. *Proceedings of the National Academy of Science*, *97*(20), 11050–11055. doi:10.1073/pnas.200033797

Fischl, B., Liu, A., & Dale, A. M. (2001). Automated manifold surgery: constructing geometrically accurate and topologically correct models of the human cerebral cortex. *IEEE Transactions on Medical Imaging*, *20*(1), 70–80. doi:10.1109/42.906426

Fischl, B., Salat, D. H., Busa, E., Albert, M., Dieterich, M., Haselgrove, C., … Dale, A. M. (2002). Whole Brain Segmentation: Neurotechnique Automated Labeling of NeuroanatomicalStructures in the Human Brain. *Neuron*, *33*(3), 341–355.

Fischl, B., Sereno, M. I., & Dale, A. M. (1999). Cortical surface-based analysis: II: inflation, flattening, and a surface-based coordinate system. Neuroimage, 9(2), 195–207. doi:10.1006/nimg.1998.0396

Fischl, B., Sereno, M. I., Tootell, R. B. H., & Dale, A. M. (1999). High-resolution inter-subject averaging and a surface-based coordinate system. Human Brain Mapping, *8*, 272–284. doi:10.1002/(SICI)1097-0193(1999)8

Fischl, B., van Der Kouwe, A., Destrieux, C., Halgren, E., Ségonne, F., Salat, D. H., … Dale, A. M. (2004). Automatically parcellating the human cerebral cortex. *Cerebral Cortex*, *14*(1), 11–22. doi:10.1093/cercor/bhg087

Friese, M. A. (2016). Widespread synaptic loss in multiple sclerosis. *Brain*, *139*(1), 2–4. doi:10.1093/brain/awv349

Gabilondo, I., Martínez-Lapiscina, E. H., Martínez-Heras, E., Fraga-Pumar, E., Llufriu, S., Ortiz, S., … Villoslada, P. (2014). Trans-synaptic axonal degeneration in the visual pathway in multiple sclerosis. *Annals of Neurology*, *75*(1), 98–107. doi:10.1002/ana.24030

Gallo, A., Bisecco, A., Bonavita, S., & Tedeschi, G. (2015). Functional plasticity of the visual system in multiple sclerosis. *Frontiers in Neurology*, *6*(Article 79), 1–3. doi:10.3389/fneur.2015.00079

Garvin, M. K., Abràmoff, M. D., Wu, X., Russell, S. R., Burns, T. L., & Sonka, M. (2009). Automated 3-D intraretinal layer segmentation of macular spectral-domain optical coherence tomography

images. *IEEE Transactions on Medical Imaging*, *28*(9), 1436–1447. doi:10.1109/TMI.2009.2016958

Geurts, J. J., Calabrese, M., Fisher, E., & Rudick, R. A. (2012). Measurement and clinical effect of grey matter pathology in multiple sclerosis. *The Lancet Neurology*, *11*(12), 1082–1092. doi:10.1016/S1474-4422(12)70230-2

Geurts, J. J. G., & Barkhof, F. (2008). Grey matter pathology in multiple sclerosis. *The Lancet Neurology*, *7*(9), 841–851. doi:10.1016/S1474-4422(08)70191-1

Gramsch, C., Nensa, F., Kastrup, O., Maderwald, S., Deuschl, C., Ringelstein, A., … Schlamann, M. (2015). Diagnostic value of 3D fluid attenuated inversion recovery sequence in multiple sclerosis. *Acta Radiologica*, *56*(5), 622–627. doi:10.1177/0284185114534413

Green, A. J., McQuaid, S., Hauser, S. L., Allen, I. V., & Lyness, R. (2010). Ocular pathology in multiple sclerosis: retinal atrophy and inflammation irrespective of disease duration. *Brain*, *133*, 1591–1601. doi:10.1093/brain/awq080

Hackmack, K., Weygandt, M., Wuerfel, J., Pfueller, C. F., Bellmann-Strobl, J., Paul, F., & Haynes, J.-D. (2012). Can we overcome the "clinico-radiological paradox" in multiple sclerosis? Journal of Neurology, 259(10), 2151–2160. doi:10.1007/s00415-012-6475-9

Hanson, J. V., Lukas, S. C., Pless, M., & Schippling, S. (2016). Optical Coherence Tomography in Multiple Sclerosis. In Seminars in Neurology (Vol. 36, pp. 177–184). Thieme Medical Publishers.

Kolappan, M., Henderson, A. P. D., Jenkins, T. M., Wheeler-Kingshott, C. A. M., Plant, G. T., Thompson, A. J., & Miller, D. H. (2009). Assessing structure and function of the afferent visual pathway in multiple sclerosis and associated optic neuritis. Journal of Neurology, 256(3), 305–319. doi:10.1007/s00415-009-0123-z

Kurtzke, J. F. (1983). Rating neurologic impairment in multiple sclerosis : An expanded disability status scale (EDSS). Neurology, 33, 1444–1452. doi:10.1212/WNL.33.11.1444

London, A., Benhar, I., & Schwartz, M. (2013). The retina as a window to the brain-from eye research to CNS disorders. Nature Reviews Neurology, 9(1), 44–53. doi:10.1038/nrneurol.2012.227

Optic Neuritis Study Group. (1991). The clinical profile of optic neuritis: experience of the Optic Neuritis Treatment Trial. Archives of Ophthalmology, 109(12), 1673–1678.

Ortiz-Perez, S., Andorra, M., Sanchez-Dalmau, B., Torre-Torres, R., Calbet, D., Lampert, E. J., … Martinez-Lapiscina, E. H. (2016). Visual field impairment captures disease burden in multiple sclerosis. Journal of Neurology, 263(4), 695–702. doi:10.1007/s00415-016-8034-2

Petzold, A., de Boer, J. F., Schippling, S., Vermersch, P., Kardon, R., Green, A., … Polman, C. (2010). Optical coherence tomography in multiple sclerosis: a systematic review and meta-analysis. *The Lancet Neurology*, *9*(9), 921–932. doi:10.1016/S1474-4422(10)70168-X

Polman, C. H., Reingold, S. C., Banwell, B., Clanet, M., Cohen, J. A., Filippi, M., … Wolinsky, J. S. (2011). Diagnostic criteria for multiple sclerosis: 2010 revisions to the McDonald criteria. *Annals of Neurology*, *69*(2), 292–302. doi:10.1002/ana.22366

Popescu, V., Schoonheim, M. M., Versteeg, A., Chaturvedi, N., Jonker, M., De Menezes, R. X., … Vrenken, H. (2016). Grey matter atrophy in multiple sclerosis: Clinical interpretation depends on choice of analysis method. *PLoS ONE*, *11*(1), 1–17. doi:10.1371/journal.pone.0143942

Riccitelli, G., Rocca, M. A., Pagani, E., Martinelli, V., Radaelli, M., Falini, A., … Filippi, M. (2012). Mapping regional grey and white matter atrophy in relapsing-remitting multiple sclerosis. *Multiple Sclerosis Journal*, *18*(7), 1027–1037. doi:10.1177/1352458512439239

Saidha, S., Syc, S. B., Durbin, M. K., Eckstein, C., Oakley, J. D., Meyer, S. A., … Calabresi, P. A. (2011). Visual dysfunction in multiple sclerosis correlates better with optical coherence tomography derived estimates of macular ganglion cell layer thickness than peripapillary retinal nerve fiber layer thickness. *Multiple Sclerosis Journal*, *17*(12), 1449–1463. doi:10.1177/1352458511418630

Sakai, R. E., Feller, D. J., Galetta, K. M., Galetta, S. L., & Balcer, L. J. (2011). Vision in multiple sclerosis (MS): the story, structure-function correlations, and models for neuroprotection. *Journal of Neuro-Ophthalmology: The Official Journal of the North American Neuro-Ophthalmology Society*, *31*(4), 362–373. doi:10.1097/WNO.0b013e318238937f

Schmidt, P., Gaser, C., Arsic, M., Buck, D., Förschler, A., Berthele, A., … Mühlau, M. (2012). An automated tool for detection of FLAIR-hyperintense white-matter lesions in Multiple Sclerosis. *Neuroimage*, *59*(4), 3774–3783. doi:10.1016/j.neuroimage.2011.11.032

Ségonne, F., Dale, A. M., Busa, E., Glessner, M., Salat, D., Hahn, H. K., & Fischl, B. (2004). A hybrid approach to the skull stripping problem in MRI. *Neuroimage*, *22*(3), 1060–1075. doi:10.1016/j.neuroimage.2004.03.032

Ségonne, F., Pacheco, J., & Fischl, B. (2007). Geometrically accurate topology-correction of cortical surfaces using nonseparating loops. *IEEE Transactions on Medical Imaging*, *26*(4), 518–529. doi:10.1109/TMI.2006.887364

Sled, J. G., Zijdenbos, A. P., & Evans, A. C. (1998). A nonparametric method for automatic correction of intensity nonuniformity in MRI data. *IEEE Transactions on Medical Imaging*, *17*(1), 87–97. doi:10.1109/42.668698

Tallantyre, E. C., & Robertson, N. P. (2016). Continuous evolution of magnetic resonance imaging in multiple sclerosis. *Journal of Neurology*, *263*(4), 835–837. doi:10.1007/s00415-016-8099-y

Talman, L. S., Bisker, E. R., Sackel, D. J., Long, D. A., Galetta, K. M., Ratchford, J. N., … Balcer, L. J. (2010). Longitudinal study of vision and retinal nerve fiber layer thickness in multiple sclerosis. *Annals of Neurology*, *67*(6), 749–760. doi:10.1002/ana.22005

Walter, S. D., Ishikawa, H., Galetta, K. M., Sakai, R. E., Feller, D. J., Henderson, S. B., … Balcer, L. J. (2012). Ganglion cell loss in relation to visual disability in multiple sclerosis. *Ophthalmology*, *119*(6), 1250–1257. doi:10.1016/j.ophtha.2011.11.032

Wegner, C., Esiri, M. M., Chance, S. A., Palace, J., & Matthews, P. M. (2006). Neocortical neuronal, synaptic, and glial loss in multiple sclerosis. *Neurology*, *67*(6), 960–967. doi:10.1212/01.wnl.0000237551.26858.39

WHO. (2006). *Neurological disorders: public health challenges*. World Health Organization.

Zimmermann, H., Oberwahrenbrock, T., Brandt, A. U., Paul, F., & Dörr, J. (2014). Optical coherence tomography for retinal imaging in multiple sclerosis. *Degenerative Neurological and Neuromuscular Disease*, *4*, 153–162. doi:http://dx.doi.org/10.2147/DNND.S73506

Zivadinov, R., & Minagar, A. (2009). Evidence for gray matter pathology in multiple sclerosis: a neuroimaging approach. *Journal of the Neurological Sciences*, *282*, 1–4. doi:10.1016/j.jns.2009.03.014

CHAPTER VI

Concluding Remarks

"The brain is a world consisting of a number of unexplored continents and great stretches of unknown territory."

Santiago Ramón y Cajal

1 CONCLUDING REMARKS

This PhD thesis explores the contemporary and highly controversial topic of the dichotomy between cortical reorganization or cortical "*plasticity*" and neurodegeneration. More specifically we focused in the study of human models of visual damage due to impairment in the retinal ganglion cell (RGC) that provides the visual information from the eye to the occipital cortex in the brain through its axons that form the optic nerve. Optic neuropathies are frequent complications that lead to visual loss by optic nerve degeneration due to inflammatory, ischemic, traumatic and/or demyelinising aetiologies. Usually, these disorders are evaluated in an ophthalmologic perspective (Behbehani, 2007). However, due to the close relation between the retina and the brain it is empirical to evaluate the status of the brain (investigative neurophthalmology approach). More importantly, it is crucial to evaluate the impact of RGCs and optic nerve degeneration in the lateral geniculate nucleus of the thalamus and the visual cortex. We asked the following fundamental question: *"Is the impairment in the most anterior part of the visual system leading to degeneration in the posterior portion of the visual system or are the neural structures still able to reorganize upon injury?"*

As introduced in the **Chapter I**, the plasticity phenomenon has been the focus of interest since the beginning of the 20th Century, despite the overall scientific scepticism. The studies of lesion and how the brain responds towards injury were the major critical points for the study of neural reorganization phenomena. Later-on, the studies regarding experience-dependent modifications and the differences observed in the brains of these individuals emphasized the singular capabilities of the brain depending of the stimulation context. Accordingly the brain is a very dynamic structure during development and very sensitive to manipulations to sensory experience, even in adulthood (even if only into a smaller extent). This issue is still very controversial and disagreement exists between studies, especially in adult participants. While some authors find clues for reorganization in visual cortex of patients with retinal lesions, others find no evidence of remapping.

Still, one pivotal question remains unanswered: ***"What are the limits of brain plasticity?"***

In this study several techniques employing Magnetic Resonance Imaging principles were used to assess the anatomy, function, neurochemistry and metabolism in human models of ganglion cell degeneration and mitochondrial dysfunction and comprehensive healthy control groups (**Chapter I**). More specifically we studied cohorts of asymptomatic carriers with Leber hereditary optic neuropathy (LHON), autosomal dominant optic atrophy (ADOA) with the OPA1 mutation, type 1 and type 2 Diabetes Mellitus patients without proliferative retinopathy and Multiple Sclerosis patients with and without Optic Neuritis. Importantly we emphasize that no direct comparisons were performed between the pathologic groups, given their clinical and demographic differences. This would be interesting to attempt in future studies, which goes beyond the scope of this thesis.

This PhD project started with the study of the cortical profile of two classical and more frequent inherited optic neuropathies (LHON and OPA1-ADOA). These have distinct aetiologies but share striking similar clinical endpoints, retinal ganglion cells (RGC) degeneration, optic atrophy, and frequently central visual loss related to mitochondrial dysfunction (Yu-Wai-Man, Griffiths, & Chinnery, 2011). Given the tight relation between retinal structures and the visual cortex the most puzzling fact in both conditions is the apparent special selectivity for RGC cells. The main challenge was to understand if the cortical visual cortex, when deprived from full visual input would degenerate or if instead it would reorganize (**Chapter II.1**). We studied of a single pedigree of asymptomatic LHON carriers with the G11778A mutation. Surprisingly we found evidence for cortical reorganization and plasticity, even when structural and functional neural loss is clinically silent and in the absence of scotomas. This evidence relied on cortical thickness estimates that were

increased in the carriers when compared to controls. The differences dominated in extrastriate cortex with indirect afferent loss and especially during relatively early developmental and preclinical stages, supporting the hypothesis of compensatory developmental plasticity. More importantly, this effect was regionally-specific given that non-visual areas did not show thickness changes. The observed effects support for a very distinct form of neural plasticity because here we studied prelesional clinical carrier stages model of ganglion cell degeneration without visual symptoms in spite of the evidence for subtle psychophysical changes, and in the absence of scotomas. We believe that our results may stem from the fact that neurodegeneration was not yet dominating and therefore plastic reorganization mechanisms could be detected. Plus the age dependency observed in this study supports for the dynamic interaction between neurodevelopmental trajectories and neurodegenerative processes that shape neuroplasticity events.

The strong functional relationship between V1 (that receives direct input from the LGN) and V2 is supported by direct feedforward and feedback projections (Sincich & Horton, 2005). This is also in line with our results in which thickness of extrastriate V2 (and into a smaller extent, V3) representations were increased, possibly as a compensatory effect mediated by local cortico-cortical connections. Several alternative explanations can be developed to at least partially explain the overall early increase in cortical thickness in LHON carriers as the lack of pruning of neuronal processes that is required for the maturation of cerebral structures (Low & Cheng, 2006; Tamnes et al., 2010) and the imbalance of growth and regressive factors (Kaas, Collins, & Chino, 2006).

Later on we looked further and correlated retinal and cortical thickness measures to evaluate the retinocortical profile of these patients (**Chapter II.2**). A constant pattern of peripheral visual field defects changing peripheral visual experience were significant but not sufficient to disrupt the retinotopic maps. Interestingly, the increased cortical thickness was especially significant in peripheral retinotopic V2/V3 regions and correlated with swelling of the macular RGC axons (due to deficits in axonal transport) at the most peripheral ring, in line with the finding of visual field peripheral loss. Also ROC analysis suggested a close coupling between retinal and cortical biological markers of LHON carrier status. Therefore one may hypothesize that in asymptomatic LHON carriers alternative pathways are formed, strengthened and/or recruited, to maintain functionality that can be more rapidly lost in V1. An alternative but not exclusive hypothesis can be considered here. Given the genetic inheritance of this disorder pervasive mitochondrial dysfunction may have induced neurodevelopmental changes. Neural proliferation and differentiation processes during development require high metabolic activity so changes in metabolic function could also induce changes in cortical thickness. In this line we aim to evaluate also the in vivo metabolism, neurotransmission and membrane status in the occipital lobe of these patients and possibly compare to in vitro mitochondrial respiratory chain activity measures. Some patients were enrolled in a preliminary study (**Chapter II.3**) of ^{1}H-MRS and ^{31}P-MRSI to assess basic metabolism (PRESS data: N-acetylaspartate, creatine, choline) and neurotransmission (PRESS data: glutamate, MEGAPRESS data: GABA) as well as membrane phospholipid and high-energy phosphate metabolism (Chemical Shift Imaging). Other indexes of readily available free energy in the cell, the efficiency of ATP production and the status of oxidative metabolism in vivo are aimed to be estimated through ^{31}P-MRSI. OCT scans will be used to obtain retinal layers thickness. However, for this future work, we still need to increase the sample size and collect the biochemical and genetic data (under analysis).

In parallel to LHON studies we performed a comprehensive study of the occipital cortex of Autosomal Dominant Optic Atrophy patients (**Chapter III**). We evaluated brain morphometry by volumetric and cortical thickness measures and studied the biochemistry of the visual cortex in these patients using 1H-MRS. Due to severe loss of central vision we decided not to use retinotopy to

define early visual areas. Instead, anatomically-defined Brodmann areas were used. The main finding in this work was a significant decrease of GABA levels (normalized to total creatine) without cortical volumetric (and thickness) changes of the occipital lobe of ADOA patients evidencing impaired cortical physiology with structural sparing. The fact that we used anatomically-defined areas could have toned down subtle changes that could occur in more explicitly localized functionally-defined early visual areas reducing the power to detect plastic changes. Therefore we also performed a volume based analysis through Voxel-based morphometry. We only found some changes in the chiasmatic area. The link of the pathophysiology of ADOA to the mitochondrial dysfunction and changes in GABA suggested that the metabolism and neurotransmission would be affected. In this study we did indeed only find changes on GABA, a surrogate marker of inhibitory neurotransmission. We speculate that such changes in the inhibitory tonus may have an impact on the structural (and perhaps functional) plasticity as verified in other models of disease (Paik & Yang, 2014). By hypothesis, lowering of GABA levels, possibly associated to the modulation of other substances such as IGF1 (Maya-Vetencourt et al., 2012) could potentially serve as a homeostatic mechanism to prevent early degeneration in the occipital cortex due to retinal ganglion cell impairment and/or trigger plasticity mechanisms.

LHON and ADOA are "classical" optic neuropathies with genetic aetiology that are tightly linked with mitochondrial dysfunction – mitochondriopathies. Another interesting question would attend to the impact of a more diffuse loss of afferent input, in disorders with acquired but not specific optic neuropathy given the involvement of other pathophysiologic systems.

Despite not being considered a "*classical*" optic neuropathy, Diabetes Mellitus (**Chapter IV**) frequently leads to visual complications due to optic nerve injury that leads to progressive visual loss. And if the anterior part of the neural visual system (the retina) has received considerable attention especially due to a frequent complication, diabetic retinopathy, the involvement of the more posterior part of the visual system (the brain) is still unclear. This is probably due to the common relation of diabetes with the metabolic and vascular abnormalities that affect several organs and systems. However it is known that despite only representing 2% of body mass, the brain expends around 20% of all body energy. Therefore, it is quite straightforward that neural tissues, especially in the brain are very sensitive to dysregulation of glucose homeostasis. Diabetes Mellitus pathophysiology has been related to the irregular modulation on the blood glucose levels, leading to hypo- and hyperglycaemic states. In addition, the human brain is an exceptionally insulin-sensitive organ, involved in memory and reward systems and eating behaviour regulation processes, and whole body metabolism, which emphasizes its susceptibility to the diabetic status (Heni, Kullmann, Preissl, Fritsche, & Häring, 2015). In turn, energy metabolism and neural activity are two non-independent, tightly coupled mechanisms. We addressed this issue by the measurement of the neurotransmitter (GABA and glutamate) and neurometabolic intermediates (NAA and Cr) levels in the occipital lobe through ^{1}H-MRS in two independent studies in the visual cortex of both type 1 and type 2 diabetes patients. Both type 1 and type 2 diabetes patients had lower tCr levels when compared to their respective control groups alerting for an energetic imbalance. However the other bioenergetics systems were relatively preserved in type 1 diabetes (except for the Cr/PCr system) while in type 2 diabetes global neurometabolic disturbances were found in the occipital cortex. These patients had a reduction of tNAA, glutamate and GABA levels suggesting that the brain may be a special target in type 2 diabetes which is in line with the central insulinoresistance concept (Blázquez, Velázquez, Hurtado-Carneiro, & Ruiz-Albusac, 2014). Moreover these metabolites are closely interconnected through the TCA cycle in the mitochondria, especially NAA and glutamate, through the interconversion of glutamate and GABA within the glutamate-glutamine-GABA cycle. NAA may be acting as non-glucose energy source and a pool of acetate to supply for acetyl-CoA

synthesis in glial cells (Moffett, Arun, Ariyannur, & Namboodiri, 2013) and the decrease in NAA levels in type 2 diabetes can indeed be related to differential anabolism and catabolism flux rates. In turn, glutamate and GABA have dual roles in the CNS as putative excitatory and inhibitory neurotransmitters and players in the astrocitic-neuronal connection through the glutamate-glutamine-GABA shuttle. Under normal conditions, glutamate has a high flux rate and is closely coupled with the high-energy demands for brain functioning contributing to replenish the substrates of the TCA cycle for energy production as an additional aspartate supply from oxaloacetate in the TCA and formation of NAA by acetylation. Additionally glucose oxidation is also tightly coupled to the synaptic activity involving the glutamate-glutamine-GABA cycle (Hertz & Rodrigues, 2014; Hyder et al., 2006; Rothman, Behar, Hyder, & Shulman, 2003; Sibson et al., 1998). One very surprising result was an intriguing positive correlation between GABA and $HbA1_c$ levels in type 2 diabetes patients linking the inhibitory neurotransmission mediated by GABA and metabolic control. This correlation with poorer metabolic control suggests that GABA reduction may actually be a homeostatic response and/or consequence of the pharmacologic treatment. In sum we established a relation between metabolic and neurotransmitter markers in type 2 diabetes that may underlie the changes in neuronal function in these patients and that were not present in type 1 diabetes. We herein promote the development of new clinical studies regarding the therapeutics effects on the neurometabolism and neurotransmission in these patients and to explore the central insulinoresistance concept that has been claimed to occur in type 2 diabetes.

Last but not the least, we are now finishing a study in a demyelinating model of diffuse optic neuropathy by comparing a comprehensive cohort of Multiple Sclerosis (MS) and age- and gender-matched control groups (**Chapter V**). Furthermore we subdivided our patients group concerning the previous occurrence of acute episodes of optic neuritis a complication caused by optic nerve inflammation. All groups performed OCT in order to estimate retinal layers thicknesses and conventional MRI to calculate volumes of cortical and subcortical brain areas. MS is still viewed as a white-matter disorder, due to inflammation of the myelin sheets. However, supporting evidence shows that there is a clear and progressive atrophy of GM. Besides, the GM pathology can even precede WM dysfunction and has been strongly related to neurological and neuropsychological measures of MS disability (Geurts, Calabrese, Fisher, & Rudick, 2012). In addition, MS patients commonly suffer from visual impairment, most particularly due to acute Optic Neuritis (ON) events (although in our sample acute episodes were not present, and therefore vision was relatively preserved). Most interestingly, these patients usually recover their vision some months after the ON episode but have always some retinal sequelae. In fact, some studies support for RNFL thinning for all MS subtypes (Saidha et al., 2011) and even without the occurrence of ON. Accordingly, one of the most curious phenomenon in MS is the called "*clinical-radiologic*" paradox that establishes a poor association between neuroradiological markers and clinical disability. For instance, the majority of visual complaints of MS patients are attributed to lesioned anterior part of visual pathway due to ON. However 10% of total lesion volume is ascribed to lesions on the more posterior portion of the visual pathway, at the optic nerve. Also these patients may recover visual clinical function despite the persistent lesion. It has been hypothesized that a critical threshold for fibre loss and/or reorganization changes at the striate and extrastriate cortical visual areas may exist and compensate for the damage (Gallo, Bisecco, Bonavita, & Tedeschi, 2015; Villoslada, 2014). Our analysis showed that cortical and thalamus volumes in MS are overall decreased compared to controls particularly in patients with previous ON. We are still segmenting the retinal layers to estimate the thickness and hope to be able to establish the retinocortical correlates in MS with and without ON. We believe that regression analysis between the cortical and retinal variables will be crucial to elucidate the "*clinical-radiologic*" paradox.

The differential profiles observed in all these potential brain reorganization or plasticity effects, at the level of structure and function (LHON and KJER) and biochemistry (ADOA and Diabetes) may be controlled (at least partially) by the mitochondria (Mattson, Gleichmann, & Cheng, 2008). This theory is consistent to the knowledge that it has pivotal role in sculpting cytoarchitecture of neural networks during the development of the nervous system and that the location or properties of mitochondria change in association with developmental processes (Cheng, Hou, & Mattson, 2010; Mattson et al., 2008). LHON (Farrar, Chadderton, Kenna, & Millington-Ward, 2013) and ADOA (Alavi & Fuhrmann, 2013) are overt genetic mitochondriopathies. One cannot exclude the possible existence of pathogenic mitochondrial mutations also modulating Diabetes Mellitus phenotypes (Reardon et al., 1992). Even if not caused by genetic effects, it is known that diabetic status and pathophysiology are closely coupled to mitochondrial (dys)function (Sivitz & Yorek, 2010) and the latter is associated to insulin sensitivity issues (Szendroedi, Phielix, & Roden, 2011). Recently Multiple Sclerosis was questioned to be also a mitochondrial disorder, not only by potential mitochondrial genome defects that increase its susceptibility (Ban et al., 2008) but also mitochondrial structural/functional alterations and overdue stress on mitochondrial function (Mao & Reddy, 2010).

To improve rehabilitation techniques and pharmacologic therapies priority should be given first to the understanding of the pathogenic mechanisms underlying the different visual deprivation and cortical reorganization patterns in these optic neuropathies. We believe that the analysis of the interplay between patterns of degeneration and plasticity in both retina and brain on optic neuropathies may be critical to define several clinical endpoints, monitor disease progression and even help promote the best window of opportunity for therapeutic intervention.

"The important thing is not to stop questioning.
Curiosity has its own reason for existing."

Albert Einstein

2 REFERENCES

Alavi, M. V., & Fuhrmann, N. (2013). Dominant optic atrophy, OPA1, and mitochondrial quality control: understanding mitochondrial network dynamics. *Molecular Neurodegeneration*, *8*(32), 1–11. doi:10.1186/1750-1326-8-32

Ban, M., Elson, J., Walton, A., Turnbull, D., Compston, A., Chinnery, P., & Sawcer, S. (2008). Investigation of the role of mitochondrial DNA in multiple sclerosis susceptibility. *PLoS ONE*, *3*(8), 1–5. doi:10.1371/journal.pone.0002891

Behbehani, R. (2007). Clinical approach to optic neuropathies. *Clinical Ophthalmology*, *1*(3), 233–246.

Blázquez, E., Velázquez, E., Hurtado-Carneiro, V., & Ruiz-Albusac, J. M. (2014). Insulin in the brain: its pathophysiological implications for states related with central insulin resistance, type 2 diabetes and alzheimer's disease. *Frontiers in Endocrinology*, *5*, 1–21. doi:10.3389/fendo.2014.00161

Cheng, A., Hou, Y., & Mattson, M. P. (2010). Mitochondria and neuroplasticity. *ASN Neuro*, *2*(5), art:e00045. doi:10.1042/AN20100019

Farrar, G. J., Chadderton, N., Kenna, P. F., & Millington-Ward, S. (2013). Mitochondrial disorders: aetiologies, models systems, and candidate therapies. *Trends in Genetics*, *29*(8), 488–497. doi:10.1016/j.tig.2013.05.005

Gallo, A., Bisecco, A., Bonavita, S., & Tedeschi, G. (2015). Functional plasticity of the visual system in multiple sclerosis. *Frontiers in Neurology*, *6*(Article 79), 1–3. doi:10.3389/fneur.2015.00079

Geurts, J. J., Calabrese, M., Fisher, E., & Rudick, R. A. (2012). Measurement and clinical effect of grey matter pathology in multiple sclerosis. *The Lancet Neurology*, *11*(12), 1082–1092. doi:10.1016/S1474-4422(12)70230-2

Heni, M., Kullmann, S., Preissl, H., Fritsche, A., & Häring, H.-U. (2015). Impaired insulin action in the human brain: causes and metabolic consequences. *Nature Reviews Endocrinology*, *11*(12), 701–711. doi:10.1038/nrendo.2015.173

Hertz, L., & Rodrigues, T. B. (2014). Astrocytic-neuronal-astrocytic pathway selection for formation and degradation of glutamate/GABA. *Frontiers in Endocrinology*, *5*, Art:42. doi:10.3389/fendo.2014.00042

Hyder, F., Patel, A. B., Gjedde, A., Rothman, D. L., Behar, K. L., & Shulman, R. G. (2006). Neuronal-glial glucose oxidation and glutamatergic-GABAergic function. *Journal of Cerebral Blood Flow & Metabolism*, *26*(7), 865–877. doi:10.1038/sj.jcbfm.9600263

Kaas, J. H., Collins, C. E., & Chino, Y. M. (2006). Plasticity of retinotopic maps in visual cortex of cats and monkeys after lesions of the retina or primary visual cortex. In *Plasticity in the Visual System: from genes to circuits* (pp. 205–227). Springer.

Low, L. K., & Cheng, H.-J. (2006). Axon pruning: an essential step underlying the developmental plasticity of neuronal connections. *Philosophical Transactions of the Royal Society of London B: Biological Sciences*, *361*(1473), 1531–1544. doi:10.1098/rstb.2006.1883

Mao, P., & Reddy, P. H. (2010). Is multiple sclerosis a mitochondrial disease? *Biochimica et Biophysica Acta (BBA)-Molecular Basis of Disease*, *1802*(1), 66–79. doi:10.1016/j.bbadis.2009.07.002

Mattson, M. P., Gleichmann, M., & Cheng, A. (2008). Mitochondria in neuroplasticity and neurological disorders. *Neuron*, *60*(5), 748–766. doi:10.1016/j.neuron.2008.10.010

Maya-Vetencourt, J. F., Baroncelli, L., Viegi, A., Tiraboschi, E., Castren, E., Cattaneo, A., & Maffei, L. (2012). IGF-1 restores visual cortex plasticity in adult life by reducing local GABA levels. *Neural Plasticity*, *2012*, ArticleID: 250421. doi:10.1155/2012/250421

Moffett, J. R., Arun, P., Ariyannur, P. S., & Namboodiri, A. M. A. (2013). N-Acetylaspartate reductions in brain injury: impact on post-injury neuroenergetics, lipid synthesis, and protein acetylation. *Frontiers in Neuroenergetics*, *5*, Art: 11. doi:10.3389/fnene.2013.00011

Paik, N.-J., & Yang, E. (2014). Role of GABA plasticity in stroke recovery. *Neural Regeneration Research*, *9*(23), 2026–2028. doi:10.4103/1673-5374.147920

Reardon, W., Pembrey, M. E., Trembath, R. C., Ross, R. J. M., Sweeney, M. G., Harding, A. E., & Luxon, L. M. (1992). Diabetes mellitus associated with a pathogenic point mutation in mitochondrial DNA. *The Lancet*, *340*(8832), 1376–1379. doi:10.1016/0140-6736(92)92560-3

Rothman, D. L., Behar, K. L., Hyder, F., & Shulman, R. G. (2003). In vivo NMR studies of the glutamate neurotransmitter flux and neuroenergetics: implications for brain function. *Annual Review of Physiology*, *65*(1), 401–427. doi:10.1146/annurev.physiol.65.092101.142131

Saidha, S., Syc, S. B., Durbin, M. K., Eckstein, C., Oakley, J. D., Meyer, S. A., … Calabresi, P. A. (2011). Visual dysfunction in multiple sclerosis correlates better with optical coherence tomography derived estimates of macular ganglion cell layer thickness than peripapillary retinal nerve fiber layer thickness. *Multiple Sclerosis Journal*, *17*(12), 1449–1463. doi:10.1177/1352458511418630

Sibson, N. R., Dhankhar, A., Mason, G. F., Rothman, D. L., Behar, K. L., & Shulman, R. G. (1998). Stoichiometric coupling of brain glucose metabolism and glutamatergic neuronal activity. *Proceedings of the National Academy of Sciences*, *95*(1), 316–321.

Sincich, L. C., & Horton, J. C. (2005). The circuitry of V1 and V2: integration of color, form, and motion. *Annual Review of Neuroscience*, *28*, 303–326. doi:10.1146/annurev.neuro.28.061604.135731

Sivitz, W. I., & Yorek, M. A. (2010). Mitochondrial dysfunction in diabetes: from molecular mechanisms to functional significance and therapeutic opportunities. *Antioxidants & Redox Signaling*, *12*(4), 537–577. doi:10.1089/ars.2009.2531

Szendroedi, J., Phielix, E., & Roden, M. (2011). The role of mitochondria in insulin resistance and type 2 diabetes mellitus. *Nature Reviews. Endocrinology*, *8*(2), 92–103. doi:10.1038/nrendo.2011.138

Tamnes, C. K., Østby, Y., Fjell, A. M., Westlye, L. T., Due-Tønnessen, P., & Walhovd, K. B. (2010). Brain maturation in adolescence and young adulthood: regional age-related changes in cortical thickness and white matter volume and microstructure. *Cerebral Cortex*, *20*(3), 534–548. doi:10.1093/cercor/bhp118

Villoslada, P. (2014). Closing the clinical-radiological paradox using the visual pathway in multiple sclerosis. *Investigative Ophthalmology and Visual Scienc*e, *55*(6), 3765. doi:10.1167/iovs.14-14765

Yu-Wai-Man, P., Griffiths, P. G., & Chinnery, P. F. (2011). Mitochondrial optic neuropathies - Disease mechanisms and therapeutic strategies. *Progress in Retinal and Eye Research*, *30*(2), 81–114.

List of Publications

Marked (⏩) publications are contemplated in this Thesis.

⏩ **d'Almeida, O. C.**, Mateus, C., Reis, A., Grazina, M. M., & Castelo-Branco, M. (2013). Long term cortical plasticity in visual retinotopic areas in humans with silent retinal ganglion cell loss. *Neuroimage*, *81*, 222-230. doi:10.1016/j.neuroimage.2013.05.032

Ribeiro, M. J., **d'Almeida, O. C.**, Ramos, F., Saraiva, J., Silva, E. D., & Castelo-Branco, M. (2014). Abnormal late visual responses and alpha oscillations in neurofibromatosis type 1: A link to visual and attention deficits. *Journal of Neurodevelopmental Disorders*, *6*(1), 1-19. doi:10.1186/1866-1955-6-4

Silva, M. F.*, **d'Almeida, O. C.***, Oliveiros, B., Mateus, C., & Castelo-Branco, M. (2014). Development and aging of visual hemifield asymmetries in contrast sensitivity. *Journal of Vision*, *14*(12), 1-11. doi:10.1167/14.12.19 (**equal contribution*)

⏩ Mateus, C.*, **d'Almeida, O. C.***, Reis, A., Silva, E., & Castelo-Branco, M. (2016). Genetically induced impairment of retinal ganglion cells at the axonal level is linked to extrastriate cortical plasticity. *Brain Structure and Function*, *221*(3), 1767-1780. doi:10.1007/s00429-015-1002-2 (**equal contribution*)

⏩ **d'Almeida, O. C.**, Violante, I. R., Quendera, B., & Castelo-Branco, M. A novel cortical neurochemical phenotype in a genetic 1 mitochondrial disorder affecting the retinal ganglion cell. (*Submitted* - 2016)

⏩ **d'Almeida, O. C.**, Violante, I. R., Quendera, B., Ferreira, C., Moreno, C., Gomes, L., Ribeiro, L., Castelo-Branco, M. Coupling vs. uncoupling of metabolism and neurotransmission in type 2 and type 1 diabetes. (*Submitted* - 2016)

Sonia Batista, S., **d´Almeida, O. C.**, Afonso, A., Freitas, S., Macário, C., Sousa, L., Castelo-Branco, M., Santana, I., & Cunha, L. Impairment of social cognition in multiple sclerosis: amygdala atrophy is the main predictor. (*Submitted* - 2016)

Sanches, M.*, Abuhaiba, S. I.*, **d'Almeida, O. C.**, Quendera, B., Gomes, L., Moreno, C., Guelho, D., & Castelo-Branco, M. Diabetic Brain or Retina? Occipital Cortex GABA as a Novel Predictor of Visual Psychophysical Performance in diabetic patients with early Non Proliferative Retinopathy. (*Submitted* - 2016; **equal contribution*)

Agradecimentos

Ao Professor Doutor Miguel Castelo-Branco, o meu orientador científico, por me ter acolhido no seu Grupo e proporcionar os meios necessários à realização de ciência com grande qualidade em Portugal. Um sincero obrigada pelo contínuo acompanhamento nesta jornada e confiança depositada em mim ao longo destes anos e incentivo à criatividade e espírito crítico. Obrigada pelo seu dinamismo e por estimular ainda mais o meu interesse pelo Conhecimento neste mundo cativante das Neurociências.

À Professora Doutora Catarina Resende de Oliveira, a minha tutora, pelo acompanhamento e apoio prestados durante o decorrer do meu Projecto de Doutoramento.

Aos médicos, técnicos e outros profissionais de saúde com quem tive o prazer de trabalhar e discutir aspetos mais clínicos e técnicos que permitiram desenvolver o meu raciocínio e explorar ao máximo o trabalho de investigação.

A todos os participantes destes estudos sem os quais seria impossível fazer Ciência.

Aos meus colegas do Laboratório das Ciências da Visão, do IBILI e do ICNAS, pelos momentos de convívio que tornaram o trabalho mais leve e animado.

Às minhas queridas colegas e amigas do gabinete 7, Monika Intaitė, Manuela, Ana Dionísio (e Teresa Sousa à hora do café ☺), por terem feito do nosso pequeno cantinho um local de trabalho muito agradável, de partilha de conhecimentos, por todo o apoio e alegria no dia-a-dia (e por me ensinares lituano Monika! *Ačiū!*).

Àqueles amigos(as) mais chegados, que tiveram sempre disponibilidade para ouvir os meus desabafos e com quem pude partilhar os momentos de maior *stress* e os de maior alegria, pela vossa preocupação e carinho.

À Eng.ª Sara Martins-Neves ☺, a minha grande amiga e companheira de luta académica, com quem percorri esta longa e árdua jornada, já desde o início dos nossos tempos de caloiras, obrigada amiga, por todo o carinho, alegria e disponibilidade com que me presenteaste estes anos todos. E à sua filha, a minha afilhada linda, Leonor, que veio trazer ainda mais alegria e vida com o seu sorriso puro e sadio.

À minha família, pelo seu apoio e carinho. Em especial aos meus avós, que trago sempre no coração. Obrigada pelos ensinamentos de vida que me transmitiram desde pequenina.

Ao meu irmão Manuel, por me incentivar a acreditar nas minhas capacidades e pelos momentos de descontração com outras temáticas, nomeadamente o futebol. :p

Um especial agradecimento aos meus pais, Elisa e José Carlos, que todos os dias me inspiram com o seu modo de ser, estar e viver. Um sentido obrigada por me apoiarem incondicionalmente, aos meus sonhos e aspirações, por todo o amor, preocupação e dedicação e pela confiança que depositam em mim.

A todos, um sincero obrigada,

Otília C. d'Almeida

SHORT *CV*

Otília C. d'Almeida was born on November 26, 1987 in Guarda, Portugal. Her secondary school education was completed at Escola Secundária Alves Martins in Viseu, Portugal. In 2005, she went to the Faculty of Sciences and Technology of the University of Coimbra to study Biomedical Engineering. For her MSc thesis, entitled "*A disease model to understand neural mechanisms of visual perception: Neurofibromatosis type-1*", she spend one year (2009/2010) doing research at the Visual Neurosciences Lab, Institute for Biomedical Imaging and Life Sciences (IBILI), Faculty of Medicine, University of Coimbra, Portugal under the scientific orientation of Professor Miguel Castelo-Branco, MD, PhD and supervision of Maria Ribeiro, PhD. Since 2011, she is enrolled in the Doctoral Programme in Health Sciences, Faculty of Medicine of University of Coimbra and she started working on her PhD project entitled "*Neural basis of visual cortical reorganization mechanisms after retinal injury in Optic Neuropathies*"at the Visual Neuroscience Laboratory, IBILI, at the Faculty of Medicine of the University of Coimbra and at the Institute for Nuclear Sciences Applied to Health, Universuity of Coimbra under the supervision of Professor Miguel Castelo-Branco.

From September 15-19 of 2014 she did a short internship in the Biomedical MR Research Group, Department of Radiology, Radboud University Nijmegen Medical Centre, Nijmegen, The Netherlands to acquire hands-on experience on how to do ^{31}P-MRS experiments of humans and learn how to process the data.

She studied the neural impact, pathophysiological mechanisms and plasticity of human retinal neuropathies on visual cortical regions acquiring hands-on experience in MRI research, in both anatomical and functional domains, and neurospectroscopy (^{1}H- and ^{31}P-MRS) in humans and learned how to process the data in a wide range of software packages such as BrainVoyager, SPM-VBM, FreeSurfer, LCModel and jMRUI and also got familiar with OCT cirrus acquisition procedures. During her PhD, Otília was involved in several Research Projects approaching different techniques and clinical populations, ranging from Diabetes, to Multiple Sclerosis, Glaucoma, ADOA and LHON, Huntington and Alzheimer's disease pathologies and healthy aging.